ANL-18/40
ISSN 1931-5007
January-June 2018

APS Science 2018 Vol. 1

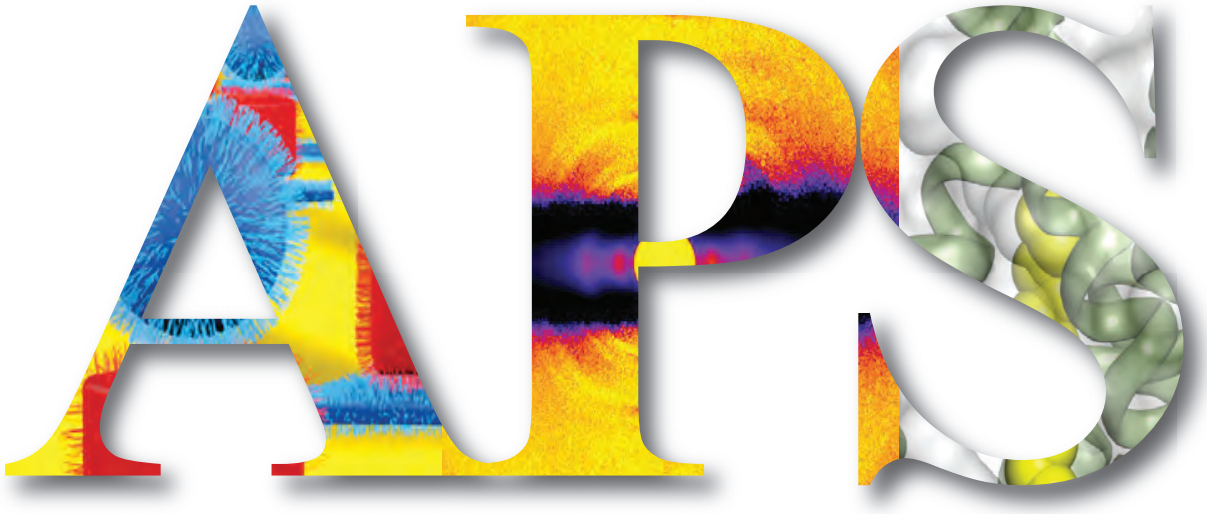

Research and engineering highlights from the Advanced Photon Source at Argonne National Laboratory

Argonne NATIONAL LABORATORY

Argonne NATIONAL LABORATORY

ANL-18/40
ISSN 1931-5007
January-June 2018

APS Science 2018 Vol. 1

Research and engineering highlights from the Advanced Photon Source at Argonne National Laboratory

Argonne is a U.S. Department of Energy (DOE) laboratory managed by UChicago Argonne, LLC.
The Advanced Photon Source is a DOE Office of Science user facility
operated for the DOE Office of Science by Argonne National Laboratory under Contract No. DE-AC02-06CH11357.

Table of Contents

Access to Beam Time at the Advanced Photon Source

Five types of beam-time proposals are available at the Advanced Photon Source (APS): general user, partner or project user, collaborative access team (CAT) member, CAT staff, and APS staff. All beam time at the APS must be requested each cycle through the web-based Beam Time Request System. Each beam-time request (BTR) must be associated with one of the proposals mentioned above.

General-user proposals and BTRs Proposals are peer reviewed and scored by a General User Proposal Review Panel, and time is allocated on the basis of scores and feasibility. A new BTR must be submitted each cycle; each cycle, allocation is competitive. Proposals expire in two years or when the number of shifts recommended in the peer review has been utilized, whichever comes first.

Partner- or project-user proposals and BTRs Proposals are peer reviewed by a General User Proposal Review Panel and reviewed further by a subcommittee of the APS Scientific Advisory Committee and by APS senior management. Although a new BTR must be submitted each cycle, a specific amount of beam time is guaranteed for up to three years.

CAT-member proposals Proposals from CAT members are typically much shorter and are reviewed by processes developed by individual CATs. Allocation/scheduling is determined by the CAT management.

CAT- and APS staff-member proposals and BTRs These proposals are also very short and are reviewed through processes developed by either the CAT or the APS. Each CAT/beamline determines how beam time is allocated/scheduled. Collaborative access team and/or APS staff may submit general user proposals, in which case the rules for general user proposals and BTRs are followed.

In addition to the above, the APS has developed an industrial measurement access mode (MAM) program to provide a way for industrial users to gain rapid access for one-time measurements to investigate specific problems. A MAM proposal expires after one visit.

The APS User Information page (www.aps.anl.gov/Users-Information) provides access to comprehensive information for prospective and current APS users.

The Advanced Photon Source Facility at Argonne National Laboratory

The APS, a national synchrotron radiation research facility operated by UChicago Argonne, LLC, and Argonne National Laborator for the U.S. Department of Energy (DOE) Office of Science-Basic Energy Sciences, Scientific User Facilities Division provides this nation's brightest high-energy x-ray beams for science. Research by APS users extends from the center of the Earth to outer space, from new information on batteries, combustion engines and microcircuits, new and improved pharmaceuticals, and nanotechnologies whose scale is measured in billionths of a meter. The APS helps researchers illuminate answers to the challenges of our high-tech world, from developing new forms of energy to sustaining our nation's technological and economic competitiveness to pushing back against the ravages of disease. Research at the APS promises to have far-reaching impact on our technology, our economy, our health, and fundamental knowledge of the materials that make up our world.

The APS occupies an 80-acre site on the Argonne campus, about 25 miles from downtown Chicago, Illinois. It shares the site with the Center for Nanoscale Materials and the Advanced Protein Characterization Facility.

For directions to Argonne, see anl.gov/directions-and-visitor-information.

Contact us

For more information about the APS send an email to apsinfo@aps.anl.gov or write to APS Info, Bldg. 401, Rm. A4115, Argonne National Laboratory, 9700 S. Cass Ave., Argonne, IL 60439.

To order additional copies of this, or previous, issues of *APS Science* send email to apsinfo@aps.anl.gov.

To download PDF versions of APS Science back issues go to www.aps.anl.gov/Science/APS-Science

Visit the APS on the Web at www.aps.anl.gov

ARGONNE NATIONAL LABORATORY 400-AREA FACILITIES

ADVANCED PHOTON SOURCE

(Beamlines, Disciplines, and Source Configuration)

ADVANCED PROTEIN CHARACTERIZATION FACILITY

CENTER FOR NANOSCALE MATERIALS

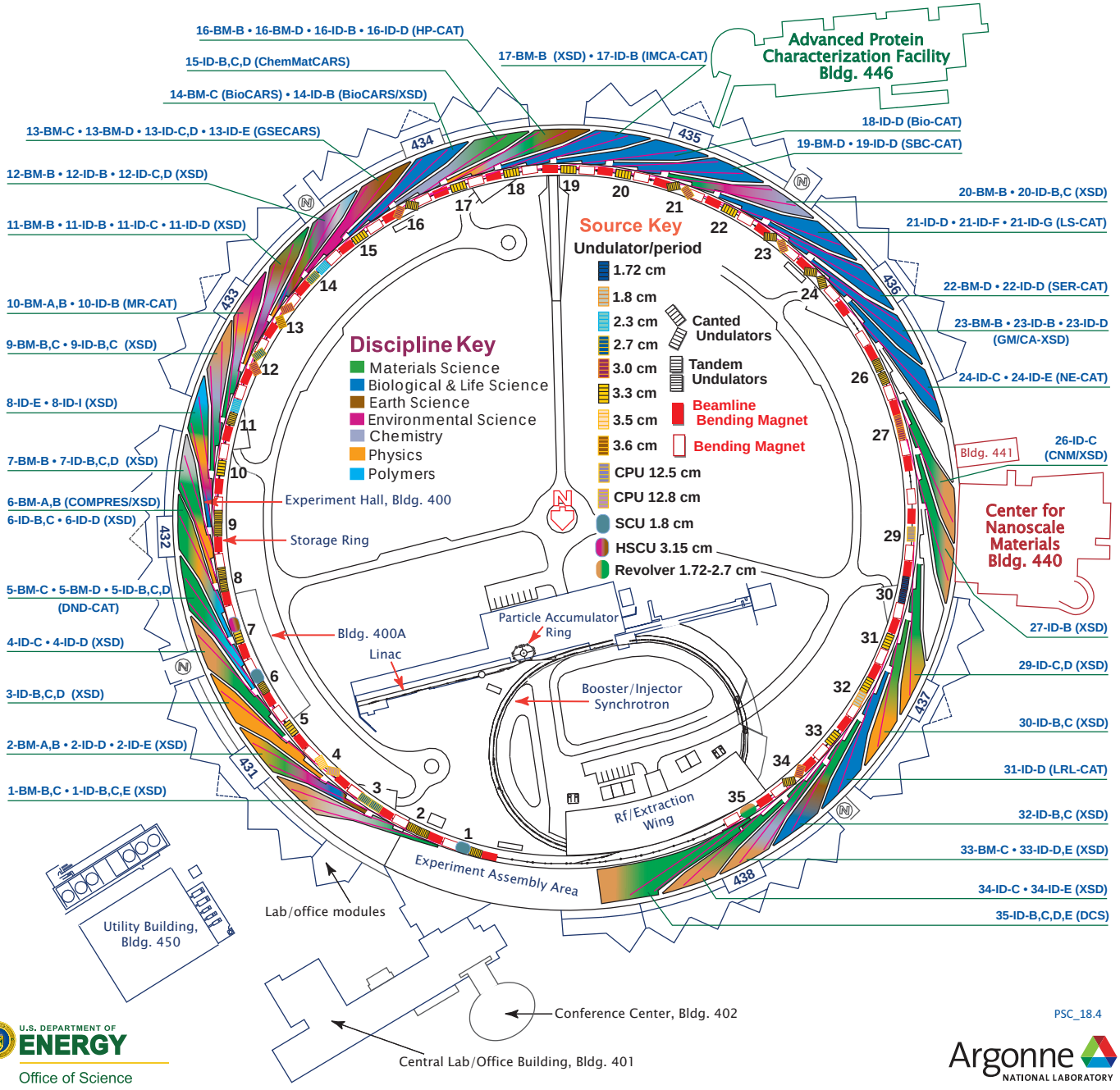

APS Sectors: At the APS, a "sector" comprises the radiation sources (one bending magnet and nominally one insertion device, although the number of insertion devices in the straight sections of the storage ring can vary) and the beamlines, enclosures, and instrumentation that are associated with a particular storage ring sector. The APS has 35 sectors dedicated to user science and experimental apparatus. X-ray Science Division sectors comprise those beamlines operated by the APS. Collaborative access team sectors comprise beamlines operated by independent groups made up of scientists from universities, industry, and/or research laboratories both federal and private.

APS Beamlines

Key: Beamline designation • Sector operator • Disciplines • Techniques • Radiation source energy • User access mode(s) • General-user status

1-BM-B,C• X-ray Science Division (XSD) • Materials science, physics, optics testing, detector testing, topography • Energy dispersive x-ray diffraction, white Laue single-crystal diffraction • 6-30 keV, 50-120 keV • On-site • Accepting general users

1-ID-B,C,E • XSD • Materials science, physics, chemistry • High-energy x-ray diffraction, tomography, small-angle x-ray scattering, fluorescence spectroscopy, pair distribution function, phase contrast imaging • 41-136 keV, 45-116 keV • On-site • Accepting general users

2-BM-A,B • XSD • Physics, life sciences, geoscience, materials science • Tomography, phase contrast imaging • 10-170 keV, 11-35 keV • On-site • Accepting general users

2-ID-D • XSD • Life sciences, materials science, environmental science • Microfluorescence (hard x-ray), micro x-ray absorption fine structure, nanoimaging • 5-30 keV • On-site • Accepting general users

2-ID-E • XSD • Life sciences, environmental science, materials science • microfluorescence (hard x-ray), tomography • 7-10.5 keV, 11-17 keV • On-site • Accepting general users

3-ID-B,C,D • XSD • Physics, geoscience, life sciences, chemistry, materials science • Nuclear resonant scattering, inelastic x-ray scattering, high-pressure diamond anvil cell • 7-27 keV, 14.41-14.42 keV • On-site • Accepting general users

4-ID-C • XSD • Physics, materials science • Magnetic circular dichroism (soft x-ray), x-ray magnetic linear dichroism, x-ray photoemission spectroscopy, x-ray photoemission electron microscopy, anomalous and resonant scattering (soft x-ray) • 500-2800 eV • On-site • Accepting general users

4-ID-D • XSD • Physics, materials science • Anomalous and resonant scattering (hard x-ray), magnetic x-ray scattering, magnetic circular dichroism (hard x-ray) • 2.7-40 keV • On-site • Accepting general users

5-ID-B,C,D • DuPont-Northwestern-Dow Collaborative Access Team (DND-CAT) • Materials science, polymer science, chemistry • Powder diffraction, x-ray standing waves, x-ray optics development/ techniques, small-angle x-ray scattering, surface diffraction, x-ray reflectivity, wide-angle x-ray scattering • 6-17.5 keV • On-site • Accepting general users

5-BM-C • DND-CAT • Materials science, polymer science, powder diffraction, tomography, wide-angle x-ray scattering • 10-42 keV • On-site • Accepting general users

5-BM-D • DND-CAT • Materials science, polymer science, chemistry • X-ray absorption fine structure, high-energy x-ray diffraction, general diffraction • 4.5-25 keV, 4.5-80 keV • On-site• Accepting general users

6-BM-A,B• COMPRES/XSD • Materials science, geoscience • Energy dispersive x-ray diffraction, high-pressure multi-anvil press • 20-1 keV • On-site • Accepting general users

6-ID-B,C • XSD • Physics, materials science • Magnetic x-ray scattering, anomalous and resonant scattering (hard x-ray), general diffraction, grazing incidence diffraction • 3.2-38 keV • On-site • Accepting general users

6-ID-D • XSD • Physics, materials science • Magnetic x-ray scattering, high-energy x-ray diffraction, powder diffraction, pair distribution function • 50-100 keV, 70-130 keV • On-site • Accepting general users

7-BM-B • XSD • Physics, radiography, tomography, microfluorescence (hard x-ray) • 5-150 keV, 6-15 keV, 25-55 keV • On-site • Accepting general users

7-ID-B,C,D • XSD • Materials science, atomic physics, chemistry • Time-resolved x-ray scattering, time-resolved x-ray absorption fine structure, phase contrast imaging • 6-21 keV • On-site • Accepting general users

8-BM-B • XSD • Chemistry, life sciences, environmental science, materials science • Microfluorescence (hard x-ray) • 5.5-20 keV, 9-18 keV • On-site • Accepting general users

8-ID-E • XSD • Materials science, polymer science, physics • Grazing incidence small-angle scattering, x-ray photon correlation spectroscopy • 7.35-7.35 keV, 11-11 keV • On-site • Accepting general users

8-ID-I • XSD • Polymer science, materials science, physics • X-ray photon correlation spectroscopy, intensity fluctuation spectroscopy, small-angle x-ray scattering • 6-12.5 keV, 10.9--10.9 keV, 7.35 keV • On-site • Accepting general users

9-BM-B,C • XSD • Materials science, chemistry, environmental science • X-ray absorption fine structure, x-ray absorption near-edge structure • 2.1-25.2 keV • On-site • Accepting general users

9-ID-B,C • XSD • Chemistry, materials science, life sciences • Nano-imaging, microfluorescence (hard x-ray), coherent x-ray scattering (hard x-ray), ultra-small-angle x-ray scattering • 4.5-30 keV • On-site • Accepting general users

10-BM-A,B • Materials Research (MR)-CAT • Materials science, chemistry, environmental science, physics • X-ray absorption fine structure • 4-32 keV • On-site • Accepting general users

10-ID-B • MR-CAT • Materials science, environmental science, chemistry • X-ray absorption fine structure, time-resolved x-ray absorption fine structure, microfluorescence (hard x-ray) • 4.3-27 keV, 4.8-32 keV, 15-65 keV • On-site • Accepting general users

11-BM-B • XSD • Chemistry, materials science, physics • Powder diffraction • 22-33 keV • On-site, mail-in • Accepting general users

11-ID-B • XSD • Chemistry, environmental science, materials science • Pair distribution function, high-energy x-ray diffraction • 58.66 keV, 86.7 keV • On-site • Accepting general users

11-ID-C • XSD • Materials science, chemistry, physics • High-energy x-ray diffraction, diffuse x-ray scattering, pair distribution function • 105.6 keV • On-site • Accepting general users

11-ID-D • XSD • Chemistry, environmental science, materials science • Time-resolved x-ray absorption fine structure, time-resolved x-ray scattering • 6-25 keV • On-site • Accepting general users

12-BM-B • XSD • Materials science, polymer science, chemistry, physics, environmental science • X-ray absorption fine structure,, x-ray reflectivity,, small-angle x-ray scattering, wide-angle x-ray scattering • 4.5-30 keV, 10-40 keV • On-site • Accepting general users

12-ID-B • XSD • Chemistry, materials science, life sciences, polymer science, physics • Small-angle x-ray scattering, grazing incidence small-angle scattering, wide-angle x-ray scattering, grazing incidence diffraction • 7.9-14 keV • On-site • Accepting general users

12-ID-C,D • XSD • Chemistry, physics, materials science • Small-angle x-ray scattering, grazing incidence small-angle scattering, wide-angle x-ray scattering, surface diffraction • 4.5-40 keV • On-site • Accepting general users

13-BM-C • GeoSoil EnviroCARS (GSECARS) • Geoscience • Environmental science • Surface diffraction, high-pressure diamond anvil cell, single-crystal diffraction • 15-15 keV, 28.6-28.6 keV • On-site • Accepting general users

13-BM-D • GSECARS • Geoscience, environmental science • Tomography, high-pressure diamond anvil cell, high-pressure multi-anvil press • 4.5-80 keV • On-site • Accepting general users

13-ID-C,D • GSECARS • Geoscience, environmental science • Microdiffraction, x-ray standing waves, x-ray absorption fine structure, resonant inelastic x-ray scattering, x-ray emission spectroscopy, high-pressure diamond anvil cell, high-pressure multi-anvil press • 4.9-45 keV, 10-75 keV • On-site • Accepting general users

13-ID-E • GSECARS • Geo science, environmental science • Microfluorescence (hard x-ray), micro x-ray absorption fine structure, microdiffraction, fluorescence spectroscopy • 2.4-28 keV, 5.4-28 keV • On-site • Accepting general users

14-BM-C • BioCARS • Life sciences • Macromolecular crystallography,

fiber diffraction, biohazards at the BSL2/3 level, subatomic (<0.85 Å) resolution, large unit cell crystallography • 8-14.9 keV • On-site • Accepting general users

14-ID-B • BioCARS • Life sciences, materials science, physics, chemistry • Time-resolved crystallography, time-resolved x-ray scattering, Laue crystallography, wide-angle x-ray scattering, biohazards at the BSL2/3 level, macromolecular crystallography • 7-19 keV • On site • Accepting general users

15-ID-B,C,D • ChemMatCARS • Materials science, chemistry • Anomalous and resonant scattering (hard x-ray), microdiffraction, high-pressure diamond anvil cell, single-crystal diffraction, liquid surface diffraction, x-ray reflectivity • 6-32 keV, 10-70 keV • On-site • Accepting general users

16-BM-B • High Pressure (HP)-CAT • Materials science, geo science, chemistry, physics • White Laue single-crystal diffraction, energy dispersive x-ray diffraction, phase contrast imaging, radiography, pair distribution function • 10-120 keV • On-site • Accepting general users

16-BM-D • HP-CAT • Materials science, geo science, chemistry, physics • Powder angular dispersive x-ray diffraction, single-crystal diffraction, x-ray absorption near-edge structure, x-ray absorption fine structure, tomography • 6-45 keV • On-site • Accepting general users

16-ID-B • HP-CAT • Materials science, geoscience, chemistry, physics • Microdiffraction, single-crystal diffraction, high-pressure diamond anvil cell • 18-60 keV • On-site • Accepting general users

16-ID-D • HP-CAT • Materials science, geo science, chemistry, physics • nuclear resonant scattering, inelastic x-ray scattering (1-eV resolution), x-ray emission spectroscopy, high-pressure diamond anvil cell • 5-37 keV, 14.41-14.42 keV • On-site • Accepting general users

17-BM-B • XSD • Chemistry, materials science • Powder diffraction, pair distribution function • 27-51 keV • On-site • Accepting general users

17-ID-B • Industrial Macromolecular Crystallography Association (IMCA)-CAT • Life sciences • Macromolecular crystallography, multi-wavelength anomalous dispersion, microbeam, single-wavelength anomalous dispersion, large unit cell crystallography • Subatomic (<0.85 Å) resolution • 6-20 keV • On-site, remote • Accepting general users

18-ID-D • Biophysics (Bio)-CAT • Life sciences • Fiber diffraction, microdiffraction, small-angle x-ray scattering, time-resolved x-ray scattering • 3.5-35 keV • On-site • Accepting general users

19-BM-D • Structural Biology Center (SBC)-CAT • Life sciences, multi-wavelength anomalous dispersion, macromolecular crystallography, single-wavelength anomalous dispersion • 6-13.5 keV • Remote, on-site, mail-in • Accepting general users

19-ID-D • SBC-CAT • Life sciences • Macromolecular crystallography, multi-wavelength anomalous dispersion, subatomic (<0.85 Å) resolution, large unit cell crystallography, single-wavelength anomalous dispersion • 6.5-19.5 keV • On-site, remote, mail-in • Accepting general users

20-BM-B • XSD • Materials science, environmental science, chemistry • X-ray absorption fine structure, microfluorescence (hard x-ray) • 2.7-32 keV, 2.7-35 keV • On-site • Accepting general users

20-ID-B,C • XSD • Materials science, environmental science, chemistry • X-ray absorption fine structure, x-ray Raman scattering, micro x-ray absorption fine structure, microfluorescence (hard x-ray), x-ray emission spectroscopy • 4.3-27 keV, 7-52 keV • On-site • Accepting general users

21-ID-D • Life Sciences (LS)-CAT • Life sciences • Macromolecular crystallography • 6.5-20 keV • On-site, remote, mail-in • Accepting general users

21-ID-F • LS-CAT • Life sciences, macromolecular crystallography • 12.7 keV • Remote, on-site, mail-in • Accepting general users

21-ID-G • LS-CAT • Life sciences, macromolecular crystallography • 12.7 keV • Remote, on-site, mail-in • Accepting general users

22-BM-D • Southeast Regional (SER)-CAT • Life sciences • Macromolecular crystallography, single-wavelength anomalous dispersion, multi-wavelength anomalous dispersion • 8-20 keV • On-site, remote • Accepting general users

22-ID-D • SER-CAT • Life sciences • Macromolecular crystallography, multi-wavelength anomalous dispersion, single-wavelength anomalous dispersion, microbeam • 6-20 keV • On-site, remote • Accepting general users

23-BM-B • National Institute of General Medical Sciences and National Cancer Institute (GM/CA-XSD) • Life Sciences • Macromolecular crystallography • 12.5-12.75 keV • On-site • Accepting general users

23-ID-B • GM/CA-XSD • Life sciences • Macromolecular crystallography, microbeam, large unit cell crystallography, subatomic (<0.85 Å) resolution, multi-wavelength anomalous dispersion, single-wavelength anomalous dispersion • 3.5-20 keV • On-site, remote • Accepting general users

23-ID-D • GM/CA-XSD • Life sciences • Macromolecular crystallography, microbeam, large unit cell crystallography, subatomic (<0.85 Å) resolution, multi-wavelength anomalous dispersion, single-wavelength anomalous dispersion • 5-20 keV • On-site, remote • Accepting general users

24-ID-C • Northeastern (NE)-CAT • Life sciences • Macromolecular crystallography, microdiffraction, single-wavelength anomalous dispersion, single-crystal diffraction, microbeam, multi-wavelength anomalous dispersion, subatomic (<0.85 Å) resolution • 6.5-20 keV • On-site, remote • Accepting general users

24-ID-E • NE-CAT • Life sciences • Macromolecular crystallography, microbeam, microdiffraction, single-wavelength anomalous dispersion, single-crystal diffraction • 12.68 keV • On-site, remote • Accepting general users

26-ID-C • Center for Nanoscale Materials (CNM)/XSD • Physics, materials science • Nanodiffraction, nano-imaging, coherent x-ray scattering • 6-12 keV • On-site • Accepting general users

27-ID-B • XSD • Physics • Resonant inelastic x-ray scattering • 5-14 keV, 5-30 keV • On-site • Accepting general users

29-ID-C,D • XSD • Physics, materials science • Resonant soft x-ray scattering, angle-resolved photoemission spectroscopy • 250-2200 eV, 2200-3000 eV • On-site • Accepting general users

30-ID-B,C • XSD • Physics, materials science • Inelastic x-ray scattering • 23.7-23.9 keV • On-site • Accepting general users

31-ID-D • Lily Research Laboratories (LRL)-CAT • Life sciences • Macromolecular crystallography, single-wavelength anomalous dispersion • 9-13.5 keV • Mail-in • Accepting general users

32-ID-B,C • XSD • Materials science, life sciences, geoscience • Phase contrast imaging, radiography, transmission x-ray microscopy, tomography • 7-40 keV • On-site • Accepting general users

33-BM-C • XSD • Materials science, physics, chemistry • Diffuse x-ray scattering, general diffraction, powder diffraction, x-ray reflectivity, grazing incidence diffraction, anomalous and resonant scattering (hard x-ray) • 5-35 keV • On-site • Accepting general users

33-ID-D,E • XSD • Materials science, physics, chemistry, environmental science • Anomalous and resonant scattering (hard x-ray), diffuse x-ray scattering, general diffraction, surface diffraction, surface diffraction (UHV), x-ray reflectivity • 4-40 keV, 6-25 keV • On-site • Accepting general users

34-ID-C • XSD • Materials science, physics • Coherent x-ray scattering • 5-15 keV • On-site • Accepting general users

34-ID-E • XSD • Materials science, physics, environmental science, geo science • Microdiffraction, Laue crystallography, microbeam, microfluorescence (hard x-ray) • 7-30 keV • On-site • Accepting general users

35-ID-B,C,D,E • Dynamic Compression Sector (DCS) • Physics, materials science, geoscience • Time-resolved x-ray scattering, phase contrast imaging, radiography • 7-35 keV, 7-100 keV, 24-24 keV • On-site • Accepting general users

APS Upgrade Achieves CD-2 Approval from the DOE

On December 12, 2018, the U.S. Department of Energy issued a Critical-Decision-2 approving the technical scope, cost estimate, and plan of work for an upgrade of the Advanced Photon Source.

The Advanced Photon Source Upgrade (APS-U) will provide a new, world-class platform to deliver breakthrough science across a wide array of disciplines and industries. By using transformative next-generation technology, the multibend achromat lattice, to deliver x-rays that are between 100 and 1000 times brighter than today's top synchrotron facilities, the new facility will open scientific frontiers that are completely inaccessible today, allowing researchers to probe and manipulate matter at the atomic level, in three dimensions. Furthermore, the project will assure continued U.S. leadership in x-ray science for decades to come. Already, the APS is one of the busiest scientific facilities in the national laboratory network, serving more than 5700 researchers a year. The upgraded facility will increase the brightness and focus of the x-rays by orders of magnitude, creating new opportunities for scientific discovery for researchers across disciplines. Studies at the APS have led to two Nobel Prizes, numerous pharmaceutical drugs (including the first drug to treat HIV), improved processes for oil extraction from shale, and new insights into additive manufacturing. The new machine will enable scientific discovery and technological innovation across a wide range of diverse disciplines, providing unprecedented access to the inner workings of matter and transforming our ability to understand and manipulate systems and materials at the nanoscale.

A vital component of the APS-U are the new and upgraded beamlines. The new beamlines for the APS-U are:

• **Polar: The Polarization Modulation Spectroscopy Beamline** enables studies of materials at the mesoscale to detect electronic/magnetic differences by means of tuning and controlling competing ground states under extreme high-pressure conditions (in the megabar range). Brilliant, polarized beams open remarkable opportunities for discovery of new phases and furthering our understanding of quantum matter.

• **The PtychoProbe Beamline** realizes the highest possible spatial-resolution x-ray microscopy for structural and chemical information, with a goal of focusing an x-ray beam to a 5-nm spot and the capability of ultra-fast scanning of the beam across the sample being studied. Scientists have unprecedented capabilities to accelerate the discovery of complex materials and establish the APS as the go-to place for hard x-ray, high-resolution microscopy.

• **The 3D Micro and Nano Diffraction Beamline** attacks many problems in materials science, physics, geoscience. The new APS will provide small, intense x-ray spots (between 50 and 200 nm) to investigate spatial variations and correlations of strain and structure that define a wide range of scientifically and technologically important materials.

• **The ATOMIC Beamline** uses the enhanced coherence of the APS-U x-ray beam for high-resolution studies of the structural, chemical, and physical properties exhibited by advanced functional materials. There is a strong need for a single technique that can acquire atomistic structural information across many length scales in full three-dimensional detail. Coherent diffractive imaging at ATOMIC combines that capability with *in situ* and *operando* environmental cells for transformative impact on many scientific disciplines.

• **The CHEX Beamlines** use coherent x-ray techniques to advance the frontier for *in situ*, real-time studies of advanced materials synthesis and chemical transformations in natural operating environments, employing condensed-matter physics and environmental science. This research promises breakthroughs in discovering, developing, and understanding the materials and processes needed to address global challenges in energy, environment, health, and security.

• **The High-Energy X-ray Microscope Beamline** investigates structure and evolution within bulk materials, often in extreme environments, with the high-energy x-ray scattering techniques and novel coherence-based techniques enabled by the APS-U. Materials subjected to these techniques are of relevance to a large range of subjects, including mechanical engineering, biophysics, irradiation/nuclear energy, energy storage, and advanced manufacturing.

• **The In Situ Nanoprobe Beamline** is designed for a relatively large optical working distance. This enables investigation of complex functional materials and materials systems such as catalysts, batteries, photovoltaic systems, and nanoscale Earth and environmental samples during synthesis, operation, and under actual environmental conditions. The beamline is designed to study these systems across many lengths scales, in two and three dimensions under *in situ* conditions.

• **The X-ray Photon Correlation Spectroscopy Beamlines** advance studies in key areas in physics and materials science and engineering, including dynamic heterogeneity, structural dynamics in super-cooled liquids, and fluctuations associated with competing mesoscale interactions in emergent materials. Correlation techniques are sensitive to the square of the brilliance of the photons, so the more than 100x increase in APS-U brilliance will lead to a more than 10,000x increase for this technique. The beamline enables dynamics-related studies in areas as diverse as *in situ* rheometry, nano-fluidic flow, and high pressure, and advances potential applications in an array of technologies, from energy and transportation to health, agriculture, and national defense.

• **The Coherent Surface-Scattering Imaging Beamline** is ideal for probing and understanding mesoscopic space-time correlations by combining a surface x-ray probe with state-of-the-art x-ray optics and detectors to study a range of materials surface and interface phenomena. These include the evolution of biological membranes and complex molecules in aqueous environments; thin-film and quantum-dot growth at surfaces and interfaces; assembly of polymer nanocomposites; and structural analysis of three-dimensional, nanoscaled electronic circuits using additive manufacturing.

Electronic & Magnetic Materials

Pinning the Bits

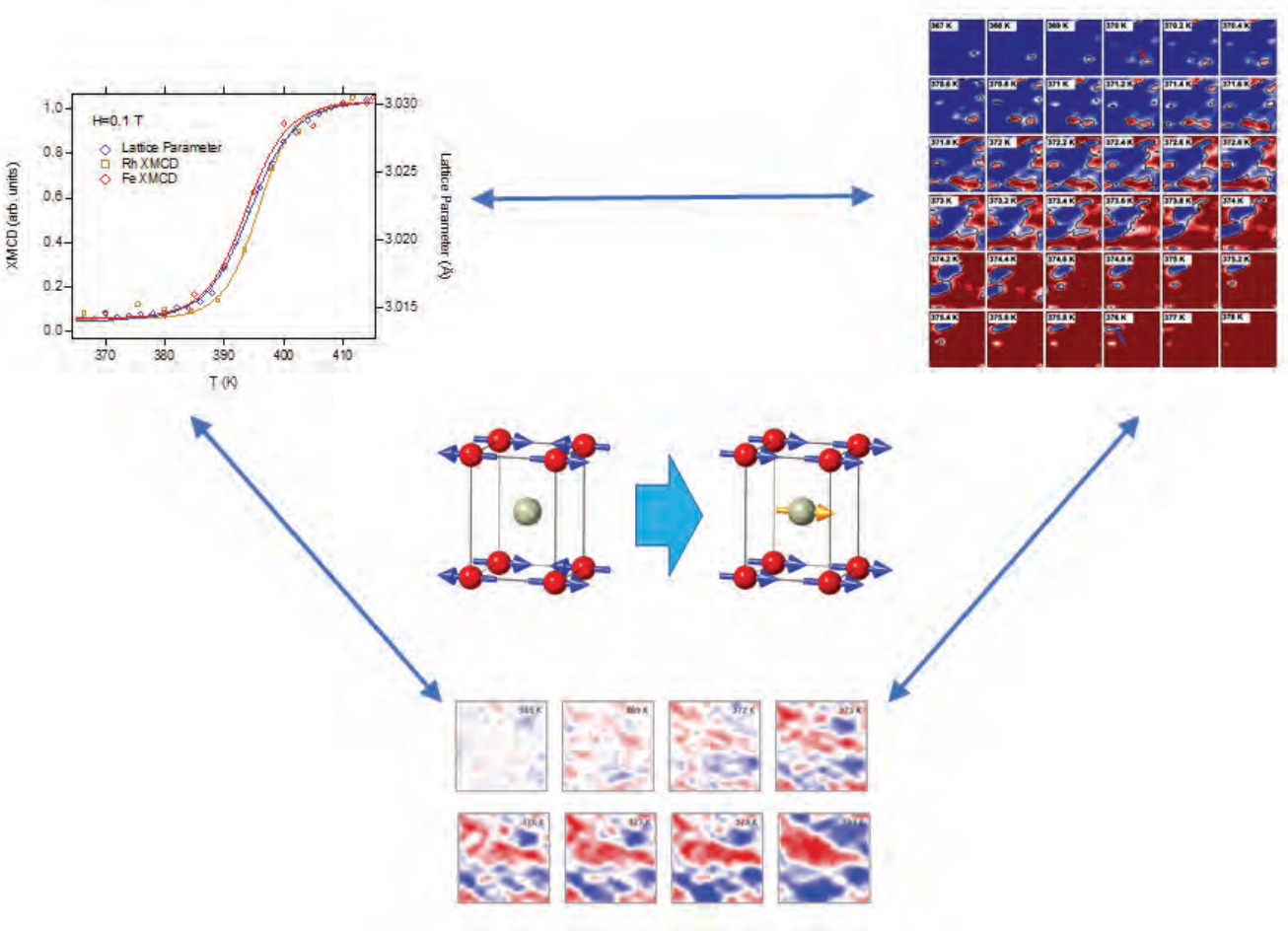

Fig. 1. The ordered alloy FeRh undergoes a structural and magnetic phase transition (shown in center image) in which the lattice parameter expands and the Rh atoms (gold spheres) acquire a magnetic moment, and the Fe atoms (red spheres) reorient their moments from antiferromagnetic to ferromagnetic order as the temperature is increased through 375 K. The structural transition (upper right) appears by the nucleation of islands that grow and eventually coalesce into a uniform phase. The growth of these islands is inhibited by the surrounding untransformed material in the kinetic arrest process, resulting in a behavior that mimics a 2nd-order phase transition. The magnetic transition (lower image) follows this behavior. In spectroscopy measurements done with common thermometry (upper left) it is shown that the structural transition and the development of Rh and Fe moments are coincident.

A team of researchers utilized a combination of high-resolution structural imaging, magnetic domain imaging, and dichroic spectroscopy on three separate x-ray beamlines at the APS to shed light on coupled structural and magnetic phase transitions. Through this combination of three individually powerful x-ray techniques, the team was able to provide added insights into the phase transition process and the nature of the coupling between the magnetic and structural order.

As information storage applications demand higher and higher bit densities, conventional magnetic storage media and memory devices become plagued by superparamagnetic behavior, which causes magnetic bits to flop about as they become smaller, resulting in a loss of the data stored in the bits. In order to keep pushing bit densities higher, a way must be found to stabilize, or pin, these bits when they are quiescent, but still allow them to be written easily.

One promising way around this problem is heat-assisted magnetic recording, in which ferromagnetic bits are coupled to an underlying antiferromagnetic layer to provide a preferred magnetic orientation, or pinning effect. Then, the structure is heated using a fast laser pulse to allow the magnetic orientation to be reset. However, the utility of this heat assisted magnetic storage approach depends on there being a fast and reliably controllable phase transition that can act as a switch for the pinning effect, and a complete understanding of how the pinning material proceeds from one phase to another.

The 50/50 alloy FeRh is an excellent candidate for use as the pinning layer in this type of memory device, since it has a phase transition from its normal antiferromagnetic state to a higher temperature ferromagnetic state at about 375 K. This magnetic transition is also coupled with a structural transition in which the lattice parameter changes by approximately 1%. The nearness of this transition to room temperature, as well as the fact that the transition temperature can be tuned by application of a magnetic field, makes FeRh very attractive for use in heat assisted recording. This material also offers a unique window into how the structure and magnetism can be intertwined in phase transitions, with implications for other types of coupled phenomena.

First, the team from Argonne, the University of California, San Diego, and the University of South Florida used the Hard X-ray Nanoprobe at the XSD/CNM 26-ID-C beamline at the APS to map the lattice parameter of crystallizing films of FeRh with 30-nm spatial resolution as the films were heated and cooled through the transition. They found that the higher-temperature ferromagnetic phase appears in tiny islands whose growth is then inhibited by the surrounding antiferromagnetic phase, a phenomenon known as “kinetic arrest.” In fact, they found that the island size follows a 2nd-order-like behavior instead of the 1st order that was expected.

Using x-ray photoemission electron microscopy (X-PEEM) at XSD beamline 4-ID-C, the researchers showed that the magnetic domain development followed that of the structure, with a similar island nucleation and growth behavior.

Finally, using x-ray magnetic circular dichroism spectroscopy and diffraction with common thermometry at XSD beamline 4-ID-D, the researchers examined how the magnetic moments in the Fe and Rh atoms develop along with the structure. They found that the magnetic and structural transitions are almost coincident in temperature (Fig. 1).

The information from these three powerful techniques combines to give a greater insight into the phase transition process, which is crucial for understanding how to use the transition in storage applications. The team showed that the transition is dominated by defect-driven nucleation and kinetic arrest. These results will help in the development of high density data storage devices using FeRh alloy and similar materials with coupled phase transitions. — David Keavney

See: David J. Keavney[1]*, Yongseong Choi[1], Martin V. Holt[1], Vojtech Uhlíř[2], Dario Arena[3], Eric E. Fullerton[2], Philip J. Ryan[1], and Jong-Woo Kim[1], “Phase Coexistence and Kinetic Arrest in the Magnetostructural Transition of the Ordered Alloy FeRh,” Sci. Rep. **8**, 1778 (2018). DOI: 10.1038/s41598-018-20101-0
Author affiliations: [1]Argonne National Laboratory, [2]University of California, San Diego, [3]University of South Florida
Correspondence: * keavney@aps.anl.gov

Work at the University of California, San Diego, was supported by U.S. Department of Energy (DOE)-Basic Energy Sciences Grant Number DE-SC0003678. Work at Argonne and use of the Advanced Photon Source, a U.S. DOE Office of Science User Facility operated for the DOE Office of Science by Argonne National Laboratory, was supported by Contract No. DE-AC02- 06CH11357.

Sensing Electric Fields under the Sea

The marine environment can be tough on materials, with water and salt working together to corrode them over time. This presents an enormous challenge for developing technologies for energy, ocean monitoring, and biological applications that will maintain their functionality under this assault. Another potential application in the marine environment is sensing; being able to respond to mild stimuli, such as electric fields, could be a boon for monitoring man-made and natural phenomena. In a new study, a team of researchers working at the APS and the Canadian Light Source report a material that can survive a harsh marine environment while also sensing electric fields. The material, samarium nickelate ($SmNiO_3$, or SNO) (which has already been investigated as an electrolyte in solid-state fuel cells, a pH sensor, and a temperature-sensitive electrical resistor) showed excellent stability in aqueous salt solutions. Further investigation showed that this material also responds to negative electrical potentials as low as millivolts by increasing its resistance, a phenomenon that occurs due to protons from the water intercalating into the SNO structure. The structure also becomes more transparent under negative potentials, allowing for a concurrent optical readout. By applying an opposing potential, these changes reverse, allowing this material to be reused again and again. The authors suggest that these characteristics make SNO an outstanding material for a variety of marine applications.

The researchers from Purdue University, Argonne, Rutgers University, the National Institute of Standards and Technology, the Massachusetts Institute of Technology, the University of Saskatchewan (Canada), Columbia University, and the University of Massachusetts started their characterization of SNO thin films by submerging them in a salt solution over a range of acidities. This material maintained its ability to change its electrical resistance in response to temperature and showed no signs of corrosion, suggesting its stability under these conditions.

After applying a negative electrical potential up to –4.0 V, the resistivity of the SNO films increased by more than 5 orders of magnitude. This change occurred regardless of the solution tested (whether it included basic potassium hydroxide, citric acid, or table salt NaCl), or the substrate used for the SNO film. Atomic force microscopy images further confirmed the stability of the film and rule out corrosion as a cause for the change in resistance.

By applying a reverse bias, the researchers were able to return the SNO films to their conducting state. The electrical resistivity of this material changed stably over multiple cycles and over a range of applied voltages, extending from those matching bioelectric potentials generated by numerous marine species to galvanic potentials from ships and unmanned underwater vehicles.

X-ray reflectivity measurements taken using the XSD 12-ID-D beamline at the APS showed that during the application of negative potentials, the SNO films' thickness increased substantially. Further investigation utilizing neutron scattering, which is sensitive to hydrogen species, suggested that protons from the hydrogen in water were entering the SNO and intercalating in its structure. Furthermore, x-ray absorption spectroscopy, which took place at the Canadian Light Source 10-ID-2 beamline, suggested that these added protons necessitated the addition of extra electrons in SNO to balance out the charge. Finally, optical spectra measurements showed that negative electric potentials increase the transparency of this material.

Each of these phenomena matched what the researchers saw in molecular dynamics simulations, a type of computer modeling technique for better understanding molecular interactions, further confirming what they observed in their experiments.

The researchers suggest that SNO seems to work like the ampullae of Lorenzini, an organ in sharks, rays, and skates that provides a "sixth sense" to detect the electrical signals generated by prey (Fig. 1). This organ also takes up protons under an electric bias, which are sensed by cells that in turn release neurotransmitters to the brain. They note that detection distance and response time of SNO and this organ are similar as well.

The authors suggest that this unusual material could offer a new and useful way to monitor electrical signals generated in marine environments, such as those from maritime vessels or sea creatures. — Christen Brownlee

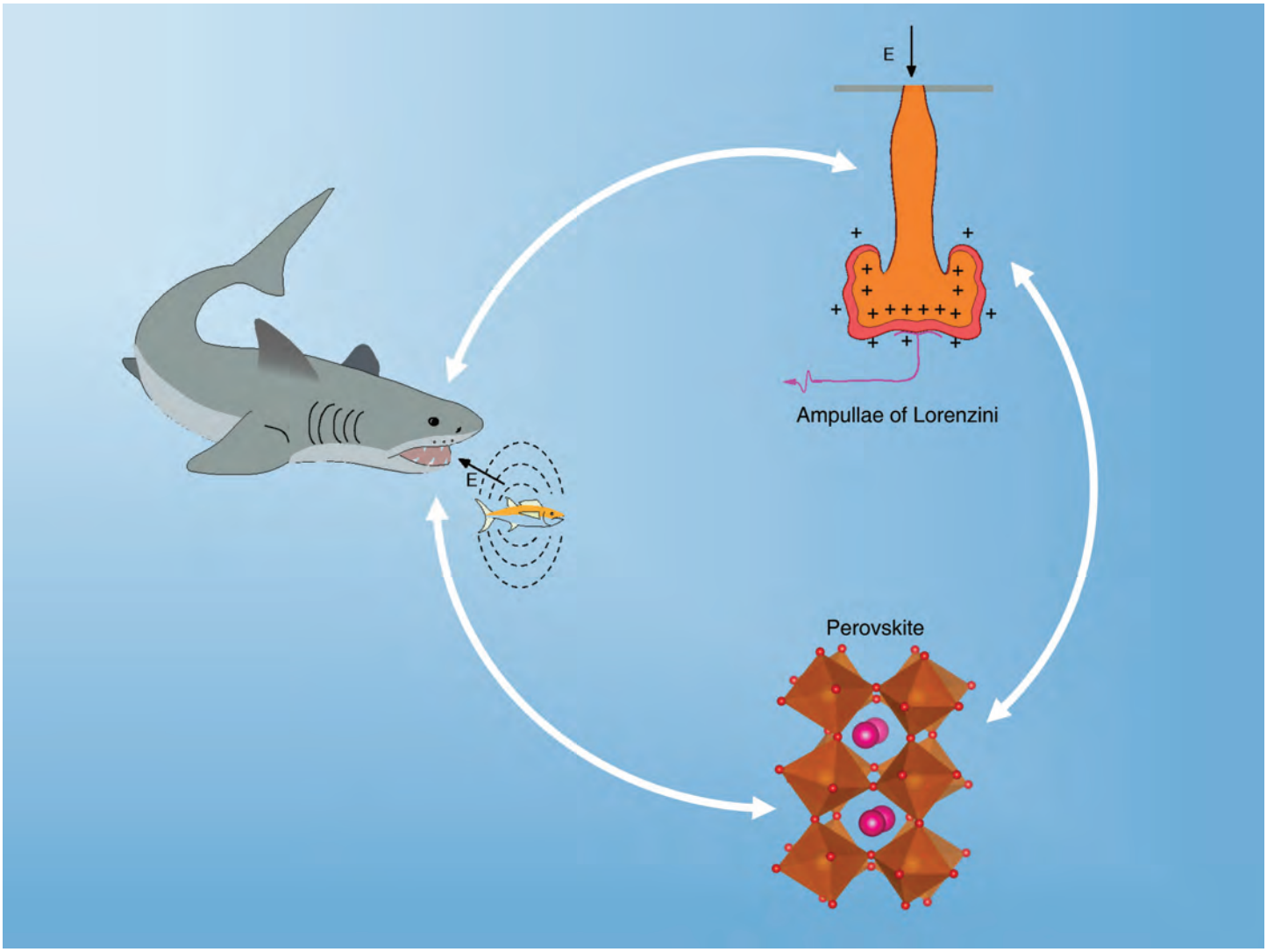

Fig. 1. Perovksite nickelates can closely mimic the function of ampullae of Lorenzinin organ in sharks. Similar to the ampullae, the perovskite can incorporate protons into the lattice under an electric field and change the resistance that can be read out.

See: Zhen Zhang[1], Derek Schwanz[1], Badri Narayanan[2], Michele Kotiuga[3], Joseph A. Dura[4], Mathew Cherukara[2], Hua Zhou[2], John W. Freeland[2], Jiarui Li[6], Ronny Sutarto[7], Feizhou He[6], Chongzhao Wu[8], Jiaxin Zhu[8], Yifei Sun[1], Koushik Ramadoss[1], Stephen S. Nonnenmann[9], Nanfang Yu[7], Riccardo Comin[5], Karin M. Rabe[3], Subramanian K.R.S. Sankaranarayanan[2], and Shriram Ramanathan[1]*, "Perovskite nickelates as electric-field sensors in salt water," Nature **553**, 68 (4 January 2018).
DOI: 10.1038/nature25008
Author affiliations: [1]Purdue University, [2]Argonne National Laboratory, [3]Rutgers University, [4]National Institute of Standards and Technology, [5]Massachusetts Institute of Technology, [6]University of Saskatchewan, [7]Columbia University, [8]University of Massachusetts-Amherst
Correspondence: * shriram@purdue.edu

The authors acknowledge financial support from the Army Research Office (W911NF-16-1-0289, W911NF-16-1-0042), the U.S. National Science Foundation (DMR-1609898, DMR-1610215), the Defense Advanced Research Projects Agency (grant D15AP00111), the Office of Naval Research (grants N00014-16-1-2442 and N00014-12-1040), and the Air Force Office of Scientific Research (grants FA9550-16-1-0159 and FA9550-14-1-0389). Use of the Center for Nanoscale Materials, an Office of Science user facility, was supported by the U.S. Department of Energy (DOE) Office of Science-Basic Energy Sciences under contract number DE-AC02-06CH11357. This research used resources of the National Energy Research Scientific Computing Center, which is supported by the Office of Science of the US DOE under contract number DE-AC02-05CH11231. An award of computer time was provided by the Innovative and Novel Computational Impact on Theory and Experiment (INCITE) programme. This research used resources of the Argonne Leadership Computing Facility at Argonne National Laboratory, which is supported by the Office of Science of the U.S. DOE under contract DE-AC02-06CH11357. S.S.N. acknowledges support from the University of Massachusetts-Amherst through start-up funding. Part of the research described in this paper was performed at the Canadian Light Source, which is supported by the Canada Foundation for Innovation, Natural Sciences and Engineering Research Council of Canada, the University of Saskatchewan, the Government of Saskatchewan, Western Economic Diversification Canada, the National Research Council Canada and the Canadian Institutes of Health Research. This research used resources of the Advanced Photon Source, a U.S. DOE Office of Science User Facility operated by Argonne National Laboratory under contract number DE-AC02-06CH11357.

Pyrochlores' Motions Solve Longstanding Mysteries

The large family of materials known as pyrochlores play a key role in applications in a variety of different fields, including catalysis, ferroelectricity, luminescence, magnetism, and nuclear waste storage. These materials have crystal structures in which two positively charged ions, which tend to be rare-earth or transition metal species, are interspersed with oxygen atoms in a corner-sharing tetrahedral arrangement. As with other materials, the structure of pyrochlores dictates their function. However, unlike many other materials, the function of pyrochlores has been shown to be extremely sensitive to minute variations in their stoichiometry, or the relative quantities of the different atoms that make up these materials. Additionally, based on pyrochlores' known structures, researchers have speculated that they should operate as ferroelectrics, or materials that have a spontaneous electric polarization that can be reversed by the application of an external electric field. Instead, these materials behave almost universally as dielectrics, electrical insulators without a permanent electric polarization, but can be polarized by an applied electrical field. To better understand these unusual attributes, a team of researchers took a closer look at the motion of the structures' corner-sharing tetrahedral, in part using the U.S. DOE's APS and Spallation Neutron Source (SNS). They found a previously undiscovered flexibility in the corners of these tetrahedra. When these corners flex and bend, it changes the expected chemical nature of these materials. This discovery helps explain some of the longstanding mysteries of these materials.

The researchers from the National Institute of Standards and Technology, Johns Hopkins University, the SuperSTEM Laboratory (UK), the University of Leeds (UK), Forschungszentrum Jülich GmbH (Germany), the University of Tokyo (Japan), and Osaka University (Japan) focused their investigation on two different pyrochlores: $Pr_2Zr_2O_7$ (PZO) and $Yb_2Ti_2O_7$ (YTO). They first employed electron diffraction to determine and analyze the crystal structure of these materials. In addition to sharp spots showing the fixed positions of atoms, the team observed diffuse lines of scattering back and forth across these structures, suggesting that the crystals' tetrahedra were displaced from their ideal positions.

To better understand this phenomenon, the researchers performed diffraction experiments utilizing the high-resolution diffractometers at the XSD 11-BM-B (for synchrotron powder x-ray diffraction) and 11-ID-B (for room-temperature x-ray pair distribution) x-ray beamlines at the APS. They carried out room-temperature time-of-flight neutron diffraction studies with the POWGEN powder diffractometer and neutron pair distribution studies with the NOMAD diffractometer, both at the Oak Ridge National Laboratory's SNS.

X-rays and neutrons tend to scatter differently from different types of atoms, but by combining the scattering data from both types of experiments, the researchers were able to get a more complete picture of each material's structure. Using this data, the researchers were able to measure the distance between atoms in PZO and YTO's crystal lattices. In materials with an ideal structure, the distance between certain atoms should be the same. However, the researchers found that these distances varied, again suggesting motion within the crystal structure.

A fourth technique, nuclear quadrupole resonance, further confirmed that the tetrahedral were flexing and bending back and forth.

To get a sense of the time scale of this motion, the researchers employed electron energy loss spectroscopy, along with high-resolution transmission electron microscopy, to identify both the position and type of atoms. Transmission electron microscopy images suggested that PZO and YTO are static on the scale of hours. However, other data suggest they fluctuate with time, at least in some samples. Other data on related pyrochlores confirm that this timescale also varies.

This inherent motion within the crystal structures of

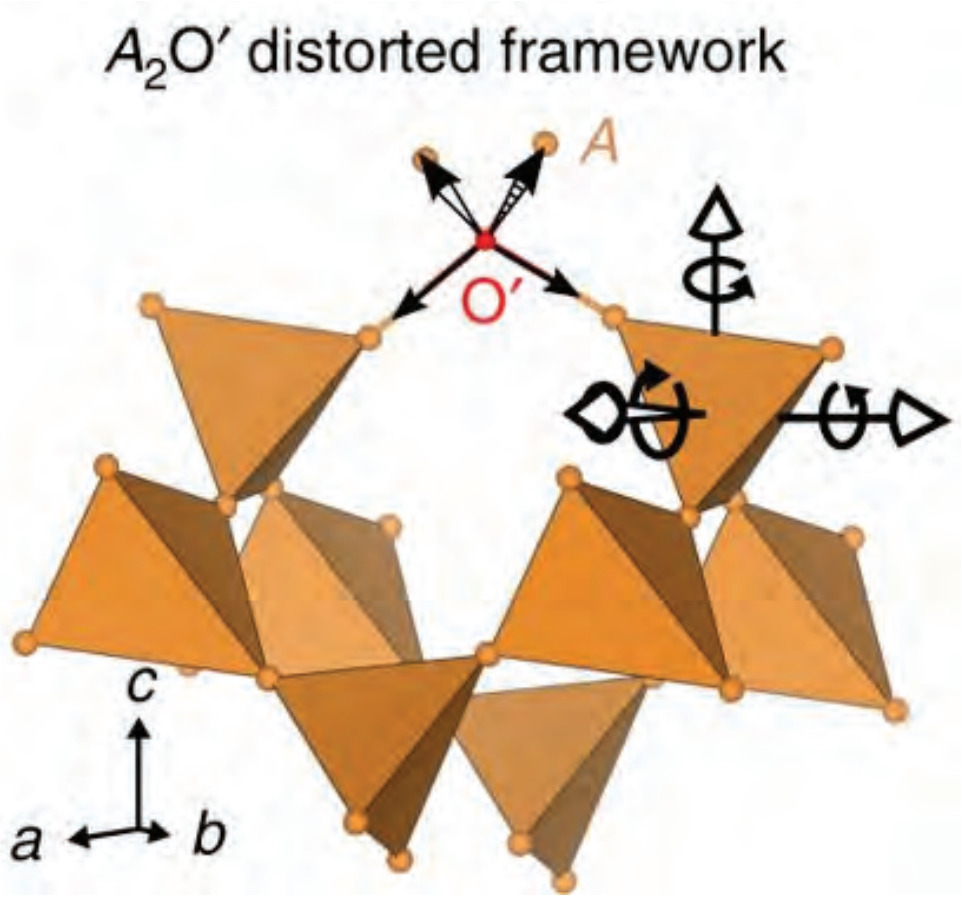

Fig. 1. The ubiquitous pyrochlore structure type harbors universal flexing due to corner-sharing topology, profoundly impacting the physics and chemistry of these materials. Adapted from B.A. Trump et al., Nat. Commun. **9**, 2619 (2018).

these materials explains why they don't display the ferromagnetic behavior that would be expected of materials with a similar static structure, the authors say. Because the tetrahedra are constantly flexing, the charges within these materials can't line up in a permanent way, leading to dielectric behavior instead.

The authors add that these findings also explain the longstanding question of why these materials are so sensitive to stoichiometry. Small changes within the chemical makeup of pyrochlores can dramatically change how flexible their tetrahedra are, significantly affecting their chemical properties. — Christen Brownlee

See: B.A. Trump[1,2], S.M. Koohpayeh[2], K.J.T. Livi[2], J.-J. Wen[2], K.E. Arpino[2], Q.M. Ramasse[3], R. Brydson[4], M. Feygenson[5], H. Takeda[6], M. Takigawa[6], K. Kimura[7], S. Nakatsuji[6], C.L. Broholm[2], and T.M. McQueen[2], "Universal geometric frustration in pyrochlores," Nat. Commun. **9**, 2619 (2018). DOI: 10.1038/s41467-018-05033-7

Author affiliations: [1]National Institute of Standards and Technology, [2]Johns Hopkins University, [3]SuperSTEM Laboratory, [4]University of Leeds, [5]Forschungszentrum Jülich GmbH, [6]University of Tokyo, [7]Osaka University
Correspondence: * mcqueen@jhu.edu

The work at IQM was supported by the U.S. Department of Energy (DOE) Office of Science-Basic Energy Sciences, Division of Materials Sciences and Engineering under grant DE-FG02-08ER46544. Use of ORNL's Spallation Neutron Source was sponsored by the Scientific User Facilities Division-Basic Energy Sciences, U.S. DOE. This work was also partly supported by the David and Lucile Packard Foundation and the Johns Hopkins University Catalyst Fund.

This research used resources of the Advanced Photon Source, a U.S. DOE Office of Basic Energy Sciences and Office of Science User Facility, operated for the DOE Office of Science by Argonne National Laboratory under contract no. DE-AC02-06CH11357.

Material Changes Hint at Superconductivity

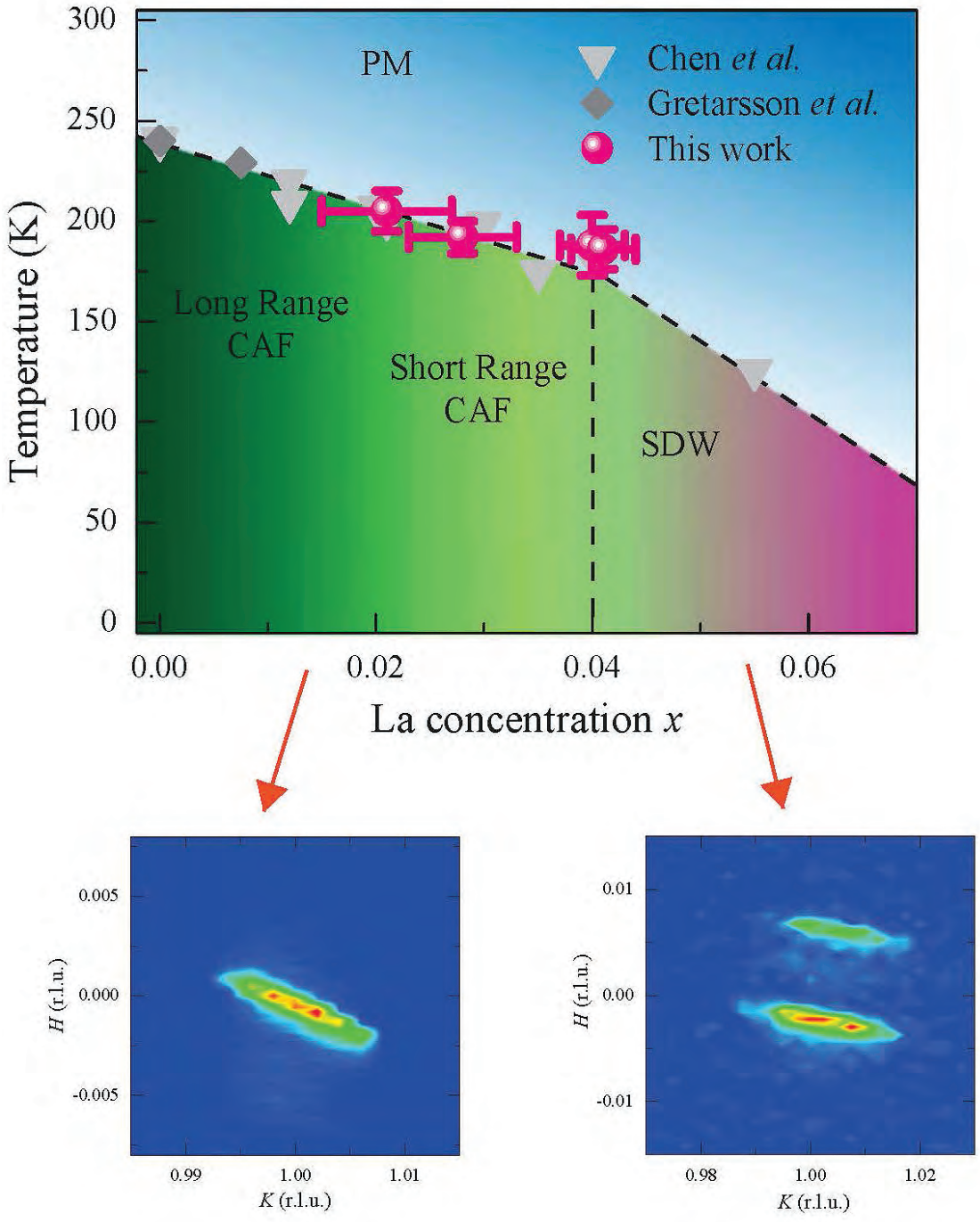

Fig. 1. As the concentration of lanthanum in the material Sr_2IrO_4 increases (top, left to right), the low-temperature magnetic ground state evolves from long-range, short-ranged canted antiferromagnetic (CAF) to spin density wave (SDW). The different magnetic states are identifiable by changes in the scattered pattern from resonant x-ray scattering on the samples below and above the critical doping (bottom, left and right).

Cooling certain materials down to the temperature of liquid helium turns them superconducting, making them able to pass current with no power loss. Scientists would like to realize the same property at room temperature, but so far have not achieved that goal. They have, however, found so-called high-temperature (high-T_c) superconductors that work above the temperature of liquid nitrogen. One group of researchers utilized the APS to study a material in order to explore its potential to be such a superconductor, possibly paving the way to further advances.

It is expensive to cool materials down to liquid helium levels at 4 K. Temperatures above liquid nitrogen, at 77 K, are less difficult to work with. Certain copper-based compounds, known as cuprates, can be made into high-T_c superconductors; one such is lanthanum copper oxide (La_2CuO_4). In its normal state, it is an insulator, blocking the flow of current. But increase the number of electrons in the material by enough, and suddenly it becomes a superconductor.

The researchers in this study, from Boston College and the University of California, Santa Barbara, decided to examine strontium iridium oxide (Sr_2IrO_4), which is also a Mott insulator. In Mott insulators, electrons are strongly correlated, so each affects the state of the others. The electronic and magnetic structures of Sr_2IrO_4 resemble those of La_2CuO_4, and both have spin-orbit coupling. Spin is a quantum mechanical property of electrons, which can be thought of as a spinning bar magnet. In spin-orbit coupling, the direction of that spin matches the direction of the electron's orbit around the nucleus.

The only problem is that, for reasons not fully understood, it is not possible to put enough electrons into Sr_2IrO_4 for the insulating state to disappear. But scientists have found that, when they add charge carriers to La_2CuO_4, its pattern of magnetic order changes in very particular ways as it approaches the superconducting state. The researchers thought that if they could show the same pattern of changes as they doped Sr_2IrO_4, it would be theoretically possible to turn it into a superconductor, too, if only they had a way to add enough electrons.

They added electrons to the material by replacing strontium atoms with lanthanum atoms. As they expected, the magnetic order in the material began to evolve in a way similar to that of La_2CuO_4. Though the result is not conclusive, it hints that Sr_2IrO_4 would become superconducting if it were is possible to replace more strontium atoms.

To measure the magnetic order, the researchers and colleagues from Argonne and Cornell University performed resonant elastic x-ray scattering experiments at the XSD 6-ID-B x-ray beamline at the APS and at the A2 and C1 beamlines at the Cornell High Energy Synchrotron Source, respectively, utilizing samples with different levels of lanthanum. The technique requires synchrotron radiation to be tuned to the resonance frequency of an element in the sample, in this case the iridium. It amplifies x-ray scattering that otherwise would be hard to see, and the scattering carries information about the magnetic state of the material.

There is not an agreed upon theoretical model for what makes a material a high-T_c superconductor. Without one, most new classes of high-T_c superconductors have been discovered more or less by accident. This work shows that there are similarities between the electronic structures of the two materials, which suggests there should be some common model that describes both. If physicists can find an accurate model, they should be able to predict other high-T_c superconductors, perhaps some that work at even higher temperatures than those currently known. — Neil Savage

See: Xiang Chen[1,2], Julian L. Schmehr[2], Zahirul Islam[3], Zach Porter[1], Eli Zoghlin[2], Kenneth Finkelstein[4], Jacob P.C. Ruff[4], and Stephen D. Wilson[2], "Unidirectional spin density wave state in metallic $(Sr_{1-x}Lax)_2IrO_4$", Nat. Commun. **9**, 103 (2018).
DOI: 10.1038/s41467-017-02647-1
Author affiliations: [1]Boston College, [2]University of California, Santa Barbara, [3]Argonne National Laboratory, [4]Cornell University
Correspondence: * stephendwilson@ucsb.edu

This work was supported by NSF Award No. DMR-1505549 (X.C. and S.D.W). Additional support was provided by ARO Award W911NF-16-1-0361 (J.S., E.Z., and Z.P.). This work is based upon research conducted at CHESS, which is supported by the U.S. National Science Foundation (NSF) and the National Institutes of Health/National Institute of General Medical Sciences under NSF award DMR-1332208. This research used resources of the Advanced Photon Source, a U.S. Department of Energy (DOE) Office of Science User Facility operated for the DOE Office of Science by Argonne National Laboratory under Contract No. DE-AC02-06CH11357.

An Elusive Magnetic Ordering in an Iron-Based, High-Temperature Superconductor

A select group of iron (Fe) compounds exhibits an unconventional type of high-temperature superconductivity. This superconducting behavior appears to be intimately connected to the unique magnetic ordering within these Fe compounds, which was previously only known to consist of two distinct types: stripe-type spin-density wave (SSDW) and spin-charge-density wave (SCDW). Nevertheless, theoretical considerations indicated the possibility of a third type of magnetic ordering: A new structural variant of the iron-based superconductors, or FeSCs, seemed to offer the potential for manifesting the elusive third type of magnetic pattern, known as spin-vortex crystal (SVC) ordering. A research team probed this new compound using several techniques, including high-energy x-ray diffraction performed at the APS. By analyzing the data from the various experimental methods, the scientists were able to deduce the presence of SVC ordering. The confirmation of this elusive magnetic ordering provides additional clues to the strong relationship between structure, magnetism, and superconductivity within the FeSCs. In turn, these new insights should aid in the ongoing effort to develop practical, high-temperature superconducting materials.

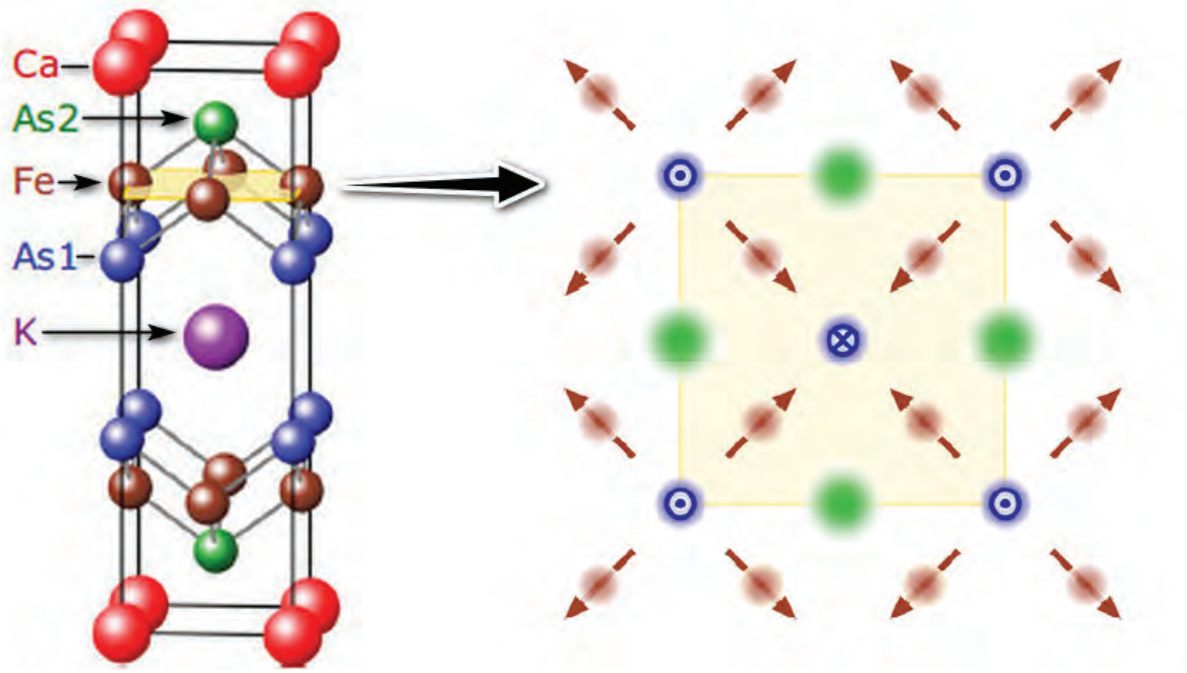

Fig. 1. Left-hand side depicts the chemical structure of the layered iron compound. The elements in the $CaKFe_4As_4$ compound are indicated by their chemical symbols. The iron atoms all lie in the same layer, highlighted for clarity. Note that two distinct layers of arsenic atoms, indicated using different colors and labeled “As1” and “As2”, reside below and above the iron layer. This asymmetric positioning is crucial to the compound’s unique magnetic ordering. Right-hand side shows the spin-vortex crystal (SVC) ordering that arises within the layer of iron atoms, whose magnetic moments (brown arrows) all point either toward or away from the arsenic atoms of the As1 layer (blue circles).

Superconductivity, which is characterized by the complete disappearance of electrical resistance, was discovered in 1911. In the decades that followed, many elements and compounds were shown to be superconducting. However, these materials generally required extremely low temperatures of 30 K or less to support superconductivity, which was typically achieved by submersion in liquid helium. The situation changed dramatically in 1986 when the first high-temperature superconductor was demonstrated, in the form of a cuprate (copper-bearing) ceramic compound. Over the years other superconducting cuprate compounds have been developed, including many that super-conduct at liquid-nitrogen temperatures (above 77 K). This development has greatly expanded the potential range of applications for superconductors.

Then in 2006, scientists discovered a new class of high-temperature superconductors containing iron and other elements. In these iron-based compounds, magnetic ordering appears to go hand-in-hand with their superconductivity. The most common type of magnetic ordering in these superconductors is the SSDW. As the name implies, stripe-type ordering occurs as parallel stripes, or rows, of magnetic moments of the iron atoms (which are analogous to tiny bar magnets). A less common magnetic pattern in these compounds is SCDW ordering. Materials scientists can manipulate the magnetic ordering within the superconducting iron layer by applying pressure to them, and/or by doping them, which entails adding small amounts of impurities. Adjusting the magnetic ordering within these compounds allows scientists to tune their superconducting properties.

In the quest to observe the potential third type of magnetic order in iron high-temperature superconductors, the researchers in this study from Iowa State University, Goethe University Frankfurt am Main (Germany), the University of Tennessee, Knoxville, Oak Ridge National Laboratory, and the University of Minnesota turned to a compound they suspected might support it. Besides iron, their compound contains calcium (Ca), potassium (K), and arsenic (As) combined in the chemical ratio $CaKFe_4As_4$. This compound forms a layered crystalline structure, as depicted on the left-hand side of Fig. 1.

The researchers produced samples of this compound doped with nickel and cobalt, which replaced a few of the compound's iron atoms and contributed additional electrons to the crystal. Following doping and other processing, the researchers needed to establish that the overall crystalline structure had not been distorted. This was confirmed via high-energy x-ray diffraction measurements performed utilizing the six-circle diffractometer at the XSD 6-ID-D x-ray beamline at the APS.

The pertinent magnetic ordering within the iron compound is confined to its iron-arsenic layers, one of which is highlighted on the left-hand side of Fig. 1. Mössbauer spectroscopy and nuclear magnetic resonance (NMR) were employed to probe the compound's magnetism at cryogenic temperatures. The researchers used the spectroscopic and NMR data to determine the most likely magnetic ordering within the sample, which matched the pattern expected from an SVC ordering.

The SVC ordering is depicted on the right side of Fig. 1. This ordering is sometimes denoted "all-in or all-out," since the magnetic moments of the iron atoms all point away or toward nearby arsenic atoms. The spin-vortex pattern is also sometimes referred to as a "hedgehog pattern," by analogy to the spikes protruding from hedgehogs.

When the magnetic phases in iron high-temperature superconductors are close to are close to degeneracy in their lowest energy state, the resulting magnetic fluctuations are thought to promote their superconductivity. The production and observation of the elusive SVC ordering provides new avenues for scientists to observe the characteristics of these unique superconductors. — Phil Koth

See: William R. Meier[1], Qing-Ping Ding[1], Andreas Kreyssig[1], Sergey L. Budko[1], Aashish Sapkota[1], Karunakar Kothapalli[1], Vladislav Borisov[2], Roser Valentí[2], Cristian D. Batista[3,4], Peter P. Orth[1], Rafael M. Fernandes[5], Alan I. Goldman[1], Yuji Furukawa[1], Anna E. Böhmer[1], and Paul C. Canfield[1]*, "Hedgehog spin-vortex crystal stabilized in a hole-doped iron-based superconductor," Quantum Mater. **3**, 5 (2018). DOI: 10.1038/s41535-017-0076-x
Author affiliations: [1]Iowa State University, [2]Goethe University Frankfurt am Main, [3]University of Tennessee, Knoxville, [4]Oak Ridge National Laboratory, [5]University of Minnesota
Correspondence: * canfield@ameslab.gov

The authors would like to acknowledge D.S. Robinson for experimental support of the x-ray scattering study. Work at the Ames Laboratory was supported by the U.S. Department of Energy (DOE) Office of Science-Basic Energy Sciences, Division of Materials Sciences & Engineering, under Contract No. DE-AC02-07CH11358. W.R.M. was supported by the Gordon and Betty Moore Foundation's EPiQS Initiative through Grant GBMF4411. V.B. and R.V. are supported by the Deutsche Forschungsgemeinschaft under grant SFB/TRR49. R.M.F. is supported by the U.S. DOE Office Science-Basic Energy Sciences, under award DE-SC0012336. P.P.O. acknowledges support from Iowa State University Startup Funds. This research used resources of the Advanced Photon Source, a U.S. DOE Office of Science User Facility operated for the DOE Office of Science by Argonne National Laboratory under Contract No. DE-AC02-06CH11357.

Electron Recovery Slows Near a Critical Temperature

Usually when photons strike a material, electrons shaken out of their normal state return pretty quickly — within a few billionths of a second. But when researchers working at the APS shook up electrons in a charge-ordered oxide, the electrons became sluggish, returning two orders of magnitude slower than expected. Their findings shed new light on "correlated" materials in which electronic, magnetic, and structural properties are intimately connected. The change in materials properties as a response to light is a novel way to engineer materials. Hidden phases that can only be accessed by light exposure exist within correlated materials, leading to new applications. Combining experiment and theory, this study gives mechanistic insight into unconventional electron behavior and on how engineering of correlated materials could be achieved to extend the lifetime of a light-induced hidden phase.

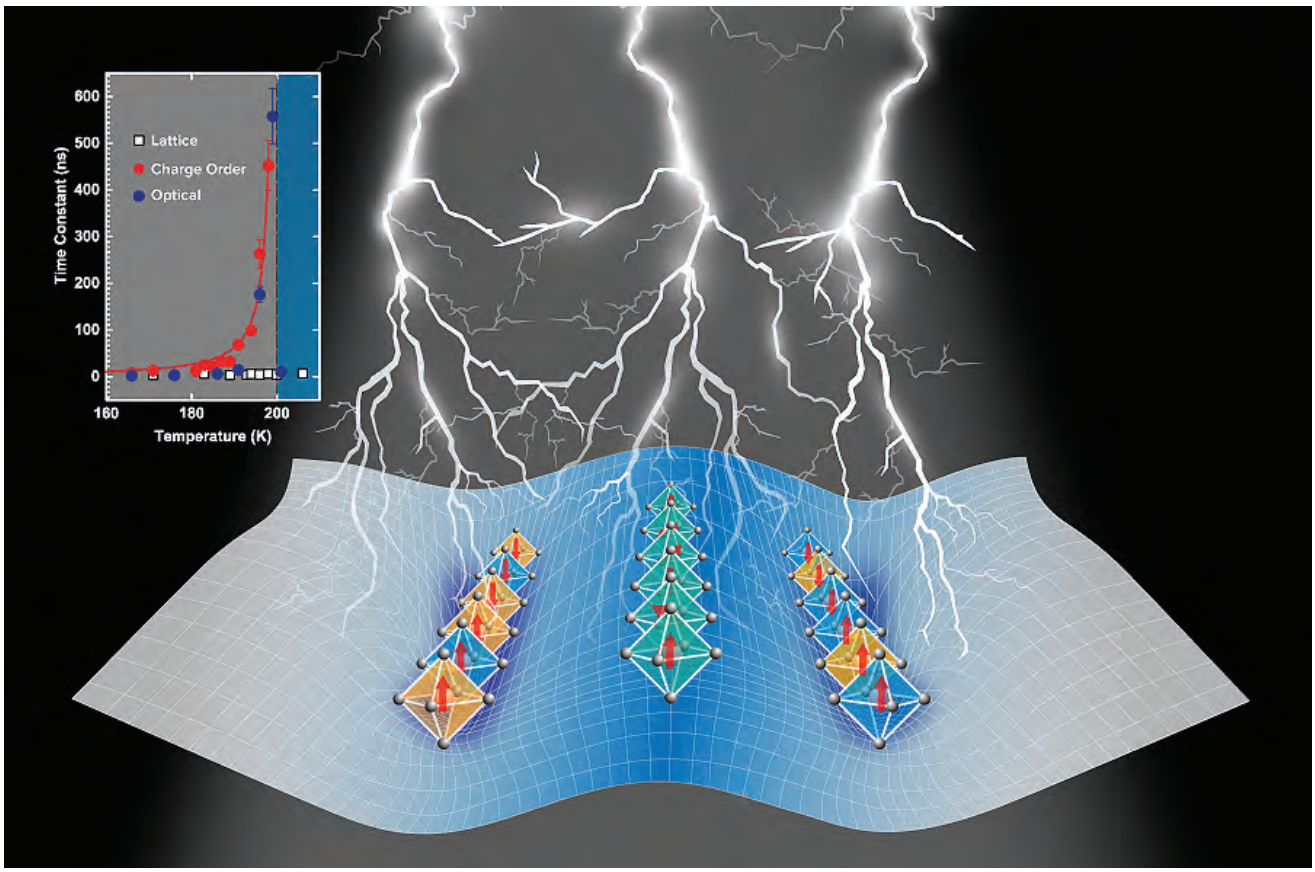

Fig. 1. After exposure to a light pulse, excited electrons within $La_{1/3}Sr_{2/3}FeO_3$ recover two orders of magnitude slower than expected, but only near a specific "critical" temperature (inset). Under this critical temperature, the correlated material undergoes a phase transition to a charge ordered state. Calculations pinpoint magnetic properties of the charge ordered state as the origin of the electron's slowdown.

Interactions within correlated materials are the basis for phenomena, like high-temperature superconductivity and metal-to-insulator phase transitions, on which emerging technologies depend. The oxide investigated in this study, lanthanum strontium ferrite ($La_{1/3}Sr_{2/3}FeO_3$), is a correlated material that undergoes a widely applicable phase transition known as the "first order phase transition." Like a liquid becoming an orderly solid below its freezing point, below a critical temperature this oxide freezes into a "charge-ordered" state. This means charges in the material localize to different sites when the temperature gets low enough — below -100° F.

It was just under this critical temperature that a slowdown of electrons was found by scientists from Argonne, Northwestern University, the University of Illinois at Chicago, and Dublin City University (Ireland). But at much lower or higher temperatures, electrons recover quickly, as expected.

Normally, electron recovery following absorption of light has the same dynamics as lattice cooling — when heat, also generated by the light, transfers from the lattice to the substrate. That is why until now, timescales beyond thermal cooling of electronic degrees of freedom had not been well studied.

The researchers were able to track the recovery of electrons employing transient optical reflectivity at the Argonne Center for Nanoscale Materials. Two ultrafast pulses of light were utilized to first excite the thin-film sample and then interrogate its reflectivity after light absorption. Reflectivity was then tracked over time, from a fraction of a picosecond to hundreds of nanoseconds, as the second pulse is delayed from the first one.

Time-resolved x-ray diffraction performed at XSD beamline 7-ID-C at the APS allowed the researchers to directly compare lattice cooling and electron recovery after light excitation. As the time delay between light absorption and an x-ray probe pulse increased, radial scans of peaks associated with the lattice structure and the charge-ordered state's structure evolved.

The electron in the charge-ordered state tracked nearly the same with these two methods, even as the temperature varied from minus 244° F to -100° F (Fig. 1, inset). Starting at around -136° F, the time constant for electron recovery began to increase steeply, changing from just a few nanoseconds to over 500 nsec. But as soon as the material exceeded the critical temperature, the time constant dropped back to a few nanoseconds. In sharp contrast, the time constant of lattice cooling remained unchanged across the entire temperature range.

Apart from the region near the critical temperature, electron recovery and lattice cooling occurred on the same timescale. Near critical temperature, the ability of electrons to go back to their original state and restore the charge-ordered state is hindered — but by what exactly?

Density functional theory calculations were done to root out the underlying cause. The researchers found that the oxide's energetics were driven by magnetic interactions, leading to two energetically similar charge-ordered states near the critical temperature. The potential energy surface of these two states is shallow, which slows electrons as they relax into one state. But at very low temperatures the two states have different energies, so the steep slope of the lower energy state acts as a strong restoring force for fast electron recovery.

In this oxide, charge ordering is accompanied by a transition from a para-magnetic metal to an antiferromagnetic insulator. This behavior could be useful as a switch — at one temperature it's electrically insulating and magnetic, but just a few degrees higher and its properties change completely. Light absorption disrupts the charge-ordered state, and the temperature-sensitive recovery of electrons controls how long the switch is flipped.

— Amanda Grennell

See: Yi Zhu[1], Jason Hoffman[1], Clare E. Rowland[1,2], Hyowon Park[1,3], Donald A. Walko[1], John W. Freeland[1], Philip J. Ryan[1,4], Richard D. Schaller[1,2], Anand Bhattacharya*[1], and Haidan Wen**[1], "Unconventional slowing down of electronic recovery in photoexcited charge-ordered $La_{1/3}Sr_{2/3}FeO_3$," Nat. Commun. **9**, 1799 (2018). DOI: 10.1038/s41467-018-04199-4
Author affiliations: [1]Argonne National Laboratory, [2]Northwestern University, [3]University of Illinois at Chicago, [4]Dublin City University
Correspondence: * anand@anl.gov, ** wen@aps.anl.gov

The authors acknowledge G. Doumy and A. M. March for assistance with the high-repetition-rate laser at APS beamline 7-ID-C.Y.Z., J.H., A.B., and H.W. acknowledge support of the U.S. Department of Energy (DOE) Office of Science-Basic Energy Sciences (BES), Materials Sciences and Engineering Division. H.P. acknowledges start-up funding from the University of Illinois at Chicago and Argonne National Laboratory (by the U.S. DOE Office of Science program) and the computing resources provided on Blues, a high-performance computing cluster operated by the Laboratory Computing Resource Center at Argonne. H.W. and J.F. acknowledge the support of data analysis by DOE-BES grant No. DE-SC0012375. The use of the Advanced Photon Source and Center for Nanoscale Materials, Office of Science user facilities at Argonne, is supported by DOE-BES under Contract No. DE-AC02-06CH11357.

Tracking the Currents of Memory

The experiences we live through are often etched into our minds, and something similar can happen for so-called "memory-resistors," or memristors. These electronic devices can hold a memory of the past in their resistance, which can be in different states depending on the last electric current that passed through them. But the mechanism underlying this electronic memory has not been entirely clear. A new x-ray study performed at the APS charts the movements of atomic defects within a memristor. The results show that memristive behavior occurs when the defect concentration is near a threshold value. Guided by this information, engineers may be able to fabricate devices that operate consistently around this threshold concentration.

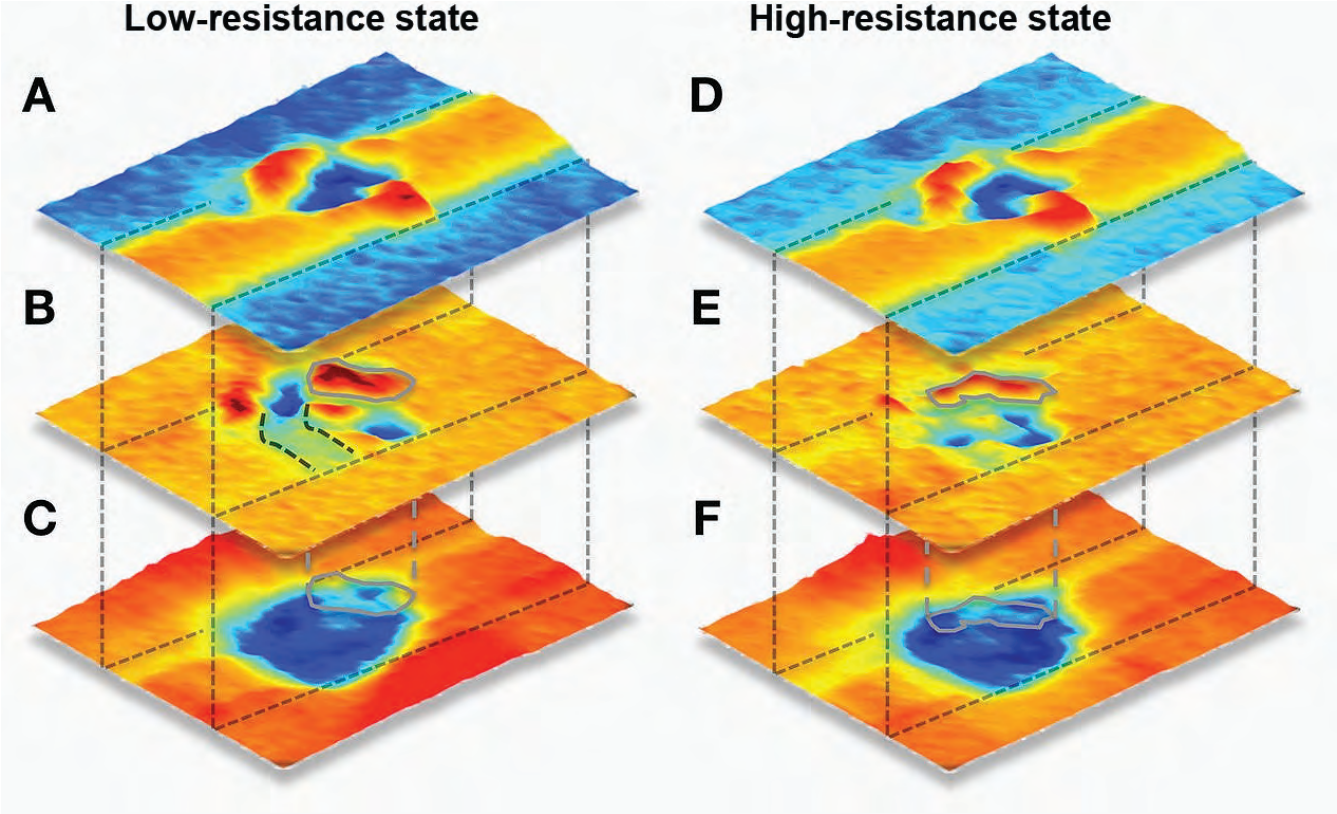

Memristors are not yet available in consumer products, but that could change in the next few years as the field is rapidly developing. Memristive memory devices have many attractive features, such as requiring low power and retaining memory after the power is shut off. Memristors also have some intriguing similarities with neurons in the brain. In analogy to synaptic connections, memristors form conduction pathways when they are exposed to a voltage. And applying a reverse voltage can reduce the pathway — leading to a kind of "forgetting" of information. Some researchers are working on memristive systems that would form brain-like neural networks in next-generation computers.

The basic picture for the conduction pathways in memristors is that they are associated with atomic defects. For this study, scientists from Argonne, the Agency for Science, Technology and Research (Singapore), the University of Science and Technology (China), and KAIST (Korea) investigated the defect behavior in a memristor made of tungsten oxide (WO_3). In the case of such a metal-oxide memristor, the defects are oxygen vacancies, which are places in the crystal structure that are missing one of their oxygen atoms. Normally, the metal oxide is an electrical insulator, but exposing it to a strong voltage can cause the oxygen vacancies to align together as a conduction pathway, or atomically-thin "wire," that allow electrons to travel back and forth between the device's electrodes.

During preliminary testing, the team varied the initial concentration of oxygen vacancies. When the vacancy concentration was near a threshold value of 8%, the material exhibited memristive behavior: it could be in one of two states: a low-resistance state and a high-resistance state. By varying the applied voltage, the team could cause the memristor to switch from one state to the other.

In order to understand this switching, the team employed multimodal, *operando* x-ray microscopy to measure both structural and chemical evolution in a working device (Fig. 1). They performed these measurements at the XSD 2-ID-D beamline at the APS. This beamline is instrumented to focus x-rays in the 10-keV range down to a 200-nm-wide spot size. As they scanned this beam over their tungsten oxide samples, the team simultaneously recorded the spatial scattering and spectral features of the outgoing x-rays. The spatial scattering data revealed the crystallinity of the material, whereas the spectral information allowed the researchers to infer the oxygen concentration. They found that the crystal structure changed significantly wherever the concentration of oxygen was depleted. Further analysis of the oxygen-vacancy images showed that the low-resistance state was associated with the formation of a vacancy-rich pathway between the electrodes. When the team switched the memristor to its high-resistance state, they observed the movement of some oxygen atoms back into pathway, effectively blocking electron motion.

These insights into the defect behavior in a memristor could help improve the design and fabrication of devices. In the future, researchers may be able to control the placement of defects in a memristor, thus ensuring that the concentration is near the threshold value. This defect engineering could lead to better device reproducibility, which is currently a big obstacle to the consumerization of memristors. For their part, the team is working on a technique called "ionic liquid gating" to manipulate the defect population and electrical properties of tungsten oxide. — Michael Schirber

< Fig. 1. Multimodal, *operando* x-ray microscopy images of the active switching region in a tungsten oxide memristor. The tungsten distribution, oxygen distribution, and degree of crystallinity are shown in (A,B,C) for the low-resistance state and (D,E,F) for the high-resistance state, respectively. These distributions are determined from the WL_3 fluorescence intensity, the W L_3 near-edge absorption spectra, and the integrated intensity of the 003 Bragg peak normalized to the thickness. For all images, the redder hues indicate larger values (log scale). Image credit: Dillon Fong (Argonne National Laboratory)

See: Huajun Liu[1,2], Yongqi Dong[1,3], Mathew J. Cherukara[1], Kiran Sasikumar[1], Badri Narayanan[1], Zhonghou Cai[1], Barry Lai[1], Liliana Stan[1], Seungbum Hong[1,4], Maria K.Y. Chan[1], Subramanian K.R.S. Sankaranarayanan[1], Hua Zhou[1]*, and Dillon D. Fong[1]**, "Quantitative Observation of Threshold Defect Behavior in Memristive Devices with *Operando* X-ray Microscopy," ACS Nano **12**, 4938 (2018). DOI: 10.1021/acsnano.8b02028
Author affiliations: [1]Argonne National Laboratory, [2]Agency for Science, Technology and Research, [3]University of Science and Technology of China, [4]KAIST
Correspondence: * hzhou@aps.anl.gov, ** fong@anl.gov

This research was supported by the U.S. Department of Energy (DOE) Office of Science-Basic Energy Sciences, Materials Sciences and Engineering Division. Use of the Advanced Photon Source and the Center for Nanoscale Materials, Office of Science user facilities at Argonne National Laboratory, was supported by the U.S. DOE Office of Science-Basic Energy Sciences, under Contract No. DE-AC02-06CH11357. H.L. acknowledges support from an A*STAR International Fellowship.

$Eu_2Ir_2O_7$ Found to Be a Potential Weyl Semimetal

Iridium oxides (iridates) exhibit many diverse and interesting electronic phases due to interplays between electron correlations and spin-orbit coupling effects. One possible such topological phase is the Weyl semimetal state, which in pyrochlore iridates can exist in the all-in–all-out (AIAO) magnetic state. Because the possible presence of this phase in pyrochlore iridates depends on the strength of the electron correlation, which remains a matter of continuing debate, a research team sought to understand the degree of electron correlation in the pyrochlore iridate $Eu_2Ir_2O_7$ as a crucial first step toward assessing the topological phase of this class of materials. In examining this issue, the researchers studied the temperature-dependent evolution of the magnetic excitation spectrum in a highly insulating single crystal of $Eu_2Ir_2O_7$ utilizing resonant inelastic x-ray scattering (RIXS) at the APS. A complementary resonant magnetic x-ray scattering experiment was also conducted at the Canadian Light Source.

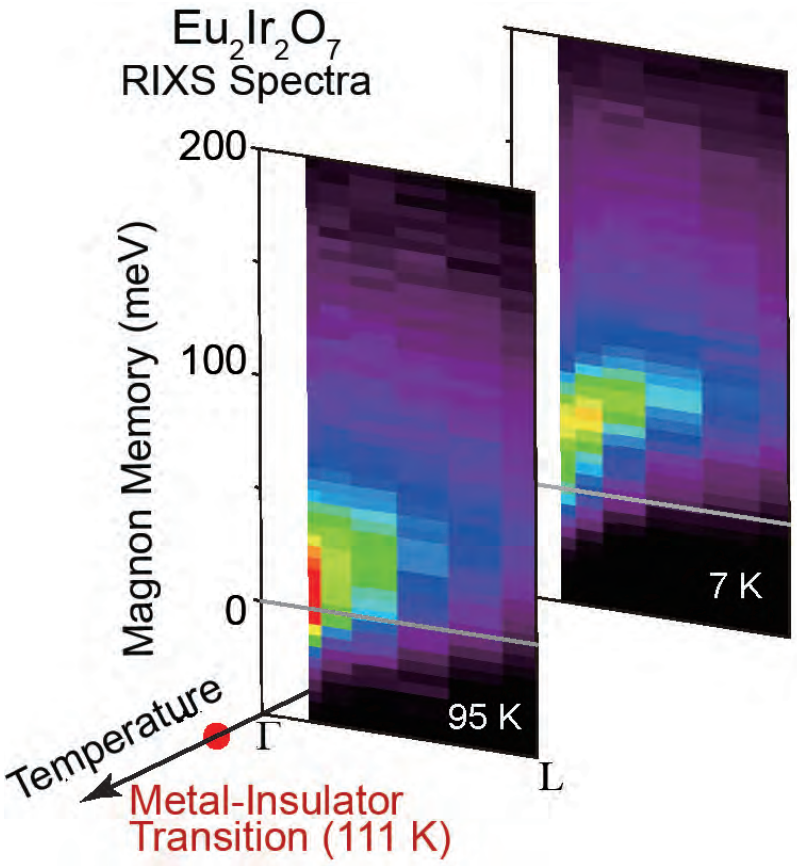

RIXS is a particularly apt way to probe the properties of correlated electrons. RIXS is sensitive to collective spin excitations called "magnons," which form a propagating wave of spinning magnetic moments. Magnons carry information about the strength of the coupling between neighboring electron spins, which in turn sheds light on the degree of electron correlation. Magnons in complex antiferromagnets like $Eu_2Ir_2O_7$ cannot be probed with other x-ray spectroscopic techniques, and even with RIXS require the extremely high-energy resolution available at the XSD 27-ID-B beamline at the APS.

The magnetic excitation spectrum obtained via RIXS at 27-ID-B exhibited a dramatic contrast between local and itinerant magnetism as the temperature of the sample was increased from 7 K to beyond the metal-insulator transition temperature of 111 K. A propagating magnon mode with a 20-meV bandwidth and a 28-meV spin gap was found at 7 K, which suggests that the sample then was predominantly a local moment system in the antiferromagnetic AIAO ordered state.

The researchers in this study, from the University of Toronto (Canada), Argonne, the Canadian Light Source, and the University of Tokyo (Japan) next investigated how magnetic order was destroyed at the phase transition at 111 K, in search of clues as to the itinerancy of the system at higher temperatures. In a completely itinerant system, the magnetic order and the metal-to-insulator transition would occur at the same time, and magnetic fluctuations would disappear above the transition temperature. On the other hand, in a purely local moment system, the local magnetic moments would lose long-range coherence, but survive into the paramagnetic phase with their moments and interactions intact.

The researchers found, however, that the magnetic excitation exhibited substantial softening as the temperature was raised toward the metal-insulator temperature of 111 K, where it turned into a highly damped excitation in the paramagnetic phase (Fig. 1). Surprisingly, the strong suppression of the excitation energy occurred throughout the whole Brillouin zone including the zone boundary. The researchers concluded that such a rigid shift of the magnetic excitation band cannot be explained by thermal magnon renormalization, as would be expected in a local moment system, but points instead to a substantial change in the electronic structure accompanying the magnetic transition. Their results strongly suggest that the electron correlation in $Eu_2Ir_2O_7$ is of intermediate strength, implying that this pyrochlore iridate is compatible with Weyl semimetal physics.

— Vic Comello

< Fig. 1. The evolution of the magnetic dispersion relation along the $\Gamma \rightarrow$ L line in reciprocal space for $Eu_2Ir_2O_7$ is shown as a function of temperature. The intensity maps of RIXS spectra at 7 K and 95 K are plotted along the temperature axis. The magnetic ordering temperature coincides with the metal-insulator transition temperature noted on the temperature axis.

See: Sae Hwan Chun[1], Bo Yuan[1], Diego Casa[2], Jungho Kim[2], Chang-Yong Kim[3], Zhaoming Tian[4], Yang Qiu[4], Satoru Nakatsuji[4], and Young-June Kim[1]*, "Magnetic Excitations across the Metal-Insulator Transition in the Pyrochlore Iridate $Eu_2Ir_2O_7$," Phys. Rev. Lett. **120**, 177203 (2018). DOI: 10.1103/PhysRevLett.120.177203
Author affiliations: [1]University of Toronto, [2]Argonne National Laboratory, [3]Canadian Light Source, [4]University of Tokyo
Correspondence: * yjkim@physics.utoronto.ca

Work at the University of Toronto was supported by the Natural Sciences and Engineering Research Council of Canada, through the Discovery and CREATE program and the Canada Foundation for Innovation. Use of the Canadian Light Source was supported by the Canada Foundation for Innovation, the Natural Sciences and Engineering Research Council of Canada, the University of Saskatchewan, the Government of Saskatchewan, Western Economic Diversification Canada, the National Research Council of Canada, and the Canadian Institutes of Health Research. Work at the University of Tokyo was supported by CREST, Japan Science and Technology Agency, by Grants-in-Aid for Scientific Research (Grants No. 16H02209 and No. 25707030), by Grants-in-Aid for Scientific Research on Innovative Areas "J-Physics" (Grants No. 15H05882 and No. 15H05883), and from the Japanese Society for the Promotion of Science. This research used resources of the Advanced Photon Source, a U.S. Department of Energy (DOE) Office of Science User Facility operated for the DOE Office of Science by Argonne National Laboratory under Contract No. DE-AC02-06CH11357.

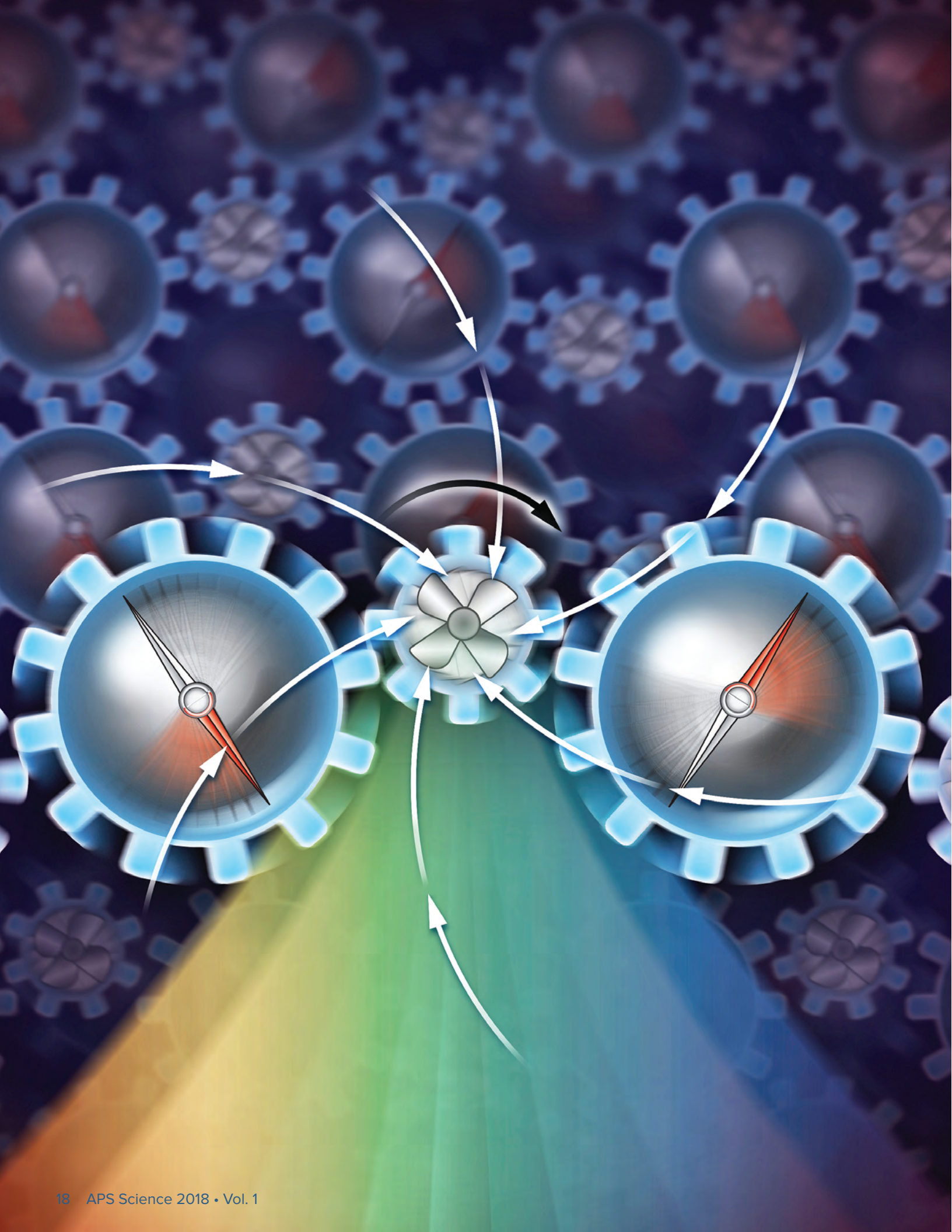

Putting a Little English on Antiferromagnets

Magnetic materials are everywhere, from the decorations on the face of your refrigerator to the GPS in your phone. Ferromagnets, the most common kind, are tremendously useful because they are easy to control, but that also means they are obvious — most of ferromagnetic devices can be easily detected or destroyed using magnets available over the counter. Engineers would like to be able to build computers and other electronic devices out of a different family of magnetic materials, called "antiferromagnets." Such devices would be magnetically invisible and thus much harder to detect than the typical ferromagnetic devices available today. They could make computers stealthier, and much, much faster. However, that also means they would be more difficult to control. Researchers utilized the APS to demonstrate a super-thin antiferromagnet that is readable and controllable using outside magnetic fields. It's the first step to building practical antiferromagnetic devices.

When the angles don't line up in a game of billiards, players will intentionally hit the cue ball off-center to make it spin. When the spinning cue ball hits another ball, it can transfer some of that spin momentum, causing the other ball to move at a curved angle it otherwise wouldn't (and hopefully fly right into the desired pocket).

Magnetic moments trading spinning electrons in a magnetic material are doing essentially the same thing. That is the key to the antiferromagnetic material built and studied by a team of researchers from the University of Tennessee, Knoxville, Brookhaven National Laboratory, the University of Tokyo (Japan), Charles University in Prague (Czech Republic), the Academy of Sciences of the Czech Republic, Dublin City University (Ireland), Oak Ridge National Laboratory, and Argonne. When a spinning electron flies from one magnetic moment to the next, it can knock over the magnetic moment it lands on. The moment flips, and in this way pairs of magnetic moments can "communicate" with each other by using different spins of the electron (Fig. 1).

The researchers layered sheets of strontium iridium oxide ($SrIrO_3$) just a single atom thick over similarly thin sheets of strontium titanium oxide ($SrTiO_3$). The iridium was the source of the antiferromagnetism, because each iridium atom has a "doublet" spin state; it can spin clockwise or counter-clockwise, also called up or down. If one iridium atom spins up, its neighbor spins down, the very definition of an antiferromagnet. But in most antiferromagnetic materials, the atoms are stuck in one orientation. Not in this one. Instead, the researchers carefully designed the layers of $SrIrO_3$ and $SrTiO_3$ to be symmetrical around the iridium atoms. Each iridium atom (and its magnetic moment) sits in an environment where it "feels" all the directions are the same. This allowed the iridium atoms to flip their magnetic moments freely, making a nice, big, easily detected response to external magnetic fields. This effect was theoretically predicted 25 years ago but never experimentally realized until the advances in material synthesis provide us the capabilities we have today.

To test whether this special arrangement of coupled magnetic moments had a magnetic response big enough to be useful, the researchers analyzed the material at two XSD beamlines at the APS. The team carried out x-ray absorption and magnetic circular dichroism measurements at XSD beamline 4-ID-D. The XSD 6-ID-B beamline end station is set up to do x-ray diffraction within a magnetic field. These experiments, which utilize resonant

"English" cont'd. on page 21

< Fig. 1. Symmetry-invariant anisotropy. Spins in an antiferromagnet are aligned to be magnetically inert. But in this paper, the researchers show that creating a material with local spin anisotropy that preserves global isotropy gears up the antiparallel spins for efficient control with a magnetic field.

X-ray Imaging of Gigahertz Ferroelectric Domain Dynamics

A team of researchers has made an important advance in broadening our understanding of light-induced mesoscale dynamics. Time-resolved x-ray diffraction microscopy, aided by a newly developed dynamical phase-field method (DPFM) , revealed how lattice waves can be excited by light pulses and the resulting local structural changes among mesoscopic domains in ferroelectrics, a widely utilized material for sensors, nanoscale positioners, and information storage devices.

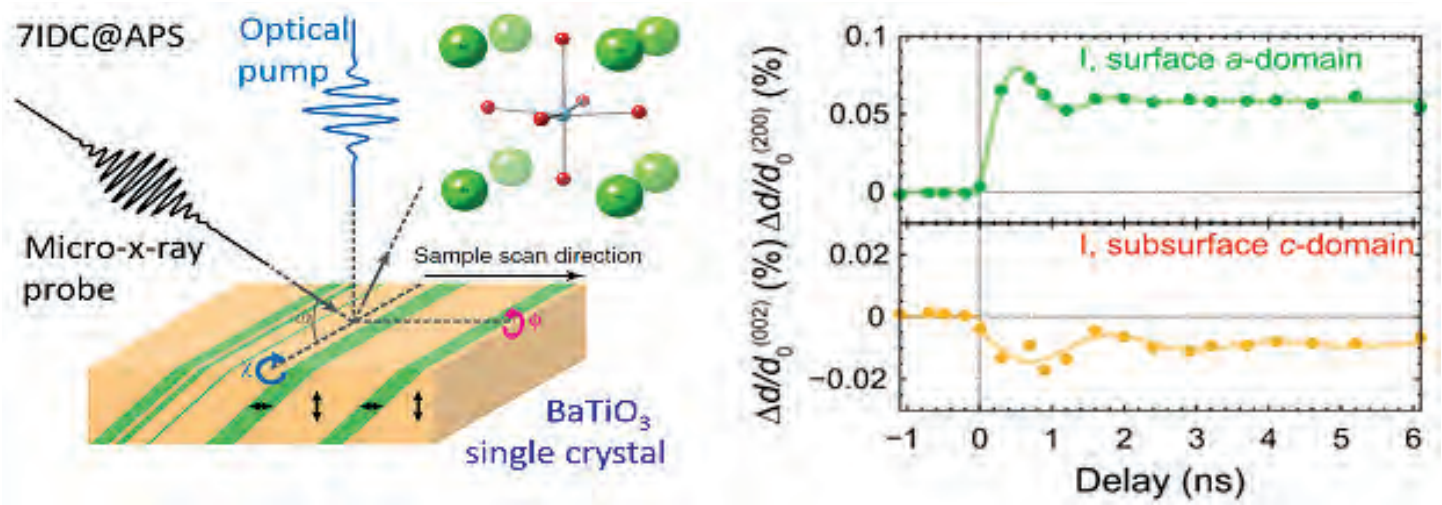

Fig. 1. Left: Schematic illustration of spatially-resolved pump-probe experiment and domain configuration of a $BaTiO^3$ single crystal sample. The inset shows a unit cell of $BaTiO^3$. Right: The measured lattice strain (dots) oscillates at gigahertz frequency that confirms the prediction by the dynamical phase-field theory (solid lines).

Light interaction with matter offers a new way of controlling material properties by harnessing energy transport and conversion in functional materials without contact on ultrafast time scales. However, the desired dynamical control is complicated by the inhomogeneous response of real materials. The ultrafast dynamics depend not only on the intrinsic properties of the compound but also, strongly, on mesoscale structures such as surfaces, domains, interfaces, and defects that govern the coupling between various degrees of freedom.

Rich mesoscale phenomena inspire new functions but pose a great challenge to characterize and understand their fundamental processes in the time domain.

The researchers from The Pennsylvania State University and Argonne shone ultrafast laser pulses on a prototypical ferroelectric single crystal, $BaTiO^3$. Due to absorption of the light, electrons are liberated from bonding states and start to move within a block of the material — a ferroelectric domain — whose lengths are on the order

"Gigahertz" cont'd. on next page

"Gigahertz" cont'd. from previous page

of a micrometer (Fig. 1). These free charge carriers can experience different local forces that pull them in certain directions depending on which domain they occupy.

As a result, the lattice start to respond to light-activated charge carriers on ultrafast time scales. To capture these local dynamics that occur on micrometer length and sub-nanosecond time scales, a focused x-ray beam from the XSD 7-ID-B,C,D x-ray beamline at the APS was utilized to probe within and across domains following optical excitation, with the lattice dynamics manifesting itself as the change of diffraction intensity from the probing x-ray beam. The local structural dynamics, including oscillatory lattice spacing and rotation at gigahertz frequency in individual domains, can be clearly resolved.

Understanding such complex behavior without modeling tools that account for spatial complexity and short time scales is an outstanding challenge. The authors have newly developed a dynamical phase-field method (DPFM) which was used to successfully predict these rich structural dynamics. This demonstration of the ability to reveal mesoscopic structural changes opens up new opportunities for understanding mesoscale phenomena and optimizing the functionalities of technologically important materials.

The continuous innovation of x-ray instruments at the APS has allowed users to enter a new spatiotemporal regime to solve challenging problems that could not previously be answered. With the APS Upgrade, higher spatial resolution and better signal-to-noise ratio will further empower these cutting-edge x-ray research tools for meeting mesoscopic energy challenges.

See: Hirofumi Akamatsu[1], Yakun Yuan[1], Vladimir Stoica[1,2], Greg Stone[1], Tiannan Yang[1], Zijian Hong[1], Shiming Lei[1], Yi Zhu[2], Ryan C. Haislmaier[1], John W. Freeland[2], Long-Qing Chen[1], Haidan Wen[2], and Venkatraman Gopalan[1]*, "Light-activated Gigahertz Ferroelectric Domain Dynamics," Phys. Rev. Lett. **120**, 096101 (2018). DOI: 10.1103/PhysRevLett.120.096101
Author affiliations: [1]The Pennsylvania State University, [2]Argonne National Laboratory
Correspondence: * vxg8@psu.edu

H.A., Y.Y., V.S., H.W., J.F., and V.G. were supported by the U.S Department of Energy (DOE) Office of Science-Basic Energy Sciences, under grant No. DE- SC0012375, for the ultrafast XRD microscopy and ultra- fast optical pump SHG probe work. G.S., S.L., R.H., and Z.H. were supported by National Science Foundation (NSF) grant NO. DMR- 1420620 for the XRD data analysis, PFM measurements, UV-vis absorption measurements, and DPFM. T.Y. and L.Q.C. acknowledge the support by NSF under grant No. DMR-1410714 for the DPFM work. This research used resources of the Advanced Photon Source, a U.S. DOE Office of Science User Facility operated for the DOE Office of Science by Argonne National Laboratory, supported by Contract No. DE-AC02- 06CH11357.

"English" cont'd. from page 19

magnetic scattering, must be carried out in a magnetic field and at a low temperature. The cryostat has a small vacuum shroud that fits within the poles of the electromagnet. The researcher can see the actual arrangement of the magnetic moments in the material, and how the arrangement changes when the magnetic field around it changes.

When they ran the experiments, the researchers saw exactly what they had hoped for: the antiferromagnet reacted to the external magnetic field in a predictable, controllable way, with a big enough signal that they could actually read it. The experiment shows that antiferromagnets could someday work as superior materials for ultrafast, stealthy computing. The two major challenges the team will work on now are making antiferromagnets that work at higher temperatures closer to room temperature, and devising a way to read them with something a little more accessible than a giant x-ray synchrotron with magnetic diffraction. — Kim Krieger

See: Lin Hao[1], D. Meyers[2], Hidemaro Suwa[1,3], Junyi Yang[1], Clayton Frederick[1], Tamene R. Dasa[1], Gilberto Fabbris[2], Lukas Horak[4], Dominik Kriegner[4,5], Yongseong Choi[6], Jong-Woo Kim[6], Daniel Haskel[6], Philip J. Ryan[6,7], Haixuan Xu[1]*, Cristian D. Batista[1,8]**, M.P.M. Dean[2]***, and Jian Liu[1]****, "Giant magnetic response of a two-dimensional antiferromagnet," Nat. Phys. **14**, 806. (August 2018). DOI: 0.1038/s41567-018-0152-6
Author affiliations: [1]University of Tennessee, Knoxville, [2]Brookhaven National Laboratory, [3]University of Tokyo, [4]Charles University in Prague, [5]Academy of Sciences of the Czech Republic, [6]Argonne National Laboratory, [7]Dublin City University, [8]Oak Ridge National Laboratory
Correspondence: * hxu8@utk.edu, ** cbatist2@utk.edu, *** mdean@bnl.gov, **** jianliu@utk.edu

The authors acknowledge experimental assistance from H.D. Zhou, E. Karapetrova, C. Rouleau, Z. Gai, J. K. Keum and N. Traynor. J.L. acknowledges support by the start-up fund and the Transdisciplinary Academy Program at the University of Tennessee. J.L. and H.X. acknowledge support by the Organized Research Unit Program at the University of Tennessee and support by the Department of Defense-Defense Advanced Research Projects Agency under grant no. HR0011-16-1-0005. M.P.M.D. and D.M. are supported by the U.S. Department of Energy (DOE) Office of Science-Basic Energy Science, Early Career Award Program under award number 1047478. H.S. and C.D.B. are supported by funding from the Lincoln Chair of Excellence in Physics. D.K. and L.H. acknowledge the support by the ERDF (project CZ.02.1.01/0.0/ 0.0/15_003/0000485) and the Grant Agency of the Czech Republic grant (14-37427 G). A portion of the work was conducted at the Center for Nanophase Materials Sciences, which is a DOE Office of Science User Facility at Oak Ridge National Laboratory. This research used resources of the Advanced Photon Source, a U.S. DOE Office of Science User Facility operated for the DOE Office of Science by Argonne National Laboratory under Contract No. DE-AC02-06CH11357.

NUMBER OF APS EXPERIMENTS (FY1998-2018)

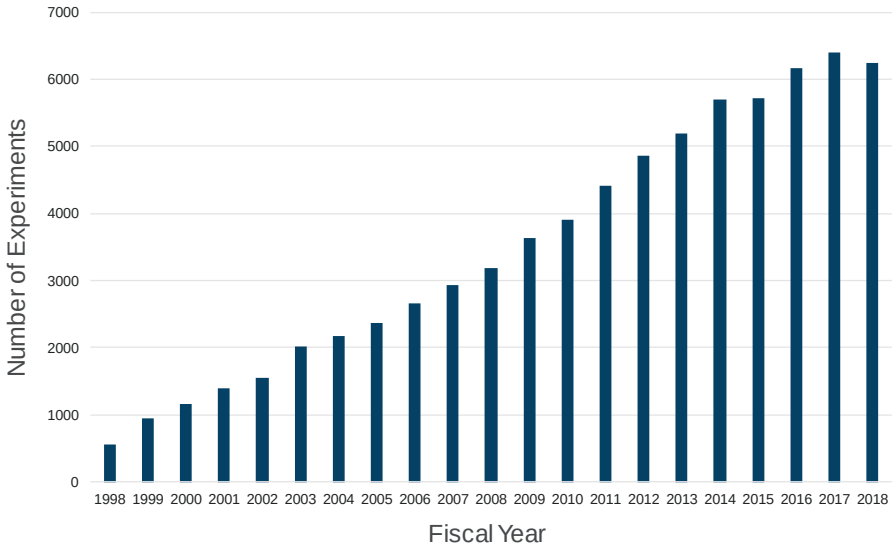

APS ON-SITE AND REMOTE USERS (FY 1998-2018)

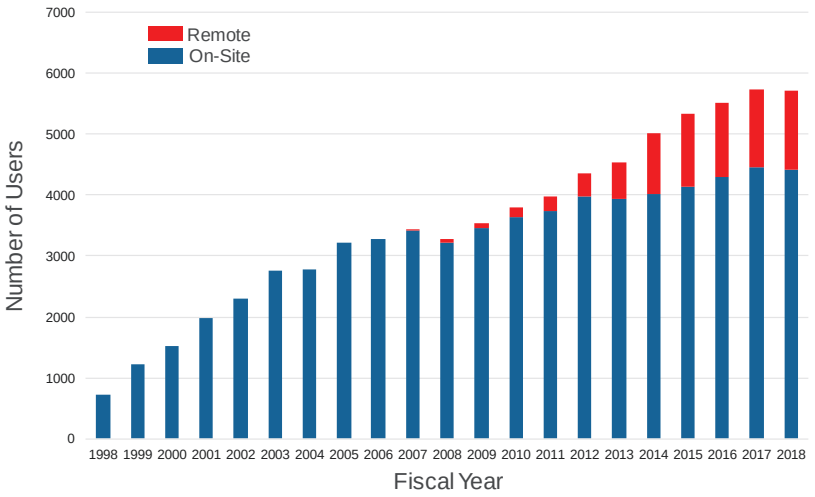

Note: Prior to FY14, mail-in users were not included in the Remote category

ON-SITE APS USERS & CO-PROPOSERS (FY 1998-2018)

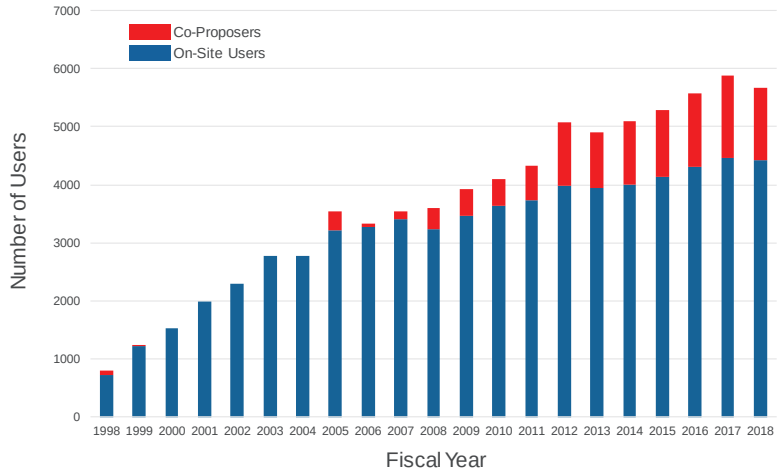

Engineering Materials & Applications

Putting the Heat on an Additive-Manufactured Alloy

As the techniques of additive manufacturing (AM), more popularly known as "3-D printing," become ever more versatile and applicable for diverse purposes, they sometimes pose unique challenges that are not present with more traditional manufacturing methods. In additive-manufactured metals and alloys, such problems can result in microstructural defects that lead to reduced strength and stress resistance, an issue commonly addressed by post-build heat treatment. But this approach can also have undesirable side effects. Researchers from the National Institute of Standards and Technology (NIST) used the APS to examine the AM alloy Inconel 625 (IN625) in an effort to better understand the effects of heat treatment on AM alloy microstructure and phase evolution.

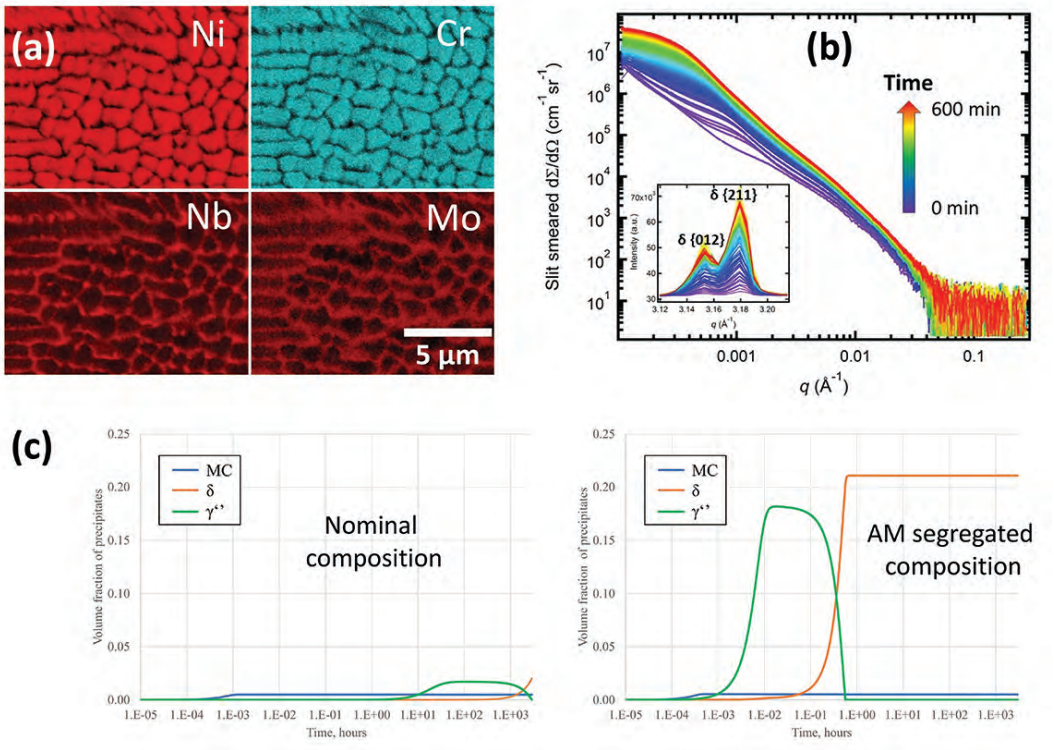

Fig. 1. (a) Energy dispersive x-ray spectrometry compositional mapping of as-built AM IN625 alloy clearly demonstrates severe elemental microsegregation introduced by rapid cooling and solidification in the AM build process. (b) Simultaneous synchrotron USAXS and XRD data reveal an unexpected, fast formation of deleterious delta phase in AM 625 and its morphological and structure transformation kinetics during a stress-relief heat treatment at 870° C. (c) Thermodynamic calculations unequivocally show that the elemental microsegregation (right panel) leads to a much accelerated (> 1 × 10^2) formation of precipitate phases comparing with the nominal composition (left panel).

A widely-used superalloy in the aerospace, marine, and nuclear industries where its high strength and corrosion resistance are critical advantages, IN625's limited machinability makes it attractive for AM as an alternative and thus a good model for studying AM alloys. Using heat-treated IN625 samples created by laser powder-bed fusion, the investigators used electron microscopy and thermodynamic modeling, and *in situ* synchrotron small-angle and ultra small-angle x-ray scattering (USAXS) and x-ray diffraction (XRD) techniques for experiments at the XSD 11-BM-B powder diffraction beamline and the XSD 9-ID-C USAXS facility.

While the AM principle of using a laser or electron beam to build up material layer by layer is very versatile, it is also a volatile and somewhat unpredictable process at the microscale, involving complex repeated cycles of heating and cooling that inevitably result in a certain degree of microstructural inhomogeneity. One form often seen in AM metals is elemental segregation, which can create defects including residual stress and nonequilibrium phase structure. These are generally alleviated by post-build stress-relief and homogenization heat treatments.

The unexpected side effects of these heat treatments were the focus of the current work, which includes some of the first detailed *in situ* investigations of the phenomenon. *Ex situ* studies of IN625 AM samples with scanning electron microscopy (SEM) and x-ray diffraction after stress-relief heat treatment at 870° C for 0.5, 1, 4, and 8 h (compared with as-built samples) reveal the phase profiles and the presence of undesired platelet-shaped delta-phase precipitates in the interdendritic regions, which are known to degrade mechanical performance of IN625.

With the *in situ* x-ray scattering and diffraction techniques at the APS USAXS facility, the researchers were able to observe the actual formation of these delta-phase precipitates. These methods also allowed both time- and temperature-dependent studies of the phase evolution kinetics within the same sample volume, including enough data for thermodynamic modeling. Across the entire temperature range of the heat treatment from 800° C to 870° C, the delta-phase precipitates were seen to grow very rapidly, beginning less than five minutes after the commencement of heat treatment, suggesting a very low nucleation barrier. Notably, the growth kinetics was found to be at least 100 times faster than with conventional alloys of similar composition.

The atomic structure of these precipitates remains stable after formation. Arrhenius analysis revealed an activation energy for these precipitates of (131.04 ± 0.69) kJ mol^{-1}, far lower than that seen in, for example, niobium (Nb) diffusion in nickel alloys. Because the precipitates initially form at interdendritic regions with high amounts of Nb, the investigators note that long-range Nb diffusion is not necessary for the initiation of the delta phase in AM IN625.

Applying a second heat treatment at 1150° C for 1 h succeeded in removing the delta-phase precipitates, resulting in a single-phase face-centered cubic structure. However, this second heat treatment was also found to promote grain growth that could possibly weaken the alloy's mechanical strength. The research team is continuing to explore, in greater detail, the benefits and adverse effects of this homogenization heat treatment.

Although the current study was confined to AM IN625, the investigators note that their general findings are applicable to many other AM alloys, since phenomena such as elemental segregation with undesired phase precipitates are an almost inevitable byproduct of AM technology. Extending the multifaceted approach taken in this work, combining *ex situ* and *in situ* EM and XRD with thermodynamic modeling, to other AM alloys will lead to a better understanding of their phase evolution in comparison with their wrought counterparts, and ultimately to new strategies to avoid or mitigate microstructural defects of additive-manufactured metal alloys.

— Mark Wolverton

See: Fan Zhang*, Lyle E. Levine, Andrew J. Allen, Mark R. Stoudt, Greta Lindwall, Eric A. Lass, Maureen E. Williams, Yaakov Idell, and Carelyn E. Campbell, "Effect of heat treatment on the microstructural evolution of a nickel based superalloy additive-manufactured by laser powder bed fusion," Acta Materialia **152**, 200 (2018). DOI: 10.1016/j.actamat.2018.03.017
Author affiliation: National Institute of Standards and Technology
Correspondence: * fan.zhang@nist.gov

We thank Jan Ilavsky and Saul Lapidus for their help at the beamlines 9-ID and 11-BM at the Advanced Photon Source. The Engineering Laboratory at NIST built the IN625 samples used in this study. This research used resources of the Advanced Photon Source, a U.S. Department of Energy (DOE) Office of Science User Facility operated for the U.S. DOE Office of Science by Argonne National Laboratory under Contract No. DE-AC02-06CH11357.

How to Make the Blackest Black

The super-black feathers found on many bird-of-paradise males have velvety microstructures that act like light traps. These super-black feathers are located adjacent to a brightly colored patch, making the colors appear almost radiant by contrast. The visual shock of the bright feathers attracts females, and males with the blackest and brightest plumage are chosen to pass their genes to the next generation. Similar microstructures could be manufactured for use in solar panels, optics, and many other technologies. To determine how the super black is created, researchers employed a variety of experiment techniques including micro-tomography at the APS.

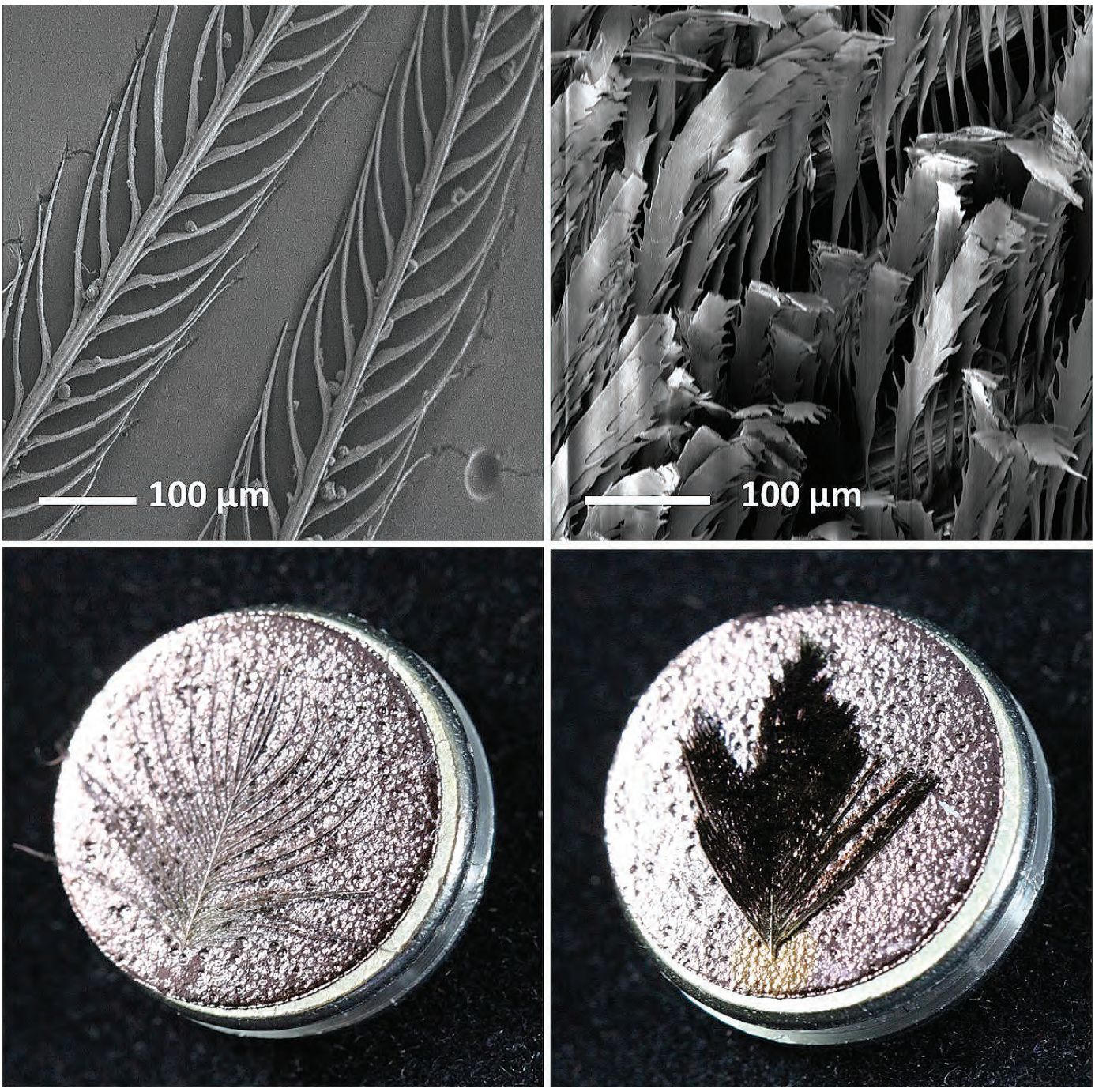

Birds of paradise inhabit the dense rain forests of Papua New Guinea and surrounding areas. Most of the 42 species in these dark forests are sexually dimorphic and polygynous: to attract mates and pass on their genes, males have engaged in a sort of evolutionary arms race. Before mating, dully feathered females evaluate males, who display their beautiful plumage during an elaborate mating dance. The male with the best plumage display wins.

Many bird-of-paradise males have super-black feathers, which absorb 99.6% of the incoming light and 99.9% when the incidence angle is 45° (black pigment absorbs only 97.5% of visible light). Since virtually no light escapes, the plumage appears profoundly darker than the normal black plumage displayed in related species. The super-black plumage is always found adjacent to or encompassing a bright, highly saturated colored patch.

The researchers from Harvard University, the Smithsonian Institution, and Yale University utilized spectrophotometry, scanning electron microscopy (SEM), optical ray-tracing simulations, and micro-tomography at the XSD 2-BM-A,B x-ray beamline at the APS. They investigated structural absorption in feathers from museum specimens of five bird-of-paradise species with super-black plumage and two with normal black plumage. Under SEM (Fig. 1), the normal black feathers display a series of barbules with open branches, somewhat like a palm frond. Margins are smooth and lie within the same plane, forming a flat surface, which reflects incident light, resulting in a glossy surface reflection. In super-black feathers, the barbule arrays look more like the bushy boughs of fir trees. The barbules curve away from the plane of the feather and are fuzzy, with microstructures sticking up to form a complex, jagged surface with intra-barbule cavities. Photons bounce around and become trapped in the cavities, until no light energy is left. The barbules are tilted vertically so the feather's appearance varies with viewing direction; the feathers are blackest when seen from head on.

Everything about the male bird-of-paradise plumage and mating dance is designed to make him look his best. The female is positioned to view him from straight ahead, so that his super-black patch appears its darkest. The adjacent colored patch appears super bright due to an optical illusion. When the cone cells in the female's eye observe the dark patch, they become hypersensitive to the photons emanating from the colored patch — making the colored patch appear extremely bright or even self-luminous. Researchers explain the evolution of such an elaborate scheme using Darwin's idea of mate choice. Female birds-of-paradise select and mate with the most impressive male, the one with the blackest black and brightest colored plumage. This ensures that his genes are passed on to the next generation. The male with one imperfect feather is out of luck.

Super-black materials appear elsewhere in natural and manufactured settings. In golden birdwing butterflies, super-black patches created by microscopic ridges collect solar radiation. In West African Gaboon snakes, super-dark scales in a vertical cone structure provide camouflage.

Manufactured super-black materials have many technological uses, including in solar panels, optics, and textiles. Currently, manufactured super-black materials are created with an irregular surface of regularly spaced cones and pits. These materials are effective, but expensive. By understanding the super-black feathers of birds-of-paradise, humans can achieve super blackness using the same structures that evolved over millions of years — and maybe at less expense. — Dana Desonie

< Fig. 1. Normal and super-black feather microstructures at 100 µm. Top left: A SEM micrograph of a normal black feather from a *Melampitta lugubris*. Top right: A SEM micrograph of a super-black feather with modified barbules *Ptiloris paradiseus*. Bottom left: When normal black feathers are painted gold, they appear gold. Bottom right: When super-black feathers are painted gold, the pigment is lost in the structure of the feather and it appears super black.

See: Dakota E. McCoy[1], Teresa Feo[2], Todd Alan Harvey[3], and Richard O. Prum[3], "Structural absorption by barbule microstructures of super black bird of paradise feathers," Nat. Commun. **9**, 1 (2018). DOI: 10.1038/s41467-017-02088-w
Author affiliations: [1]Harvard University, [2]Smithsonian Institution, [3]Yale University
Correspondence: * dakotamccoy@g.harvard.edu

Xianghui Xiao and the 2-BM beamline of the X-ray Imaging Group aided with computed tomography scanning and analysis at the APS. This research was funded by the W. R. Coe Fund of Yale University, by a Sigma XI student research fellowship to D.E.M., and by a Mind, Brain, and Behavior Graduate Student Award to D.E.M. D.E.M. was supported by the Department of Defense through the National Defense Science and Engineering Graduate Fellowship Program. D.E.M. was also supported by a Theodore H. Ashford Graduate Fellowship in the Sciences. T.J.F. was supported by a U.S. National Science Foundation (NSF) Post-doctoral Fellowship in Biology (#1523857). This work was performed in part at the Harvard University Center for Nanoscale Systems, a member of the National Nanotechnology Coordinated Infrastructure Network, which is supported by the NSF under NSF ECCS award no. 1541959. This research used resources of the Advanced Photon Source, a U.S. Department of Energy (DOE) Office of Science User Facility operated for the DOE Office of Science by Argonne National Laboratory under contract number DE-AC02-06CH11357.

Finding Unusual Performance in Unconventional Battery Materials

Even as our electronic devices become ever more sophisticated and versatile, battery technology remains a stubborn bottleneck, preventing the full realization of promising applications such as electric vehicles and power-grid solar energy storage. Among the limitations of current materials are poor ionic and electron transport qualities. While strategies exist to improve these properties, and hence reduce charging times and enhance storage capacity, they are often expensive, difficult to implement on a large scale, and of only limited effectiveness. An alternative solution is the search for new materials with the desired atomic structures and characteristics. This is the strategy of a group of researchers who, utilizing ultra-bright x-rays from the APS, identified and characterized two niobium tungsten oxide materials that demonstrate much faster charging rates and power output than conventional lithium electrodes.

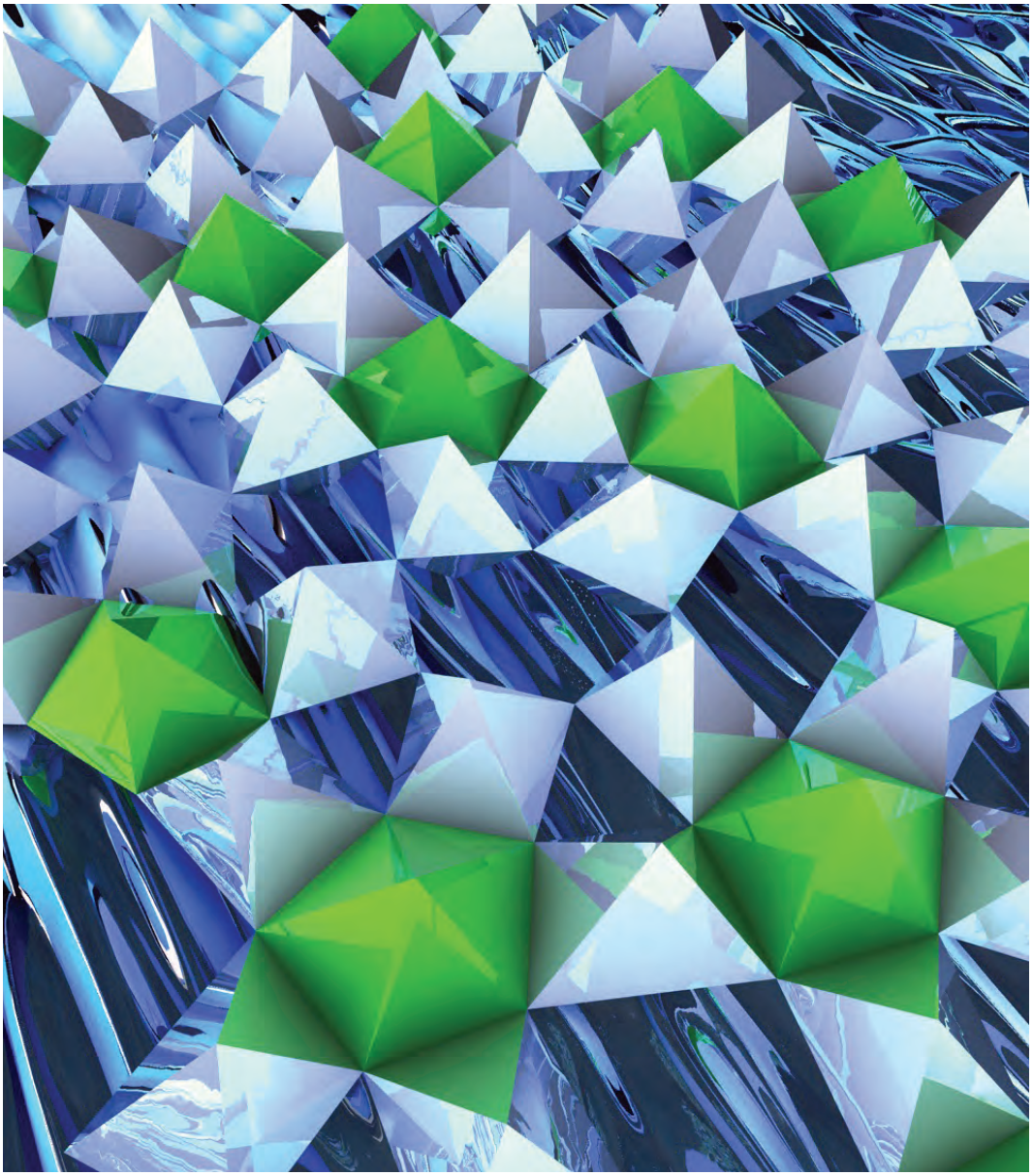

Fig. 1. Artist's impression of rapidly flowing lithium through the niobium tungsten oxide structure. Image credit: Ella Maru Studio

Currently, the usual approach for wringing extra capacity and performance from lithium-ion batteries involves the creation of electrode materials with nanoscale structures, which reduces the diffusion distances for lithium ions. However, this also tends to increase the practical volume of the material and can introduce unwanted additional chemical reactions. Further, when graphite electrodes are pushed to achieve high charging rates, irregular dendrites of lithium can form and grow, leading to short circuits, overheating, and even fires. Measures to prevent these dendrites generally cause a decrease in energy density. These issues seriously limit the use of graphite electrodes for high-rate applications.

In the present work, the team from the University of Cambridge (UK) together with colleagues from Argonne and the Diamond Light Source at the Harwell Science and Innovation Campus (UK) explored an alternative approach with materials featuring a different three-dimensional crystal structure (Fig. 1) and larger active particle size that allows freer movement of lithium ions while avoiding the swelling and other stresses that impede transport in graphite. They concentrated on the niobium tungsten oxides $Nb_{16}W_5O_{55}$ and $Nb_{18}W_{16}O_{93}$, studying their ionic transport characteristics under pulsed-field gradient nuclear magnetic resonance spectroscopy. Among other studies, the experimenters also conducted *operando* powder x-ray diffraction and absorption spectroscopy measurements at the APS, using the AMPIX cell (developed at Argonne) at the XSD 9-BM-B,C and 17-BM-B x-ray beamlines, respectively; and *ex situ* x-ray absorption spectroscopy performed at beamline B18 of the Diamond Light Source.

The team's observations confirmed that, as they had theorized, the different crystallographic natures of the niobium tungsten oxides resulted in high diffusion rates. The $Nb_{16}W_5O_{55}$ material is composed of 4 x 5 $(Nb, W)O_6$ octahedra connected at shear planes, while the $Nb_{18}W_{16}O_{93}$ structure is bronze-like, with "pillars" of oxygen that hold open tunnels in the crystal lattice. This inherent anisotropy of both systems allows free and rapid passage of lithium ions while also leading to greater rigidity and stability and reduced volume expansion. The testing shows that both NbW oxides feature storage densities and room-temperature diffusion rates that exceed current electrode materials by several orders of magnitude, even with micrometer-sized active particles.

The investigators note that cells using these niobium tungsten oxides may result in lower voltages for a given battery weight. However, the greatly increased charging rate can offset this disadvantage for applications requiring fast charging. Also, while the creation of nanoscale material electrodes is complex and costly, the synthesis of large amounts of these niobium tungsten oxides is relatively simple and inexpensive. If needed, their capabilities can be further enhanced by the usual nano-scaling or carbon coating techniques.

This demonstration of the exceptional capabilities that can be achieved in unconventional battery materials opens great potential for further explorations, yet still circumvents the limitations that have dogged past efforts to achieve next-generation batteries. In conjunction with encouraging the development and maturation of technological systems requiring fast charging and high power output, expanding the repertoire of materials available for energy storage can also make possible new approaches to the fundamental design of electrodes in ways that may make them more customizable for specific needs. The researchers offer the example of solid-state batteries with greater similarities in diffusion qualities between electrodes and electrolyte. The present research shows that the continued quest for new approaches, new materials, and new solutions is always worth the effort.

— Mark Wolverton

See: Kent J. Griffith[1], Kamila M. Wiaderek[2], Giannantonio Cibin[3], Lauren E. Marbella[1], and Clare P. Grey[1]*, "Niobium tungsten oxides for high-rate lithium-ion energy storage," Nature **559**, 556 (26 July 2018). DOI: 10.1038/s41586-018-0347-0
Author affiliations: [1]University of Cambridge, [2]Argonne National Laboratory, [3]Diamond Light Source
Correspondence: * cpg27@cam.ac.uk

K.J.G. acknowledges support from The Winston Churchill Foundation of the United States, a Herchel Smith Scholarship, and a Science and Technology Facilities Council Futures Early Career Award. K.J.G. and C.P.G. thank the EPSRC for a LIBATT grant (EP/M009521/1). L.E.M. acknowledges support from the European Union's Horizon 2020 research and innovation program under the Marie Skłodowska–Curie grant agreement number 750294, and a Charles and Katharine Darwin Research Fellowship. We thank O. Borkiewicz from the APS and A. Kasam from the University of Cambridge for diffraction data reduction scripts. We thank Diamond Light Source for access to beamline B18. This research used resources of the Advanced Photon Source, a U.S. Department of Energy (DOE) Office of Science User Facility operated for the DOE Office of Science by Argonne National Laboratory under contract number DE-AC02-06CH11357.

Boosting Sodium-Ion Battery Performance Via Self-assembly of a Titania-Graphene Anode

Lithium-ion batteries have enabled leaps and bounds in the advancement of lightweight electronics and electric cars. But lithium availability won't last forever. That's why a team of scientists developed an easy-to-assemble electrode material that targets sodium storage instead of lithium. Not only does their titania-graphene hybrid material boast an ultrahigh capacity and long-term cycle stability, studies done at the APS helped pin down the mechanisms behind such high performance — an electrostatic attraction between titania and graphene. Computer modelling shows that their method can be extended to other common ions, providing a new paradigm for ion battery technology.

Both graphene and titania (TiO_2) have been studied as promising electrode materials for ion batteries. Titania is inexpensive and Earth-abundant and can easily take sodium ions into its crystal structure, a process called "intercalation." Nanocrystals of titania are especially attractive due to increased conductivity, a shorter diffusion length for sodium, and a flexibility that helps cope with the strain of adding many new ions to its lattice.

Previous studies have integrated titania nanocrystals with graphene to increase conductivity and promote sodium storage at the interface of the two materials. But the main routes for fabrication of these materials require high temperatures, long waiting times, and complicated steps. Any new battery with commercial intent must be easy to scale up for mass production, so researchers from Argonne, the University of Duisburg-Essen (Germany), Xiamen University (China), and the University of North Carolina set out to find a new route. But they didn't just find a better synthesis — they were able to enhance sodium storage in the process.

Their titania-graphene hybrid is based on self-assembly driven by electrostatic attraction between titania nanocrystals and graphene. The nanocrystals, grown in a spray-flame reactor, end up with a positively charged surface while preparation of graphene oxide sheets come out negatively charged. When mixed in solution, these opposites attract, with nanocrystals neatly arranging themselves on the graphene oxide sheets. A simple chemical reduction using vitamin C turns the graphene oxide into graphene by crosslinking the sheets — permanently trapping the nanocrystals inside a three-dimensional hydrogel.

A combination of synchrotron x-ray probe experiments, transmission electron microscopy (TEM), and computational modelling allowed the researchers to examine the insertion and extraction of sodium ions, which is the basis of battery performance. They found that the electrostatic interaction between titania nanocrystals and graphene helps facilitate intercalation of sodium into the bulk titania lattice, but also enhances sodium ion build-up at the interface between the two components. This interfacial storage drastically boosts the performance of the material as a battery electrode, demonstrated by electrochemical experiments where the hybrid material was tested as an anode in a coin cell (Fig. 1).

Together, high-energy x-ray diffraction (HEXRD) done on XSD beamlines 11-ID-C and 11-ID-D at APS and x-ray absorption near edge spectroscopy (XANES) done at XSD beamline 20-BM-B, also at the APS, provided strong evidence that the self-assembly is driven by electrostatic interactions, rather than chemical reactions. Compared to titania nanocrystals alone, the HEXRD pattern of the hybrid material is the same, suggesting no structural changes. In the XANES experiment, no titanium-carbon

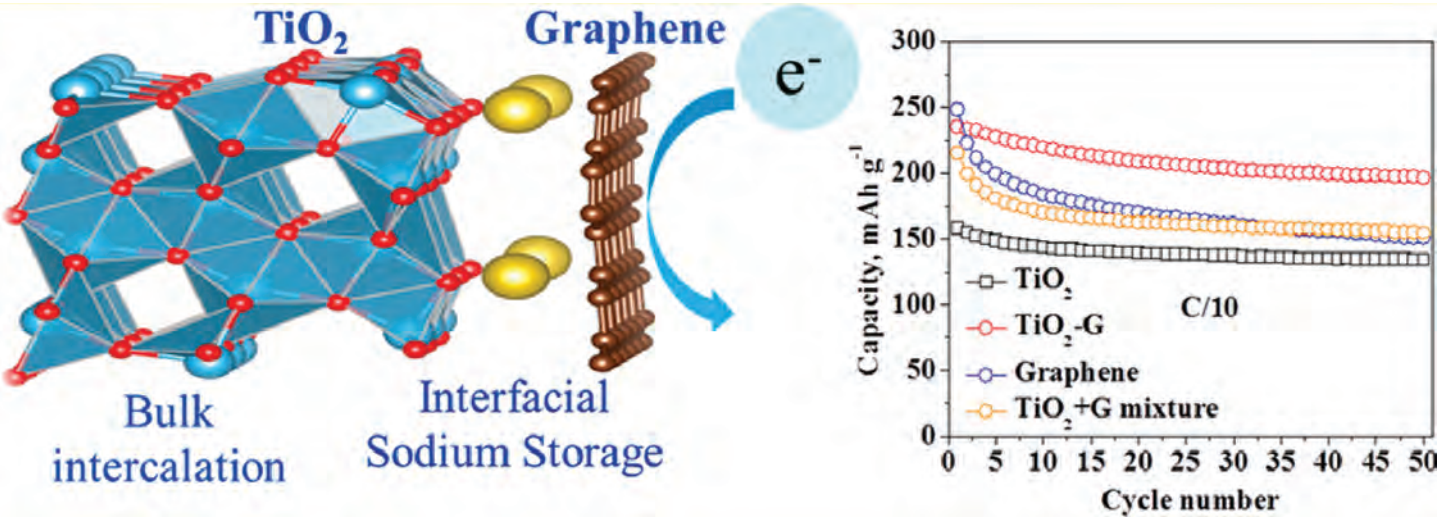

Fig. 1. Left: Model of a titania nanocrystal (blue and red) electrostatically attracted to a graphene sheet (brown). This strong attraction leads to better sodium ion storage both in the titania lattice and at the interface between the nanocrystal and graphene. (Sodium shown in yellow). Right: Ultrahigh capacity and long-term cycle stability are observed for a coin cell with the titania-graphene hybrid (red) as the anode.

bonds were observed, indicating that nanocrystals are not chemically attached to the graphene.

Intercalation of sodium ions was examined with HEXRD, taken in situ at multiple points in a charge/discharge cycle. During initial discharging, the HEXRD pattern did not change, thus the researchers propose the interfacial sodium leaves first. A subsequent decrease in integrated intensity signified a loss in crystallinity, likely from the outer shell of nanocrystals as sodium ions leave the lattice. This change was also accompanied by a downshift in the $NaxTiO_2$ peak, confirming a change in sodium intercalation.

Density functional theory calculations of the binding energy for sodium on a titania surface demonstrated that the presence of electrostatically attracted graphene stabilizes sodium ions by lowering their binding energy. The binding energy continues to decrease as more sodium ions are added. Thus, more sodium ions can be stabilized on the titania surface when graphene is present. Similar binding energy calculations showed that Li^+, K^+, Mg^{2+}, and Al^{3+}, are also stabilized on titania by graphene.

As sodium storage mechanisms are debated in the literature, there is a clear need to correlate structure with behavior. Unravelling ion storage mechanisms, as demonstrated by this research, can guide design of better battery materials. For the three-dimensional titania-graphene hybrid studied here, both intercalation and interfacial storage play a role in boosting performance. This results in a promising anode material and a general strategy for developing advanced battery systems.

— Amanda Grennell

See: Gui-Liang Xu[1], Lisong Xiao[2], Tian Sheng[3], Jianzhao Liu[1], Yi-Xin Hu[1,4], Tianyuan Ma[1], Rachid Amine[1], Yingying Xie[1], Xiaoyi Zhang[1], Yuzi Liu[1], Yang Ren[1], Cheng-Jun Sun[1], Steve M. Heald[1], Jasmina Kovacevic[2], Yee Hwa Sehlleier[2], Christof Schulz[2], Wenjuan Liu Mattis[5], Shi-Gang Sun[3], Hartmut Wiggers[2]*, Zonghai Chen[1]**, and Khalil Amine[1]***, "Electrostatic Self-Assembly Enabling Integrated Bulk and Interfacial Sodium Storage in 3D Titania-Graphene Hybrid," Nano Lett. **18**, 336 (2018). DOI: 10.1021/acs.nanolett.7b04193
Author affiliations: [1]Argonne National Laboratory, [2]University of Duisburg-Essen, [3]Xiamen University, [4]University of North Carolina, [5]Microvast Power Solutions
Correspondence: * hartmut.wiggers@uni-due.de, ** zonghai.chen@anl.gov, *** amine@anl.gov

The authors gratefully acknowledge support from the U.S. Department of Energy (DOE) Vehicle Technologies O ce. Research at State Key Lab of Xiamen University was funded by National Natural Science Foundation of China (Grant 21321062). Part of this work has been funded from the European Union's Horizon 2020 Research and Innovation Programme, under Grant 646121 (NanoDome). L.S.X. acknowledges the financial support of "Programm zur Forderung des exzellenten wissenschaftlichen Nachwuchses" from University of Duisburg-Essen. The authors also thank the support from Clean Vehicles-U.S.-China Clean Energy Research Center. This research used resources of the Advanced Photon Source, a U.S. Department of Energy (DOE) Office of Science User Facility operated for the DOE Office of Science by Argonne National Laboratory under contract number DE-AC02-06CH11357.

Visualizing Degradation in Lithium-Ion Batteries

For our devices to become faster, cheaper, and longer-lived, improvements in batteries are crucial. Lithium-ion (Li-ion) batteries have high energy density, low self-discharge, no need for priming, and low maintenance relative to other rechargeable battery types. Connected in a parallel circuit, lithium-ion batteries can power electric cars; singly, they keep our personal electronics humming. The Curiosity rover has been exploring Mars since August 6, 2012, powered by two rechargeable lithium-ion batteries connected to solar panels. Nevertheless, one major downside to lithium-ion batteries is capacity fade, in which the amount of charge a battery delivers at the rated voltage decreases with use. To learn how to slow the processes that cause batteries to degrade and capacity to fade, researchers employed high-brightness x-rays from the APS to image and model a battery's inner workings at the nanoscale. Their work revealed the primary cause of degradation in the battery, providing a new materials model for minimizing capacity fade in Li-ion batteries and helping to create the next generation of powerful of these important batteries.

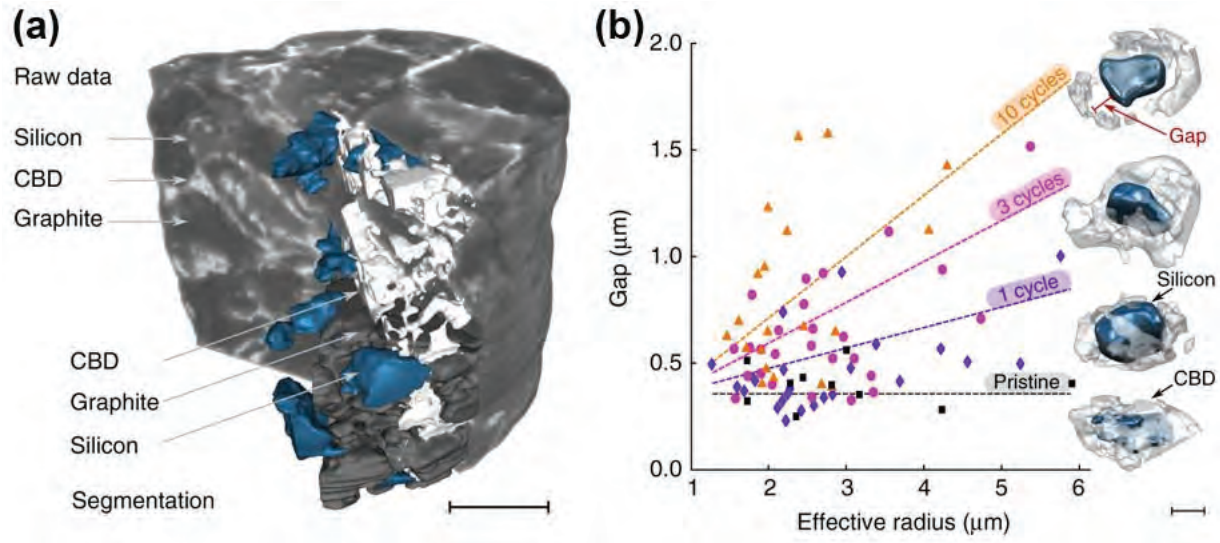

Electrodes in Li-ion batteries contain electrochemically active silicon particles that are mechanically stabilized by a polymeric binder. Nanoscale carbon black particles, dispersed in the binder, form a network that electrochemically connects the active particles. During each charge-discharge cycle, the silicon particles undergo small volumetric changes. Expansion and contraction cause them to detach from the carbon black-binder network, which causes capacity fade.

Nano-imaging battery degradation is challenging since spatial resolution that is high enough leads to a weak signal and weak image contrast. For this work, researchers from ETH (Switzerland) and Argonne replaced 50 vol% of the carbon black with carbon-coated copper nanoparticles, which provided better contrast but did not change the electrochemical performance of the material. The researchers used scanning electron microscopy and attenuation-based transmission x-ray tomographic microscopy at the XSD 32-ID-C beamline of the APS to obtain three-dimensional electrode microstructures (Fig. 1).

Imaging allows researchers to depict the detachment process during cycling. In a pristine battery, silicon particles are surrounded by the carbon-black binder domain. After one cycle, volumetric changes in the silicon particles shrink, which causes a gap between the silicon particles and the carbon black-binder domain. After three cycles the silicon particles begin to crack and a solid electrolyte interphase (SEI) layer forms on the silicon surface, causing additional mechanical deformation. After 10 cycles, the binder and the graphite particles remain in contact but the silicon particles are almost completely detached. Ultimately, each silicon particle detaches and can no longer participate in electrochemical reactions.

This work showed that the dominant degradation mechanism is the electric isolation of the silicon particles: the larger the distance between the silicon particle surface and its environment, the greater the rate of electrochemical degradation. Modelling simulates how detachment and capacity fade are impacted by different parameters, such as active particle size, viscoelastic criteria of the composite electrode, adhesion between the silicon and the carbon black-binder domain, and the SEI growth rate. However, it is difficult to determine the optimal parameters for reducing capacity fade: smaller silicon particles undergo smaller volumetric changes and so are less likely to detach, but since smaller particles have greater surface area to volume, there is an increase in other reactions.

Imaging reveals the structure of these networks in porous electrodes. It helped researchers building a new model determine how to minimize degradation and other undesirable traits. By visualizing and quantifying the detachment of silica in a carbon black-binder, materials engineers can choose active particle size, binder type, and the use of electrolyte additives to optimize the desired traits. Improving these transport characteristics together with the mechanical properties is a key step for better performance in next-generation battery electrodes.

— Dana Desonie

< Fig. 1. Transmission x-ray tomographic microscopy. (a) Tomographic raw data of a pristine silicon-graphite electrode shown with multi-phase segmentation, whereby the silicon particles (blue), the graphite particles (dark gray), the carbon black-binder domain (light gray), and the pore space can be distinguished. Scale bar: 15 µm. (b) Average gap between the surface of a silicon particle and the corresponding carbon black-binder domain as a function of the respective particle effective radius. The data have been acquired in electrodes in the pristine state (black squares) and in fully delithiated electrodes after one cycle (purple diamonds), after three cycles (magenta circles), and after ten cycles (orange triangles). Gaps increase with increasing cycle number and increasing silicon effective particle radius, which is confirmed by renderings of individual particles extracted from the segmented tomographic data. The dotted lines are included to guide the eye. Scale bar: 5 µm. From Müller et al., Nat. Commun. **9**, 2340 (2018)

See: Simon Müller[1], Patrick Pietsch[1], Ben-Elias Brandt[1], Paul Baade[1], Vincent De Andrade[2], Francesco De Carlo[2], and Vanessa Wood[1]*, "Quantification and modeling of mechanical degradation in lithium-ion batteries based on nanoscale imaging," Nat. Commun. **9**, 2340 (2018). DOI: 10.1038/s41467-018-04477-1
Author affiliations: [1]ETH, [2]Argonne National Laboratory
Correspondence: * vwood@ethz.ch)

The authors gratefully acknowledge funding from the European Research Council, the Commission for Technology and Innovation, and the Competence Center for Energy and Mobility. This research used resources of the Advanced Photon Source, a US Department of Energy (DOE) Office of Science User Facility operated for the DOE Office of Science by Argonne National Laboratory under Contract No. DE-AC02-06CH11357.

An Abundant and Inexpensive Alternative for Energy Storage in Li-Ion Batteries

One of the key components of a lithium-ion (Li-ion) battery is the cathode, which forms its positive electrode. The cathodes of most Li-ion batteries currently incorporate metals that are problematic. One alternative is to use the abundant and inexpensive element manganese (Mn). Up until now, manganese-rich cathodes have been limited in their ability to carry enough charge. In a quest to enhance their performance, researchers demonstrated a unique design incorporating manganese in a cathode that is durable and inexpensive, yet exhibits the requisite high-charge capacity and high-energy output exhibited by conventional cathodes. High-energy x-ray measurements performed at the APS and at the Advanced Light Source (ALS) were crucial in revealing the chemical changes in the new cathode material during repeated charge-discharge cycles. Further development of this new material could provide a safer, less-toxic, and cheaper alternative for the cathodes of next-generation Li-ion batteries.

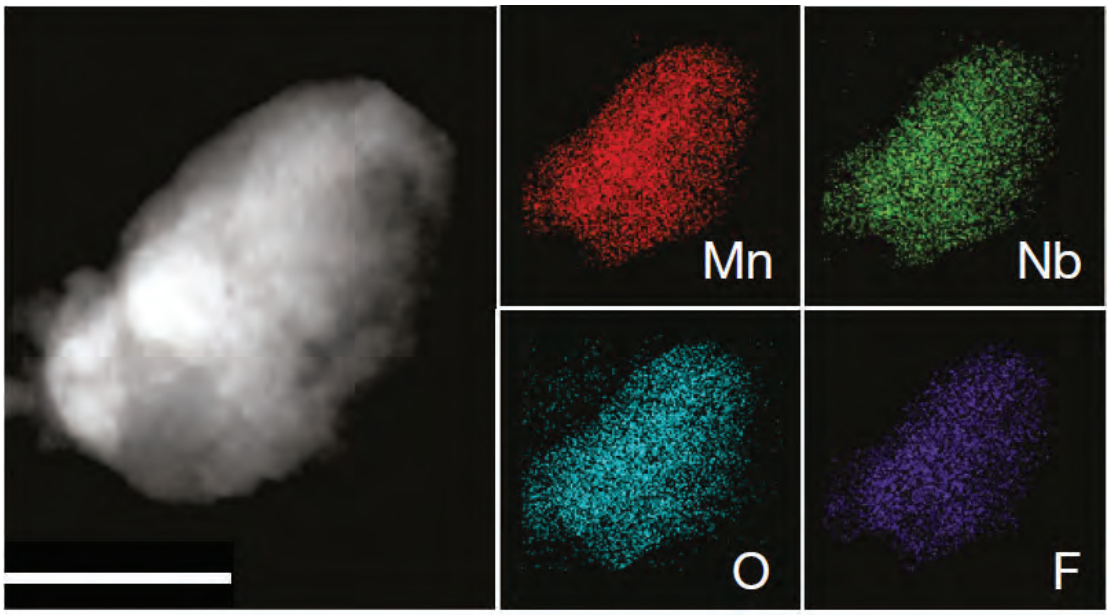

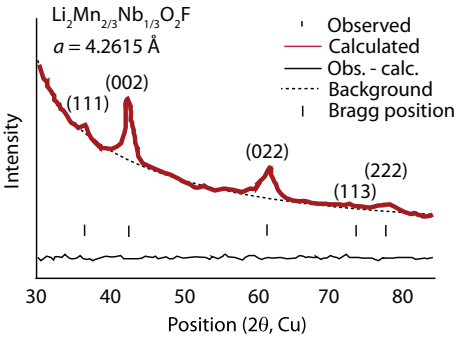

Fig. 1. The electron micrograph in the left panel shows a single particle of the manganese-based cathode material ($Li_2Mn_{2/3}Nb_{1/3}O_2F$) that was examined in this study. Scale bar at bottom of the panel represents 100 nm. The four smaller, color-coded panels were produced from energy-dispersive spectroscopy mapping of the compound's elemental distribution (EDS). The vivid colors in each panel indicate that the compound's manganese (Mn), niobium (Nb), oxygen (O), and fluorine (F) were evenly distributed. Inset lower right: The x-ray diffraction pattern of $Li_2Mn_{2/3}Nb_{1/3}O_2F$. From J. Lee et al., Nature **556**, 185 (12 April 2018). © 2018 Springer Nature Publishing AG

Due to their high energy density and other favorable characteristics, Li-ion batteries are increasingly in demand for vehicles, power grid energy storage, and numerous consumer products. Remarkably, nearly all Li-ion batteries use cathodes that incorporate the metals nickel (Ni) and/or cobalt (Co). Unfortunately, these two metals have several drawbacks. Nickel, and in particular cobalt, are relatively expensive and rare, and mining their ore presents heightened environmental risks. In spite of these drawbacks, efforts to eliminate these metals from Li-ion batteries have been largely unsuccessful. Cobalt, for instance, remains a key cathode ingredient because it is

very efficient at retaining the layered structure used in conventional Li-ion cathodes over many charge-discharge cycles.

In the search for substitute cathode materials, in 2014 a team of researchers (which included researchers in this study) found a novel material that retained its high-storage capability even when its ions became fully disordered, making a structure similar to the mineral rocksalt. Using computational modeling to understand this unusual behavior, the researchers realized they had found a potentially very large class of novel cathode materials with diverse and rich chemistry. Most importantly, by avoiding the layered structure required by conventional Li-ion high-performance cathodes, cobalt and nickel could be eliminated.

Research into disordered rocksalt as a viable high-performance cathode material has steadily progressed. Its cation structure (its distribution of positive ions) supports the insertion of a variety of elements that can be utilized to tune the material's performance characteristics. Manganese, for one, is abundant, environmentally-friendly, inexpensive, and features good safety behavior.

The oxidation state of the elements in a Li-ion cathode can be crucial to how it interacts with the battery's lithium ions as they flow in-and-out over repeated charge-discharge cycles. The oxidation state of an element indicates the sharing of electrons within a compound. Changes in an element's or compound's oxidation state occur as part of reduction-oxidation (or redox) reactions, which are ubiquitous in nature and in batteries. A simple example involves the sodium chloride in table salt. A redox reaction between these two elements occurs when a sodium atom gives up an outer electron to a chlorine atom; the sodium is said to be oxidized while the chlorine is reduced.

The research team in this study from the University of California, Berkeley, and the Massachusetts Institute of Technology focused on finding a material that allows manganese to vary its oxidation state between +2 and +4, which is referred to as a "double redox" state and abbreviated Mn^{2+}/Mn^{4+}. This combination, which is similar to the Ni^{2+}/Ni^{4+} double redox present in many layered cathodes, allows for high charge and energy capacity in the battery.

A compound containing lithium, manganese, oxygen, fluorine, and niobium was utilized, with the chemical formula $Li_2Mn_{2/3}Nb_{1/3}O_2F$. The addition of fluorine limited over-oxidation of the compound during repeated charge-discharge cycles. The compound structure was gauged using x-ray diffraction, while spectral analysis indicated the distribution of its constituent elements (Figure 1). To track changes in the oxidation state of the manganese, the team and colleagues from Argonne and Lawrence Berkeley National Laboratory (LBNL) carried out x-ray absorption near-edge structure measurements at XSD beamline 20-BM-B at the APS, and soft x-ray absorption spectroscopy measurements on beamline 8.0.1.1 (iRIXS end station) of the ALS at LBNL. The combined data indicated that the compound exhibited high performance characteristics (charge and power capacity), with the oxidation state of the manganese cycling as anticipated.

The researchers demonstrated that common and inexpensive elements can be utilized to achieve high performance in disordered rocksalt cathodes, which could eliminate the need for cobalt and nickel in Li-ion batteries. Several large research programs on disordered rocksalts are currently under way, as the nature of this material provides ample opportunity for improving its performance as a cathode material. — Phil Koth

See: Jinhyuk Lee[1*‡], Daniil A. Kitchaev[2], Deok-Hwang Kwon[1], Chang-Wook Lee[3], Joseph K. Papp[1], Yi-Sheng Liu[4], Zhengyan Lun[1], Raphaële J. Clément[1], Tan Shi[1], Bryan D. McCloskey[1,4], Jinghua Guo[4,5], Mahalingam Balasubramanian[3], and Gerbrand Ceder[1,4**], "Reversible Mn^{2+}/Mn^{4+} double redox in lithium-excess cathode materials," Nature **556**, 185 (12 April 2018).
DOI: 10.1038/s41586-018-0015-4
Author affiliations: [1]University of California, Berkeley, [2]Massachusetts Institute of Technology, [3]Argonne National Laboratory, [4]Lawrence Berkeley National Laboratory, [5]University of California, Santa Cruz ‡Present address: Massachusetts Institute of Technology
Correspondence: * jinhyuk@mit.edu, ** gceder@berkeley.edu

Work by J.L., D.A.K., D.-H.K., Z.L., R.J.C., and G.C. was supported by Robert Bosch, LLC, Umicore Specialty Oxides and Chemicals, and the Assistant Secretary for Energy Efficiency and Renewable Energy, Vehicle Technologies Office, of the U.S. Department of Energy (DOE) under Contract No. DE-AC02-05CH11231, under the Advanced Battery Materials Research Program. This research used resources of the Advanced Photon Source, a U.S. DOE Office of Science User Facility operated for the DOE Office of Science by Argonne National Laboratory under contract No. DE-AC02-06CH11357. Work at the Advanced Light Source is supported by DOE Office of Science-Basic Energy Sciences User Facilities under contract no. DE-AC02-05CH11231. Work at the Molecular Foundry was supported by the DOE Office of Science-Basic Energy Sciences, under contract No. DE-AC02-05CH11231. J.K.P. acknowledges the U.S. National Science Foundation Graduate Research Fellowship (grant no. DGE-1106400). B.D.M. acknowledges support from the Assistant Secretary for Energy Efficiency and Renewable Energy, Vehicle Technologies Office, U.S. DOE, under contract no. DEAC02-05CH11231, under the Advanced Battery Materials Research Program.

The Variables Controlling Thin-Film Structure in Organic Solar Cells

Organic solar cells (OSCs) are photovoltaic devices that convert sunlight into electricity. OSCs consist of multiple thin layers of organic (carbon-based) soft-matter materials that are lightweight, flexible, inexpensive, and generally less resource-intensive to manufacture than the inorganic and silicon-based variety. The so-called active layers within OSCs are responsible for converting light into electricity. To boost the light-conversion efficiency of OSCs, researchers manipulate the morphology (the distribution, quantity, etc.) of the light-capturing molecules within their active layers. However, improvements in OSC morphology attained in the laboratory are sometimes difficult to carry over into mass-produced devices. Much of this difficulty is due to differences in fabrication: While scientists typically utilize spin-coating to create OSC prototypes, manufacturers employ entirely different techniques. To better translate laboratory advances into mass-produced OSCs, researchers undertook to quantify the many variables affecting OSC fabrication during the spin-coating process using the APS. These x-ray experiments allowed researchers, for the first time, to precisely delineate the many variables affecting the morphological properties of different OSC layers during an actual spin-coating process. These new insights will help transition laboratory advancements to the high-volume production of improved organic solar cells.

OSCs can be classified by the light-sensitive compounds they contain: either small-molecule or polymers consisting of long chains of smaller molecular units. Prior to creating an organic solar cell, its light-sensitive compounds (polymers or small-molecule) are suspended within a liquid, which also contains various chemical additives and solvents. To create a single active layer of an organic solar cell, the liquid is spread out into a thin film where it begins to dry and crystallize. This basic process is followed whether in the laboratory or the factory.

Spin-coating is typically employed to produce OSC prototypes. In this technique, a substrate is placed on a revolving turntable where small amounts of liquid are deposited. The liquid is quickly and evenly distributed over the substrate surface and dries to form a solid thin film. Repeated cycles of liquid application and solidification build up the multiple layers within an OSC. The basic spin-coating process is depicted in Fig. 1.

The researchers conducted grazing incidence wide-angle x-ray scattering (GIWAXS) experiments at the XSD 8-ID-E beamline of the APS, and solution-scattering experiments at the DND-CAT 5-ID-B,C,D beamline at the APS in order to observe and measure the primary aspects of OSC fabrication during an actual spin-coating process. This non-destructive x-ray method developed in collaboration with Joel Strzalka (XSD) to install an inline spin coater at beamline 8-ID-E provided real-time, high-resolution data about thin-film formation. For instance, the GIWAXS data revealed details of the liquid-to-crystalline phase transition, and the intermediate phases that the film encountered before its final morphology (structure) was achieved. Optical reflectance was used to gauge thin-film thickness.

This study analyzed three light-sensitive compounds (which are considered semi-conducting materials) to produce OSCs. Two were polymers, the semi-crystalline P3HT and less-crystalline PTB7, and the crystalline small-molecule p-DTS(FBTTh$_2$)$_2$. Three solvents and four processing additives were also surveyed. A large variety of thin films was subsequently generated using different combinations of the semi-conducting compounds, solvents, and additives.

As individual solutions were spin-cast, they dried to form a solid film. During this process, two-dimensional GIWAXS images were recorded every 10 msec over a period of a few hundred seconds to 2 h. These “molecular

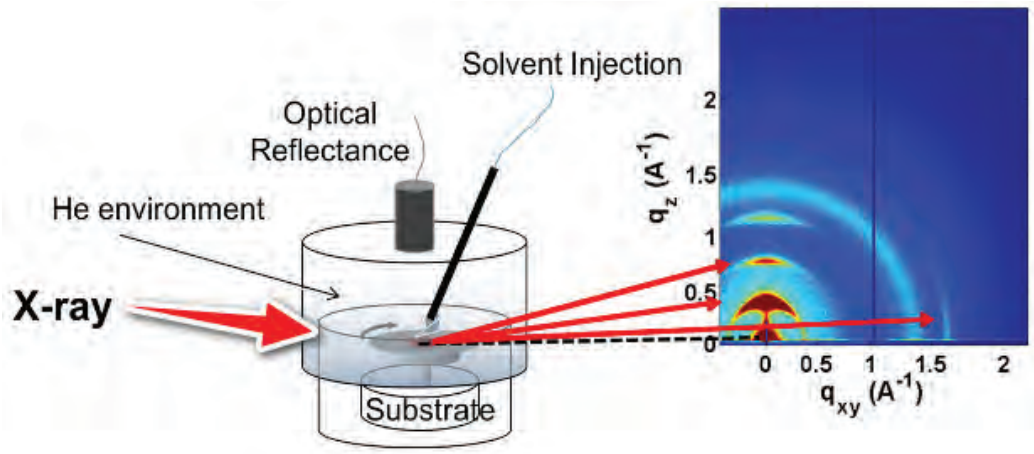

Fig. 1. Basic experimental setup is shown at the center of the figure. Using an actual spin-coating device allowed thin layers of organic solar cells to be spin-cast while both high-resolution x-ray (GIWAXS) and optical measurements were made of the process. "He environment" refers to the helium atmosphere within the spin-cast device. Colored image at right illustrates GIWAXS data of a thin film during spin-casting.

movies" helped to identify the role of solvents and additives in tuning the evolution of domain sizes, crystalline phases, and molecular packing corresponding to each stage of thin-film formation. Data from one of the molecular movies is summarized in Fig. 2.

Analysis of the GIWAXS data yielded a couple of general conclusions about the formation of thin films produced by a spin-coating process. First, the solvents used in some experiments led to a too-rapid onset of thin-film crystallization that sometimes locked in multiple crystalline orientations and/or divergent crystalline structures, resulting in lowered solar cell efficiency. Second, for thin films processed using both solvents and additives, the evolving structure of the thin film proceeds step-wise over a duration lasting anywhere from seconds to hours, depending upon the specific conditions involved.

These results will aid in rationally defining the conditions for desirable morphologies in high-performance OSCs, an approach sometimes referred to as "intelligent processing", and should have a direct impact on advancing efficient and effective OSC industrial production. The experimental results should also be helpful to materials engineers in the design of next-generation OSCs.

— Phil Koth

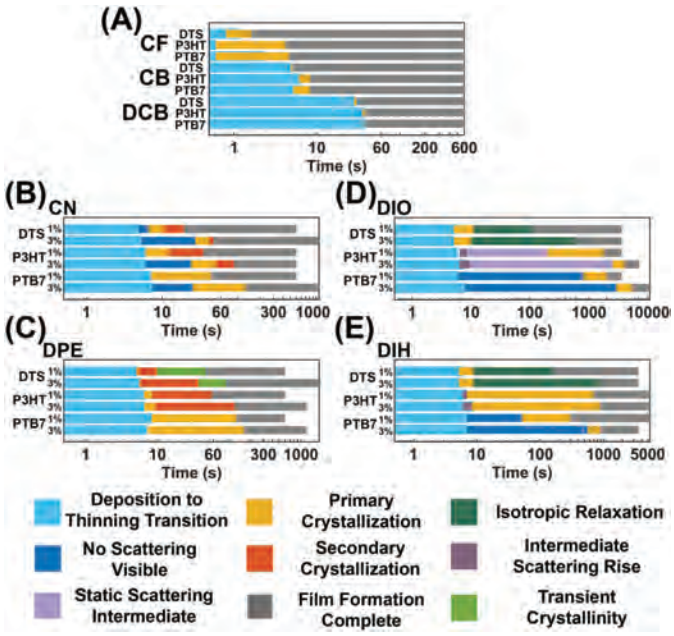

Fig. 2. The various bar graphs summarize the morphological evolution for all single-solvent and all additive-containing chlorobenzene (CB) films. Chlorobenzene was one of three solvents studied. The different bar graphs are grouped according to the particular additives that were used in order to easily compare film evolution across the three light-converting semiconductors, namely the two polymers P3HT and PTB7, and the small-molecule p-DTS(FBTTh2)2 (identified simply as "DTS"). Different phases of formation (the deposition-to-thinning transition, primary and secondary crystallizations of the thin-films, etc.) are labeled according to the colored key-code at bottom. Gray areas in the bars indicate that no further evolution was detected.

See: Eric F. Manley[1,2], Joseph Strzalka[2], Thomas J. Fauvell[1,2], Tobin J. Marks[1]*, and Lin X. Chen[1,2]**, "In Situ Analysis of Solvent and Additive Effects on Film Morphology Evolution in Spin-Cast Small-Molecule and Polymer Photovoltaic Materials," Adv. Energy Mater. **8**, 1800611 (2018). DOI: 10.1002/aenm.201800611
Author affiliations: [1]Northwestern University, [2]Argonne National Laboratory
Correspondence: ** l-chen@northwestern.edu or lchen@anl.gov
* t-marks@northwestern.edu

E.F.M., T.J.F., T.J.M. and L.X.C. acknowledge financial support from the Argonne-Northwestern Solar Energy Research Center, an Energy Frontier Research Center funded by the U.S. Department of Energy (DOE) Office of Science-Basic Energy Sciences under Award Number DE-SC0001059, and by the U.S. DOE Office of Science-Basic Energy Sciences under Award Number DE-FG02-08ER46536. E.F.M. was also supported by the Qatar NPRP Grant 7-286-1-046. DND-CAT is supported by the Northwestern University, E.I. DuPont de Nemours & Co., and The Dow Chemical Company. Solution scattering data were collected using an instrument funded by the National Science Foundation under Award Number 0960140. This research used resources of the Advanced Photon Source, a U.S. DOE Office of Science User Facility operated for the DOE Office of Science by Argonne National Laboratory under Contract No. DE-AC02-06CH11357.

Watching Fuel-Cell Catalysts in Action

Fuel cells could power the next Industrial Revolution, as these devices can very efficiently combine hydrogen and oxygen to produce electricity with only water coming out of the "exhaust pipe." Fuel cells are often compared to batteries, as both convert the energy released by a chemical reaction into electric power. But fuel cells don't need to be recharged; they will deliver electricity as long as fuel (hydrogen) is supplied. To run the chemistry inside a fuel cell, catalysts are needed to facilitate the energy-releasing reactions. However, most catalysts do not perform as well as expected when they are inserted into a fuel cell. To help figure out why, a team of researchers developed an x-ray method for observing the catalyst behavior in a working fuel cell. As a demonstration of this *in operando* technique, the team investigated several catalysts utilizing extreme-brightness x-rays from the APS. Their experiments revealed structural changes of the catalyst material that disrupt its chemical functioning. The results could help in finding catalysts that are more structurally stable under fuel cell conditions.

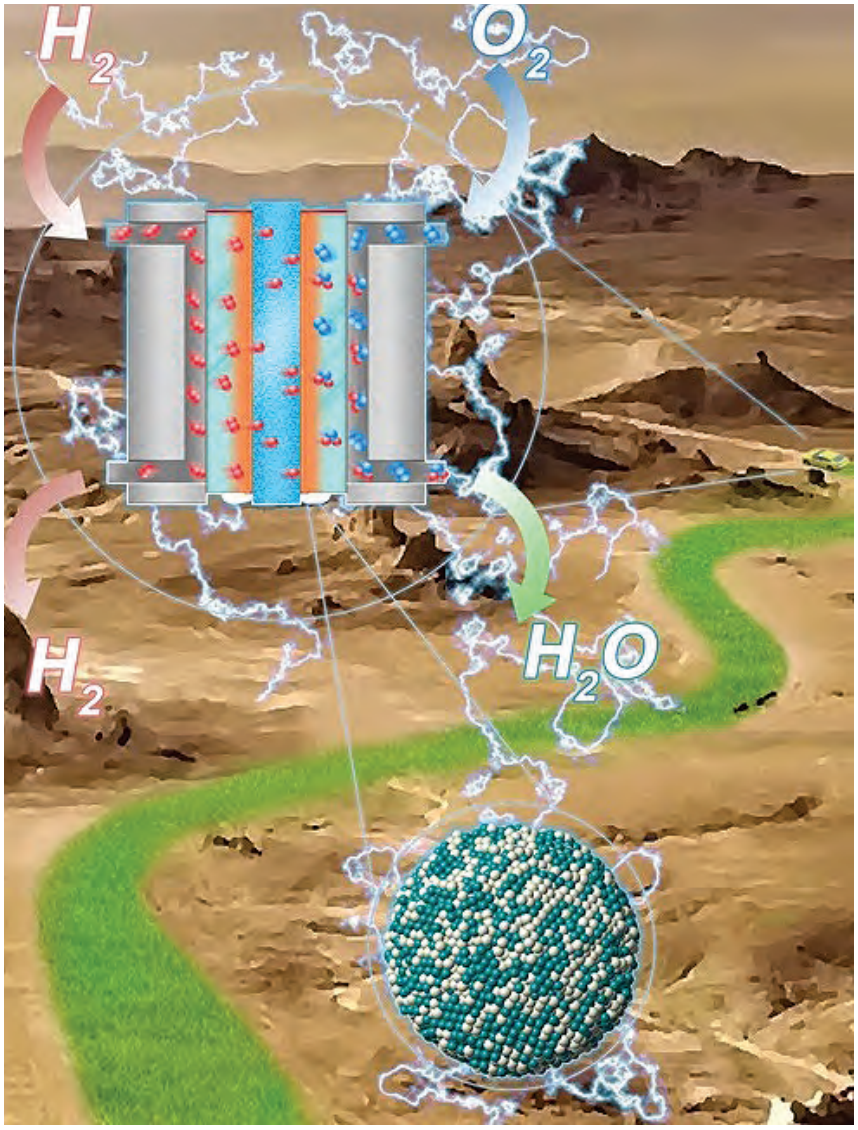

Of the many types of catalysts that are available, one of the best options is platinum, but this noble metal is very rare and expensive. For this reason, scientists are exploring the potential of nanoalloy catalysts, which could provide the same chemical boost as platinum but at a fraction of the cost. These nanoalloys contain noble metals (e.g., platinum and palladium), transition metals (e.g., nickel and iron), and post-transition metals (e.g., tin and lead). In laboratory tests, nanoalloy catalysts have proven to be as effective as pure platinum nanoparticles in driving the oxygen reduction reaction (ORR), which is a key step in the fuel-cell chemical process.

Despite their positive lab results, nanoalloy catalysts tend to underperform — dropping roughly 70% in efficiency — when exposed to actual operating conditions. This decline is in part due to the highly corrosive environment inside fuel cells. To understand what's going on at the atomic level, researchers from Central Michigan University, the State University of New York at Binghamton, and Argonne have developed an experimental approach for catalyst characterization that combines energy dispersive x-ray spectroscopy (EDS) and high-energy total x-ray scattering. The EDS measurements allow the researchers to track composition changes, while the scattering data helps to identify atomic structure evolution. This is the first time these two techniques have been combined to study a catalyst during its operation.

The team investigated two types of nanoalloy catalysts: one made of palladium and tin (Pd-Sn) and the other consisting of platinum, nickel, and copper (Pt-Ni-Cu). The researchers placed these catalysts in a specially-designed fuel cell that was optimized for x-ray studies. They then exposed each sample to the high flux of focused, high-energy x-rays (100 keV) from the XSD 1-ID-C x-ray beamline at the APS. Analyzing the data required techniques for removing the effect from the cell's hardware.

< Fig. 1. Fuel cells could power a greener future by combining hydrogen fuel (H_2) with oxygen (O_2) from the atmosphere to produce electricity, with the only by-product being water (H_2O). The fuel cell's chemical reactions require a catalyst, depicted in the magnified inset as a nanoalloy particle composed of several thousand green and white atoms. A new high-energy x-ray method has been developed for tracking structural changes of the catalyst during fuel-cell operation. Credit: Valeri Petkov (Central Michigan University)

Once this background was subtracted, the EDS and scattering observations revealed the structural and chemical evolution of the sparse collection of catalyst particles with approximately 1-minute time resolution and 30-μm spatial resolution. While collecting the x-ray data, the team also monitored the electric current produced by the cell, allowing them to relate changes in the catalyst to the fuel-cell performance.

The combined measurements revealed structural transformations of the nanoalloy catalysts that reduce their ORR activity — and thus downgrade the efficiency of the fuel cell. The researchers recognized that, in part, these structural transformations are caused by fast diffusion of atomic species within the catalyst particles. One way to minimize this diffusion is to choose a different shape for the nanometer-sized particles that make up the catalyst. In this vein, the team tried using cube-shaped particles, whose geometry conformed with their cubic-type atomic structure. They found that the atoms in these nanocubes were limited in how they could hop to a new position, and this restricted hopping resulted in slower diffusion and a more stable structure during fuel-cell operation.

The group is planning more experiments — using EDS and scattering data — to explore other promising families of catalysts for proton exchange membrane fuel cells. The hope is that the information collected on structural changes will guide the development of better catalysts that can make fuel cells more commercially viable.

— Michael Schirber

See: Valeri Petkov[1]*, Yazan Maswadeh[1], Yinguang Zhao[2], Aolin Lu[2], Hannah Cronk[2], Fangfang Chang[2], Shiyao Shan[2], Haval Kareem[2], Jin Luo[2], Chuan-Jian Zhong[2], Sarvjit Shastri[3], and Peter Kenesei[3], "Nanoalloy catalysts inside fuel cells: An atomic-level perspective on the functionality by combined *in operando* x-ray spectroscopy and total scattering," Nano Energy **49**, 209 (2018). DOI: 10.1016/j.nanoen.2018.04.049
Author affiliations: [1]Central Michigan University, [2]State University of New York at Binghamton, [3]Argonne National Laboratory
Correspondence: * petko1vg@cmich.edu

This work was supported by U.S. Department of Energy (DOE)-Basic Energy Sciences Grant DE-SC0006877. This research used resources of the Advanced Photon Source, a U.S. DOE Office of Science User Facility operated for the DOE Office of Science by Argonne National Laboratory under Contract No. DE-AC02-06CH11357.

High Shear Stress on Submicron Scales

Catastrophic failure of pliable (ductile) materials under tensile strain is typically preceded by the appearance of shear bands, narrow layers of the material distorted by intense shear strain. Working at the APS, researchers employed x-ray diffraction measurements with high spatial resolution to follow the evolution of shear bands in a stainless steel. The interplay of external strain with the local orientation of grains and their lattice structure leads to extremely high strain gradients on submicron scales near shear bands. The resulting high local shear stress may induce material damage and even trigger premature failure. Failure studies of austenitic steel have shown that as the number of loading cycles increases, failure tends to occur sooner than standard models would imply. The results of this new study suggest that intensified shear strain on very small scales may have an outsize effect in determining the behavior of the sample as a whole, and provide new information about potentially catastrophic, fatigue-induced failure of critical materials.

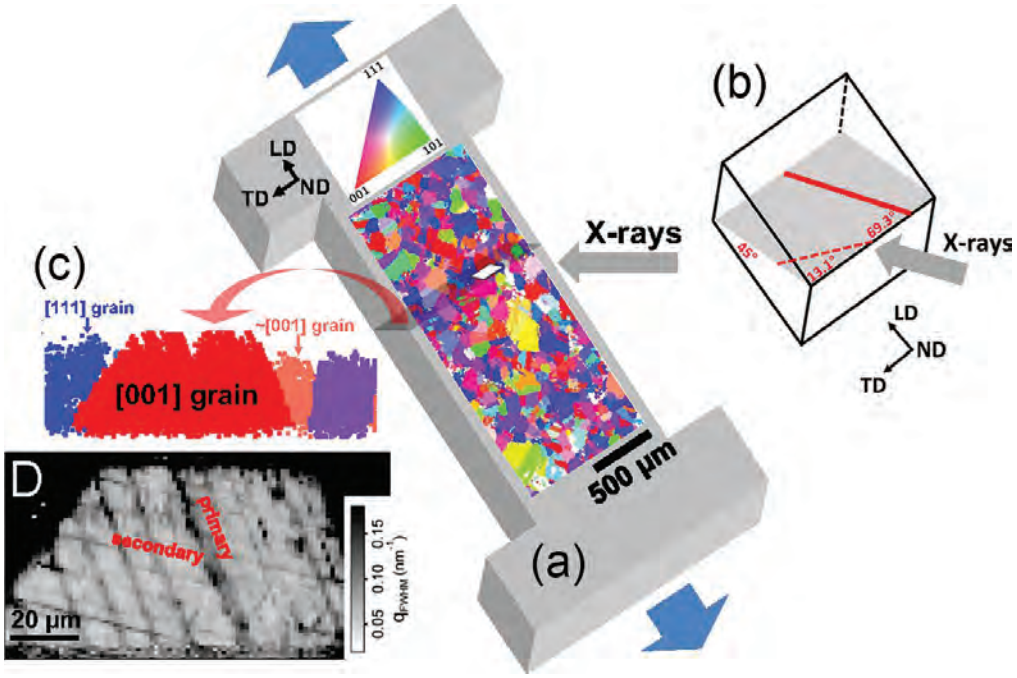

After a material has been subjected to strain, examination of shear bands by transmission electron microscopy reveals details of dislocations and other changes in the affected area. But such post-mortem studies do not reveal how the shear band structure came to be, nor indicate how it will evolve under further strain. Researchers from the University of Science and Technology Beijing (China), Argonne, Northeastern University (China), Chongqing University (China), and the Georgia Institute of Technology used a three-dimensional (3-D) x-ray diffraction technique with micrometer-scale resolution to characterize shear patterns in a sample of steel and to examine those shear patterns changed in real time when greater stress was applied.

The team studied austenitic stainless steel (24 wt% nickel, 20 wt% chromium, 6.2 wt% molybdenum, 0.22 wt% nickel), an alloy known to develop a network of planar slip bands when subjected to fatigue cycling. Such planar slip bands are a common type of microscopic shear band formed in metal alloys. At the XSD 34-ID-E APS beamline, the team obtained two-dimensional diffraction patterns utilizing an x-ray beam of 0.5-μm diameter, and simultaneously derived data in the third dimension by using a differential aperture technique to scan along the beam direction. The combination of high-intensity x-rays with high-speed data collection makes it possible to perform 3-D mapping of lattice structures and overall grain orientations over significant sample volumes (Fig. 1).

The study began by putting a steel sample through 29,000 loading cycles with a tensile strain amplitude of 0.3%. The 3-D x-ray diffraction technique applied to a small "dog bone"-shaped piece cut from the steel revealed grains of about 100 μm in size, randomly oriented, and also showed lattice dislocations within those grains. The researchers identified one grain in particular that showed a striking pattern of shear bands aligned in two distinct directions. The geometry of these bands corresponded to the primary and secondary dislocation slip planes of the steel. In principle, such a grain would be expected to show tensile strain in the direction of the applied strain and compressive strain perpendicularly, but further examination of the grain revealed a mix of tensile and compressive strains near shear bands whose directions were influenced by the orientation of the grain lattice. Where the primary and secondary shear bands crossed, tensile and compressive strains ran into each other, creating intense local shear that varied on a submicron scale.

The team then continued the experiment by performing *in situ* x-ray diffraction measurements as the sample was subjected slowly to an additional 0.5% strain. The pattern of tensile and compressive strains in the selected grain changed considerably. Close scrutiny of locations where the shear bands intersected showed that, although the macroscopic increase in strain on the sample was modest, local shear strain changed by much larger amounts as the grain, influenced by its setting in the steel's polycrystalline matrix, tried to adjust to the new conditions. Computer simulations of strain distribution in the material supported this interpretation and were consistent with the magnitude of the observed local shear.

— David Lindley

< Fig. 1. Experiment setup and results of *in situ* x-ray micro-diffraction (μXRD) testing. (a) Schematic of a tensile specimen cut from a fatigued sample of stainless steel. The specimen is covered with a crystal orientation map of near-surface grains from μXRD measurement. The map is colored by the loading direction (LD) inverse pole figure, with the color scheme shown in the orientation triangle. (b) Schematic of an incident x-ray slicing plane (in gray) at 45° to the sample surface. The specimen orientations are represented in terms of the LD, surface normal direction (ND), and transverse direction (TD). The primary and secondary shear bands are represented by the solid and dashed lines, respectively. (c) A crystal orientation map slicing along the x-ray beam direction, measured with polychromatic x-rays. The [001]//LD grain is red. (d) A map of the (480) diffraction peak full width half maximum of the same [001] grain shown in (c), measured with monochromatic x-rays. The primary and secondary shear bands, as marked in the map, can be readily identified according to the gray scale. All measurements have a spatial resolution of ~1 μm in three dimensions.

See: Runguang Li[1], Qingge Xie[1], Yan-Dong Wang[1]*, Wenjun Liu[2]**, Mingguang Wang[3], Guilin Wu[4], Xiaowu Li[3], Minghe Zhang[1], Zhaoping Lu[1], Chang Geng[3], and Ting Zhu[5]***, "Unraveling submicron-scale mechanical heterogeneity by three-dimensional X-ray microdiffraction," Proc. Natl. Acad. Sci. USA **115**(3), 483 (January 16, 2018). DOI: /10.1073/pnas.1711994115
Author affiliations: [1]University of Science and Technology Beijing, [2]Argonne National Laboratory, [3]Northeastern University, [4]Chongqing University, [5]Georgia Institute Technology
Correspondence: * ydwang@ustb.edu.cn, ** wjliu@anl.gov, *** ting.zhu@me.gatech.edu

The authors acknowledge financial support from National Natural Science Foundation of China Grants 51231002, 51471032, and 51527801; the Fundamental Research Funds for the Central Universities Grant 06111020; and the fundamental research fund at the State Key Laboratory for Advanced Metals and Materials (2014Z-01). Q.X. acknowledges financial support from the China Postdoctoral Science Foundation (2014M560884) and Fundamental Research Funds for the Central Universities (FRF-TP-14-047A1). This research used resources of the Advanced Photon Source, a U.S. Department of Energy (DOE) Office of Science User Facility operated for the DOE Office of Science by Argonne National Laboratory under Contract No. DE-AC02-06CH11357.

Topological Excitations from a Vibrating Crystal Lattice

It has long been known that the properties of materials are crucially dependent on the arrangement of the atoms that make up the material. For example, atoms that are further apart will tend to vibrate more slowly and propagate sound waves more slowly. Now, researchers from Brookhaven National Laboratory have used the APS to discover "topological" vibrations in iron silicide (FeSi). These topological vibrations arise from a special symmetrical arrangement of the atoms in FeSi and endow the atomic vibrations with novel properties such as the potential to transmit sound waves along the edge of the materials without scattering and dissipation. Looking to the future, one might envisage using these modes to transfer energy or information within technological devices.

In quantum mechanics, atomic motions in crystals are described in terms of vibrational modes called phonons. Similar to electrons moving in metals, phonons can also propagate through materials. The detailed properties of these excitations determine many of the thermal, mechanical and electronic properties of the material. In 2017, part of the current collaborative team from the Chinese Academy of Science theoretically predicted the existence of the topological phonons in transition metal monosilicides. As shown in Fig. 1, these topological phonons are formed by two Dirac-cones with different slopes and are protected by symmetry. Since the mathematical description of each Dirac-cone is intimately related to the famous Weyl-equation that was originally proposed in high-energy physics, these topological phonons are consequently called double-Weyl excitations.

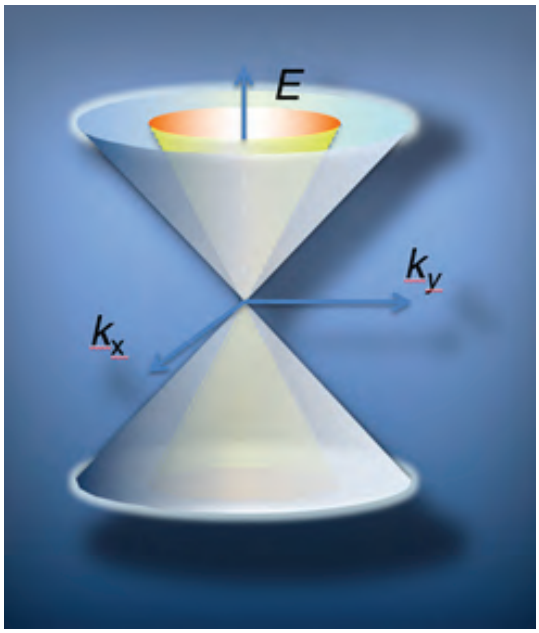

Fig. 1. Schematic view of the double-Weyl phonon dispersion. Image: Brookhaven National Laboratory

To experimentally prove the existence of these novel phonon excitations, one needs a technique that can probe the full bulk phonon dispersion with high energy and momentum resolution. The HERIX beamline at the XSD 30-ID,B,C beamline of the APS is among the very few machines in the world in which this experiment can be done. The research team performed comprehensive inelastic x-ray scattering measurements on high-quality, single-crystal FeSi and successfully resolved double Weyl phonon dispersions beautifully consistent with theoretical predictions.

See: H. Miao[1*], T.T. Zhang[2,3], L. Wang[2,3], D. Meyers[1], A.H. Said[4], Y.L. Wang[1], Y.G. Shi[2], H.M. Weng[2,5], Z. Fang[2,5] and M.P.M. Dean[1**], "Observation of Double Weyl Phonons in Parity-Breaking FeSi", Phys. Rev. Lett. **121**, 035302 (18 July 2018).
DOI: 10.1103/PhysRevLett.121.035302
Author affiliations: [1]Brookhaven National Laboratory, [2]Institute of Physics, Chinese Academy of Sciences, [3]University of Chinese Academy of Sciences, [4]Advanced Photon Source, [5]Collaborative Innovation Center of Quantum Matter
Correspondence: * hmiao@bnl.gov, ** mdean@bnl.gov

This material is based upon work supported by the U.S. Department of Energy (DOE)-Basic Energy Sciences, Early Career Award Program under Award No. 1047478. Work at Brookhaven National Laboratory was supported by the U.S. DOEOffice of Science-Basic Energy Sciences under Contract No. DE- SC0012704. Support was provided by the National Key Research and Development Program of China (Grant No. 2016YFA0300600), the National Natural Science Foundation of China (Grants No. 11674369 and No. 11774399), and the Chinese Academy of Sciences (XDB07020100 and QYZDB-SSW-SLH043). This research used resources of the Advanced Photon Source, a U.S. DOE Office of Science User Facility operated for the DOE Office of Science by Argonne National Laboratory under Contract No. DE-AC02-06CH11357.

A New Material Could Store Data in 3-D with Light

An intense research effort is under way worldwide on replacing electrons with photons in solid-state switching devices. An international research team reported the outcome of experiments at the APS: the first-ever confirmed synthesis of an osmium sulfur dioxide ammine complex and the testing of its properties for solid-state optical switching. Such switches have applications in optical data storage and quantum computing, but their adoption has been hampered by interactivity problems between light and the material.

Single crystals of the $[Os(NH_3)_5(SO_2)]$-$[Os(NH_3)_5(HSO_3)]Cl_4$, complex were prepared, collected by vacuum filtration, washed with CH_3OH, and dried. By means of synchrotron x-ray diffraction at the ChemMatCARS beamline 15-ID-B,C,D of the APS, the crystal structures of the dark- and light-induced states were then captured at a temperature of 100 K. The results showed that stimulation of the crystal with 505-nm light for 2.5 h induced a metastable state, whereby 9.3% of the SO_2 ligands with one bond to the osmium (η^1-SO_2) was photo-converted to SO_2 with two bonds (η^2-SO_2), as shown in Fig. 1a. The remaining 90.7% retained the dark-state structure. This photoisomerization caused little structural deformation to the crystal. These results suggest that osmium can better stabilize sulfur dioxide photoisomers than its ruthenium counterparts, which had been previously investigated.

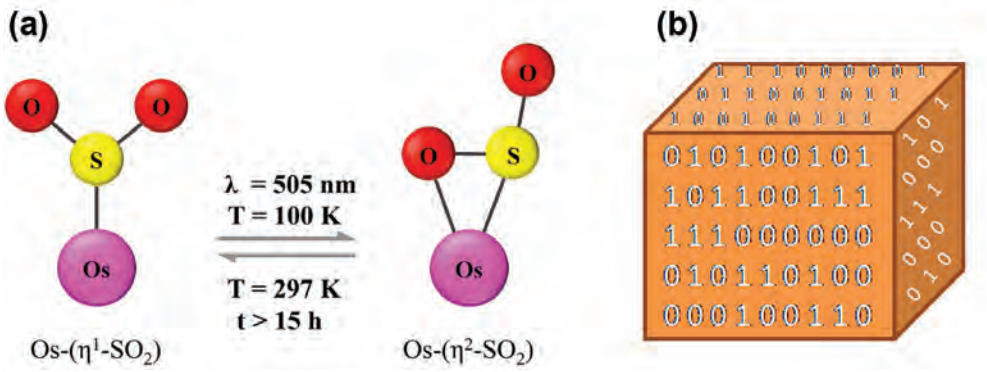

Fig. 1. (a) Thermal reversibility of SO_2 photoconversion in osmium sulfur dioxide ammine complex and (b) prospective application of crystalline photo-isomers in 3-D optical data storage.

The authors, from the University of Cambridge (UK), the Rutherford Appleton Laboratory (UK), Argonne, and The University of Chicago, further investigated the optical properties of the osmium sulfur dioxide ammine complex by means of concerted optical spectroscopy and microscopy, experiments that were performed at the Argonne Center for Nanoscale Materials.

The dark-state single crystal was found to undergo photoinduced "bleaching" upon 2.5 h of exposure to 505-nm light at 100 K, where the optical absorption decreased by about 50% across most of the visible spectrum. The SO_2 ligands appeared to be responsible for this bleaching effect. After warming to 275 K over 15 h, the crystal exhibited progressive recovery of its optical absorption, but had not yet returned to the panchromatic absorption of the dark-state single crystal. By contrast, their previously investigated metastable ruthenium sulfur dioxide complex counterparts had returned to the dark state in a few seconds or minutes. These results demonstrate that the above osmium sulfur dioxide complex is a rare example of a material that can be developed into a promising osmium-based, solid-state, optical switch.

For example, one can imagine the dark-state SO_2 ligand (η^1-SO_2) as a 0 and the photoisomer (η^2-SO_2) as a 1 in binary nomenclature. Since the molecular configurational changes in Fig. 1a take place within a single osmium-based crystal, one can then envision this crystal tailored with optically switchable 0s and 1s that express encoded forms of data – thus achieving three-dimensional optical data storage, as illustrated in Fig. 1b.

This capability is significant because bottom-row transition metals like osmium stand to offer linkage photoisomerism with the greatest photoconversion levels and

"Store" cont'd on page 47

Dominant Deformation Mechanisms in Shocked Single Crystals

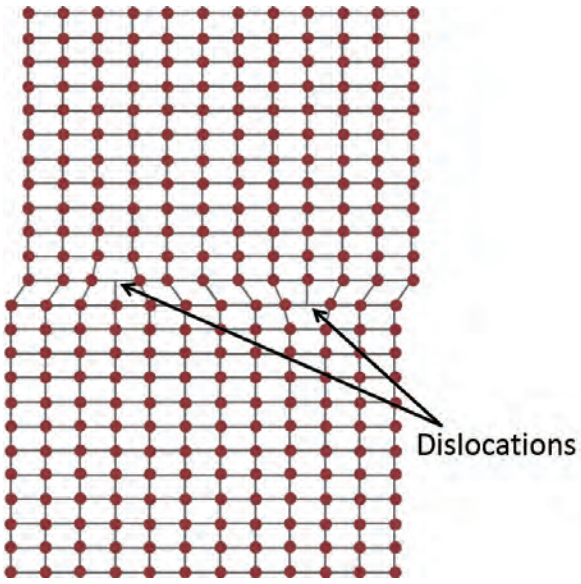

Fig. 1. Conceptual drawing of dislocations in a crystal lattice.

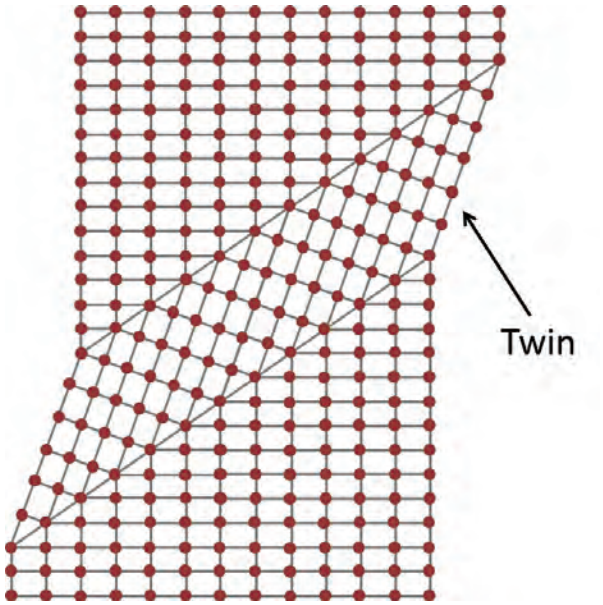

Fig. 2. Conceptual drawing of twinning in a crystal lattice.

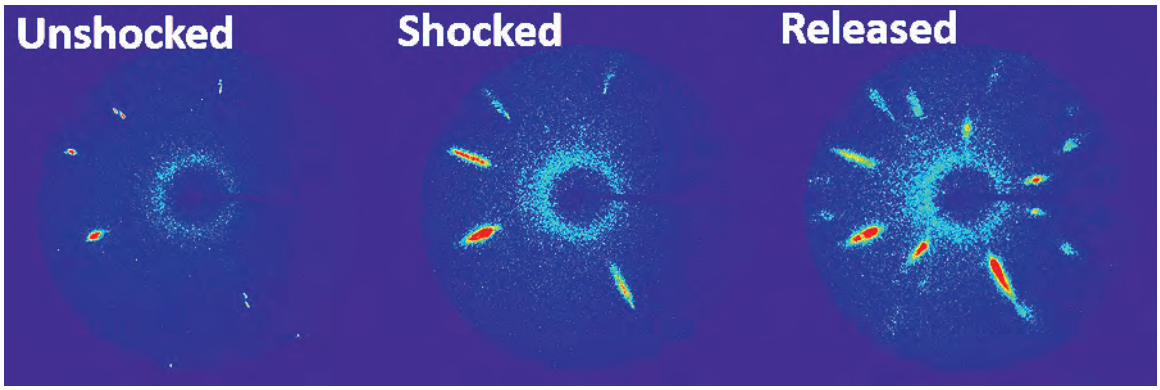

Fig. 3. X-ray diffraction patterns for magnesium single crystals. The three different patterns correspond to unshocked (ambient) Mg, Mg shock-compressed along the c-axis of the crystal, and Mg after release of stress from the shock-compressed state. The additional spots appearing in the third pattern are due to twinning in the Mg crystal.

Despite almost 50 years of plane shockwave studies of single crystals, understanding the specific inelastic deformation mechanisms operating during shock compression remains a long-standing scientific need. Real-time microscopic measurements of deformation mechanisms during shockwave loading stand at the forefront of dynamic compression science. Single-crystal studies are ideal for examining fundamental mechanisms governing plastic deformation mechanisms such as twinning and dislocation slip under shockwave loading, in part because studying shock waves along different crystal axes allows for selective activation of different deformation mechanisms. Such experiments aid in the development of models that can accurately predict material response to dynamic compression, a quality that is essential when developing or improving materials that will be exposed to high-velocity impacts and explosions. In pursuit of this critical information, researchers working at the APS carried out real-time x-ray diffraction (XRD) experiments that were the first *in situ* observations of active deformation mechanisms in shock-compressed and released single crystals.

Employing a combination of synchrotron x-rays with plate-impact experiments at the DCS 35-ID x-ray beamline at the APS, the researchers from Washington State University studied the effect of flat polycarbonate projectiles impacting magnesium (Mg) crystals along the c axis (Fig. 1). These XRD measurements were used to examine the deformation mechanisms during shock compression and during subsequent release. Using broadband x-rays, four real-time x-ray diffraction patterns of (~ 100-ps duration; 153.4 ns between frames) were recorded during each plate impact experiment.

A possible deformation mechanism during both shock compression and release along the c axis is pyramidal $\langle \mathbf{c} + \mathbf{a} \rangle$ dislocation slip. In addition, two types of deformation twinning are possible: during shock compression (longitudinal stress > lateral stress), contraction twins or double twins are possible; during release (lateral stress > longitudinal stress) extension twins are possible. Changes in the measured XRD patterns were utilized to determine which of these possible deformation mechanisms were active. Figures 1 and 2 display conceptual drawings of these mechanisms.

Laue diffraction spots observed in the shocked state were similar to those observed before the Mg was impacted, but the spots were elongated. New Laue spots appeared only after the shock wave reflected as a release wave. These new Laue spots arise due to changes in the crystal orientation within twinned regions of the crystal. Thus, these measurements revealed that deformation twinning occurred only during release.

In order to further understand which deformation mechanisms were active during compression and release, a comparison of XRD simulations incorporating crystallographic changes was made with the measured XRD patterns. This revealed that dislocation slip is the dominant cause of deformation during compression, while during release extension twinning was activated.

These results provide important insight into the micromechanisms governing inelastic deformation in shocked single crystals, and how those micromechanisms relate to the material response at different length scales. Moreover, time-resolved XRD measurements during both shock compression and release in a single experiment will be valuable for gaining insight into shock-induced inelastic deformation for a range of technologically relevant materials, such as hexagonal-close-packed metals and body-centered-cubic metals. — Gwenevier Johnson

See: Stefan J. Turneaure, P. Renganathan, J. M. Winey, and Y. M. Gupta*, "Twinning and Dislocation Evolution during Shock Compression and Release of Single Crystals: Real-Time X-Ray Diffraction," Phys. Rev. Lett. **120**, 265503 (2018).
DOI: 10.1103/PhysRevLett.120.265503
Author affiliation: Washington State University
Correspondence: * ymgupta@wsu.edu

Yoshi Toyoda, Travis Volz, Paulo Rigg, and the DCS staff are thanked for assistance with the plate impact experiments. This publication is based upon work supported by the U.S. Department of Energy (DOE), National Nuclear Security Administration (NNSA) under Award No. DE-NA0002007. This publication is also based upon work performed at the Dynamic Compression Sector supported by the DOE/NNSA under Award No. DE-NA0002442 and operated by Washington State University. This research used resources of the Advanced Photon Source, a DOE Office of Science User Facility operated for the DOE Office of Science by Argonne National Laboratory under Contract No. DE-AC02-06CH11357.

Flexible Crystals Can Heal Themselves

From a materials science perspective, crystals have several advantages. They are well-ordered rigid systems, but that rigidity also makes them brittle and vulnerable to cracking. On the other hand, soft materials such as hydrogels can bend and stretch without mechanical failure, but lack the molecular order and rigidity of crystals. Now scientists using the APS have shown they can create a hybrid material that combines the advantages of each, making crystals that are able to expand to greater than five times their original volume. Giving crystals the ability to expand and self-heal could lead to a range of applications, for instance trapping biomolecules within a crystal lattice for later drug delivery or for creating a crystalline scaffold for catalysis. The researchers are also using this method with other polymer compositions and protein lattices to see how generalizable their method is and derive some structural principles.

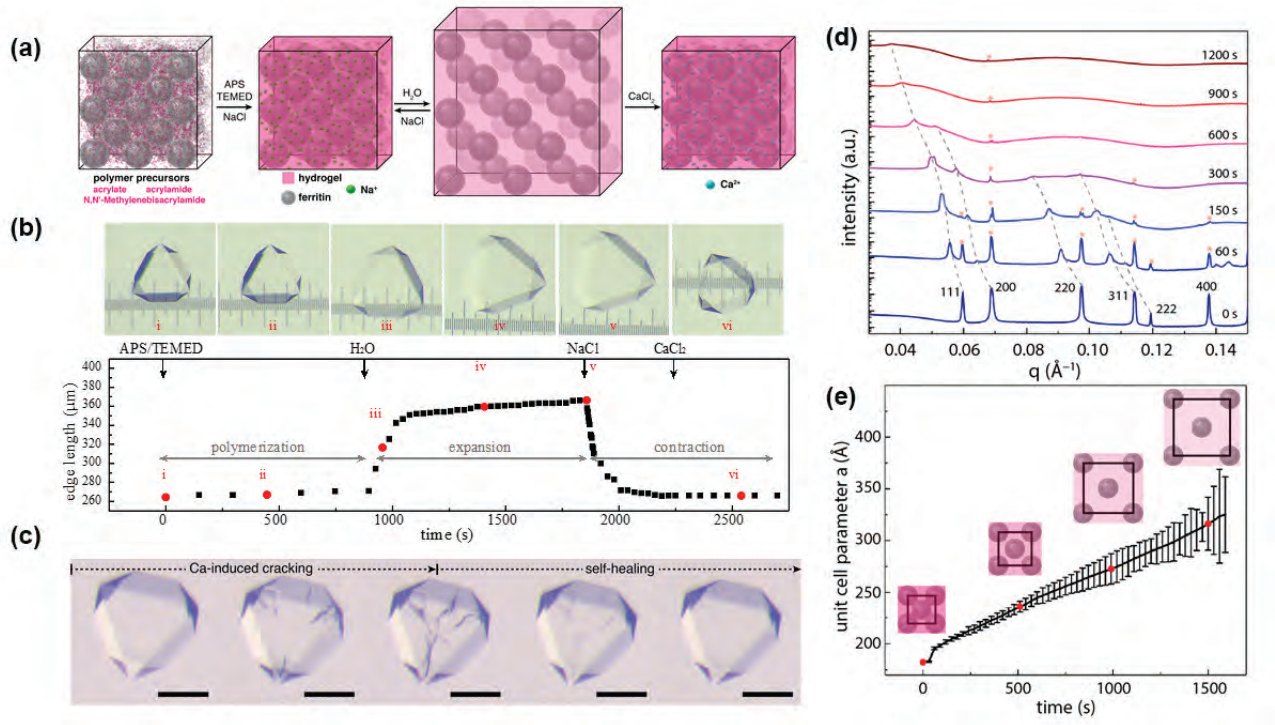

Fig. 1. A schematic (a) shows the formation, expansion, and contraction of ferritin-hydrogel hybrids, while a graph analyzing microscope images (b) shows the expansion and contraction of a single crystal in solutions of different ionic strength. Additional microscope images (c) show cracks caused by the addition of calcium, followed by self-healing of the crystal. SAXS profiles (d) allow researchers to calculate changes in the unit cell parameters of the lattice (e).

The researchers started with ferritin, a protein that stores iron in human cells. They selected the protein because it crystallizes into a lattice with nanometer-sized pores. They filled the pores with polymer precursors, then polymerized the mixture, creating superabsorbent poly(acrylate-acrylamide) copolymer hydrogels throughout the crystal lattice. The polymer interacts with the protein through noncovalent bonds, allowing it to maintain connectivity of the lattice during expansion.

In low ionic strength solutions, the polymer absorbed water and expanded at the same rate in all three dimensions. The expansion separated individual ferritin cages, while the connections between protein and polymer maintain some of the periodic order throughout the crystal lattice. This was true even when the proteins were separated by approximately 50 Å, which is a large distance on the atomic scale.

The researchers in this study from the University of Califirnia, San Diego, then added concentrated salt solutions — either sodium chloride or calcium chloride — to the system. The increase in ionic strength of the solution caused the polymers to expel water and shrink, drawing the proteins back into their original positions. The contacts between the proteins — mediated by calcium — formed anew, and the crystal regained its original structure. However, the addition of salt would often create an uneven spatial gradient, leading one side of the crystal to contract more quickly leading to the formation of cracks. Normally, cracks in crystals are not able to repair themselves, but the polymer network in these materials pulls everything back into place and repairs the crystal lattice.

To observe the changes in crystallinity during expansion and contraction of the hybrid materials, the research team performed small-angle x-ray scattering (SAXS) at the DND-CAT beamline 5-ID-D of the APS. That beamline includes a syringe injector that allowed team to add water or salt during x-ray data collection to monitor the changes in the lattice in real-time. The SAXS technique enabled them to examine the long-range periodicity of the hybrid material, while separate high-angle x-ray diffraction measurements let them look at changes in the positioning of individual atoms in the contracted lattice. They also performed similar SAXS measurements on single crystals at beamline 4-2 at the Stanford Synchrotron Radiation Lightsource at the SLAC National Accelerator Laboratory.

The technique the team employed may provide a way to improve protein crystallography, which is widely used to characterize proteins. Often, protein crystals lack perfect periodicity, which impairs scientists' ability to obtain high-resolution structures. Integrating the ferritin crystals with the hydrogel, then putting them through an expansion and contraction cycle, rearranged the lattice and improved the structural order, allowing for higher-resolution diffraction images. — Neil Savage

See: Ling Zhang, Jake B. Bailey, Rohit H. Subramanian, Alexander Groisman, and F. Akif Tezcan*, "Hyperexpandable, self-healing macromolecular crystals with integrated polymer networks," Nature **557**, 86 (3 May 2018). DOI: 10.1038/s41586-018-0057-7
Author affiliation: University of California, San Diego
Correspondence: * tezcan@ucsd.edu

This work was primarily funded by the U.S. Department of Energy (DOE) Office of Science-Basic Energy Sciences, Division of Materials Sciences, Biomolecular Materials Program, DE-SC0003844 to F.A.T.). Additional funding was provided by the U.S. National Science Foundation (NSF) (DMR-1602537 to F.A.T. for SAXS studies). DND-CAT is supported by Northwestern University, E.I. DuPont de Nemours & Co., and The Dow Chemical Company; data was collected using an instrument funded by the NSF under Award Number 0960140. The Stanford Synchrotron Radiation Lightsource and the Advanced Photon Source are supported by the DOE Office of Science-Basic Energy Sciences under contracts DE-AC02-76SF00515 and DE-AC02-06CH11357, respectively.

"Store" cont'd from page 43

thermal stability. Proposed future work is to produce chemical derivatives of the osmium sulfur dioxide complex that will generate even higher η^2-SO_2 photoconversion fractions and to search for other types of SO_2 photoisomers in the osmium complex family.

— Joseph E. Harmon

See: Jacqueline M. Cole[1,2,3]*, Jose de J. Velazquez-Garcia[1], David J. Gosztola[3], SuYin Grass Wang[4], and Yu-Sheng Chen[4], "η^2-SO^2 Linkage Photoisomer of an Osmium Coordination Complex," Inorg. Chem. **57**, 2673 (2018).
DOI: 10.1021/acs.inorgchem.7b03032
Author affiliations: [1]University of Cambridge, [2]Rutherford Appleton Laboratory, [3]Argonne National Laboratory, [4]The University of Chicago
Correspondence: * jmc61@cam.ac.uk.

J.M.C. thanks the 1851 Royal Commission of the Great Exhibition for the 2014 Fellowship in Design, hosted by Argonne National Laboratory, where work done was supported by the U.S. Department of Energy (DOE) O ce of Science-Basic Energy Sciences, and used research resources of the Center of Nanoscale Materials and the Advanced Photon Source (APS), O ce of Science User Facilities operated for the DOE O ce of Science by Argonne National Laboratory, supported by the U.S. DOE, all under contract No. DE-AC02-06CH11357. ChemMatCARS Sector 15 is principally supported by the Divisions of Chemistry (CHE) and Materials Research (DMR), U.S. National Science Foundation (NSF), under grant number NSF/CHE-1346572. Use of the PILATUS3 X CdTe 1M detector is supported by the NSF under the grant number NSF/DMR-1531283. J.d.J.V. is indebted to the National Council of Science and Technology of Mexico (CONACyT) and the Cambridge Trust for a Ph.D. Scholarship (217553)

Forging the Links to Building Better Metal Oxides

Metal oxides such as titanium dioxide (TiO_2) are fascinating and versatile substances that can be used in many applications, including photovoltaic devices, batteries, and other vital technologies. But the utility of a particular material for a particular purpose may be limited, and common techniques to chemically "fine tune" their properties to fit specific parameters, such as doping or surface coating, are not always practical or effective. A group of researchers from a diverse set of institutions decided to try a different strategy by cross-linking metal oxide molecules with boron to create clusters of hybrid networks with new chemical and electrical properties and then characterizing the material at the APS. Their work opens possibilities for the precise tailoring of such materials for specific purposes.

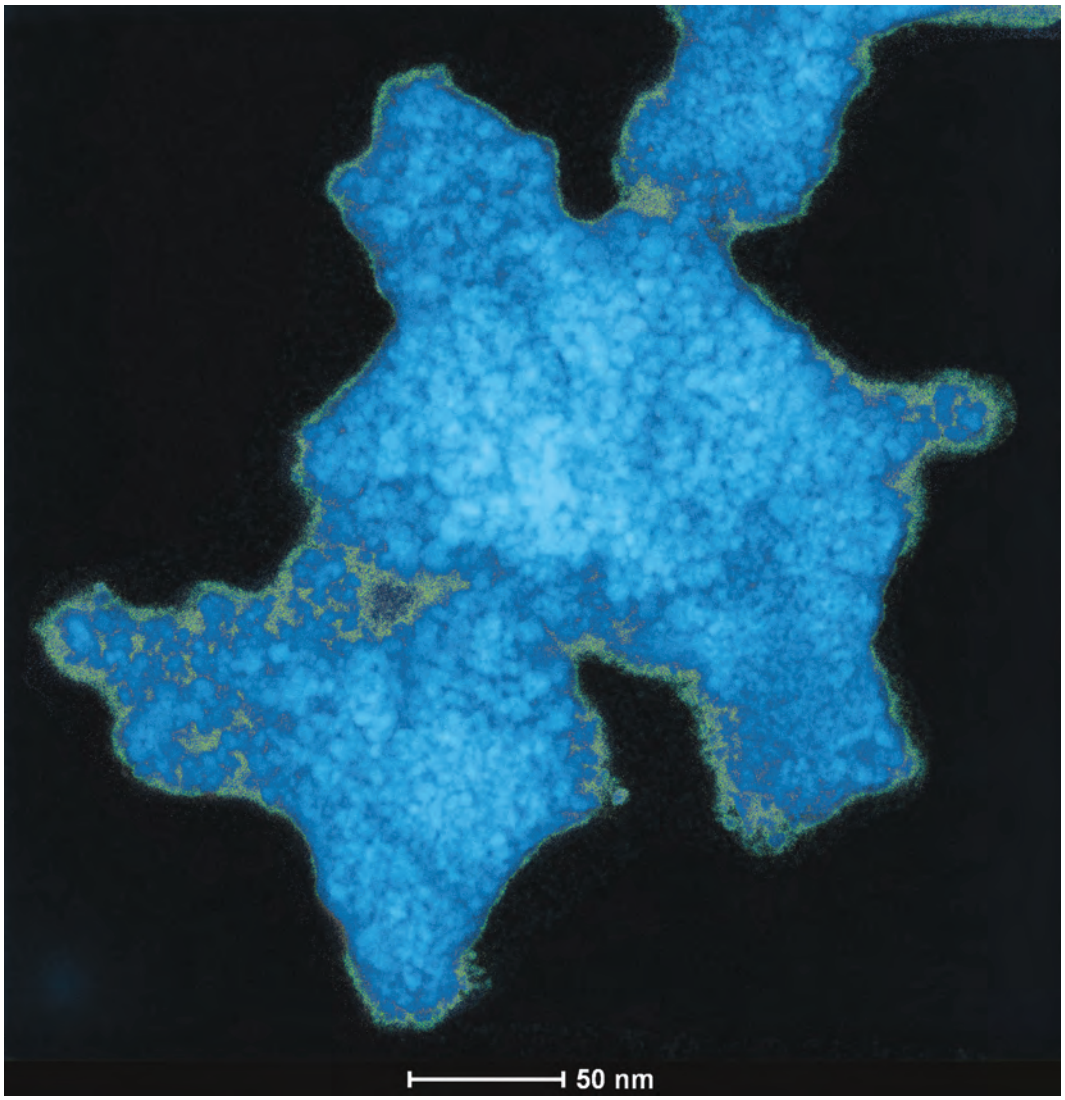

Fig. 1. A scanning transmission electron microscope image of TiO_2 nanoparticles cross-linked with boron-rich clusters.

The team's approach involved identifying a robust boron-containing cluster capable of withstanding the harsh conditions inherent in the cross-linking processes. The researchers from the University of California, Los Angeles, the University of California, Santa Barbara, Cairo University (Egypt), Purdue University, Argonne, and the University of Oregon settled on a three-dimensional aromatic benzene analog, $[N^nBu_4]_2[B_{12}(OH)_{12}]$, which is a derivative of dodecaborate of the $[B_{12}(OH)_{12}]^{2-}$ type. After annealing a bulk sample at 500° C in air, creating a cross-linked polymer of clusters and boron oxide, the researchers combined the substance with titanium tetraisopropoxide, resulting in the formation of a shiny black solid hybrid material. They used various techniques to analyze this material's physical and electrochemical characteristics, including x-ray absorption spectroscopy at the MR-CAT 10-BM-A,B x-ray beamline at the APS, and total scattering data suitable for pair distribution function (PDF) analysis collected at the XSD 11-ID-B beamline at the APS.

Structural analysis of the material utilizing a variety of methods including powder x-ray diffraction, scanning electron microscopy, transmission electron microscopy (Fig. 1), x-ray photoelectron spectroscopy, nuclear magnetic resonance imaging, and PDF showed crystalline anatase TiO_2 in densely embedded nanocrystals. B_{12}-based clusters were also present, leading to the present model of a hybrid molecular boron oxide comprised of cross-linked intact boron clusters and boron oxide, with embedded nanocrystals of anatase TiO_2.

The team next investigated the material's electronic properties. Because dodecaborate derivatives have been previously shown to exhibit pseudo-metallic redox activity, the researchers looked for clusters in redox states. Electroparamagnetic resonance spectroscopy and superconducting quantum interference device magnetometry showed that the material is paramagnetic, which appears to be related to the cross-linked molecular boron oxide material. The material also showed an electron transfer rate considerably higher than that of either anatase or rutile TiO_2, indicating its ability to enhance electronic properties when linked to metal oxides.

To further investigate these characteristics, the experimenters constructed pouch-cell supercapacitors using the material in the active layer. These showed superior capacitance and performance compared to both TiO_2 forms, which appears to be directly related to the cross-linked molecular nature of the hybridized material. Combined with the reduced charge-transfer and ionic diffusion resistance of nanosized TiO_2, these properties could make this material highly desirable for energy storage applications.

The team also examined the hybrid material's potential use in visible light photochemical processes by testing it as a photocatalyst in the decomposition of various water contaminants. Under a low-power LED red-light source, three common dye contaminants showed markedly faster degradation with the new material than with a pristine TiO_2 control. Visible light excitation appears to stimulate electron transfer and generate reactive oxygen species that efficiently break down organic contaminants. The lack of precious metal elements in the new material makes it an even more attractive and inexpensive candidate for such applications.

While the current experiments provide an excellent demonstration of how the properties of common metal oxide materials can be altered and enhanced through molecular cross-linking techniques, the researchers note that further work is needed to better understand the underlying chemistry and enable more exact and controlled modifications. One possibility is to expand the technique with the use of other metal oxides such as ZrO_2. Nevertheless, the significantly enhanced properties achieved in the material synthesized in these experiments makes this relatively simple, room-temperature approach to molecular customization enormously promising, not only for TiO_2 but also other metals and materials. — Mark Wolverton

See: Dahee Jung[1], Liban M.A. Saleh[1], Zachariah J. Berkson[2], Maher F. El-Kady[1], Jee Youn Hwang[1], Nahla Mohamed[1,3], Alex I. Wixtrom[1], Ekaterina Titarenko[1], Yanwu Shao[1], Kassandra McCarthy[1], Jian Guo[1], Ignacio B. Martini[1], Stephan Kraemer[2], Evan C. Wegener[4], Philippe Saint-Cricq[1], Bastian Ruehle[1], Ryan R. Langeslay[8], Massimiliano Delferro[5], Jonathan L. Brosmer[1], Christopher H. Hendon[6], Marcus Gallagher-Jones[1], Jose Rodriguez[1], Karena W. Chapman[5], Jeffrey T. Miller[4], Xiangfeng Duan[1], Richard B. Kaner[1], Jeffrey I. Zink[1], Bradley F. Chmelka[2], and Alexander M. Spokoyny[1]*, "A molecular cross-linking approach for hybrid metal oxides," Nat. Mater. **17**, 341 (April 2018). DOI: 10.1038/s41563-018-0021-9
Author affiliations: [1]University of California, Los Angeles, [2]University of California, Santa Barbara, [3]Cairo University, [4]Purdue University, [5]Argonne National Laboratory, [6]University of Oregon
Correspondence: * spokoyny@chem.ucla.edu

A.M.S. thanks the University of California, Los Angeles, Department of Chemistry and Biochemistry for start-up funds, 3M for a Non-Tenured Faculty Award, and the Alfred P. Sloan Foundation for a research fellowship in chemistry. Z.J.B. was supported by a grant from the BASF Corporation. E.C.W. and J.T.M. were supported by the U.S. National Science Foundation (NSF) Energy Research Center for Innovative and Strategic Transformations of Alkane Resources (CISTAR) under the cooperative agreement no. EEC-1647722. J.I.Z. thanks the Student and Research Support Fund for financial support. R.R.L. and M.D. were supported by the U.S. Department of Energy (DOE), Office of Science-Basic Energy Sciences, Division of Chemical Sciences, Biosciences and Geosciences under Contract DE-AC02-06CH11357. MR-CAT operations are supported by the DOE and the MR-CAT member institutions. This research used resources of the Advanced Photon Source, a U.S. DOE Office of Basic Energy Sciences and Office of Science User Facility, operated for the DOE Office of Science by Argonne National Laboratory under contract no. DE-AC02-06CH11357.

Engineering Metal Alloys that are Less Susceptible to Failure

Although crucial to modern life, metal alloys can fail, possibly leading to bridge collapse or other disasters. One cause of failure about which little has been understood is hydrogen embrittlement, which occurs when hydrogen from water propagates a crack. In this work, researchers from academia and DOE national laboratories utilized the APS to analyze the micro-structure of a preexisting crack in a nickel superalloy in order to determine the susceptibility of individual grain boundaries to hydrogen embrittlement. By understanding fracture behavior, researchers and industry can better predict metal failure and how to design failure-resistant alloys.

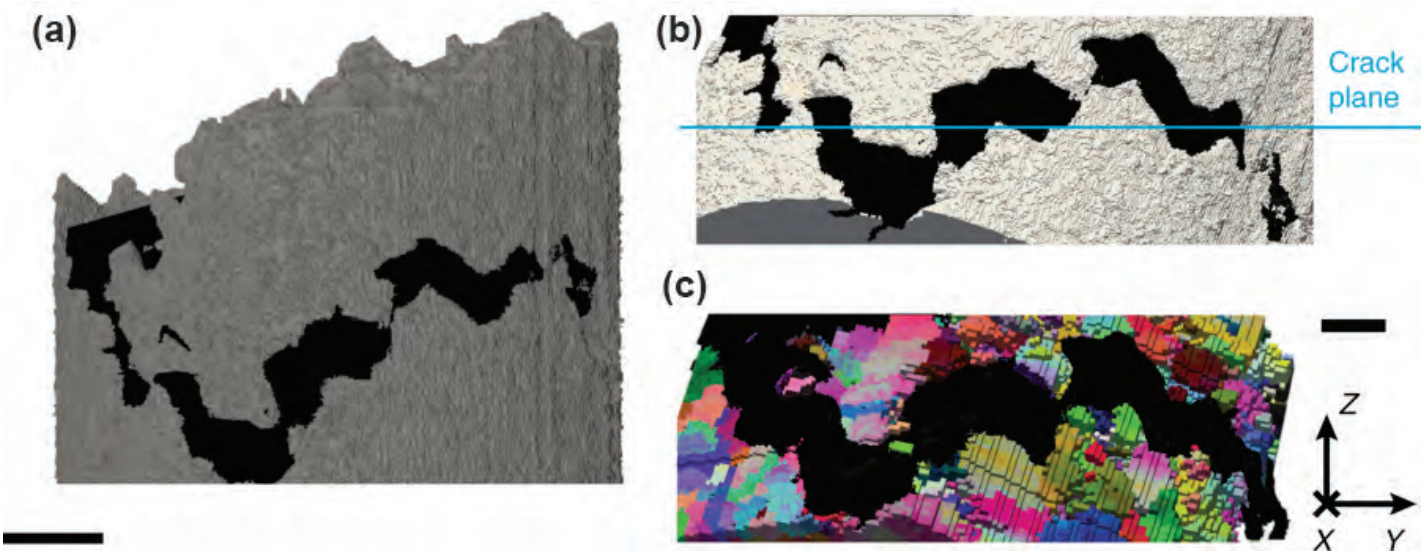

Fig. 1. Three-dimensional sample reconstruction. (a) X-ray attenuation tomography data with metal shown in gray and void space inside the secondary crack shown in black. Scale bar: 200 µm. (b) Isolated section of the XRAT reconstruction with an edge-on view of the nominal crack plane (X–Y), indicated in blue. The nominal crack propagation direction (X) is into the page. (c) High-energy diffraction microscopy (HEDM) reconstruction of the microstructure viewed from the same direction as (b). Each voxel is colored according to the crystallographic orientation of the crystal at that location relative to the laboratory reference frame. Scale bar for (b) and (c): 100 µm. The black void space indicating the space inside the crack was obtained from the XRAT reconstruction and digitally fused with the HEDM data. From J.P. Hanson et al., Nat. Commun. **9**, 3386 (2018).

During the 1989 Loma Prieta earthquake, the upper deck of the eastern span of the San Francisco-Oakland Bay Bridge collapsed. Engineers constructed a new earthquake-resistant span, but before the span opened, they discovered that one-third of the steel rods had fractured due to hydrogen embrittlement (HE). While this discovery averted a potential disaster, the opening of the span was delayed by a few years and the fix was extremely costly.

Metal alloys are made of microscopic crystal grains. When hydrogen, typically from water, infiltrates the metal, it propagates cracks along microstructural defects at grain boundaries. This reduces the cohesive strength of the grain boundaries and allows dislocations to nucleate, resulting in sudden fracture. Since the mechanisms of HE are poorly understood, researchers have been unable to predict which metal alloys will fail. At this time, engineers reduce the chance of metal failure by adding additional material, which was the solution to make the eastern span safe. A better understanding of HE has the potential to save time and realize huge economic benefits.

In the past, engineers learned about metal failure by analyzing the separated pieces of a fractured component. But now there are new tools to help solve this old problem. For this paper, the researchers experimented with nickel (Ni)-base superalloy 725. Although engineered for high strength and corrosion resistance, the alloy is very susceptible to HE fractures. Researchers electrically charged a 1 mm cylindrical sample of alloy 725 with H and loaded it to failure in tension. Within the sample they placed the tip of a large, intergranular secondary fracture. Two non-destructive, synchrotron-based techniques revealed the total crystallographic character of individual grain boundaries, including grain orientations: near-field, high-energy diffraction microscopy (HEDM) to image grain shapes and orientations, and x-ray absorption tomography (XRAT) to reveal the interconnections of individual grain boundaries with crack morphology (Fig. 1). Both were done on XSD 1-ID-B,C,E beamline at the APS.

The researchers in this study, from the Massachusetts Institute of Technology, Johns Hopkins University, Carnegie Mellon University, Lawrence Livermore National Laboratory, Argonne, and Texas A&M University identified ten microscopic structures that contained grain boundaries especially resistant to crack propagation from HE. These grain boundaries deflected a propagating crack to a meandering path, increasing the crack's surface area and the work necessary for it to grow, making the material less susceptible to fracturing. Nine of these fracture-resistant microscopic structures were "BLIPs," or grain boundaries with low-index planes, where at least one of the grains had a low Miller index facet. The strongest section of a grain boundary determined the ability of the material to stop or deflect a crack. No cracks were initiated in the sample interior, suggesting that all cracks in the Ni-alloy initiated at free surfaces.

As a result of this work, engineers can use microstructure design techniques to create a more HE-resistant metal alloy. They also can predict the chance of HE failure based on the density and distribution of BLIPs in the microstructures. Although BLIPs are resistant to HE fractures, the researchers did not discover if non-BLIPs preferentially form cracks. In the future, engineers working on bridges will have the tools to design HE-resistant metals. Meanwhile, the microstructure of existing metal components can be imaged to predict their susceptibility to failure. — Dana Desonie

See: John P. Hanson[1], Akbar Bagri[1,2], Jonathan Lind[3,4], Peter Kenesei[5], Robert M. Suter[3], Silvija Gradecak[1,] and Michael J. Demkowicz[6]*, "Crystallographic character of grain boundaries resistant to hydrogen-assisted fracture in Ni-base alloy 725," Nat. Commun. **9**, 3386 (2018). DOI: 10.1038/s41467-018-05549-y
Author affiliations: [1]Massachusetts Institute of Technology, [2]Johns Hopkins University, [3]Carnegie Mellon University, [4]Lawrence Livermore National Laboratory, [5]Argonne National Laboratory, [6]Texas A&M University
Correspondence: * demkowicz@tamu.edu

This work was supported by the BP-MIT Materials and Corrosion Center. Access to shared experimental facilities at MIT was provided by the MIT Center for Materials Science Engineering, supported in part by the MRSEC Program of the U.S. National Science Foundation (NSF) under award number DMR-0213282. Work at CMU was supported by U.S. DOE Office of Science-Basic Energy Sciences grant DESC0002001. Computational support for this research was provided by grant TG-DMR130061 from the NSF Extreme Science and Engineering Discovery Environment advanced support program. A.B. acknowledges support from the NSF, Grant No 1150862, for support in HEDM data analysis. J.P.H. acknowledges the DOE Office of Science Graduate Fellowship Program, made possible in part by the American Recovery and Reinvestment Act of 2009, administered by ORISE-ORAU under contract no. DE-AC05-06OR23100. This research used resources of the Advanced Photon Source, a U.S. DOE Office of Science User Facility operated for the DOE Office of Science by Argonne National Laboratory under Contract No. DE-AC02-06CH11357.

APS USER INSTITUTIONS BY INSTITUTION TYPE (FY 2018)

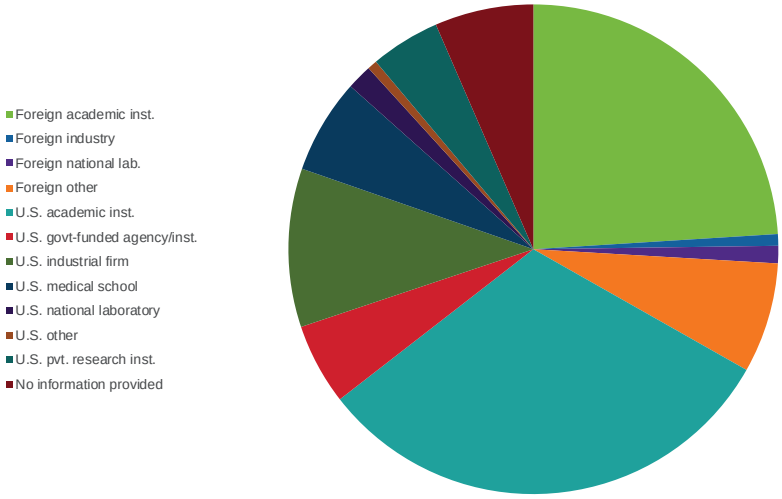

APS USERS BY USER TYPE (FY 2018)

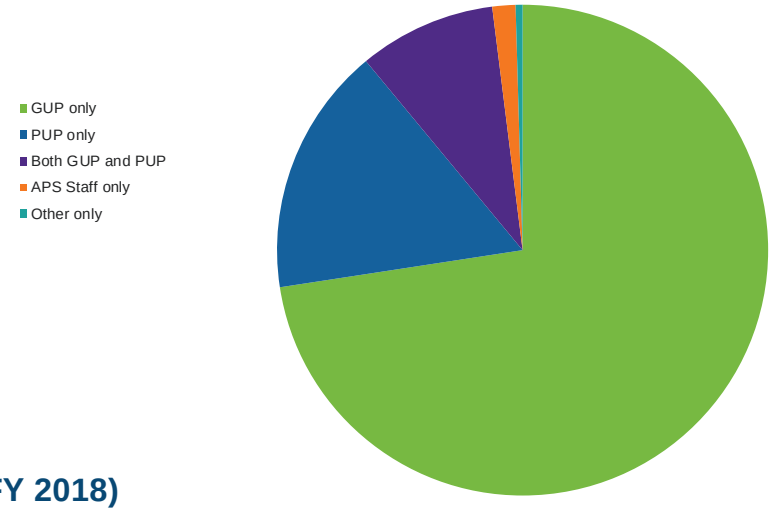

APS USERS BY PROPRIETARY TYPE (FY 2018)

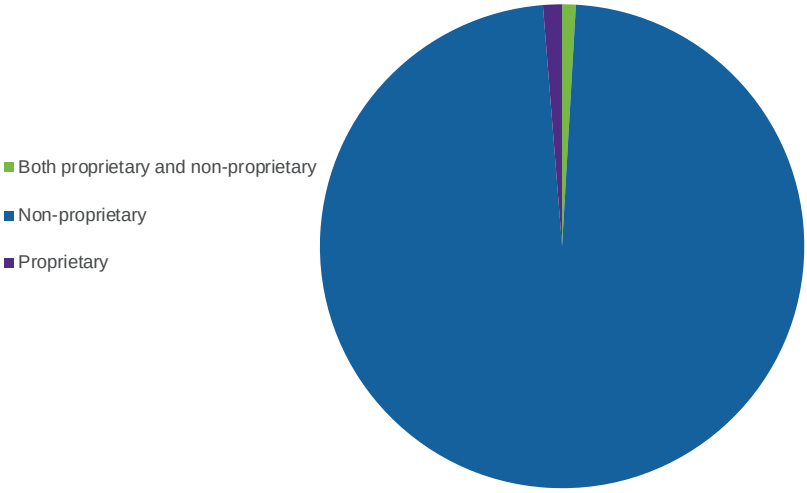

Soft Materials & Liquids

Evidence for a Low-Density Liquid Phase in Supercooled Water

To explain some of the puzzling properties of water, notably the fact that ice floats, many theorists have embraced a model in which the molecular structure of liquid water fluctuates between two phases with different densities. By means of high-resolution x-ray diffraction measurements on ice that is allowed to rapidly decompress, researchers working at the APS have found strong evidence for the existence of the hypothesized low-density liquid phase in supercooled water. The work suggests that the relationship of the two phases may partly explain water's unusual characteristics.

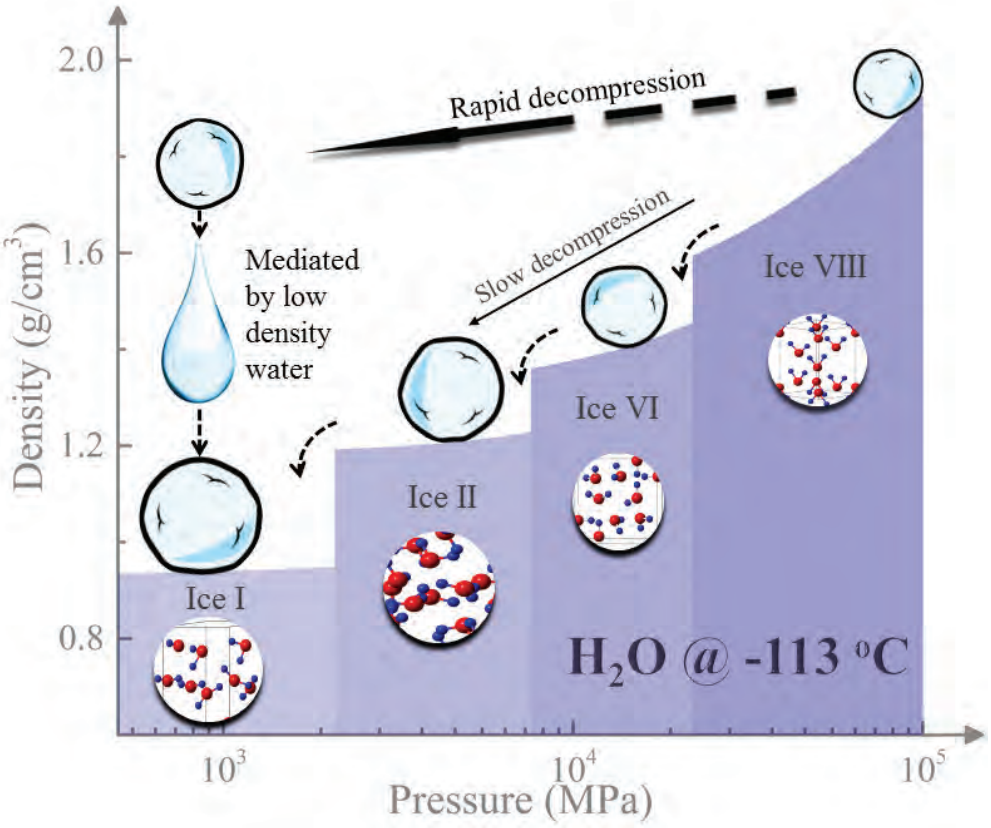

Water at atmospheric pressure can be carefully supercooled to a temperature of about 230 K without crystallizing into ice. Below that temperature, ice formation appears inevitable. On the other hand, a glassy ice that may be formed below 100 K can be warmed to about 140 K before a liquid phase begins to appear. This same behavior persists, with somewhat different upper and lower temperatures, when water is subjected to pressures as high as 3 GPa, or 30,000 times atmospheric pressure. These temperature and pressure limits define what has been called a "no-man's land" in the phase diagram of water, a region characterized by metastable liquid water, but experimentally not accessible.

In the two-phase hypothesis for the structure of liquid water, the lattice has local tetrahedral coordination in both phases, but in one phase, the next nearest oxygen is much closer than in the other. The former phase has roughly an approximately 30% higher density than the latter, and contributes significantly to the density of water at room temperature and pressure. When water freezes under ambient pressure, it adopts a bigger lattice structure than the high density liquid, making ice less dense than water.

As water is supercooled, the lower density phase is theorized to become more stable, but the line in the phase diagram at which the two phases coexist sits within the no-man's land, making it hard to investigate experimentally. Researchers with HP-CAT sought to enter the no-man's land via novel route. They created tiny samples of ice, about one-tenth a millimeter across, by compressing water in a diamond anvil cell at temperatures from 140 K to 165 K, at 5 K intervals. Under these conditions, water crystallized into the phase known as "ice-VIII." Placing the samples in the beamline, the researchers then abruptly released the pressure while keeping the temperature constant. They tracked the changing structure of the sample during this rapid decompression by conducting x-ray diffraction measurements at the HP-CAT 16-ID-B x-ray beamline at the APS, with a time resolution of 5 ms (Fig. 1).

< Fig. 1. The phase that water attains at a given temperature and pressure depends on the route taken. When ice at 160 K slowly decompresses from 10 GPa, it passes through a series of distinct crystalline phases. Rapid decompression, however, leads to the appearance of a non-crystalline phase that researchers have identified as a low-density liquid.

The diffraction results showed that the ice-VIII transformed into a low-density, non-crystalline phase, then began to revert to a different crystalline form, cubic ice-Ic. By contrast, an ice-VIII sample that was allowed to slowly decompress went through several transformations, from ice-VI to ice-II to ice-Ic, but never passed through a non-crystalline phase.

The timescale on which the non-crystalline phase turned into ice-Ic varied enormously with temperature. For the 140 K sample, full conversion took about 2000 sec; at 155 K only 120 sec elapsed; and at 165 K, the process was complete in a couple of hundredths of a second.

Using the time-resolved diffraction data, the researchers plotted graphs of the percentage conversion into ice-Ic as function of time, and found curves of a sigmoid shape governed by a single parameter. These trends are characteristic of a diffusion-controlled process, suggesting that the ice-Ic fraction arises through the formation of numerous separate crystals in a liquid. In addition, the large variation of timescale with temperature is typical for a liquid near the glass transition.

The researchers conclude that their results strongly imply that the non-crystalline phase arising during rapid decompression is a low-density liquid. Even at much higher temperatures, however, the presence of the low-density phase may influence water's properties. Above about 319 K (46° C), water is almost entirely in the high-density phase and behaves as a normal liquid, for examples with heat capacity and compressibility that increase with temperature. Below that temperature, fluctuations between the low- and high-density phases become important, influencing water's properties. — David Lindley

See: Chuanlong Lina, Jesse S. Smitha, Stanislav V. Sinogeikina, and Guoyin Shen*, "Experimental evidence of low-density liquid water upon rapid decompression," Proc. Natl. Acad. Sci. **115**(9), 2010 (February 27, 2018). DOI: 10.1073/pnas.1716310115
Author affiliation: Carnegie Institute for Science
Correspondence: * gshen@ciw.edu

This research was supported by the U.S. Department of Energy (DOE) Office of Science-Basic Energy Sciences, Division of Materials Sciences and Engineering under Award DE-FG02-99ER45775. High Pressure Collaborative Access Team operations are supported by DOE, National Nuclear Security Admin-istration under Award DE-NA0001974. This research used resources of the Advanced Photon Source, a U.S. DOE Office of Science User Facility operated for the DOE Office of Science by Argonne National Laboratory under Contract No. DE-AC02-06CH11357.

Mixing Materials for Muscle-like Polymers

Scientists would like to build synthetic materials that behave like muscles, turning chemical energy into mechanical motion. Such materials might one day act as muscles for soft, deformable robots, or serve as actuators in other applications. Now a team of researchers, with an assist from the APS, have taken a step toward this goal by combining two different materials to build polymer tubes that move in response to changes in temperature.

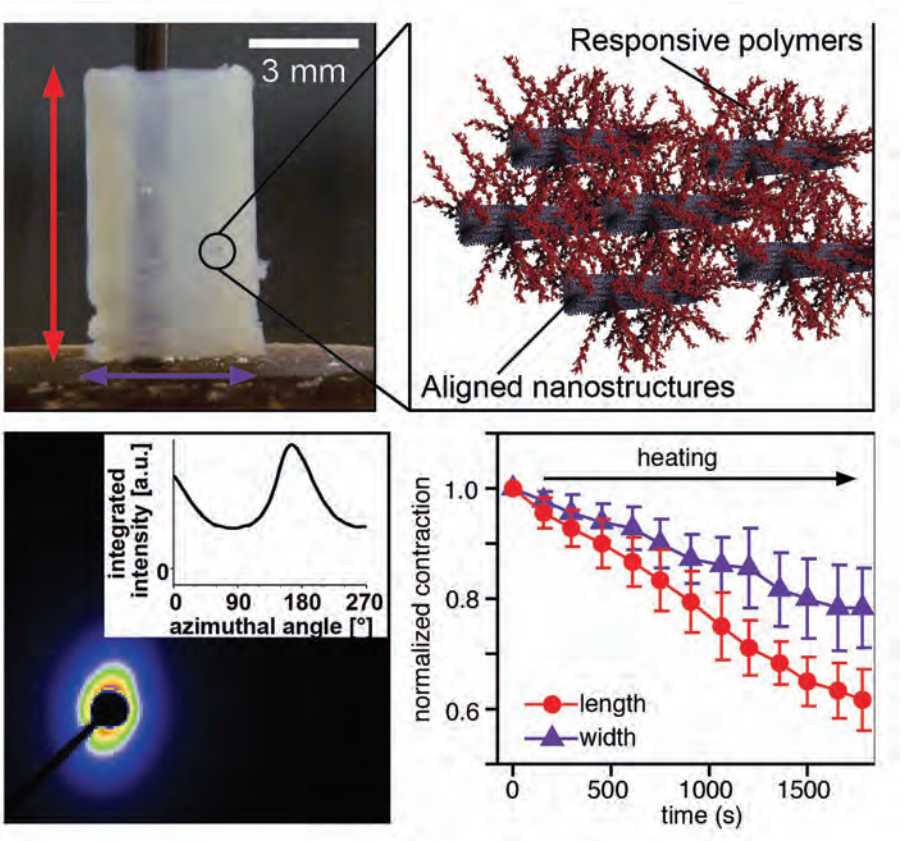

Fig. 1. A hybrid polymer actuator (top left) consists of responsive polymers covalently bonded to aligned nanostructures (top right). SAXS measurements at the APS (bottom left) show that the fibers are aligned, so that when heated, the actuator contracts (bottom right).

The tubes are made from a hydrogel, a polymer swollen by water that is often used in medical applications. Hydrogels change shape in response to various stimuli, but because the polymer network lacks order, it is difficult to control how they move. To provide the material with structure, a multidisciplinary team of researchers from Northwestern University combined the material with nanofibers made of water-soluble peptide molecules that could easily be made to align with each other, giving the hybrid material order. When the hybrid material, placed in water, was heated to 40° C, it expelled water and contracted. When it cooled, it took in more water and expanded to its original shape.

The researchers began by synthesizing two different peptide molecules and dissolving them in hexafluoroisopropanol, then removing the solvent and dissolving them in an aqueous buffer. Heating that to 80° C for 30 min caused the peptides to grow into fibers approximately 10 nm in diameter and 10- to 20-μm long, known as "supramolecular fibers." They placed what was now essentially a liquid crystal of nanofibers into a glass mold with a rotating central rod. The large difference between the fibers' thickness and their length meant that applying even the small amount of energy from the rod's turning caused the fibers to align around the circumference of the tube. The researchers removed the rod and added calcium chloride, forming a gel, which they then removed from the mold.

Finally, they placed the gel into a solution containing different monomers, then used a process called "atom transfer radical polymerization" to create the actuator, in which all the polymer molecules were covalently bonded to the nanofiber construct. When heated, the actuator got thinner and shorter, contracting more along its length than its width. It shrank to 62% of its original length, perpendicular to the direction of the nanofibers, but to only 79% of its original width. Computer modeling showed that both mechanical and chemical mechanisms contributed to the action.

In order to check that the nanofibers were aligned the way researchers had hoped, they performed small-angle x-ray scattering measurements at the DND-CAT beamline 5-ID-D at the APS. The hybrid was approximately 97% water and only 3% organic content, creating a low-contrast material that required the intensity of the beamline to be visible. The researchers could easily identify actuators with the nanofibers aligned along the circumference versus those aligned along the axis, both of which were distinguishable from material with no alignment.

The heat-induced contraction took approximately 30 min, while the cooling and expansion back to the original state took about 1 hour. The researchers would like to speed the process up, and so plan to explore other actuation mechanisms, including those induced by light, magnetic fields, or chemical reactions.

They also tried creating the materials through three-dimensional printing, rather than rotating them in a tube. The shear induced by pushing the liquid through the printer's nozzle provided enough energy to trigger alignment, and they were able to print materials aligned in different directions. Heated up, the aligned hydrogels bent, while unaligned versions simply wrinkled. The researchers say that three-dimensional printing will give them the ability to create a much wider variety of shapes than they can with a tubular mold. — Neil Savage

See: Stacey M. Chin, Christopher V. Synatschke, Shuangping Liu, Rikkert J. Nap, Nicholas A. Sather, Qifeng Wang, Zaida Álvarez, Alexandra N. Edelbrock, Timmy Fyrner, Liam C. Palmer, Igal Szleifer, Monica Olvera de la Cruz, and Samuel I. Stupp*, "Covalent-supramolecular hybrid polymers as muscle-inspired anisotropic actuators," Nat. Commun. **9**, 2395 (2018).
DOI: 10.1038/s41467-018-04800-w
Author affiliation: Northwestern University
Correspondence: * s-stupp@northwestern.edu

This work was primarily supported by the Center for Bio-Inspired Energy Science, an Energy Frontier Research Center funded by the U.S. Department of Energy (DOE) Office of Science-Basic Energy Sciences under Award # DE-SC0000989. The three-dimensional printing experiments were supported by the Air Force Research Laboratory under agreement number FA8650-15-2-5518. S.M.C. and A.N.E. acknowledge graduate research fellowships through the U.S. National Science Foundation. C.V.S. acknowledges a Feodor Lynen-postdoctoral fellowship through the Humboldt Foundation. Z.A. has received postdoctoral support from the Beatriu de Pinós Fellowship 2014 BP-A 00007 (Agència de Gestió d'Ajust Universitaris i de Recerca, AGAUR), and by Grant #PVA17_RF_0008 from the PVA Research Foundation. N.A.S. was supported by the Department of Defense, Air Force Office of Scientific Research, through the National Defense Science and Engineering Graduate Fellowship, 32 CFR 168a, and also acknowledges support from Northwestern University International Institute for Nanotechnology through a Ryan Fellowship. DND-CAT is supported by Northwestern University, E.I. DuPont de Nemours & Co., and The Dow Chemical Company. This research used resources of the Advanced Photon Source, a U.S. DOE Office of Science User Facility operated for the DOE Office of Science by Argonne National Laboratory under Contract No. DE-AC02-06CH11357.

APS USERS BY EXPERIMENT SUBJECT (FY 2018)

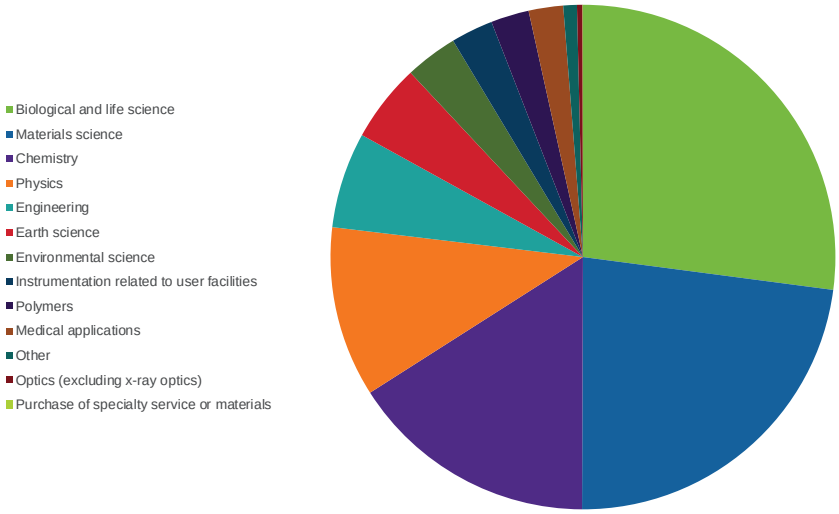

APS USERS BY SOURCE OF SUPPORT (FY 2018)

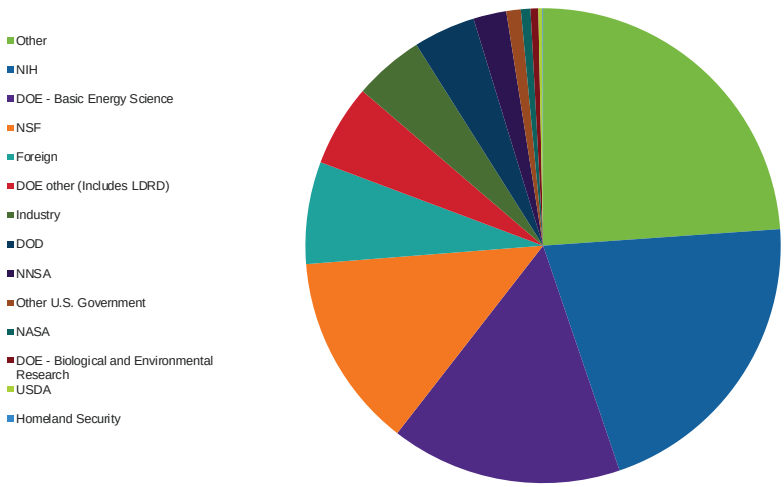

APS USERS BY EMPLOYER (FY 2018)

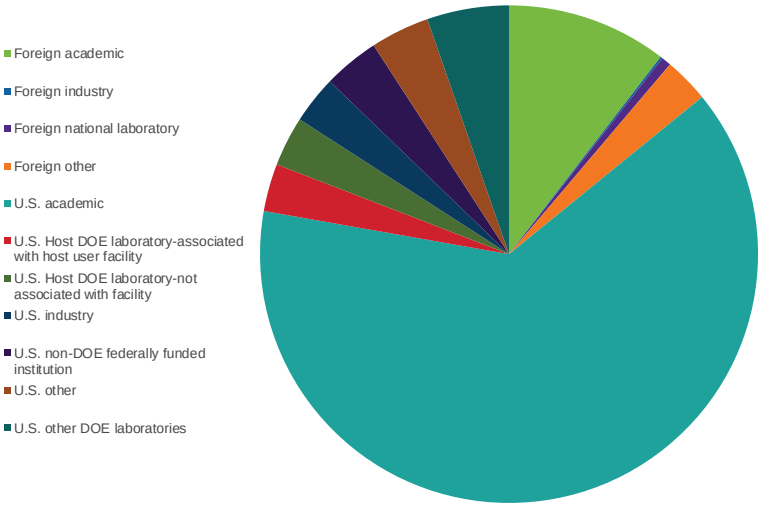

Chemical Science

Solidifying Catalyst Selectivity

Solid catalysts are utilized in approximately 9 out of 10 processes in the chemical industry to speed up the manufacture of everything from pharmaceuticals to pesticides. Solid catalysts are easily separated from the reaction mixture once the reaction is complete because all the other materials involved are gas or dissolved in solvent. Unfortunately, solid catalysts have a major drawback: They are less selective than soluble catalysts and so the products they make can contain more side products. A new type of solid catalyst based on platinum promises to change all that. Scientists working at the APS characterized the new catalysts, which display better selectivity than the commercially available variety.

Technically speaking, such catalysts are known as heterogeneous catalysts. This term distinguishes them from homogeneous catalysts which are dispersed or dissolved in the same state, or phase, as the reaction mixture. Heterogeneous catalysts are commonly very small solid metal particles supported on materials with huge surface area, on which starting materials, the reactants, can come together in the mixture, and react to form the desired products.

The separation benefits of heterogeneous catalysts mean lower costs in the final step of extracting product from reaction mixture.

However, their use represents something of a compromise because such catalysts are less selective in the way in which they allow the starting materials to react. They not only speed up the main reaction but also side reactions leading to byproducts and lower percentage yields of the target compound. The lower selectivity of solid catalysts is due to different ways in which the reactive chemical groups are arranged around different types of metal centers in the catalyst. The problem is particularly acute when chemists hope to add useful functional groups to simple hydrocarbon compounds, chemicals containing strings of carbon atoms to which are attached the simplest “group,” hydrogen atoms. Converting simple hydrocarbons into more complicated molecules is often the first step in constructing pharmaceuticals, pesticides, and other important products.

Chemists have spent many years looking for ways to improve heterogeneous catalysts and some progress has been made in improving their selectivity. One promising approach involves the use of single-site catalysts (SSC). These materials have well-defined, uniform metal centers that are atomically dispersed through the surface of supporting materials, so that reactive groups interact with all metal centers in the same way. Also, no metal centers are buried in the body of particles, so they are used more efficiently. Finding relatively straightforward ways to make SSCs and testing them for a range of industrial reactions have been the focus of many investigations. Unfortunately, there is an obvious obstacle in the way of their wider development: the single metal atoms needed in such catalysts are thermodynamically unstable and the active sites can stick together as soon as, or even before any reaction is initiated, effectively self-poisoning the catalyst and rendering it useless.

One approach to circumvent this obstacle involves dispersing the SSCs on another carrier solid, such as an oxide, an inactive metal, or a carbon support. These have been tested with some success. Another approach involves chemically anchoring soluble single-site metal compound to a solid support but this also has stability problems as well as being costly and so commercially untenable. Yet other approaches involve the formation of porous materials, such as metal-organic frameworks (MOFs) where the active metal centers of the SSC is essentially encapsulated in its own support material. This latter option often involves complex multicomponent solution mixtures, ultra-high vacuum and/or vapor deposition preparation procedures that have, so far, limited its practicality in an industrial setting.

Nevertheless, the ability to tune the design of some of the approaches and the high selectivity and chemical activity possible mean that researchers are now striving to overcome the complexity of setting up SSCs and reducing costs to make them a viable alternative to conventional heterogeneous catalysts in the chemical industry.

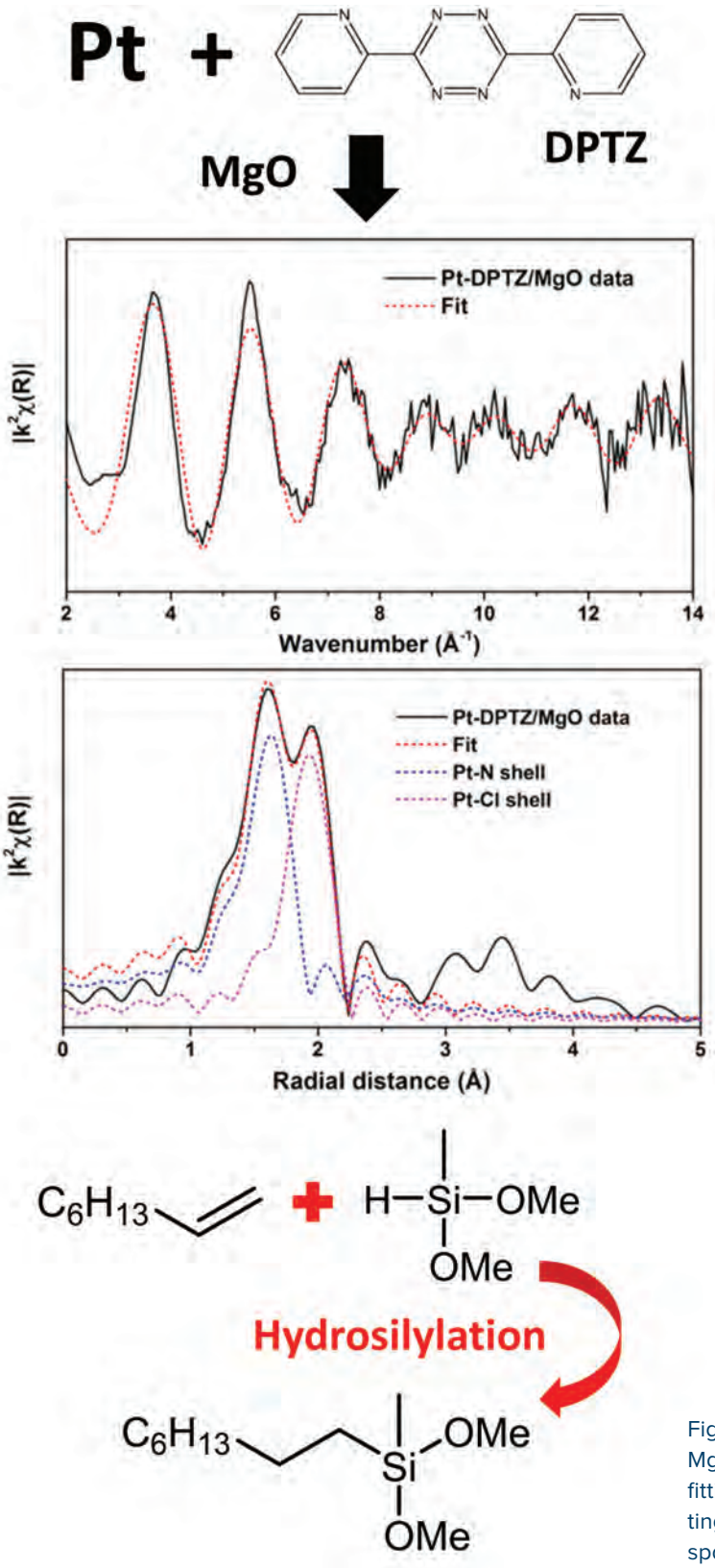

Critically, finding a way to make metal-ligand single-sites on high surface area catalyst supports without the need for complex preparation conditions is an important target in this area.

It has now been demonstrated that it is possible to impregnate platinum and an organic ligand — 3,6-di-2-pyridyl-1,2,4,5-tetrazine (DPTZ) — in a single-step process to create Pt-DPTZ single-site catalytic centers on powdered magnesium oxide, aluminum oxide, and cerium oxide. The resulting powerful and selective catalysts have been characterized using x-ray adsorption spectroscopy measurements at the XSD 9-BM-B,C x-ray beamline at the APS (Fig. 1). For the magnesium oxide example, 90% of the platinum centers are single-site centers. Tests of their catalytic performance in industrially relevant hydrosilylation reactions were demonstrated, satisfactorily showing better selectivity than commercially available homogeneous catalysts and revealing a new strategy for the development of supported single-site catalysts that can potentially be applied in various metal-ligand systems. — David Bradley

See: Linxiao Chen[1], George E. Sterbinsky[2], and Steven L. Tait[1]*, "Synthesis of platinum single-site centers through metal-ligand self-assembly on powdered metal oxide supports," J. Catal. **365**, 303 (2018). DOI: 10.1016/j.jcat.2018.07.004
Author affiliations: [1]Indiana University Bloomington, [2]Argonne National Laboratory
Correspondence: * tait@indiana.edu

This work was supported by the U. S. Department of Energy (DOE) Office of Science-Basic Energy Sciences, Chemical Sciences program, DE-SC0016367. This research used resources of the Advanced Photon Source, a U.S. DOE Office of Science User Facility operated for the DOE Office of Science by Argonne National Laboratory under Contract No. DE-AC02-06CH11357.

Fig. 1. EXAFS spectra of single-site Pt-DPTZ on a powdered MgO support formed in a single-step process. The first-shell fitting is shown in k-space (top) and R-space (bottom). The fitting was performed in R-space, and then plotted back into k-space. This single-site catalyst shows excellent activity for the hydrosilylation reaction illustrated in the scheme in the lower part of the figure. Fit parameters are available in the paper from which this figure is adapted: L. Chen et al., J. Catal. **365**, 303 (2018).

Making Fuels from Shale Gas with Atomic-Level Catalyst Design

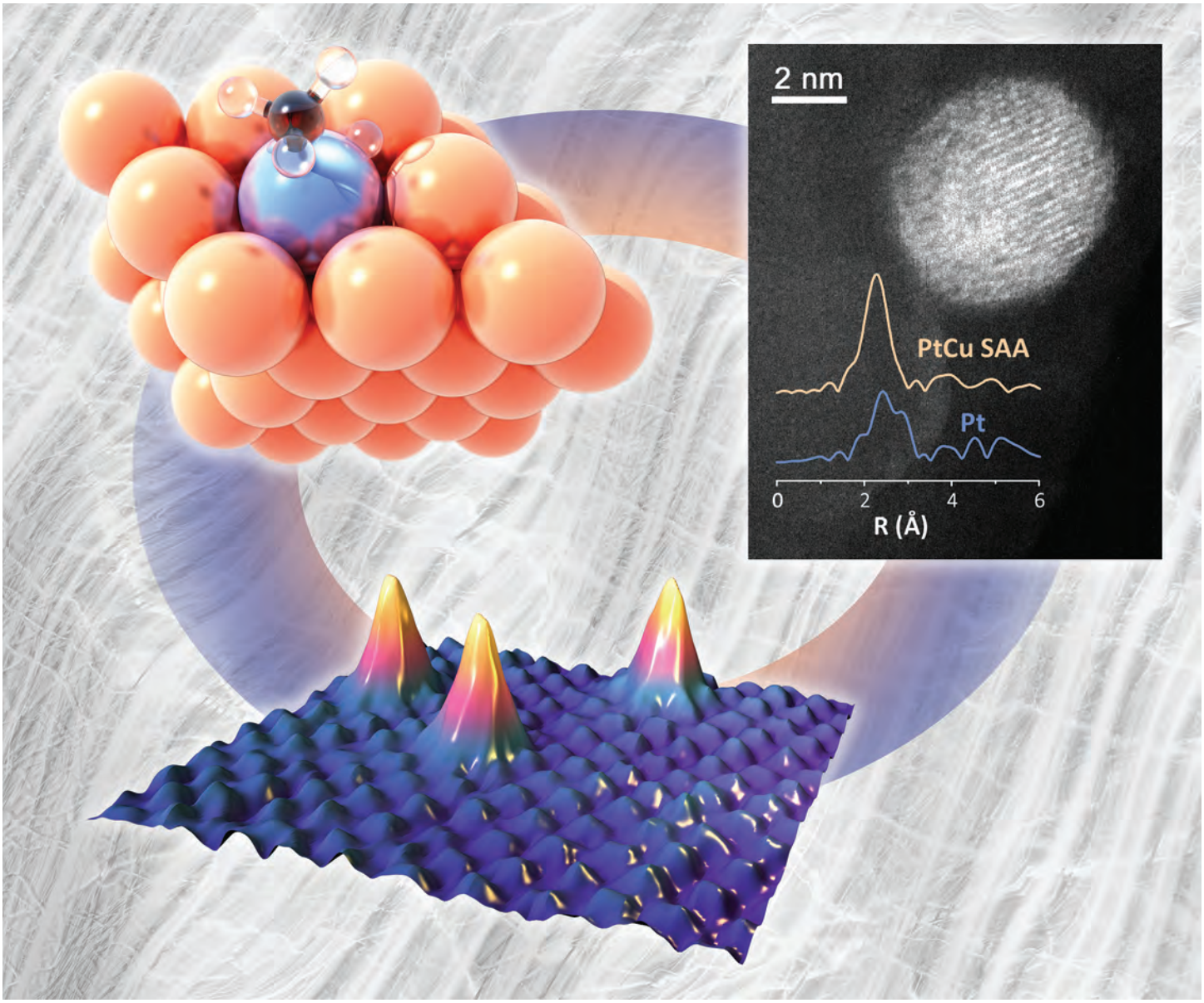

Dilution may not be the solution to pollution, but it is useful nonetheless. By alloying just a small amount of platinum with copper, researchers have made a new catalyst that subverts the well-known problem of "coking." In research at the APS, the single-atom alloy's structure was shown to consist of highly active platinum atoms surrounded by coke-resistant copper. This new catalyst is a less expensive and more energy efficient way to transform shale gas into fuels and useful chemicals. Catalysts that suffer from coking must be cleaned periodically to continue working, sapping away time and energy precious to a large industrial plant. But with this discovery of coke-resistant single-atom alloys, catalysts for small hydrocarbons become much easier to work with. The catalyst isn't expensive either – with relatively cheap copper as the main component, the high price of platinum is mitigated.

The boom in fracking for shale gas has boosted supplies of small hydrocarbon alkanes like methane, ethane, and propane. These simple molecules can act as building blocks for complex molecules, like the octane found in gasoline or fine chemicals. But the current practice of "steam cracking" that transforms these alkanes takes too much energy and is 60% efficient at best. Fortunately, these chemical reactions are much more efficient when aided by catalysts. Platinum and nickel act as catalysts to break carbon-hydrogen (C-H) bonds — the first step in converting alkanes to more useful molecules. But often these catalysts go too far, breaking hydrocarbons down into a carbon-rich soot called "coke," which coats the catalyst surface and blocks reactions from happening.

The researchers in this study from Tufts University and University College London (UK) knew copper is resistant to coking, but it isn't an active catalyst until very high temperatures are reached. Instead, copper was chosen as a host material for platinum, which is very efficiently catalyzes C-H bond breaking. By combining these elements in a single-atom alloy, each platinum atom was surrounded by coking-resistant copper at a ratio of 1:100, suppressing platinum's ability to completely break down hydrocarbons.

The catalyst was tested by the team utilizing a combination of experiments and computer simulations.

< Fig. 1. Top left: A single-atom alloy of platinum and copper acts as a catalyst for C-H bond activation that is resistant to coking. Copper (orange) is only able to break bonds between carbon (black) and hydrogen (clear) in methane at higher temperatures. But a single atom of platinum (blue) in the surface layer of the alloy can break C-H bonds at lower temperatures without forming coke. Top right: X-ray absorption spectrum of platinum (blue) and the alloy (yellow), performed at the APS and a ac-HAADF-STEM image of an alloy nanoparticle. Bottom: STM image of atoms attached to the alloy surface during catalysis.

Nanoparticles of the alloy were prepared to maximize surface area, and the catalytic process was carried out in a flow reactor at atmospheric pressure, simulating an industrial environment. The desorption of molecules off the alloy's surface as catalysis took place was monitored with temperature programmed reaction (TPR) experiments. The surfaces of the alloy nanoparticles were investigated with scanning tunneling microscopy (STM) and x-ray absorption spectroscopy. Supercomputers were used to simulate each step in the reaction at an atomic level to build a mechanism for catalysis and coke-resistance.

The hallmark of a single-atom alloy (that individual atoms of one of the metals are isolated) was confirmed by x-ray absorption spectroscopy conducted along with an Argonne colleague at XSD beamline 12-BM-B at the APS (Fig. 1, top right). Consistent with STM observations, this assured the researchers that platinum atoms were isolated from one another by the copper host.

Both TPR and flow reactor studies showed that the catalyst becomes active at 100-300 K cooler than nanoparticles made from only copper, depending on the reaction studied. While platinum nanoparticles suffer from deactivation after just one catalytic cycle of butane dehydrogenation in the flow reactor, the alloy is active for many cycles, and stable up to 54 h at 400° C, indicating that coke is not impeding catalysis. STM studies of a reaction with methyl iodide also confirmed that no coking occurs; only methyl and iodide groups were observed on the alloy surface.

When pure platinum and copper were compared to the alloy in computer simulations, the researchers observed rapid C-H bond breaking by platinum and found the same bond breaking is a million times slower when performed by copper at higher temperatures. The alloy

"Shale" cont'd. on page 65

Transparent under Pressure

As light becomes ever more important to our computers, communications, and power supply, semiconductors that can work with light become critical ingredients in our infrastructure. Right now, one of the best semiconductors for working with light is cadmium telluride; it is used in thin-film solar cells, and when alloyed with various heavy metals it can be used to detect infrared, x-ray, and gamma ray light, as well as other types of nuclear radiation. But cadmium telluride is expensive, difficult to mine, toxic, and the supply is controlled by nations sometimes hostile to the United States. Researchers seeking substitutes for cadmium telluride have found a clue to potential materials of the future: tin nitride (Sn_3N_4). Abundant and relatively non-toxic, tin nitride is an opaque semiconductor at room temperature and pressure. Researchers utilized high-energy x-rays from the APS to show that when squeezed at tremendously high pressures, tin nitride goes through a dramatic transformation: It becomes transparent and allows light to shine through, acting like an optical semiconductor. This behavior — changing from an opaque to a transparent substance under pressure — is the opposite of what most materials tested under pressure have exhibited. Understanding how tin nitride does this could be the key to making related compounds that do the same thing at everyday pressure and temperatures.

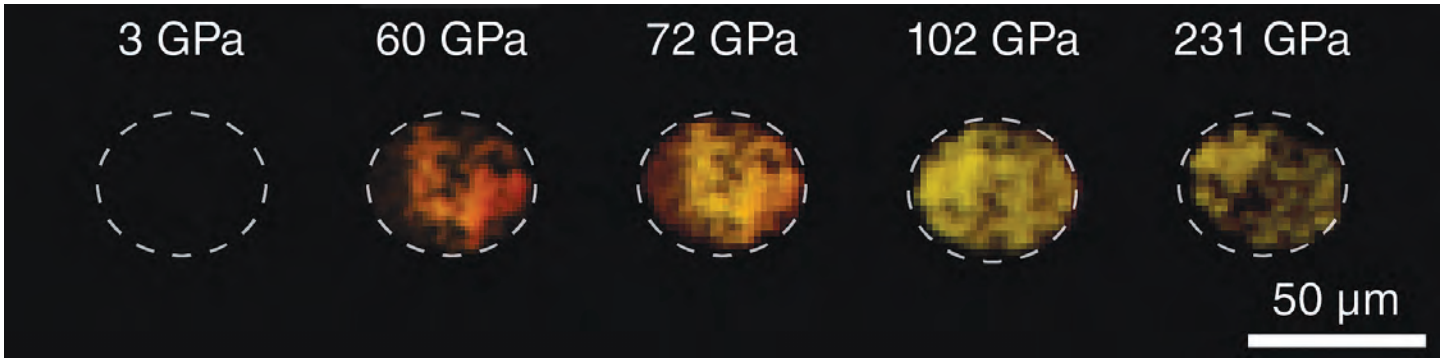

Fig. 1. Photomicrographs show how the tin nitride is opaque at relatively low pressures (3 GPa), but gradually transmits red and then all optical light (60 GPa to 102 GPa) before dimming again near 231 GPa. Image: Ashkan Salamat (University of Nevada, Las Vegas)

Tin is an old, familiar material, abundant in Earth's crust and used by humans since at least 3000 B.C.E. Although it looks and behaves more like a metal, chemically tin is more similar to non-metallic elements. Tin nitride shares its electrons covalently — that is, fairly equally — between the tin and nitrogen atoms, which makes it akin to other non-metallic compounds; think of stone or wood. But, material scientists had predicted that if Sn_3N_4 was squeezed to incredibly high pressure normally found only near the center of Earth, its electrons would change their ways. Instead of being distributed covalently, they would crowd closer to the atoms to which they belonged. A gap with no electrons in it would gradually open up in the material, and that gap would be just the right energy to allow visible light to pass through.

To test this, researchers from University of Nevada, Las Vegas, the Carnegie Institution for Science, the University of Southampton (UK), the University of Cambridge (UK), Universität Basel (Switzerland), and Tohoku University (Japan) performed a unique experiment possible only at the HP-CAT 16-BM-D and 16-ID-B beamlines at the APS. The researchers slowly squeezed a piece of tin nitride and watched how it changed. At 600,000 atm, the tin nitride turned red. At one million atm, it became completely transparent (Fig. 1).

The HP-CAT beamlines have specific capabilities that make them the only place in the world this experiment could be done. In addition to the high brilliance and flux

"Transparent" cont'd. on next page

"Transparent" cont'd. from previous page

of the APS x-rays, HP-CAT has a carbon dioxide laser operating at 10.6 μm installed specifically to heat non-metallic materials such as tin nitride at pressure (many lasers employed in high-pressure experiments work only on metals).

The team used x-ray diffraction to reveal how the atomic-level crystalline structure of tin nitride changed as the pressure and temperature climbed. The diffraction images showed that as the atoms did indeed get closer together under pressure. Further analysis showed that the electrons also were behaving as predicted. They hugged closer to their native atoms, allowing an energy gap to open in the material, a gap with no electrons inhabiting it.

Now that the researchers have confirmed that the unique geometry of tin nitride's electron orbitals causes a band gap to open, and that this band gap can be tuned to different energies using pressure, they want to figure out other chemical structures that may behave similarly. Synthetic chemists might be able to design semiconductors that have optical bandgaps similar to tin nitride but operate closer to room pressure. If these semiconductors can be made from tin nitride or similarly abundant materials, that would make optical electronics more affordable, greener, and less dependent on trade and geopolitics, making a more stable and environmentally friendly U.S. economy. — Kim Krieger

See: John S.C. Kearney[1], Migle Grauzinytė[2], Dean Smith[1], Daniel Sneed[1], Christian Childs[1], Jasmine Hinton[1], Changyong Park[3], Jesse S. Smith[3], Eunja Kim[1], Samuel D.S. Fitch[4], Andrew L. Hector[4], Chris J. Pickard[5,6], José A. Flores-Livas[2], and Ashkan Salamat[1]*, "Pressure-Tuneable Visible-Range Band Gap in the Ionic Spinel Tin Nitride," Angew. Chem. Int. Ed. **57**, 11623 (2018). DOI: 10.1002/anie.201805038
Author affiliations: [1]University of Nevada, Las Vegas, [2]Universität Basel, [3]Carnegie Institution for Science, [4]University of Southampton, [5]University of Cambridge, [6]Tohoku University
Correspondence: * salamat@physics.unlv.edu

This research was sponsored in part by the National Nuclear Security Administration (NNSA) under the Stewardship Science Academic Alliances program through U.S. Department of Energy (DOE) Cooperative Agreement no. DE-NA0001982. C.P. and J.S.S. acknowledge the support of DOE-Basic Energy Sciences Materials Sciences and Engineering Division under Award DE-FG02-99ER45775. HP-CAT operation is supported by DOE-NNSA under Award No.DE-NA0001974, with partial instrumentation funding by the U.S. National Science Foundation. C.J.P. acknowledges financial support from the Engineering and Physical Sciences Research Council of the UK under Grant No. EP/P022596/1. C.J.P. is also supported by the Royal Society through a Royal Society Wolfson Research Merit Award. This research was partially supported by the NCCR MARVEL, funded by the Swiss National Science Foundation.

"Shale" cont'd. from page 63

splits the difference: Breaking C-H bonds at intermediate temperatures, and not doing it so quickly as to form coke. This occurs because the activation barrier increases for every subsequent C-H bond broken, though it is still lower than copper, requiring lower temperatures. In platinum, subsequent C-H bond breaking is either similar or lower in energy, driving the rapid stripping of hydrogens that leads to coking.

The alloy was also able to connect two or three methyl fragments of the molecule methane, the next step to creating useful chemicals, due to the ability of copper to make carbon-carbon bonds.

Further studies that couple surface science, catalysis, and simulations can engineer coke-resistant catalysts based on palladium and nickel as well. Thus, single-atom alloys could be a new low-cost route to many C-H chemistries. — Amanda Grennell

See: Matthew D. Marcinkowski[1], Matthew T. Darby[2], Jilei Liu[1], JoshuaM. Wimble[1], Felicia R. Lucci[1], Sungsik Lee[3], Angelos Michaelides[2], Maria Flytzani-Stephanopoulos[1]*, Michail Stamatakis[2]**, and E. Charles H. Sykes[1]***, "Pt/Cu single-atom alloys as coke-resistant catalysts for efficient C–H activation," Nat. Chem **10**, 325 (March 2018). DOI: 10.1038/NCHEM.2915
Author affiliations: [1]Tufts University, [2]University College London, [3]Argonne National Laboratory
Correspondence: * maria.flytzani-stephanopoulos@tufts.edu, ** m.stamatakis@ucl.ac.uk, *** charles.sykes@tufts.edu

All surface science studies (M.D.M., F.R.L., and E.C.H.S.) were performed with support from the U.S. Department of Energy (DOE) Office of Science-Basic Energy Sciences, Division of Chemical Sciences, CPIMS Program, under grant no. FG02-10ER16170. J.L. and M.F-S. acknowledge the U.S. DOE (DE-FG02-05ER15730) for financial support of the catalysis work. M.T.D is funded by the Engineering and Physical Sciences Research Council UK as part of a Doctoral Training Grant (Award Ref. 1352369). The theoretical portion of the research also used resources of the Oak Ridge Leadership Computing Facility, which is a DOE Office of Science User Facility supported under contract no. DE-AC05-00OR22725. Access to the Oak Ridge facility was provided via the Integrated Mesoscale Architectures for Sustainable Catalysis (IMASC), an Energy Frontier Research Center funded by the U.S. DOE Office of Science-Basic Energy Sciences under award #DE-SC0012573. A.M. is supported by the European Research Council under the European Union's Seventh Framework Programme (FP/2007-2013)–European Research Council grant agreement no. 616121 (HeterolCe project). A.M. is also supported by the Royal Society through a Royal Society Wolfson Research Merit Award. This research used resources of the Advanced Photon Source, a U.S. DOE Office of Science User Facility operated for the U.S. DOE Office of Science by Argonne National Laboratory under Contract No. DE-AC02-06CH11357.

Converting Atmospheric Carbon Dioxide into Carbon-Neutral Fuels

A unique phenomenon — reversible restructuring of metal-complex structures that enables high electrocatalytic performance — has been discovered by researchers employing high-brightness x-rays to carry out structural characterization of samples at the APS. This work has the potential for positive impacts in the realms of energy conservation and industrial chemistry.

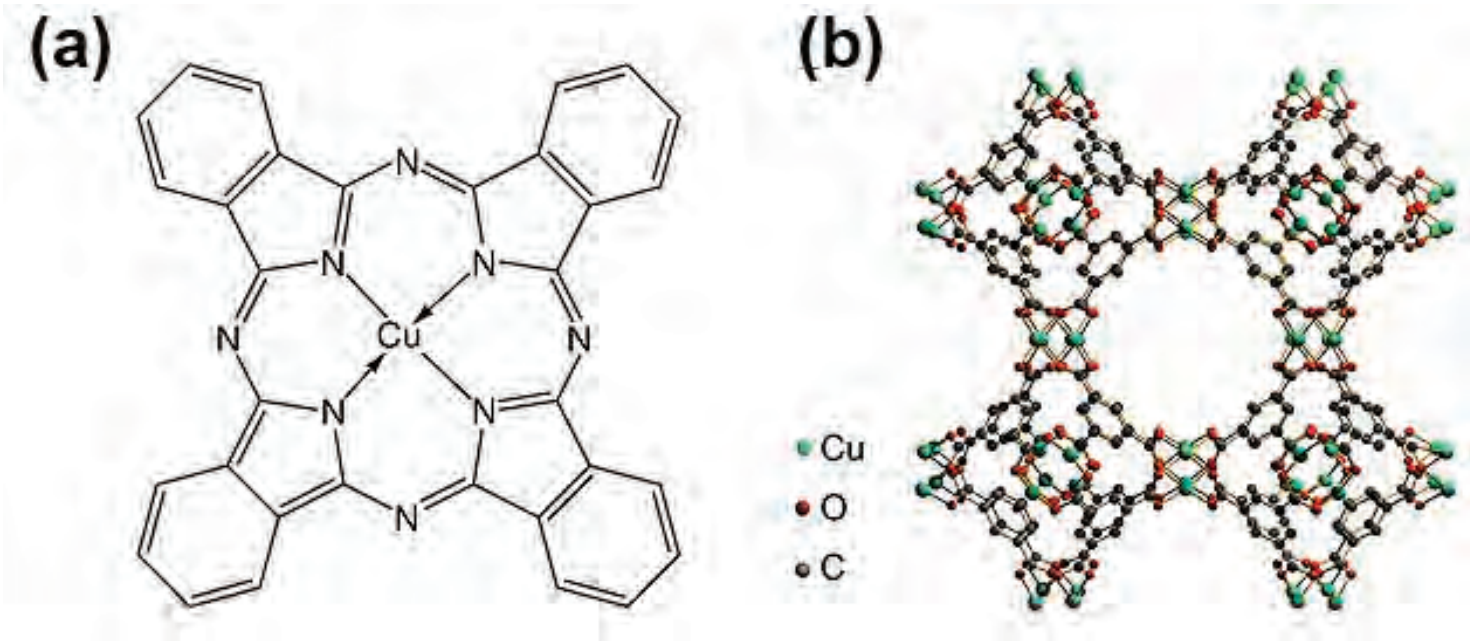

Fig. 1. Molecular structures for three cupper-complex materials: (a) CuPc, (b) HKUST-1, and (c) [Cu(cyclam)]Cl_2.
Figures adapted from Z. Wang et al., Nat. Commun. **9**, 415 (2018). © 2018 Springer Nature Publishing AG

In theory, electrocatalysts can be used to convert the ever-growing carbon dioxide (CO_2) in the Earth's atmosphere to carbon-neutral fuels or other value-added chemicals. Doing so on a large scale would diminish the environmental problems associated with the atmospheric CO_2 and also benefit energy storage and chemical production. One attractive proposal is to power catalytic CO_2 conversion with electricity generated from renewable energy sources, such as wind or solar energy. This electrocatalytic CO_2 reduction would work under ambient conditions in aqueous media. However, this process requires cost-effective electrocatalysts for the reaction. The research team in this study led by Yale University, Oregon State University, and South University of Science and Technology had earlier discovered a promising candidate, a copper porphyrin, which is able to convert CO_2 to methane in a neutral aqueous electrolyte.

It is known that the structures of many catalysts change under reaction conditions. This restructuring can be caused by various conditions, including temperature, pressure, electrical potential, and chemical environment. The structures formed during the reaction conditions are responsible for the resulting catalytic properties.

Using *in situ* and *operando* x-ray absorption spectroscopy (XAS) at the DND-CAT 5-BM-D beamline at the APS, the team was able to follow the restructuring that occurred under CO_2 reduction conditions in an aqueous electrolyte for three copper catalysts: copper(II) phthalocyanine (CuPc), copper(II) benzene-1,3,5-tricarboxylate (HKUST-1), and copper(II) 1,4,8,11-tetraazacyclotetradecane ([Cu(cyclam)]Cl_2) (Fig. 1).

Samples were prepared for analysis by drop drying an ink solution containing the catalysts on carbon fiber paper (2.5 by 1.5 cm^2). Supplementary analyses of the samples included scanning electron microscopy, x-ray diffraction, and electrocatalytic measurements.

The authors correlated the catalyst structures determined from the XAS and other data to the observed cat-

alytic properties. Of the three electrocatalysts, CuPc was clearly the most efficient for electrochemical reduction of CO_2 to methane (66% Faradaic efficiency) and attained the highest current density (13 mA/cm^2). The XAS structural data showed that during the conversion reaction the CuPc molecules restructure to metallic copper clusters (size of around 2 nm), which are the active sites for the electrocatalysis (Fig. 2). Then, the copper nanoclusters reverse back to the original CuPc structure after the negative electrode potential is removed. By contrast, the other two samples decompose to much larger copper nanostructures, and do not return to the original structure. The excellent performance of the CuPc electrocatalyst is due to its reversible formation of the copper nanoclusters. The earlier reported copper porphyrin catalyst shows a similar restructuring behavior as CuPc.

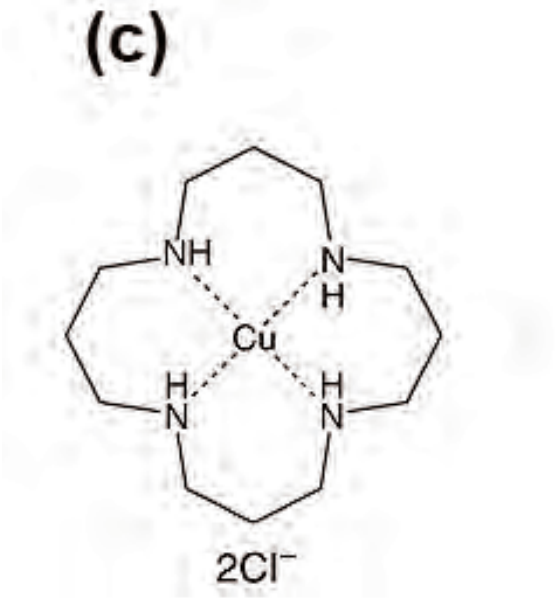

The authors also performed density functional theory calculations on the restructuring of the CuPc material. These calculations revealed that the causes of its good reversibility were the small size of the copper nanoclusters and the strong affinity of the copper ions and phthalocyanine ligands.

The results from this study provide valuable insight into strategies for developing other high-performance electrocatalysts. The team is developing other heterogenized molecular catalysts with new functionalities and high performance for electrochemical CO_2 conversion.

— Joseph E. Harmon

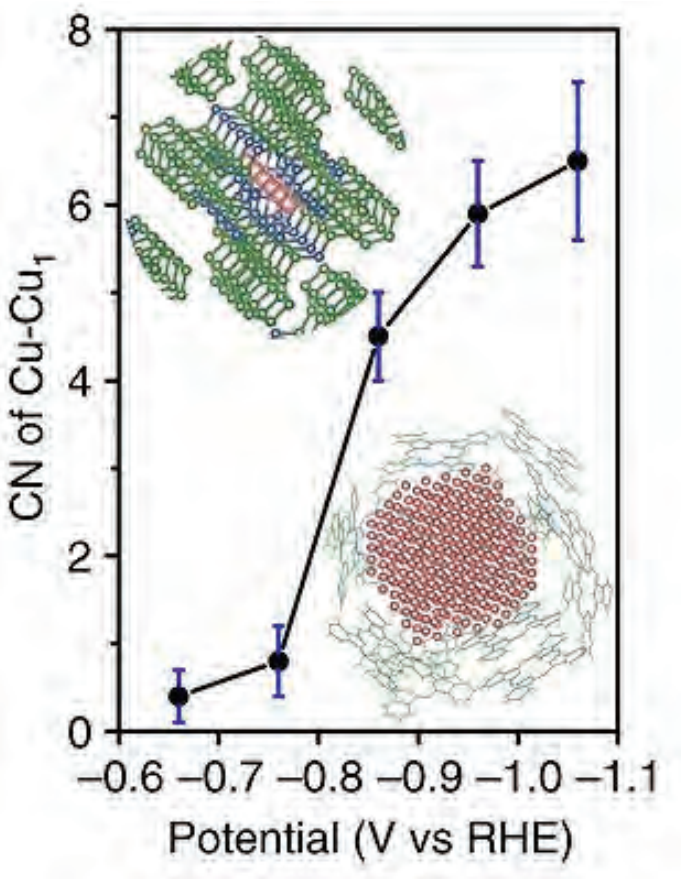

Fig. 2. Coordination number of first shell copper-copper bond of the CuPc catalyst at different potentials. Upper left shows the CuPc structure; right inset shows a possible configuration of the Cu nanoclusters generated under electrocatalytic conditions. Green, carbon; blue, nitrogen; pink, copper.

See: Zhe Weng[1,2], Yueshen Wu[2], Maoyu Wang[3], Jianbing Jiang[2], Ke Yang[2], Shengjuan Huo[2,4], Xiao-Feng Wang[5], Qing Ma[6], Gary W. Brudvig[2], Victor S. Batista[2], Yongye Liang[1*], Zhenxing Feng[3**], and Hailiang Wang[2***], "Active sites of copper-complex catalytic materials for electrochemical carbon dioxide reduction," Nat. Commun. **9**, 415 (2018). DOI: 10.1038/s41467-018-02819-7
Author affiliations: [1]South University of Science and Technology of China, [2]Yale University, [3]Oregon State University, [4]Shanghai University, [5]University of South China, [6]Northwestern University
Correspondence: * liangyy@sustc.edu.cn, ** zhenxing.feng@oregonstate.edu, *** hailiang.wang@yale.edu

The work was supported by the National Science Foundation (Grant CHE-1651717), a Doctoral New Investigator grant from the ACS Petroleum Research Fund, a Global Innovation Initiative from the Institute of International Education, and the Callahan Faculty Scholar Endowment Fund from Oregon State University. The synthetic work was supported by the U.S. Department of Energy (DOE), Chemical Sciences, Geosciences, and Biosciences Division, Office of Sciences–Basic Energy Sciences (Grant DEFG02-07ER15909). Additional support was provided by a generous donation from the TomKat Foundation. V.S.B. acknowledges support from the Air Force Office of Scientific Research grant FA9550-13-1-0020 and supercomputing time from the NERSC. Y.L. acknowledges financial support from Shenzhen Fundamental Research Funding (JCYJ20160608140827794) and Peacock Plan (KQTD2014063 0160825828). DND-CAT is supported by Northwestern University, E.I. DuPont de Nemours & Co., and The Dow Chemical Company. This research used resources of the Advanced Photon Source, a U.S. Department of Energy (DOE) Office of Science User Facility operated for the DOE Office of Science by Argonne National Laboratory under Contract No. DE-AC02-06CH11357.

With These Liquid Crystals, the Action Is On the Surface

Liquid crystals (LCs) can be described as an interesting hybrid, an "in-between" matter state occupying the region between solid, hard crystal, and free-flowing liquid. The different orientations adopted by their long rod-like molecules in their various phases as they respond to various stimuli make LCs suitable for a wide variety of applications, including their most familiar use in liquid-crystal electronics displays. Interfacial dynamics at the LC-air boundary are key to these applications, because molecular ordering at the LC surface can propagate into the LC and control molecular orientations into the bulk crystal. While this phenomenon has been studied to some degree in smectic (layered) phase LCs, little work has been done on nematic (long-range parallel ordered) LCs. Researchers working at the APS employed advanced x-ray synchrotron reflectivity studies and molecular dynamics simulations to examine how LC interfaces can serve as what the authors call "high-fidelity reporters of molecular events."

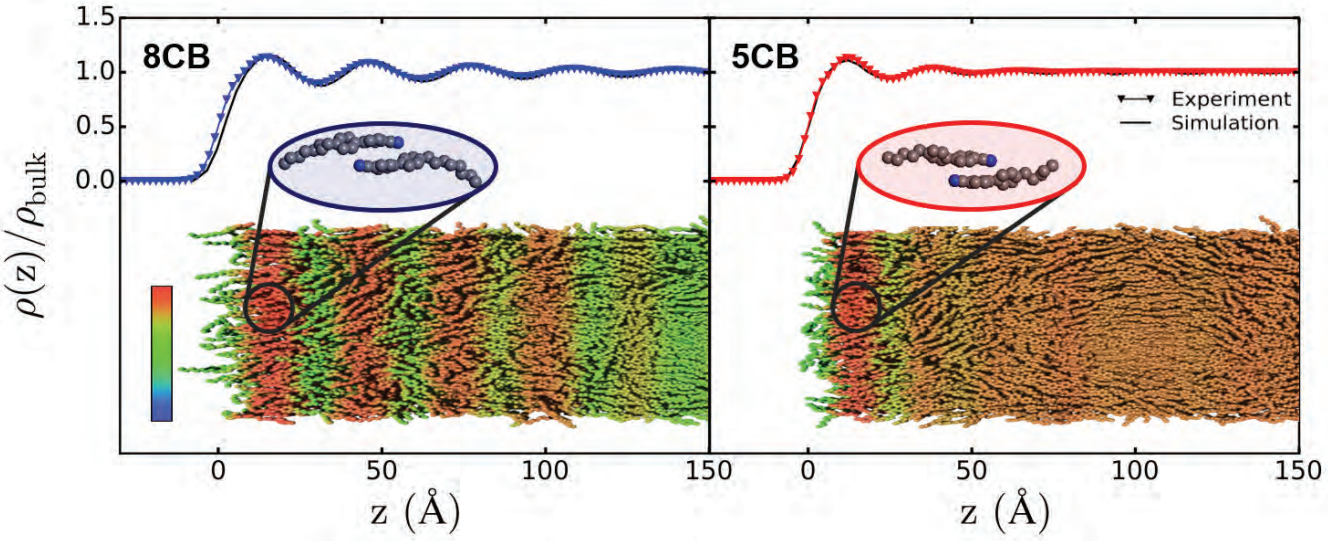

Fig. 1. Comparison of the electron density extracted from the x-ray reflectivity measurements (symbols connected by lines) with the profiles obtained from the molecular dynamics simulations (continuous lines) along with the average orientation of 8CB and 5CB molecules with respect to a predefined axis along the surface normal.

The research team from The University of Chicago, the University of Illinois at Chicago, the University of Wisconsin-Madison, and Argonne focused on the air-liquid interface of two widely-used LCs, the nematic liquid crystal 4-pentyl-4′-cyanobiphenyl (5CB) and 4-octyl-4′-cyanobiphenyl (8CB), which is also capable of forming smectic and isotropic phases. At room temperature, 5CB is nematic, while 8CB exhibits a smectic A phase until transitioning to a nematic state with increasing temperature. The synchrotron x-ray reflectivity studies were performed at the ChemMatCARS 15-ID-B,C,D x-ray beamline at the APS, and then combined with detailed simulations using the Nanoscale Molecular Dynamics package.

The x-ray studies showed that in the 8CB samples, surface-induced smectic layering began to form and the reflectivity peaks became markedly sharper as the phase transition temperature of 33.5° C approached. In 5CB, however, this molecular ordering appears to be nearly independent of temperature. Although electron density profiles from the isotropic phases of both 5CB and 8CB showed a single dominant smectic surface layer, this changed in the nematic phase, in which 5CB formed two surface-induced smectic interfacial layers, while 8CB showed multiple distinct smectic layers at the air interface with very deep bulk penetration. The LC orientations of both 5CB and 8 CB were homeotropic with the interfaces. The authors posit that the overlapping alkyl tails of the 5CB and 8CB molecules, though each of slightly different sizes, result in bilayer structures somewhat larger than the individual molecule.

Because the x-ray studies showed only one-dimensional surface information, molecular dynamics simulations allowed the experimenters to infer three-dimensional structures and dynamics. These showed good quantitative agreement with the experimental observations, revealing that the air interface imparted a high degree of molecular order that propagated deeply into the liquid-crystal bulk structure. Orientational order decayed steadily and became more isotropic with increasing distance from the surface interface, while calculations of polarization density profiles showed oscillations of the molecular layer dipoles that canceled out into the bulk regions (Fig. 1).

The present work, utilizing x-ray synchrotron measurements at the APS, has yielded detailed molecular-scale information on the nature of LC-air interfacial structures that previous spectroscopic techniques were unable to provide because of their comparatively limited resolution. Based on these studies, the team plans to extend their x-ray reflectivity studies to investigate LC-aqueous electrolyte interfaces, which will provide greater insights into the effects of electrostatic interactions on LC orientational ordering. They expect that such knowledge will be instrumental in extending the versatility of LCs into even more applications, such as responsive interfaces for the detection of various molecules. — Mark Wolverton

See: Monirosadat Sadati[1,4], Hadi Ramezani-Dakhel[1], Wei Bu[1], Emre Sevgen[1], Zhu Liang[2], Cem Erol[2], Mohammad Rahimi[1], Nader Taheri Qazvini[1,4], Binhua Lin[1], Nicholas L. Abbott$_3$, Benoît Roux[1*], Mark L. Schlossman[2**], and Juan J. de Pablo[1,4***], "Molecular Structure of Canonical Liquid Crystal Interfaces," J. Am. Chem. Soc. **139**, 3841 (2017). DOI: 10.1021/jacs.7b00167
Author affiliations: [1]The University of Chicago, [2]University of Illinois at Chicago, [3]University of Wisconsin-Madison, [4]Argonne National Laboratory
Correspondence: * roux@uchicago.edu, ** schloss@uic.edu, *** depablo@uchicago.edu

The simulations of structure and deformation of structured liquid crystal interfaces and the analysis of the x-ray reflectivity data were supported by U.S. National Science Foundation (NSF) DMR-1420709. The design of triggerable materials based on liquid crystals with engineered bulk responses to interfacial perturbations was supported by the U.S. Army Research O ce through the MURI program (W911NF-15-1-0568). The experimental assembly of supported liquid-crystal films for characterization by reflectivity was supported by NSF DMR-1121288. The validation of force fields for prediction of liquid crystal structure from first principles was supported by the U.S. Department of Energy (DOE) Office of Science-Basic Energy Sciences, Materials Science Division, through the Midwest Integrated Center for Computational Materials. ChemMatCARS is principally supported by the Divisions of Chemistry and Materials Research, NSF, under grant number NSF/CHE-1346572. We acknowledge the University of Chicago Research Computing Center for allocation of computing resources. We further acknowledge the computing resources provided on Blues, a high-performance computing cluster operated by the Laboratory Computing Resource Center at Argonne National Laboratory. This research used resources of the Advanced Photon Source, a U.S. Department of Energy (DOE) Office of Science User Facility operated for the DOE Office of Science by Argonne National Laboratory under Contract No. DE-AC02-06CH11357.

This highlight was inadvertantly omitted from *APS Science 2017*.

APS USERS BY AGE (FY 2018)

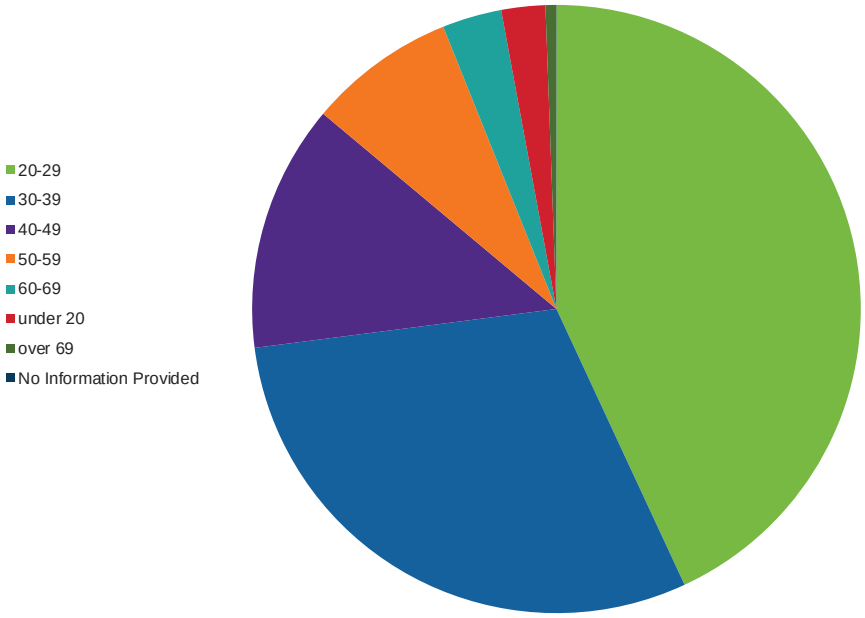

APS USERS BY EMPLOYMENT LEVEL (FY 2018)

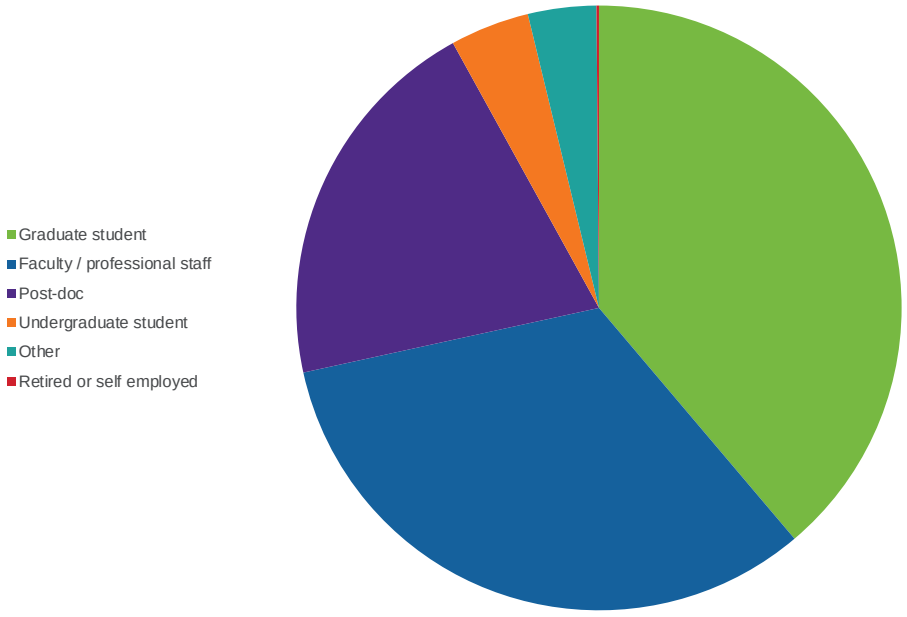

Life Science

A Super-relaxed Myosin State to Offset Hypertrophic Cardiomyopathy

At its most basic level, the proper functioning of the heart depends upon the intricate interaction of proteins that trigger, maintain, and control the muscular contractions and relaxations of this vital organ. Disruption of those interactions can cause serious pathologies such as hypertrophic cardiomyopathy (HCM). Such disruptions can originate with mutations in the primary motor protein involved in heart contraction, ß-cardiac myosin, which can alter the rate of ATP hydrolysis and have been hypothesized to destabilize its super-relaxed state (SRX). Researchers utilizing electron microscopy together with low-angle x-ray diffraction studies carried out at the APS investigated the stabilizing action of mavacamten, a cardiac drug currently in phase-3 clinical trials, on the ß-cardiac myosin super-relaxed state and its possible therapeutic effects on HCM.

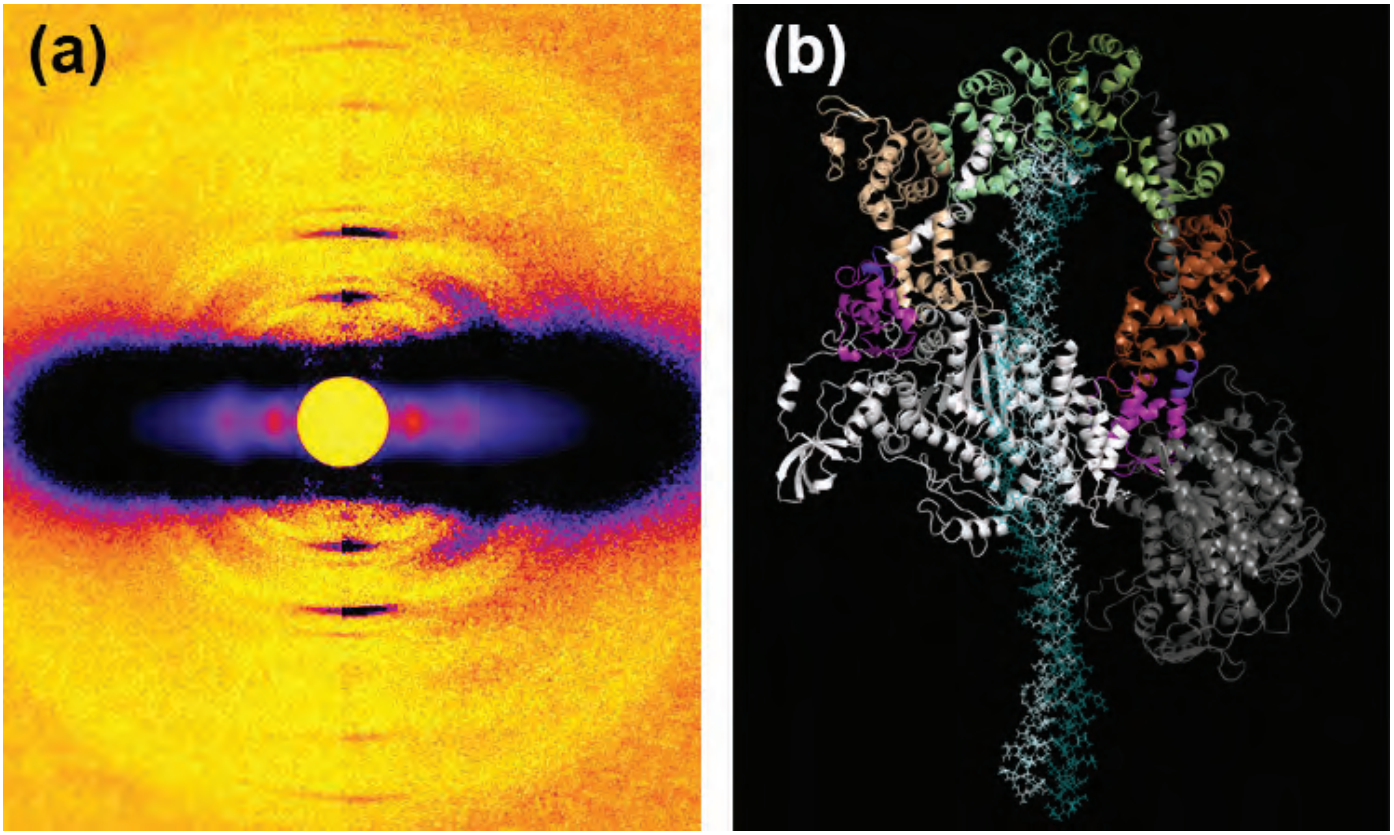

Fig. 1. (a) A diffraction pattern from untreated muscle compared to treated muscle on the right. Intensification of the x-ray reflections from the treated muscle indicate a highly ordered "super-relaxed" state of myosin motors. (b) The myosin heads in the compact "interacting head motif," which the heads adopt in the super-relaxed state allowing them to be packed closely and tightly on the surface of muscle thick filaments.

Previous work had hinted that a folded state of the myosin protein, seen both in purified form and in isolated filaments and known as the interacting-heads motif or IHM, could be analogous to the SRX state, although this has not yet been demonstrated experimentally. It has been proposed that mutations causing HCM disrupt this state, resulting in a higher percentage of myosin heads being available for interaction with actin and leading to the hypercontractility of cardiac tissue seen in HCM. These investigators, from MyoKardia, Inc., the Stanford University School of Medicine, the Illinois Institute of Technology, Exemplar Genetics, the Harvard Medical School, and the University of California, San Francisco, first studied this possibility using three separate purified ß-cardiac myosin constructs (25-heptad heavy meromysin [HMM], two-heptad HMM, and short S1), finding that a fraction of their basal ATPase rates were within the range of 0.002-0.004 s^{-1} which defines the SRX state.

After confirming the slow basal ATPase rate, the team hypothesized that they were observing a folded structural state biochemically similar to SRX. This was supported by electron microscopy that visualized a folded-back myosin structure. They also demonstrated that mavacamten slowed ATPase rates to SRX levels and promotes the formation of folded-back myosin molecules, suggesting that it acts by stabilizing a SRX state.

The research team also investigated the action of mavacamten in porcine and human cardiac fibers. Both showed similar marked effects, with an increase in SRX and decreased tension. The low-angle x-ray diffraction studies carried out at the Bio-CAT 18-ID-D beamline at the APS showed a significant increase in ordering of the porcine myosin heads in both relaxed and contracting fibers on the thick filament backbone (Fig. 1). The presence of mavacamten appears to shift the on-off state equilibrium of myosin to an off/folded-back state.

To study one of the best-described ß-cardiac myosin mutations in HCM, R403Q, the researchers used a large-animal model of the Yucatan minipig. This showed a sharp decrease in SRX levels in R403Q cardiac fibers compared to those from wild-type pigs, consistent with the role of this mutation in causing hypercontractility. Treatment with mavacamten restored SRX levels to normal and reduced fiber tension. The XRD images again showed increase in ordering of myosin heads along the thick filament backbone. Further studies of human cardiac fibers with the R663H mutation showed similar results, showing the destabilizing effects of the HCM mutations on the SRX state in both humans and pigs.

The experimenters emphasize that although the present work does not establish an equivalency of the folded-back SRX state with the IHM state, it demonstrates some striking insights, particularly that specific myosin mutations weaken SRX enough to lead to the hypercontractility seen in HCM. The results also confirm the importance of the tail region of myosin for a stable SRX state, although uncertainties persist regarding the exact molecular structures and charge interactions. Further work to better characterize and understand these phenomena promises new insights and therapeutic possibilities for the treatment of hypertrophic cardiomyopathy.

— Mark Wolverton

See: Robert L. Anderson[1], Darshan V. Trivedi[2], Saswata S. Sarkar[2], Marcus Henze[1], Weikang Ma[3], Henry Gong[3], Christopher S. Rogers[4], Joshua M. Gorham[5], Fiona L. Wong[1], Makenna M. Morck[2], Jonathan G. Seidman[5], Kathleen M. Ruppel[2], Thomas C. Irving[3], Roger Cooke[6], Eric M. Green[1]*, and James A. Spudich[2]**, "Deciphering the super relaxed state of human -cardiac myosin and the mode of action of mavacamten from myosin molecules to muscle fibers," Proc. Natl. Acad. Sci. **115**(35), E8143 (2018). DOI: 10.1073/pnas.1809540115

Author affiliations: [1]MyoKardia, Inc., [2]Stanford University School of Medicine, [3]Illinois Institute of Technology, [4]Exemplar Genetics, [5]Harvard Medical School, [6]University of California, San Francisco

Correspondence: * egreen@myokardia.com,
** jspudich@stanford.edu

This work was funded by National Institutes of Health (NIH) Grants GM33289 and HL117138 (to J.A.S.), AR062279 (to R.C.), and HL084553 (to J.G.S.). D.V.T. is supported by Stanford Lucile Packard Child Health Research Institute Postdoctoral Award UL1 TR001085 and American Heart Association Postdoctoral Fellowship 17POST33411070. The EM project described was supported, in part, by American Recovery and Reinvestment Act Award 1S10RR026780-01 from the National Center for Research Resources. This project was supported by Grant 9 P41 GM103622 from the National Institute of General Medical Sciences of the NIH (to T.C.I.). This research used the Nikon Imaging Center, University of California, San Francisco and the resources of the Advanced Photon Source, a US Department of Energy (DOE) Office of Science User Facility operated for the DOE Office of Science by Argonne National Laboratory under Contract DE-AC02-06CH11357.

The Molecular Drivers of Dilated Cardiomyopathy

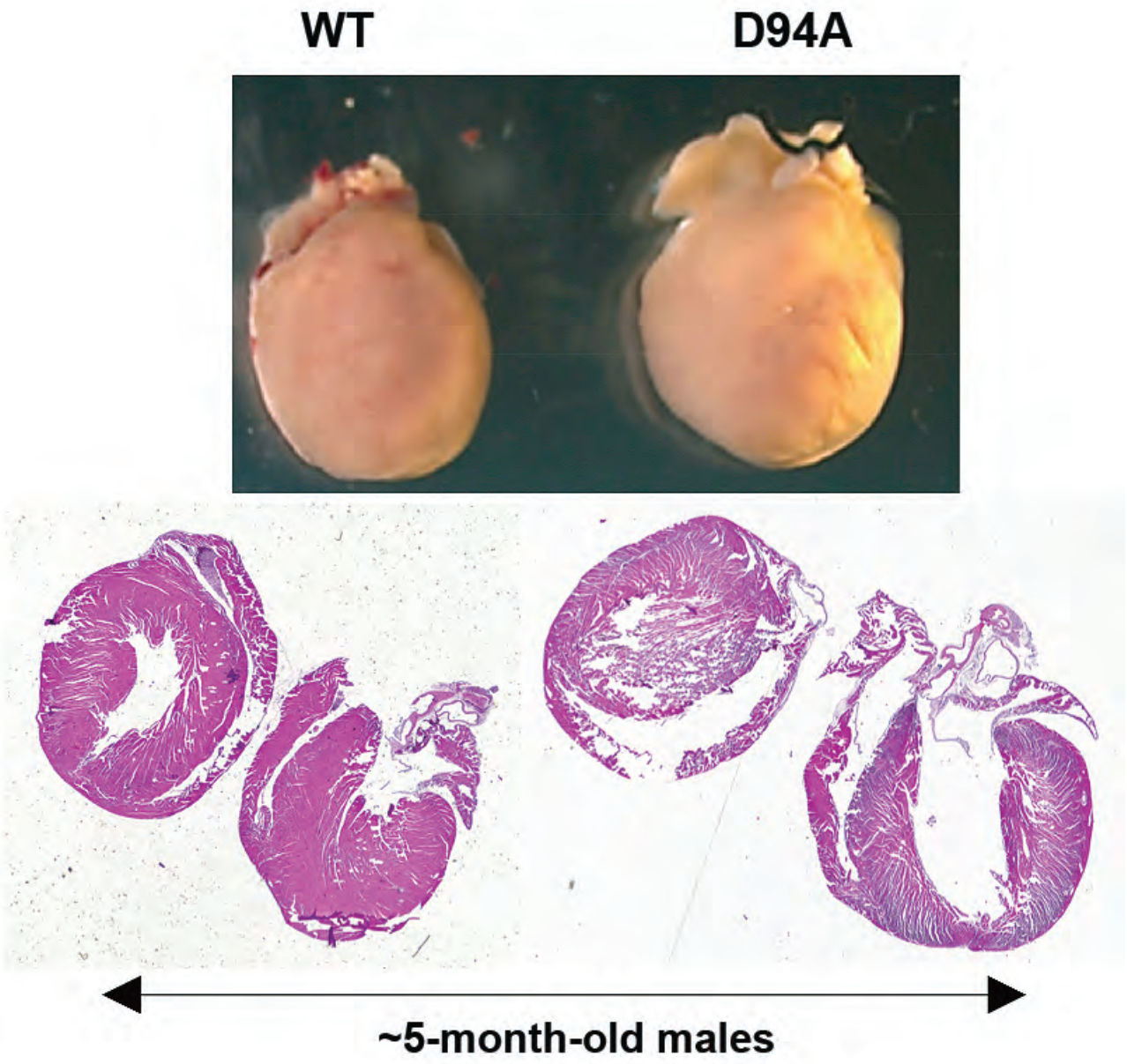

Dilated cardiomyopathy (DCM) is a serious and progressive heart disease that affects over 1 million people in the United States, annually. One hallmark of DCM is a reduced ability of the heart muscle to contract, and thus failure of the heart to adequately pump blood throughout the body. To build upon the recent discovery of the D94A mutation in the gene *MYL2*, in a family affected by DCM, researchers evaluated the hearts of transgenic mice expressing either normal or D94A human *MYL2*. Coupled with findings from functional assessments, examination of tissue samples using small-angle x-ray scattering at the APS show that D94A gives rise to the hypocontractile activity, reduced ejection fraction, and dilated left ventricle, supporting a direct role for the mutation in DCM. Showing that D94A is likely a causative mutation for DCM paves the way for new DCM therapies that may target MYL2.

Dilated cardiomyopathy has a number of causes, with sporadic cases arising from ischemia, alcohol toxicity, or viral infection, and inherited cases arising from genetic mutations in any one of approximately 40 currently known genes. Some 25% of DCM cases have a known genetic component, and each of the identified genes is involved in some way with the function of the cardiovascular musculature. This work by researchers from the University of Miami Miller School of Medicine and the University of California, Davis, builds on a recent discovery of a new mutation, D94A that is associated with DCM in a family pedigree. *MYL2* encodes a portion of the myosin protein, a subcellular filament that is a primary building block of muscle tissue. Myosin works like a motor, burning chemical energy to contract muscle tissue, including the muscle that makes up the heart.

To better understand the relationship between D94A and the clinical manifestations of DCM, researchers developed a transgenic mouse that expressed either the normal or D94A mutated human *MYL2* gene. The hearts of D94A mice had increased ventricular chamber size (Fig. 1) that correlated with reduced cardiac function, and microscopic evaluation showed tissue remodeling and fibrosis that is characteristic of DCM pathology in humans. Finally, male D94A mice were more susceptible to DCM than females, mirroring DCM clinical patterns in humans. Together, these patterns are highly suggestive of a direct role for D94A in DCM.

To understand the molecular mechanism of the DCM phenotype in D94A mice, researchers used small-angle x-ray diffraction at the Bio-CAT 18-ID-B beamline at the APS to measure the spacing of the myosin fibers within the D94A mouse heart tissue. They found that the position of the "motor" portion of the myosin fibers was abnormal in the D94A mice and consistent with a more stable inactive state. This finding, together with the observation that D94A muscle fibers are less sensitive to stimulation with Calcium ions than normal heart tissue reveal illustrate how the D94A mutation likely leads to reduced function in heart tissue and eventually, to myopathy.

The impact of this work is twofold. First, the development of the clinical mouse model paves the way for more in depth exploration of other genes known to play a part in DCM. Second, the improved understanding of how D94A leads to clinical manifestations may lead to development of therapies that can be used to treat DCM.

— Emma Nichols

< Fig. 1. Normal mouse hearts (top, WT) and hearts with a mutation (top, D94A). The D94A mutation causes dilated cardiomyopathy, evidenced in part by the impact of the mutation on heart structures (bottom). Adapted from C.-C. Yuan et al., Proc. Nat. Acad. Sci. USA **115**(10) (2018). Copyright ©2018 National Academy of Sciences.

See: Chen-Ching Yuan[1], Katarzyn[1], Kazmierczak[1], Jingsheng Liang[1], Zhiqun Zhou[1], Sunil Yadav[1], Aldrin V. Gomes[2], Thomas C. Irving[3], and Danuta Szczesna-Cordary[1]*, "Sarcomeric perturbations of myosin motors lead to dilated cardiomyopathy in genetically modified *MYL2* mice," Proc. Nat. Acad. Sci. USA **115**(10) (2018). DOI: 10.1073/pnas.1716925115
Author affiliations: [1]University of Miami Miller School of Medicine, [2]University of California, Davis, [3]Illinois Institute of Technology
Correspondence: * dszczesna@med.miami.edu

This work was supported by NIH-HL123255 (to D.S.-C.), NIH-HL096819 (to A.V.G.), and NIH-NIGMS 9P41-GM103622 (to T.C.I.), and American Heart Association Grants 15PRE23020006 (to C.-C.Y.), 17PRE33650085 (to S.Y.), and 15POST25080302 (to Z.Z.). This research used resources of the Advanced Photon Source, a U.S. Department of Energy (DOE) Office of Science User Facility operated for the DOE Office of Science by Argonne National Laboratory under Contract DE-AC02-06CH11357.

Deposits in Protein Data Bank — Light Sources Worldwide*

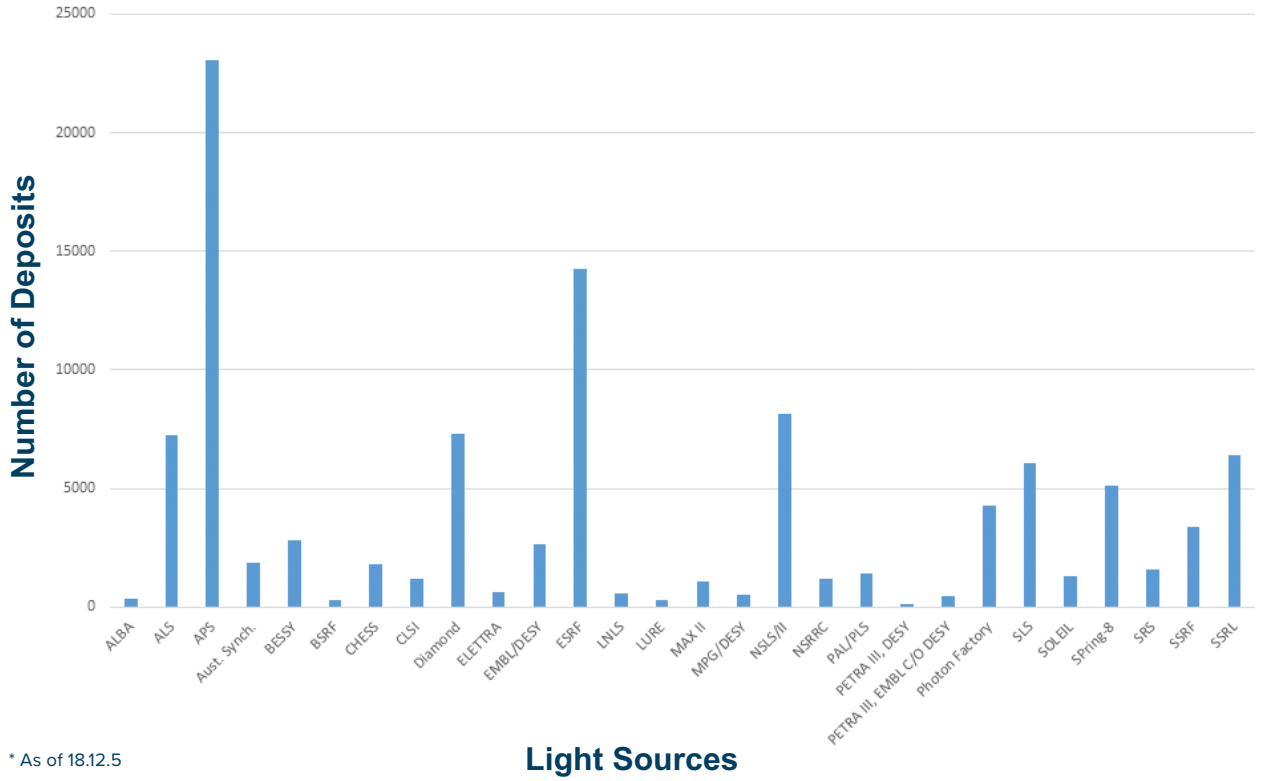

* As of 18.12.5

Number of APS Publications, Calendar Years 1998-2016
Recorded as of 18.12.11

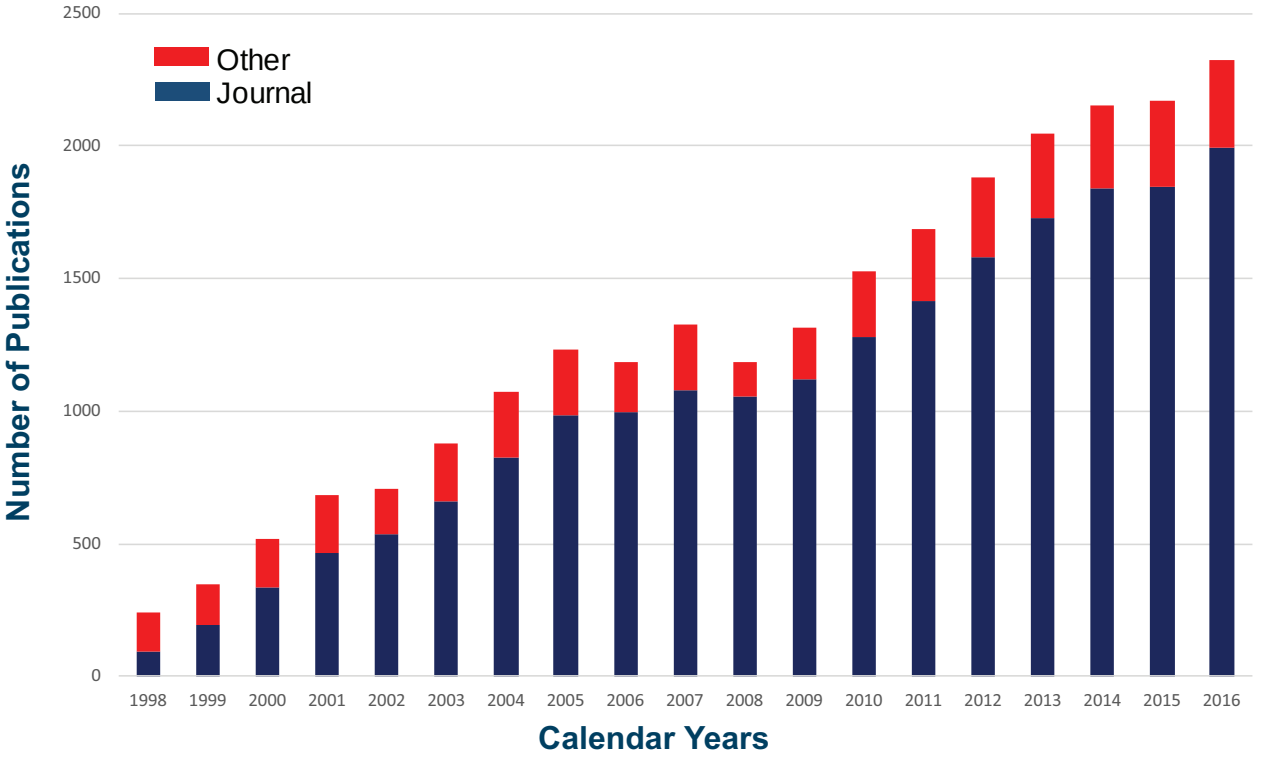

To search lists of APS publications see https://beam.aps.anl.gov/pls/apsweb/pub_v2_0006.review_start_page

Structural Biology

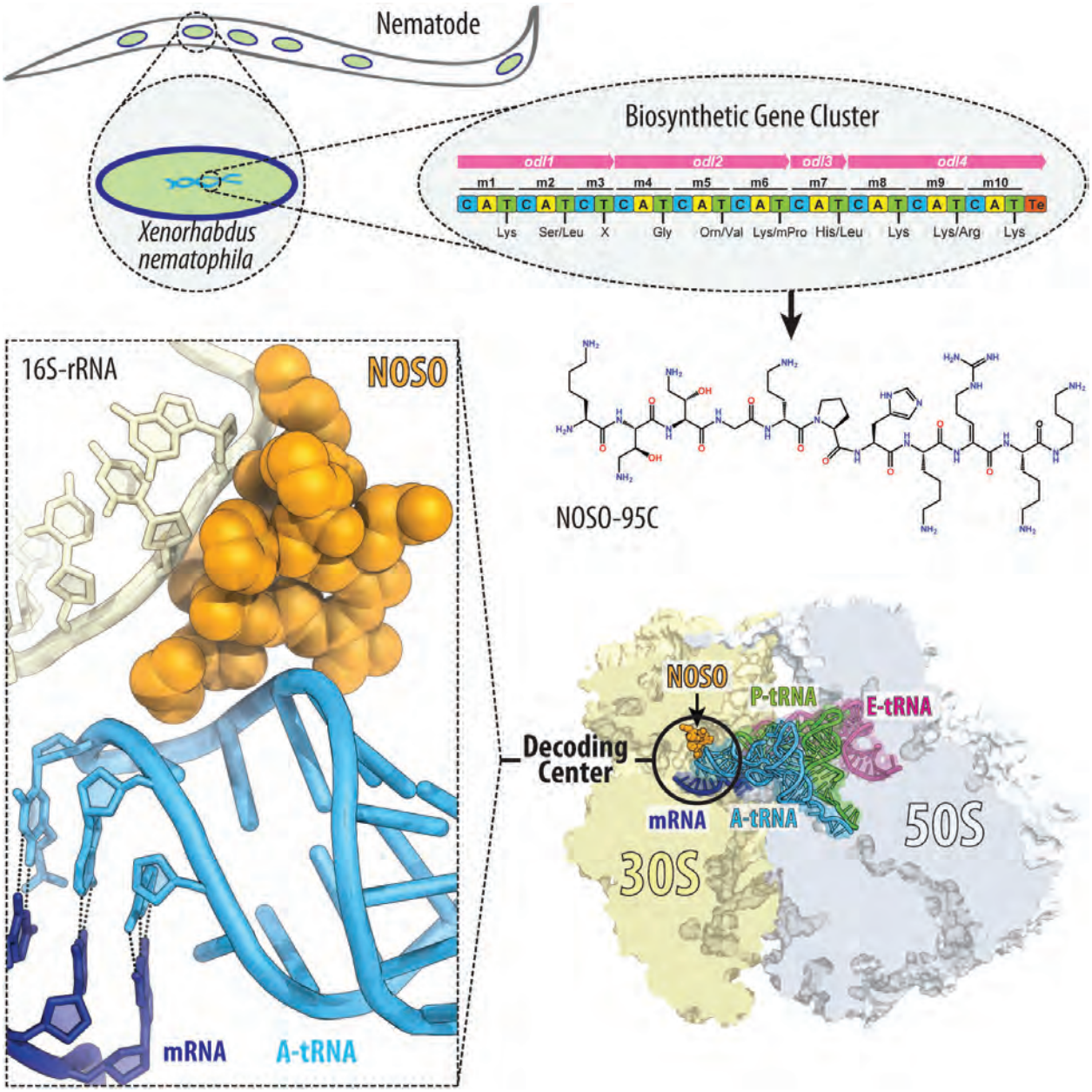

Fig. 1. A new antibiotic NOSO-95C, discovered in the symbiotic bacteria *Xenorhabdus nematophila* that infects nematode worms, occupies a unique binding site on the ribosome, the cell's protein manufacturer. NOSO-95C make contacts with both rRNA and tRNA within the ribosome and interrupts the proper building of proteins, likely by promoting the binding of the wrong version of tRNA.

A New Way to Kill Deadly Bacteria

The growing resistance of pathogenic bacteria to antibiotics and the lack of new drug development by the pharmaceutical industry has created an enormous global-health crisis. According to the World Health Organization, antibiotic resistance is one of the biggest threats to global health today and a significant contributor to longer hospital stays, higher medical costs, and increased mortality. Scientists are continuously in search of new sources of antibiotics that pathogenic bacteria are unfamiliar with and to which they have not yet evolved defense mechanisms. This threat has driven the exploration of unconventional sources of antibiotics and the identification of inhibitors able to exterminate drug-resistant bacteria. An international team of researchers recently identified a novel class of antibiotics produced by the nematode-symbiotic bacterium *Xenorhabdus nematophila*. Research with high-brightness x-ray beams from the APS and other experiments have led to clinical trials on one of these new antibiotics.

The new class of antibiotics discovered by researchers from Nosopharm (France), the University of Illinois at Chicago, Institut Charles Gerhardt Montpellier (France), Université de Montpellier (France), the University of Wisconsin-Milwaukee, Aix-Marseille Université (France), Statens Serum Institut (Denmark), and Uppsala University (Sweden) exhibit a unique way to kill bacteria. The new antibiotics, called "odilorhabdins," or ODLs, latch onto a specific binding site of a cell's protein-producing machine, called the ribosome, and gum up the works so badly that the cell makes defective versions of life-sustaining proteins. While many clinically useful antibiotics target the ribosome, ODLs bind to a site that has never been used by other known antibiotics.

ODLs are produced by symbiotic bacteria, *Xenorhabdus nematophila*, found in soil-dwelling nematode worms that colonize insects for food. The bacteria help to kill the insects and, importantly, secrete the antibiotic to keep competing bacteria away. Until now, these nematode-associated bacteria and the antibiotics they make have not been studied extensively.

To identify the antibiotic, the Nosopharm research team screened 80 cultured strains of *X. nematophila* for antimicrobial activity. They then isolated the active compounds, studied their chemical structures, and engineered more potent derivatives. After the team screened and isolated the most potent ODL derivatives, they showed that ODLs can neutralize Gram-positive and Gram-negative pathogens, including a family of highly antibiotic-resistant bacteria called "carbapenem-resistant *Enterobacteriacae*." The team then demonstrated that ODLs kill bacteria by crippling protein synthesis. X-ray crystal structural analyses conducted at the NE-CAT 24-ID-C and 24-ID-E x-ray beamlines at the APS further revealed that ODLs bind to the small ribosomal subunit of the Gram-negative eubacterium *Thermus thermophilus* at a site not exploited by current antibiotics. The researchers discovered that when bound to the ribosome, ODLs make contacts with both rRNA and tRNA and stimulate miscoding in the cell-free translation system and in the living cell, likely by promoting the binding of the wrong version of tRNA (Fig. 1). This illegitimate binding phenomenon impacts the reading ability of the ribosome and causes the organelle to make mistakes when translating the genetic code during the creation of new proteins. The result is that the cell is flooded with misshapen proteins, leading to the death of the bacterial cell.

The team confirmed the potency of ODLs with experiments in which the new antibiotics eradicated infections in a mouse model. Because ODLs are found in an unconventional source and because they employ a distinct method of killing bacteria, the compounds may be particularly effective at treating drug-resistant or hard-to-treat bacterial infections.

The researchers then tested the ODL compounds against bacterial pathogens, including many known to develop antibiotic resistance. They found that the ODL compounds cured mice infected with several pathogenic bacteria and demonstrated activity against both Gram-

"Bacteria" cont'd. on page 81

Chasing the Next Penicillin

The story of the discovery of penicillin and its use as an antibiotic is a classic. As the result of a serendipitous set of circumstances and a smart observation, one of the most effective, life-saving treatments ever was discovered accidentally. Now, however, overuse and bacterial evolution have combined to create a situation in which we need new antibiotics because bacteria have become resistant to the old ones. Penicillin has been shown to be so effective because it disrupts essential cell wall building enzymes in the bacterial membrane, halting bacterial growth. However, some bacteria can tolerate a complete removal of these essential genes and continue wall building without pause. Why? It turns out that bacteria have another set of enzymes, the SEDS proteins, that also appear to make the same cell wall components. Although we know SEDS are widely distributed among bacterial species, very little is known about their structure or function. Recent work has shown that one of these SEDS proteins, called RodA, acts as a peptidoglycan polymerase, just like the proteins targeted by penicillin. A team of researchers who carried out experiments at the APS has reported using a novel approach to overcome challenges in solving the structure of RodA that may open the door to finding the next penicillin, the hard way.

The researchers from Harvard University started by growing RodA crystals that diffracted to a resolution of 2.9 Å. Diffraction data from the macromolecule crystals were collected at the GM/CA-XSD beamline 23-ID-B at the APS. Unfortunately, the database of three-dimensional (3-D) structures had no closely-related protein structures that they could use as a model for phase calculation by molecular replacement. This is the most widely-used method of solving the crystallographic "phase problem," which refers to the fact that the amplitude of the signal is retained in diffraction data, but phase information is lost and must be deduced after data collection. After trying other established methods of solving this problem without success, the team decided to adapt a method called "evolutionary coupling analysis" to create a crude model of the RodA 3-D structure that would succeed in phase calculation by molecular replacement. Evolutionary co-variation is based on the idea that amino acid residues that interact with each other will co-evolve to maintain their interactions in a structure. Imagine two amino acids that have a positive and a negative charge and contact each other in the structure. Over time, these two would evolve together because their interaction is important to the overall structure of the protein.

Using this type of analysis and the amino acid sequences of a very large number of proteins related to RodA, researchers can deduce these interactions and build structural constraints that form a scaffold for structure design. The Harvard team developed 100 possible RodA models based on evolutionary constraints and tested whether each model could have produced the measured diffraction data. Of the initial 100, they found 22 plausible structures that eventually led them to a final refined crystal structure.

Their hard work paid off. The structure of RodA shows a unique fold with 10 transmembrane domains connected by small intracellular and large extracellular loops, suggesting that the extracellular domains are where the action happens. On the outer side of the membrane, between transmembrane domains 2 and 3, a long hydrophobic groove penetrates the membrane. The groove has the right characteristics to be the binding site for the lipid substrate that the enzyme acts on. In addition, the hydrophobic groove is adjacent to a water-filled central cavity that contains a conserved salt bridge (Fig. 1). Disruption of this evolutionarily conserved bridge causes growth problems for the bacteria and blocks the catalytic activity of the enzyme, suggesting this bridge might be a good target for an antibiotic. The fact that this central cavity is water-filled and on the outside of the membrane also means that it could be accessible to small-molecule drugs. *"Penicillin" cont'd. on next page*

"Penicillin" cont'd. from previous page

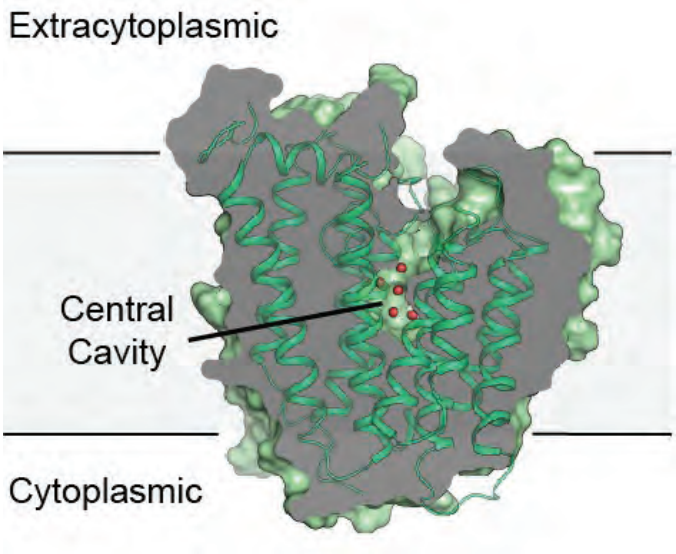

Fig. 1. The structure of RodA reveals a large water-filled central cavity that is a prime target for small-molecule inhibitor design. The green protein is sliced vertically (dark gray surface) to reveal bound water molecules (red) in the central cavity that is open to the extracytoplasmic surface. The surrounding membrane is light gray.

Using this work as a foundation, the team next plans to determine exactly how RodA and other related SEDS proteins work in order to understand how to block them. — Sandy Field

See: Megan Sjodt[1], Kelly Brock[1], Genevieve Dobihal[1], Patricia D. A. Rohs[1], Anna G. Green[1], Thomas A. Hopf[1], Alexander J. Meeske[1], Veerasak Srisuknimit[2], Daniel Kahne[2], Suzanne Walker[1], Debora S. Marks[1], Thomas G. Bernhardt[1], David Z. Rudner[1], and Andrew C. Kruse[1]*, "Structure of the peptidoglycan polymerase RodA resolved by evolutionary coupling analysis," Nature **556**, 118 (5 April 2018). DOI: 10.1038/nature25985
Author affiliations: [1]Harvard Medical School, [2]Harvard University
Correspondence: * andrew_kruse@hms.harvard.edu

Financial support for the work was provided by National Institutes of Health (NIH) grant U19AI109764 (A.C.K., D.Z.R., T.G.B., S.W. and D. K.), NIH grant R01GM106303 (D.S.M.), and a CIHR doctoral research award to P.D.A.R. GM/CA-XSD has been funded in whole or in part with Federal funds from the National Cancer Institute (ACB-12002) and the National Institute of General Medical Sciences (AGM-12006). The Eiger 16M detector was funded by an NIH–Office of Research Infrastructure Programs, High-End Instrumentation Grant (1S10OD012289-01A1). We thank GM/CA-XSD beamline staff for technical support during x-ray data collection. This research used resources of the Advanced Photon Source, an Office of Science User Facility operated for the U.S. DOE Office of Science by Argonne National Laboratory under contract no. DE-AC02-06CH11357, and the Canadian Light Source and its funding partners.

"Bacteria" cont'd. from page 79

negative and Gram-positive pathogens, notably including carbapenem-resistant *Enterobacteriacae*, or CRE, which are a family of highly drug-resistant microbes. CRE are a common cause of surgical site infections and mortality rates for infected individuals are close to 50%.

While many antibiotics can slow bacterial growth, such drugs that actually kill bacteria, called bactericidal antibiotics, are rare. The bactericidal mechanism of ODLs and the fact that they bind to a site on the ribosome not exploited by any known antibiotic are very strong indicators that ODLs have the potential to treat infections that are unresponsive to other antibiotics.

Although ODLs have yet to be thoroughly investigated for their therapeutic potential, the findings have encouraged further research. Researchers at Nosopharm plan to launch the first clinical trials of ODL NOSO-502 in humans in 2020. — Chris Palmer

See: Lucile Pantel[1], Tanja Florin[2], Malgorzata Dobosz-Bartoszek[2], Emilie Racine[1], Matthieu Sarciaux[1], Marine Serri[1], Jessica Houard[1], Jean-Marc Campagne[3], Renata Marcia de Figueiredo[3], Camille Midrier[3], Sophie Gaudriault[4], Alain Givaudan[4], Anne Lanois[4], Steve Forst[5], André Aumelas[1], Christelle Cotteaux-Lautard[6], Jean-Michel Bolla[6], Carina Vingsbo Lundberg[7], Douglas L. Huseby[8], Diarmaid Hughes[8], Philippe Villain-Guillot[1], Alexander S. Mankin[2]*, Yury S. Polikanov[2]**, and Maxime Gualtieri[1]***, "Odilorhabdins, Antibacterial Agents that Cause Miscoding by Binding at a New Ribosomal Site," Mol. Cell **70**, 83 (April 5, 2018) DOI: 10.1016/j.molcel.2018.03.001
Author affiliations: [1]Nosopharm, [2]University of Illinois at Chicago, [3]Institut Charles Gerhardt Montpellier, [4]Université de Montpellier, [5]University of Wisconsin-Milwaukee, [6]Aix-Marseille Université, [7]Statens Serum Institut, [8]Uppsala University
Correspondence: * shura@uic.edu, ** yuryp@uic.edu, *** m.gualtieri@nosopharm.com

We thank the staff at NE-CAT beamline 24-ID-C for help with data collection and freezing of the crystals. NE-CAT beamlines are funded by the National Institute of General Medical Sciences from the National Institutes of Health (NIH) (P41 GM103403). The Pilatus 6M detector on the 24-ID-C beamline is funded by an NIH-ORIP HEI grant (S10 RR029205). The Eiger 16M detector on the 24ID-E beamline is funded by an NIH-ORIP HEI grant (S10 OD021527). The work on this project was supported by research grants from Nosopharm (to Y.S.P. and A.S.M.) and Illinois State startup funds (to Y.S.P.). This work has received financial support from OSEO and Region Languedoc-Roussillon under grant agreement A1010014J and from DGA un-der grant agreement 122906117. The research leading to these results has also received support from the Innovative Medicines Initiative Joint Undertaking under grant agreement 115583, the resources of which are composed of financial contributions from the European Union Seventh Framework Program (FP7/2007-2013) and EFPIA companies in kind contribution. This research used resources of the Advanced Photon Source, a Department of Energy (DOE) Office of Science User Facility operated for the DOE Office of Science by Argonne National Laboratory under contract DE-AC02-06CH11357.

Evolution of a Zinc Finger

The 20,000 or so genes in the human genome contain a lot of information; too much information for a cell to use at any given time. So the cell has evolved a complex system to regulate gene expression, which includes zinc finger proteins. Zinc finger proteins, as the name suggests, have finger-like segments that press down onto specific sequences of DNA in a 1-finger to 3 base ratio to either increase or block gene expression. Scientists understand these binding properties so well that zing finger proteins can be engineered to bind to specific DNA segments and regulate genes of choice. But a new finding suggests that scientists may not understand zinc fingers as well as they thought, and that zinc finger binding properties are fluid. Using structural data collected at the APS, a research team discovered a protein with zinc fingers that can interact with two, three, or four bases, suggesting a level of evolutionary tunability that hadn't before been realized.

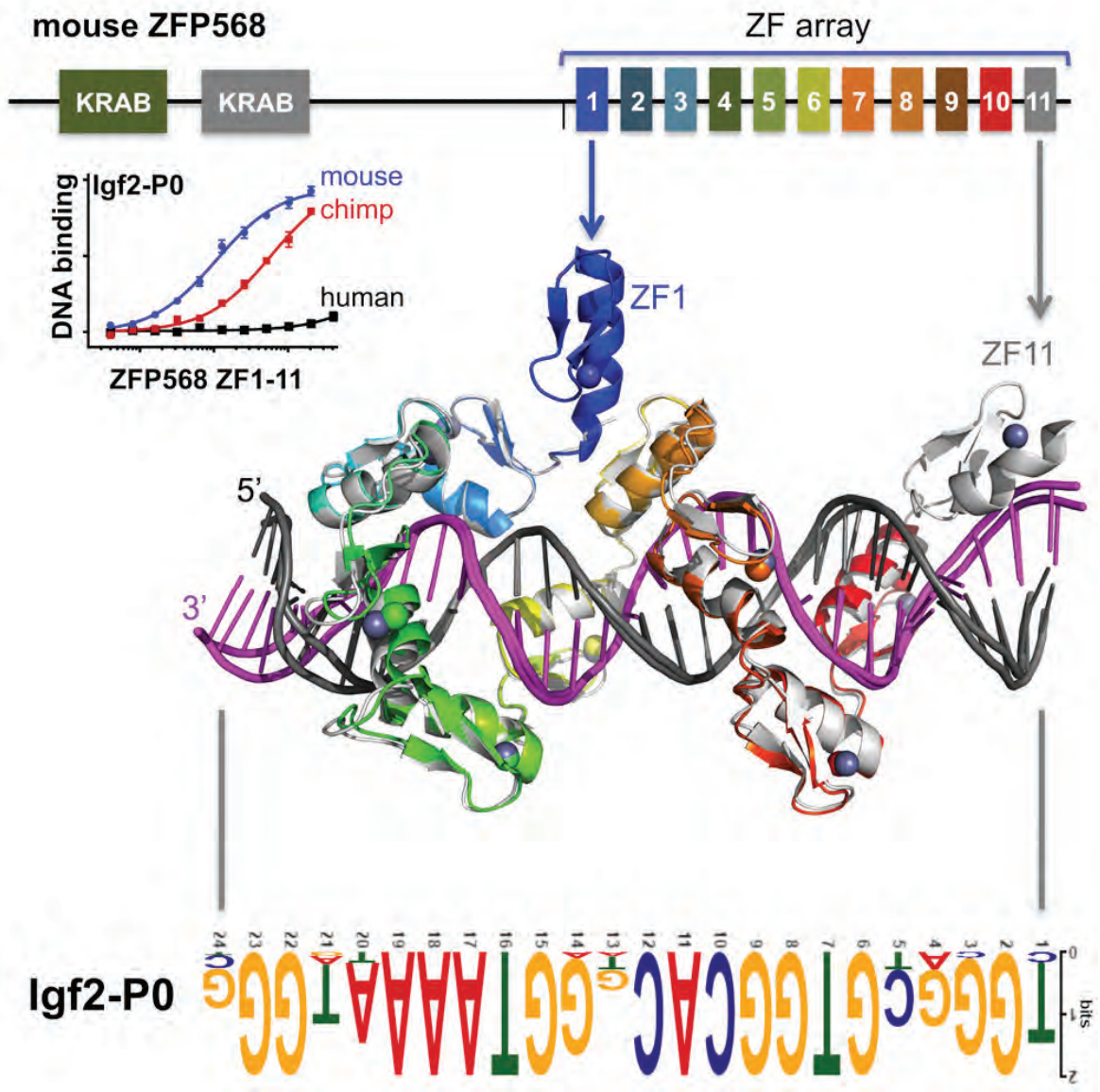

The KRAB-ZF family of zinc finger proteins include tandem repeats of zinc fingers from 3 to 35 fingers in length, with 11 to 13 fingers on average. The KRAB-ZF proteins have been around for a while, originating in the common ancestor of the coelacanth (an enormous bottom-dwelling fish), birds, and tetrapods (four-footed animals). About two-thirds of the KRAB-ZF proteins bind to transposable elements, bits of DNA that can jump from one part of the genome to another. Transposons can be disruptive, and KRAB-ZF proteins may have evolved to help mitigate the damage transposons can cause when they invade an important stretch of DNA. Yet, few KRAB-ZF proteins have been studied in molecular detail, leaving a gap in scientists understanding of their structure function relationship. In this study, the researchers from the Emory University School of Medicine, The Eunice Kennedy Shriver National Institutes of Child Health and Human Development, and The University of Texas MD Anderson Cancer Center focused on one particular member of the KRAB-ZF family, ZFP568, to better understand how zinc finger structures evolve to solve cellular problems.

In the very earliest stages of mouse development, as the single layer blastula undergoes gastrulation to become a multi-layered pocketed gastrula, ZFP568 regulates the morphogenesis of the tissue that extends beyond the embryo and forms the beginnings of the placenta. Specifically, ZFP568 is responsible for repressing the expression of an insulin-like growth factor in mouse placental tissues during early development. To accomplish this, ZFP568's 11 zinc fingers bind to a specific 24-base segment of mouse DNA in a promoter region upstream of the insulin-like growth factor gene. Employing macromolecular x-ray crystallography at the SER-CAT 22-ID-D beamline of the APS, the team obtained x-ray diffraction data that allowed them to determine the three-dimensional structure of ZFP568 bound to the DNA , which revealed unexpected binding properties that significantly diverge from typical zinc finger binding behavior (Fig. 1).

The structure showed that, near the ends of the DNA sequence, ZFP568 follows the canonical one finger to three base rule, while the interactions in the middle vary from a one finger to two base ratio to a one finger to four base ratio. The difference may have to do with the DNA sequence, with the ends being GC-rich and the middle AT-rich. AT-rich sequence has altered widths of DNA major and minor grooves from that of GC-rich sequence, suggesting that zinc fingers may have more options when binding to AT-rich regions than GC-rich regions of DNA.

To better understand the evolution of zinc finger proteins and their binding sites, the team also studied the human counterparts of ZFP568. In previous research, the researchers identified the human ZFP568 as a rapidly evolving gene. A comparison of mouse and human ZFP568 gene sequences and their corresponding binding sites suggested that the human version may have evolved mutations that would disrupt zinc finger binding, and thus may have lost its function. This was supported by data showing that human ZFP568 did not in fact bind to its corresponding promoter. Together, these findings suggest that human ZFP568 may be evolving new functions. — Erika Gebel Berg

< Fig. 1. Evolutionary and structure-function dynamics of zinc finger-DNA interactions reveal unconventional recognition codes and co-evolution of ZFP568 and its target gene Igf2 in mammals. Credit: Xiaodong Cheng; from A. Patel et al., Cell **173**, 221 (March 22, 2018). ©2018 Elsevier Inc.

See: Anamika Patel[1], Peng Yang[2‡], Matthew Tinkham[2], Mihika Pradhan[1], Ming-An Sun[2], Yixuan Wang[2‡], Don Hoang[2], Gernot Wolf[2], John R. Horton[3], Xing Zhang[3], Todd Macfarlan[2*], and Xiaodong Cheng[1,3**], "DNA Conformation Induces Adaptable Binding by Tandem Zinc Finger Proteins," Cell **173**, 221 (March 22, 2018). DOI: 10.1016/j.cell.2018.02.058
Author affiliations: [1]Emory University School of Medicine, [2]The Eunice Kennedy Shriver National Institutes of Child Health and Human Development, [3]The University of Texas MD Anderson Cancer Center ‡Present address: Tongji University
Correspondence: * todd.macfarlan@nih.gov,
** xcheng5@mdanderson.org

This work was supported by grants from the National Institutes of Health (GM049245-24 to X.Z. and X.C. and 1ZIAHD008933 to T.M.), and the Cancer Prevention Research Institute of Texas (RR160029) to X.C. The Department of Biochemistry of Emory University School of Medicine supported the use of the SER-CAT beamline. SER-CAT is supported by its member institutions (see www.ser-cat.org/members.html), and equipment grants (S10_RR25528 and S10_RR028976) from the National Institutes of Health. This research used resources of the Advanced Photon Source, a U.S. Department of Energy (DOE) Office of Science User Facility operated for the DOE Office of Science by Argonne National Laboratory under Contract No. DE-AC02-06CH11357.

An Enzyme May Improve Drug Design for Common Forms of Cancer

Membrane-embedded enzymes belonging to the DHHC family modify nearly 1000 human proteins, including epidermal growth factor receptors (EGFRs), a family of receptors implicated in a range of cancers. These enzymes, also known as "palmitoyltransferases," modify cell membrane-bound and soluble proteins by attaching fatty acids of differing lengths, which can lead to changes in a number of properties of the target protein including location, stability, and function inside of the cell. Researchers utilizing high-brightness x-rays from the APS determined the three-dimensional structure of the human DHHC20 enzyme using x-ray crystallography. While inhibiting DHHC activity to boost first-line treatments for breast and lung cancer has been proposed, there are no approved drugs aimed at specific DHHC enzymes. Better understanding the structure of these enzymes can make it possible to target them with new drugs.

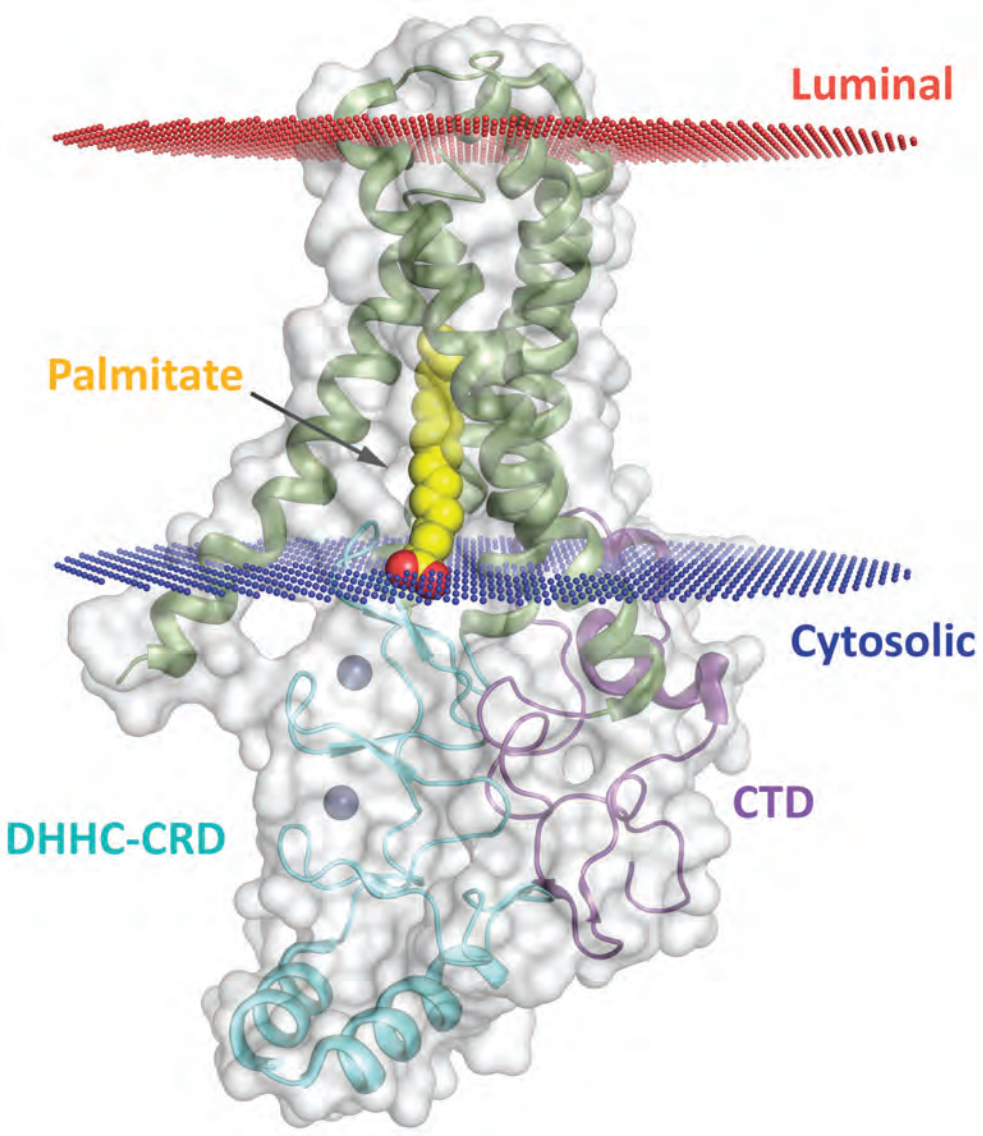

DHHC enzymes modify other proteins by attaching to them a certain kind of lipid called fatty acids. The predominant fatty acid used by these enzymes is the sixteen-carbon palmitic acid which is why this kind of modification is also called palmitoylation, although fatty acids of other chain length can also be used. Palmitoylation can change many properties of a target protein, such as the membrane association of peripheral membrane proteins, protein targeting to membrane subdomains, protein-protein associations, and protein trafficking.

Unlike most forms of posttranslational lipidation, protein palmitoylation is a potentially reversible modification. This enables dynamic modulation of the hydrophobicity of substrate proteins, which in turn results in protein palmitoylation playing important roles in a wide range of physiological processes such as Ras signaling, localization of neuronal scaffolding proteins, intracellular trafficking, activity of ion channels, and host-pathogen interactions. Because these processes are critical to normal cellular function, protein palmitoylation can play a prominent role in diseases such as cancers and neuropsychiatric disorders.

There are 23 DHHC enzymes in humans that modify an estimated 1,000 human proteins, including EGFRs. A well-known EGFR is HER2, which is overactivated in aggressive forms of breast cancer. EGFRs can also be overactivated in colon cancer, and non-small cell lung cancer, the most common type of lung cancer.

Scientists have proposed blocking DHHC activity to boost the effectiveness of first-line treatments against common forms of lung and breast cancer. Several EGFR inhibitors are already on the market, but some cancers can develop resistance to this class of drugs. However, there are currently no licensed drugs that target specific DHHC enzymes.

A team of researchers from the National Institutes of Health employed x-ray crystallography to study the atomic-level structure of a human DHHC enzyme, DHHC20 (Fig. 1), and the zebrafish version of another DHHC enzyme, DHHC15. They collected the x-ray crystallography data sets at the NE-CAT 24-ID-C, GM/CA-XSD 23-ID-D and 23-ID-B, and SER-CAT 22-ID-D beamlines at the APS. Importantly, DHHC20 is the enzyme that palmitoylates EGFR. Previous studies have shown that blocking DHHC20 makes cancer cells more vulnerable to existing treatments that target EGFR.

The research team identified a cavity within the structure of DHHC20 where the fatty acid tail is inserted. The amino acid residues lining this cavity form numerous contacts with the fatty acyl chain that the enzyme attaches to other proteins. Although some of these residues are conserved across all DHHC enzymes, there is considerable sequence diversity in the other residues between different subgroups of DHHC enzymes. These residues vary not only in their size, but also in their polarity, and likely alter the chemical properties of the cavity in a complex manner. Guided by the structure, the researchers designed mutations of specific residues that altered the relative size of the cavity, causing DHHC20 to use shorter or longer lipid chains. These changes may significantly alter target protein function and localization.

Based on these experiments, the researchers propose that the structure of this site explains why different DHHC enzymes have different fatty acid preferences. The structures reported by the team may be starting points for developing a structure-guided research program for the creation of human DHHC20 inhibitors that could lead to therapeutic interventions. — Chris Palmer

< Fig. 1. X-ray crystal structure of DHHC-CRD enzyme. The enzyme spans the cell membrane, with a luminal portion outside the cell and larger cytosolic portion, including the c-terminus domain (CTD) (mauve), inside the cell. The binding site for fatty acids, such as palmitate (yellow), resides within the bi-lipid membrane. Changes to the binding site can alter the length of fatty acids that DHHC can attach to proteins. Such changes can have significant effects of protein structure and function.

See: Mitra S. Rana[1], Pramod Kumar[1], Chul-Jin Lee[1], Raffaello Verardi[1], Kanagalaghatta R. Rajashankar[2], and Anirban Banerjee[1]*, "Fatty acyl recognition and transfer by an integral membrane S-acyltransferase," Science **359**(6372), eaao6326 (12 January 2018). DOI: 10.1126/science.aao6326
Author affiliations: [1]National Institutes of Health, [2]Cornell University
Correspondence: * anirban.banerjee@nih.gov

This work was supported by the Intramural Research Program of the National Institutes of Health (NIH), the National Institutes of Child Health and Human Development (1ZIAHD008928 to M.S.R., P.K., C.-J.L., R.V., and A.B.), and the National Institute of Neurological Disorders and Stroke (to R.V. and A.B.). NE-CAT is funded by the National Institute of General Medical Sciences from the NIH (P41 GM103403). The Pilatus 6M detector on the 24-ID-C beamline (NE-CAT) is funded by a NIH-ORIP HEI grant (S10RR029205). GM/CA-XSD has been funded in whole or in part with federal funds from the National Cancer Institute (ACB-12002) and the National Institute of General Medical Sciences (AGM-12006). The Eiger 16M detector at GM/CA-XSD was funded by a NIH, Office of Research Infrastructure Programs, High-End Instrumentation Grant (1S10OD012289-01A1). SER-CAT is supported by its member institutions (www.ser-cat.org/members.html) and equipment grants (S10_RR25528 and S10_RR028976) from the NIH. This research used resources of the Advanced Photon Source, a U.S. Department of Energy (DOE) Office of Science User Facility operated for the DOE Office of Science by Argonne National Laboratory under contract no. DE-AC02-06CH11357.

How Bacterial Architects Set Up House – In Your Cells

Legionellae are bacteria normally found in aquatic environments where they infect other microorganisms and generally leave people alone. However, in some situations, they can infect susceptible individuals and cause severe, potentially fatal pneumonia. They do this by subverting the action of immune cells in the lungs called "macrophages" that are tasked with killing them. Normally, macrophages engulf bacterial invaders and then break them down in a specialized membrane compartment, the lysosome, that is akin to a cellular recycling center. However, *Legionella pneumophila* counters this action by injecting 300 proteins into the macrophage and, over a few hours, builds itself its own membrane compartment to live and grow in. Many of the effector proteins involved in this hostile takeover have been identified by the similarity of their amino acid sequence to known proteins. But some of them, like the Lem4 protein, have resisted identification. In an effort to identify these potentially important antibiotic targets, researchers turned to x-ray beams from the APS and the Canadian Light Source to solve the structure of some of these proteins to try to identify them based on their three-dimensional similarity to known proteins. Their findings confirm the function of Lem4 as a phosphatase and suggest it plays an important role in *Legionella pneumophila* infection while also providing a variety of potentially fruitful opportunities for future studies and insight into how these clever bacteria take over our cellular machinery to set up house.

This project, conducted by a team from the University of Saskatchewan and McGill University (both Canada), started with crystallization of Lem4. The protein has two domains; the C-terminal end is hypothesized to bind to membranes and the function of the N-terminal end is unknown. Macromolecular crystallography studies carried out at the the LRL-CAT 31-ID-D beamline at the APS and at the 08ID-CMCF beamline at the Canadian Light Source, were successful in determining the structure of a stable fragment of the N-terminal end predicted to house the functional domain of the protein. Comparison of the Lem4 structure to a database of structures showed that it is closely related to a mouse protein phosphatase (MDP-1), a class of enzymes that plays a critical role in cellular signaling by removing phosphate groups from other proteins.

In vitro assays showed that Lem4 acts to remove phosphates from tyrosine residues, rather than serine or threonine, and has similar kinet-

Fig. 1. Structural representation of the N-terminal phosphatase domain of Lem4. Important active site amino acids are shown as sticks oriented toward the phosphate group (orange and red ball and stick structure) and magnesium ion (purple ball) substrates.

ics to the MDP-1 phosphatase from mice. Screening with a panel of 360 peptides which present the phosphorylated tyrosine in the context of different amino acid sequences, allowed the team to identify the preferred substrate sequence for Lem4. Intriguingly, this preferred sequence is found in a protein, called colony stimulating factor 1 receptor (CSF1R), that is important in macrophage signaling, making it a potential target for Lem4 action in cells. Further co-precipitation experiments identified a number of other potential targets and showed that the presence of Lem4 in cells causes an increase in phosphorylated proteins in the cell. This suggests that its dephosphorylating actions lead to activation of proteins downstream providing rich opportunities for future study.

Once they confirmed that Lem4 was indeed a phosphatase, the team was able to go back to the MDP-1 structure and compare its active site to their Lem4 structure. They identified the critical active site residues at the base of a deep tunnel approximately 9 Å from the surface of the protein. Like MDP-1, the Lem4 active site entrance appears to be restricted by the sidechains of the surface residues which may play a role in substrate specificity.

To understand more about the role of Lem4 in cells and the role of the C-terminal domain (hypothesized to be the membrane-binding domain), they expressed each end and the whole protein in cells. These experiments confirmed the role of the C-terminal domain as important to membrane localization and showed that the protein localized to lysosomes and the plasma membrane, findings that are consistent with a role for Lem4 in early *Legionella* infection. — Sandy Field

See: Ksenia Beyrakhova[1], Lei Li[1], Caishuang Xu[1], Alla Gagarinova[1], and Miroslaw Cygler[1,2]*, "Legionella pneumophila effector Lem4 is a membrane-associated protein tyrosine phosphatase," J. Biol. Chem. **293**(34), 13044 (2018). DOI: 10.1074/jbc.RA118.003845
Author affiliations: [1]University of Saskatchewan, [2]McGill University
Correspondence: * miroslaw.cygler@usask.ca

The Canadian Light Source is supported by the Canada Foundation for Innovation, Natural Sciences and Engineering Research Council of Canada, the University of Saskatchewan, the Government of Saskatchewan, Western Economic Diversification Canada, the National Research Council Canada, and the Canadian Institutes of Health Research. Use of the Lilly Research Laboratories Collaborative Access Team (LRL-CAT) beamline at Sector 31 of the Advanced Photon Source was provided by Eli Lilly, which operates the facility. This research used resources of the Advanced Photon Source, a U.S. Department of Energy (DOE) Office of Science User Facility operated for the DOE Office of Science by Argonne National Laboratory under Contract No. DE-AC02-06CH11357.

Knowing Legionellosis

Legionellosis, which includes Legionnaires' disease and Pontiac fever, is a respiratory disease caused by a type of bacteria called *Legionella*, which was discovered after an outbreak in 1976 among people who went to a Philadelphia convention of the American Legion. Those who were affected suffered from a type of pneumonia (lung infection) that eventually became known as Legionnaires' disease.

The first identified cases of Pontiac fever occurred in 1968 in Pontiac, Michigan, among people who worked at and visited the city's health department. It wasn't until *Legionella* was discovered after the 1976 outbreak in Philadelphia that public health officials were able to show that the same bacterium causes both diseases.

In the U.S., the rate of reported cases of Legionnaires' disease has grown by nearly five and a half times since 2000. It is unclear whether this increase is due to increased awareness and testing, increased susceptibility of the population, increased *Legionella* in the environment, or some combination of factors. Health departments reported almost 7500 cases of Legionnaires' disease in the U.S. in 2017. But because Legionnaires' is likely underdiagnosed, this number may underestimate the true incidence. More illness is usually found in the summer and early fall, but it can happen any time of year.

Legionella is a type of bacterium found naturally in freshwater environments, like lakes and streams. It can become a health concern when it grows and spreads in human-made building water systems like showerheads and sink faucets, cooling towers (structures that contain water and a fan as part of centralized air cooling systems for building or industrial processes), hot tubs that aren't drained after each use, decorative fountains and water features, hot water tanks and heaters, and large plumbing systems. Home and car air-conditioning units do not use water to cool the air, so they are not a risk for *Legionella* growth.

After *Legionella* grows and multiplies in a building water system, water containing Legionella then has to spread in droplets small enough for people to breathe in. Less commonly, people can get sick by aspiration of drinking water containing *Legionella*. This happens when water accidently goes into the lungs while drinking. People at increased risk of aspiration include those with swallowing difficulties.

In general, people do not spread Legionnaires' disease and Pontiac fever to other people. However, this may be possible under rare circumstances.
Source: Centers for Disease Control and Prevention, https://bit.ly/2sNpV3a

Facilitating Faster Folding Following

The direct tracking of protein structural dynamics during folding and unfolding processes is important for understanding the formation of functional proteins. In an effort to monitor such dynamics, a team of researchers turned to the APS to investigate structural changes during the folding of the cytochrome c, a large transmembrane protein involved in the respiratory electron transport chain. Their results demonstrate how different environmental conditions can change the nature of interaction between a protein's active site and its overall conformation, even within the same metalloprotein, which subsequently affect folding structural dynamics. The team believes that the experimental technique employed here, time-resolved x-ray solution scattering or TRXSS, coupled to jumps in pH, electron transfer, and previously reported jumps in temperature, will make it possible to perform detailed studies of biologically relevant processes in non-photoactive proteins with high structural sensitivity and high temporal resolution at the same time.

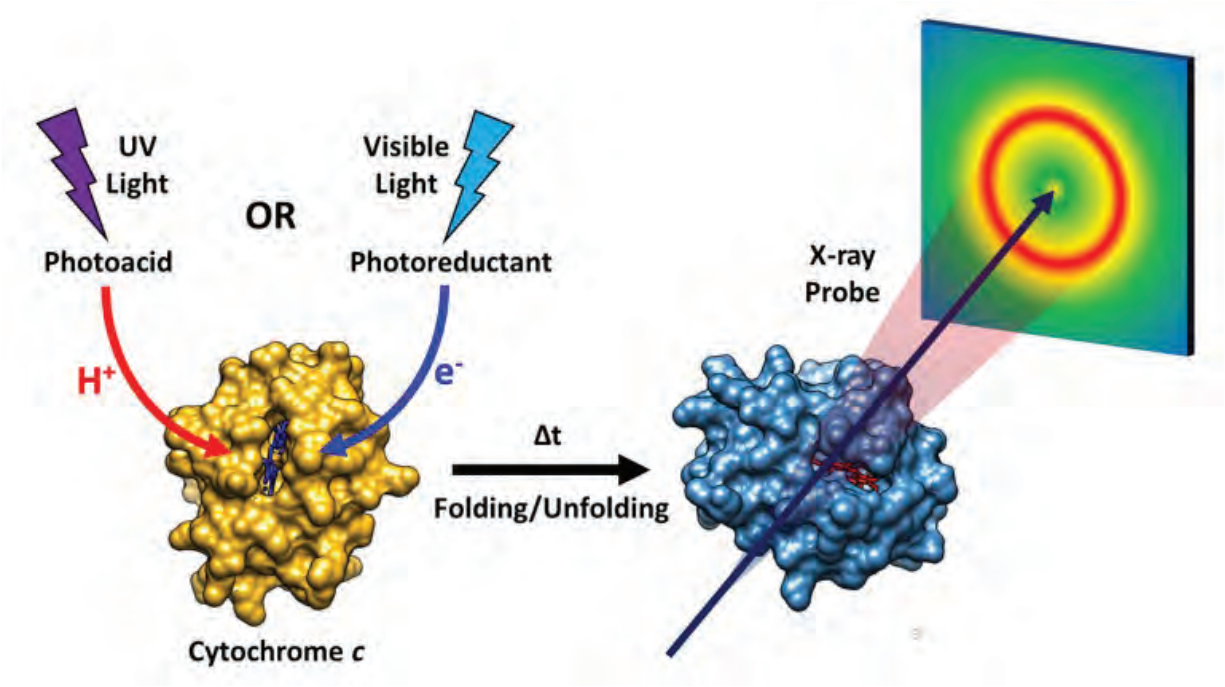

Fig. 1. Experimental scheme for the TRXSS experiment utilizing photoinduced pH jump/photoreduction initiation. The protein responds to the change in the local environment by undergoing structural changes that can be probed by x-ray scattering on nanosecond to second timescales.

Protein structure-function relationships are known to be sensitive to environmental conditions, such as temperature, pH, and the presence of compounds that trigger redox reactions. Within cells, protein environment, structure, and function work together to regulate a protein's biological functions via conformational gating or ligand binding. Protein folding dynamics typically span multiple timescales and can range from nanoseconds to milliseconds for fast folding proteins.

Traditional time-resolved structural biology methods, such as stopped flow or continuous flow mixing, typically cannot resolve the first 100 μsec from initiating mixing and the beginning of kinetics observations, making these methods not suited to tracking dynamics on short timescales. In contrast, pulsed laser-based methods can initiate reactions on timescales as short as femtoseconds, making them well suited to observations of short-lived intermediate states.

Still, laser-based approaches are limited in that naturally occurring light-driven proteins are rare and an intrinsic chromophore is needed to drive the dynamics and probe structural changes. The team of researchers from Northwestern University, the University of Delaware, The University of Chicago, and Argonne devised a new technique for studying protein folding dynamics that eliminated the need for an intrinsic chromophore by employing laser excitation to perturb the protein environment. They then probed the resulting structural changes with TRXSS, carried out at the BioCARS 14-ID-B beamline at the APS, which is capable of directly tracking protein tertiary structural dynamics, which gives it an important advantage over spectroscopic methods such as optical transient absorption (OTA) that indirectly infers global protein conformation. The team also collected steady-state scattering patterns of proteins at different temperature at the DND-CAT 5-ID-B,C,D beamline at the APS. These patterns served as reference in data analysis to extract transient protein structures.

The protein that the researchers investigated, cytochrome c, is a heme metalloprotein that takes part in the mitochondrial electron transport chain. It also plays a role in apoptosis, or programmed cell death. In their study, the researchers triggered protein conformational changes in cytochrome c by either bombarding the protein with UV light to induce a jump in pH or with visible light to induce electron transfer. Both experiments utilized TRXSS to directly observe the resulting structural dynamics as the protein underwent folding and unfolding (Fig. 1).

Starting from partially unfolded cytochrome c, a sudden pH drop caused a structural contraction within microseconds, followed by active site restructuring and unfolding within milliseconds. In contrast, the reduction of iron in the heme embedded within cytochrome c produced by photoinduced electron transfer did not affect the protein's conformational stability at sub-millisecond timescales, despite changes to active site coordination geometry.

The team found the TRXSS experiments to be sensitive to both the active site dynamics and the global structural rearrangements in cytochrome c. These properties of TRXSS allowed the researchers to directly observe the formation of a previously unseen intermediate state in the pH-jump experiments, which did not affect the active site dynamics directly and would therefore have been missed with OTA. — Chris Palmer

See: Dolev Rimmerman[1], Denis Leshchev[1], Darren J. Hsu[1], Jiyun Hong[1], Baxter Abraham[2], Robert Henning[3], Irina Kosheleva[3], and Lin X. Chen[1,4]*, "Probing Cytochrome c Folding Transitions upon Phototriggered Environmental Perturbations Using Time-Resolved X-ray Scattering," J. Phys. Chem. B **122**, 5218 (2018). DOI: 10.1021/acs.jpcb.8b03354

Author affiliations: [1]Northwestern University, [2]University of Delaware, [3]The University of Chicago, [4]Argonne National Laboratory

Correspondence: * l-chen@northwestern.edu or lchen@anl.gov

This work was supported by the National Institutes of Health (NIH), under contract no. R01-GM115761. B.A. acknowledges support from the U.S. Department of Energy (DOE) Office of Science Graduate Student Research program, administered by the Oak Ridge Institute for Science and Education, managed by ORAU under contract number DE-SC0014664, as well as from the U.S. DOE Office of Science-Basic Energy Sciences, under award number DE-SC0016288. Use of BioCARS was also supported by the National Institute of General Medical Sciences of the NIH under grant number R24GM111072. Time-resolved setup at Sector 14 was funded in part through collaboration with Philip Anfinrud (NIH/NIDDK). The authors also acknowledge Guy Macha (BioCARS) for his assistance in designing the sample holder. The DuPont-Northwestern-Dow Collaborative Access Team is supported by Northwestern University, E.I. DuPont de Nemours & Co., and The Dow Chemical Company. Data were collected using an instrument funded by the National Science Foundation under award number 0960140. This research used resources of the Advanced Photon Source, a U.S. DOE O ce of Science User Facility operated for the DOE O ce of Science by Argonne National Laboratory under contract no. DE-AC02-06CH11357.

A "New" Ligase Upends a Canonical Enzyme Reaction

Just when scientists thought they knew an enzyme superfamily, they discovered a member that doesn't fit the mold. The activation of carboxylates (salts or esters of a carboxylic acid) with coenzyme A (CoA-SH) is a fundamental biological reaction, underpinning the metabolism of fatty acids and the synthesis of amino acids, among many other critical reactions. The enzymes that perform this reaction are termed "acyl-CoA ligases," and they all catalyze a two-step reaction including an adenylation step, the process of attaching an AMP molecule to carboxylic acids to afford acyl-adenylates, compounds with the functional group AMP-CO-R, and a thioesterification step, which converts acyl-adenylates, in the presence of CoA-SH, into thioesters, compounds with the functional group CoA–S–CO–R. All, that is, until a research team working at the APS discovered the first non-adenylating acyl-CoA ligase, opening up new avenues for biological inquiry.

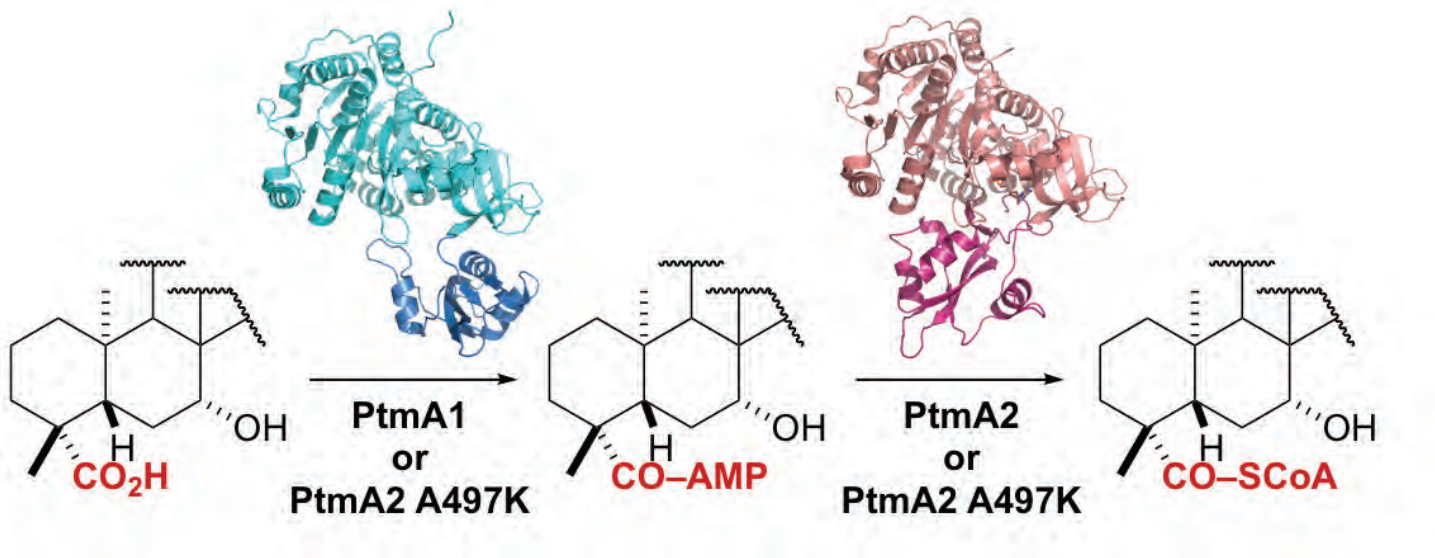

Fig. 1. A naturally separated acyl-CoA ligase reaction was discovered in the biosynthesis of the antibiotics platensimycin and platencin. PtmA1 and PtmA2 act sequentially to activate a free acid to an acyl-CoA via an acyl-adenylate intermediate. The canonical bifunctionality of PtmA2 was restored by a single active site mutation. The depicted crystal structures highlight the ability of PtmA2 to alternate between the two conformations necessary for both adenylation and thioesterification. Credit: Ben Shen (The Scripps Research Institute)

Scientists had long assumed that it was necessary that acyl-CoA ligases (enzymes that bring about ligation of carboxylic acids with CoA-SH) perform thioesterification directly after adenylation in the same enzymatic active site due to the extreme reactivity of the intermediate. It was an accident that the team from The Scripps Research Institute and Rice University discovered otherwise. They had been studying the bacterial biosynthesis of two fatty acid synthase inhibitors. These molecules, platensimycin and platencin, are produced by the bacteria *Streptomyces platensis* and are being investigated as potential antibiotics and diabetes medications. Evidence suggested that a key step in their biosynthesis was the activation of a carboxylate, indicating the participation of

an acyl-CoA ligase. After scanning the genome of *S. platensis* looking for the responsible enzyme, the researchers identified one candidate, PtmA2, which, according to its sequence, should have been a canonical adenylating acyl-CoA ligase. However, inactivation of PtmA2 in *S. platensis* caused an accumulation of adenylates, suggesting that the enzyme may not be involved in adenylation after all.

So the question became, where were the adenylated species coming from? The researchers looked toward another potential acyl-CoA ligase they'd identified in the genome of *S. platensis*, called PtmA1. When PtmA1 was inactivated in *S. platensis*, they observed an accumulation of free acids, suggesting that species were not being adenylated. Thus, PtmA1 must be the counterpart to PtmA2, the yin to PtmA2's yang. PtmA1 performed the

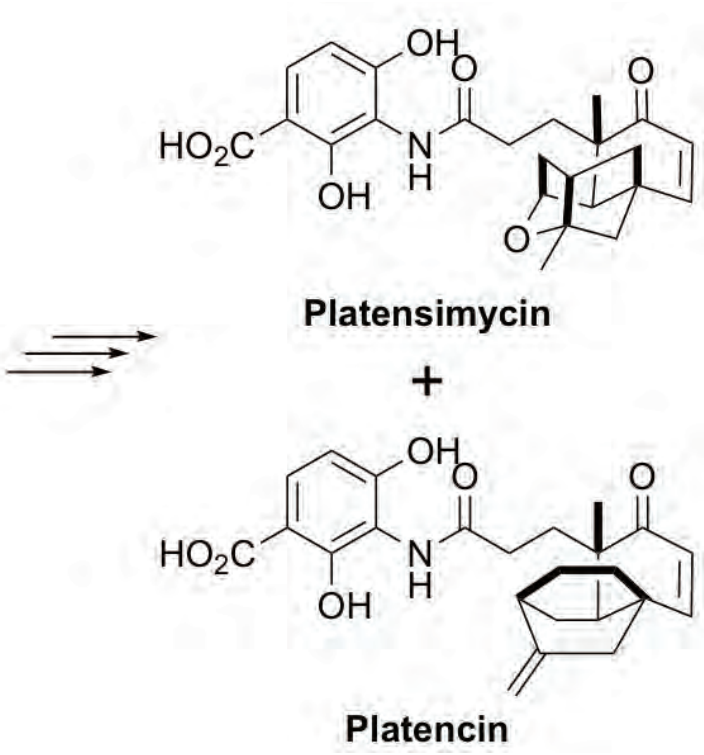

adenylation half of the acetylation reaction, while PtmA2 finished the job with thioesterification. Together, PtmA1 and PtmA2 behave as the functional equivalent of a canonical acyl-CoA ligase. When Shen's team scanned other species' genomes looking for other PtmA2-like non-adenylating acyl-CoA ligases, they found a bunch, and many had a PtmA1-like protein sequence in close genomic proximity, suggesting coexpression.

As a next step, the researchers, with colleagues from Argonne, solved the structure of the novel enzyme PtmA2 via single-wavelength x-ray diffraction data collected at the peak wavelength of 0.9792 Å and 100 K temperature at the 19-BM-D and 19-ID-D beamlines of the SBC-CAT at the APS. The structure of PtmA2 turned out to look a lot like adenylating acyl-CoA ligases. So, at first the team wasn't sure why PtmA2 lacked adenylation activity. But a closer look at the protein's structure revealed one key difference in the active site. Among adenylating acyl-CoA ligases, there is a conserved lysine in the active site that is essential to the adenylation reaction and is believed to track the negative charge during the adenylation half of the reaction. In PtmA2, the corresponding residue at that position is an alanine. When the team mutated PtmA2 to replace that alanine with a lysine, they restored adenylating activity, albeit with less catalytic efficiency than is typical of a full strength enzyme (Fig. 1).

The discovery of a non-adenylating CoA ligase has some interesting biological implications, according to the authors. The explanation for why, in this case, biology chose to use two enzymes to perform this reaction instead of one is unclear, but there are multiple possibilities, including the addition of a layer of regulation. Future studies will explore how, and why, this counterintuitive enzymatic duo evolved and if other metabolic pathways utilize the same strategy. — Erika Gebel Berg

See: Nan Wang[1], Jeffrey D. Rudolf[1], Liao-Bin Dong[1], Jerzy Osipiuk[2], Catherine Hatzos-Skintges[2], Michael Endres[2], Chin-Yuan Chang[1], Gyorgy Babnigg[2], Andrzej Joachimiak[2], George N. Phillips, Jr.[3], and Ben Shen[1]*, "Natural separation of the acyl-CoA ligase reaction results in a non-adenylating enzyme," Nat. Chem. Biol. **4**, 730 (July 2018). DOI: 10.1038/s41589-018-0061-0
Author affiliations: [1]The Scripps Research Institute, [2]Argonne National Laboratory, [3]Rice University
Correspondence: * shenb@scripps.edu

This work is supported in part by the National Institute of General Medical Sciences Protein Structure Initiative grants GM094585 (A.J.) and GM098248 (G.N.P.) and National Institutes of Health grants GM109456 (G.N.P.) and GM114353 (B.S.). Use of SBC-CAT beamlines was supported by U.S. Department of Energy (DOE) Office of Science-Biological and Environmental Research grant DE-AC02-06CH11357 (A.J.). N.W. is supported in part by the Institute of Applied Ecology, Chinese Academy of Sciences, and a scholarship from the Chinese Scholarship Council (201504910034). J.D.R. is supported in part by an Arnold O. Beckman Postdoctoral Fellowship. C.-Y.C. is supported in part by the Fellowship of Academia Sinica–The Scripps Research Institute Postdoctoral Talent Development Program. This research used resources of the Advanced Photon Source, a U.S. DOE Office of Science User Facility operated for the DOE Office of Science by Argonne National Laboratory under Contract No. DE-AC02-06CH11357.

Safer Opioids Taking Shape

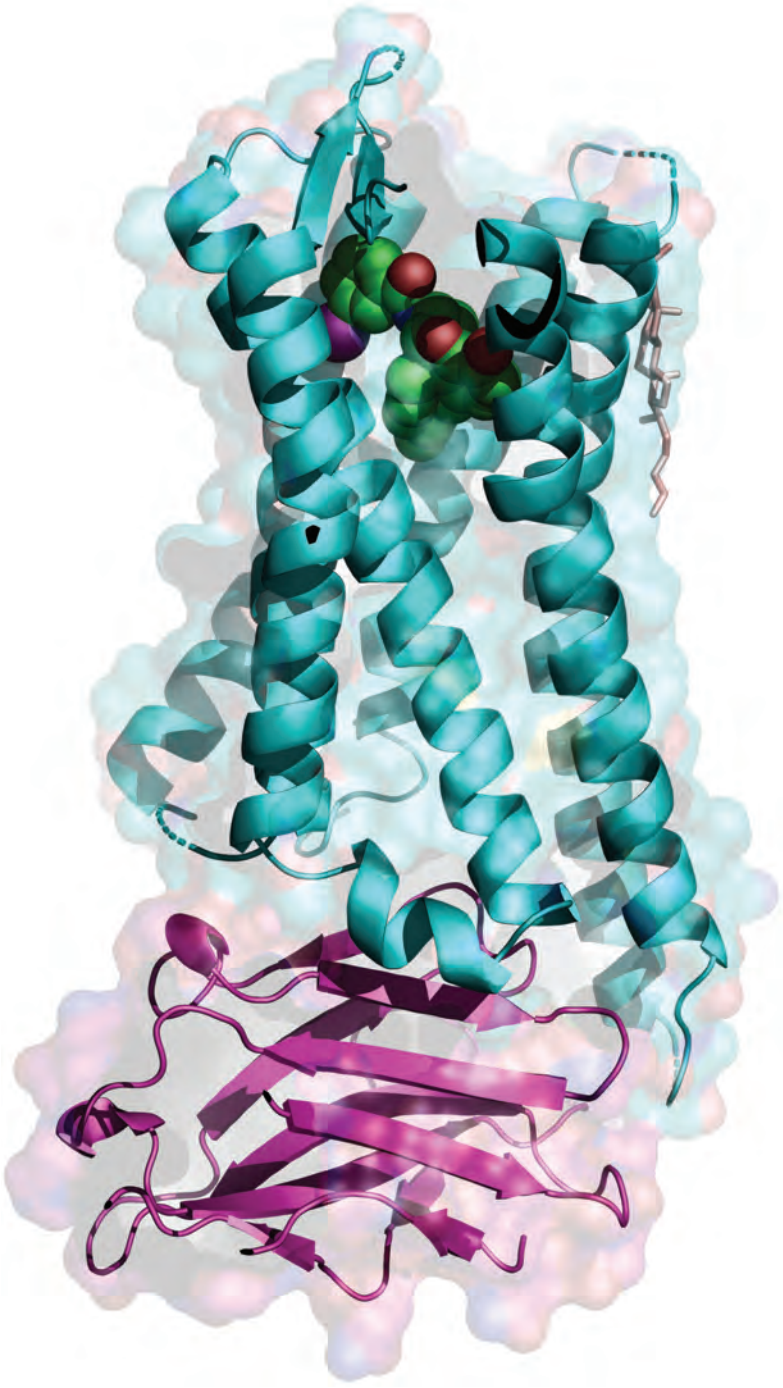

Opioids play a very important role in providing pain relief to millions of people, through the activation of analgesic, or painkilling, pathways found in cells throughout the brain and peripheral nervous system. However, the primary opioid receptors — delta, kappa, and mu — are also linked to chemical signaling pathways tied to a variety of side effects, ranging from nausea and constipation to lethal respiratory problems. One particular type of opioid receptor, called the "kappa receptor," triggers analgesia as well as a handful of non-lethal side effects. Finding a drug that activates kappa in a way that only elicits pain relief has been challenging. Knowing the exact structure of the kappa receptor can likely help researchers identify or synthesize a safer pain relief molecule. An international team of nearly two dozen researchers carrying out studies at the APS derived the structure of a complex of the human kappa opioid receptor bound by the morphine derivative MP1104 and an antibody that helps stabilize the receptor in its active state. Comparisons between inactive- and active-state opioid receptor structures revealed significant changes in the shape of the binding pocket and in the regions of kappa that face the inside and outside of the cell. These molecular insights offer the potential to accelerate the structure-guided design of safer and more effective therapeutic compounds that target kappa opioid receptors.

Most opioids bind to several different kinds of opioid receptors — primarily the delta, kappa, and mu receptors — on the surface of cells throughout the brain and peripheral nervous system. Drugs such as fentanyl, heroin, morphine, and oxycodone latch onto the mu opioid receptor particularly well. Unfortunately, while the mu receptor facilitates these drugs' analgesic, or painkilling, properties, it's also responsible for their addictive properties and a variety of side effects, including respiratory depression, which plays a prominent role in the deaths of tens of thousands of people per year in the U.S.

Like mu, the kappa opioid receptor can mediate pain relief. But the side effects associated with kappa — frequent urination, hallucinations, and unhappiness — are non-lethal. In addition, recent evidence suggests the possibility of finding specific drugs that can act at the kappa receptor to trigger signaling pathways relevant to pain relief, but not to those associated with side effects.

But whether such selective activation is possible depends on the receptor's structure, which changes shape when an opioid molecule binds, thereby kicking off one or more signaling cascades inside the cell. Scientists typically determine the three-dimensional structures of proteins with the x-ray crystallography technique, in which the protein is constrained in a crystal that is then bombarded with a high-energy x-ray beam, revealing the protein's structure based on how the crystal diffracts the x-rays.

< Fig. 1. A schematic view of an x-ray crystal structure of the kappa opioid receptor (teal) determined using a 10-μm minibeam at GM/CA-XSD at the APS, in complex with the morphine derivative MP1104 (green and red atoms, near top) and the antibody Nb39 (purple, near bottom).

Because the structure of an active kappa receptor is far more flexible than its previously described inactive form, the researchers had to add a few more steps to their crystallography procedure. Using a method called "lipidic cubic phase crystallization," the team first suspended the kappa receptor in a custom water-lipid mixture and slowly removed the water. Then, they utilized a tiny antibody to stabilize the receptor in its active state when it was bound to a derivative of morphine called MP1104. The effect was akin to unlocking a door with a key, then using a door stop to keep it open long enough to take a picture of it. The researchers tried this procedure several hundred times and stitched together a 3.1-Å-resolution crystal structure from just a couple of dozen successful attempts (Fig. 1). The x-ray data were collected at the GM/CA-XSD 23-ID-B and 23-ID-D beamlines at the APS.

Some members of the team then employed computer models of thousands of potential receptor-binding molecules to figure out which parts to chemically modify to make the molecules bind more tightly to kappa, but not

"Opioids" con't'd. on page 95

Kinked Protein Sheets That Know How to Network

Unlike the more familiar golgi apparatus (a complex of vesicles and folded membranes within the cytoplasm of most eukaryotic cells, involved in secretion and intracellular transport) or mitochondria, which are organelles found in large numbers in most cells, in which the biochemical processes of respiration and energy production occur, some organelles, such as P bodies, stress granules, and nuclear paraspeckles are not bound by membranes. Their presence is fluid, forming and dispersing depending on a cell's needs. One common feature of membraneless organelles is proteins that include low-complexity domains (or LCDs), sequence segments containing only a few of the 20 common amino acids. Scientists are learning how these proteins tend to associate, glomming together to form hydrogels. To better understand the forces that drive LCD assembly, researchers collected structural data at the APS on five short segments of LCDs. They discovered a common structural motif; these segments formed kinked stacks of β sheets, termed low-complexity aromatic-rich kinked segments (LARKS), held together by polar and aromatic side chain interactions. The finding provides insights into how membraneless organelles form, but may also have broader impact, as LCDs are extremely common in the proteome, the entire complement of proteins that is or can be expressed by an organism.

Despite their prevalence, LCDs are rare in the protein structure database, leaving a dearth of molecular-scale information. Previous electron microscopy and x-ray diffraction studies suggested that LCDs form fibrils with a "cross-β" structure reminiscent of those found in disease-associated amyloid fibrils, but with far less stability. To gain additional structural insights, the research team from the University of California, Los Angeles, searched for segments they suspected may form crystals, identifying five such LCD segments. Three of the segments were from the FUS protein and one was from hnRNP1, both found associated with stress granules, while the other was from nucleoprotein 98. They crystallized as micron-sized needles, and their structures were determined with x-ray diffraction data collected at the NE-CAT 24-ID-E beamline at the APS.

All five LCD segments crystals showed similar structures: pairs of kinked β sheets. The β sheets ran the length of the micron-sized needle crystals, a stack some 300,000 segments long. The kinks occurred at either glycines or aromatic

"Kinked" cont'd. on next page

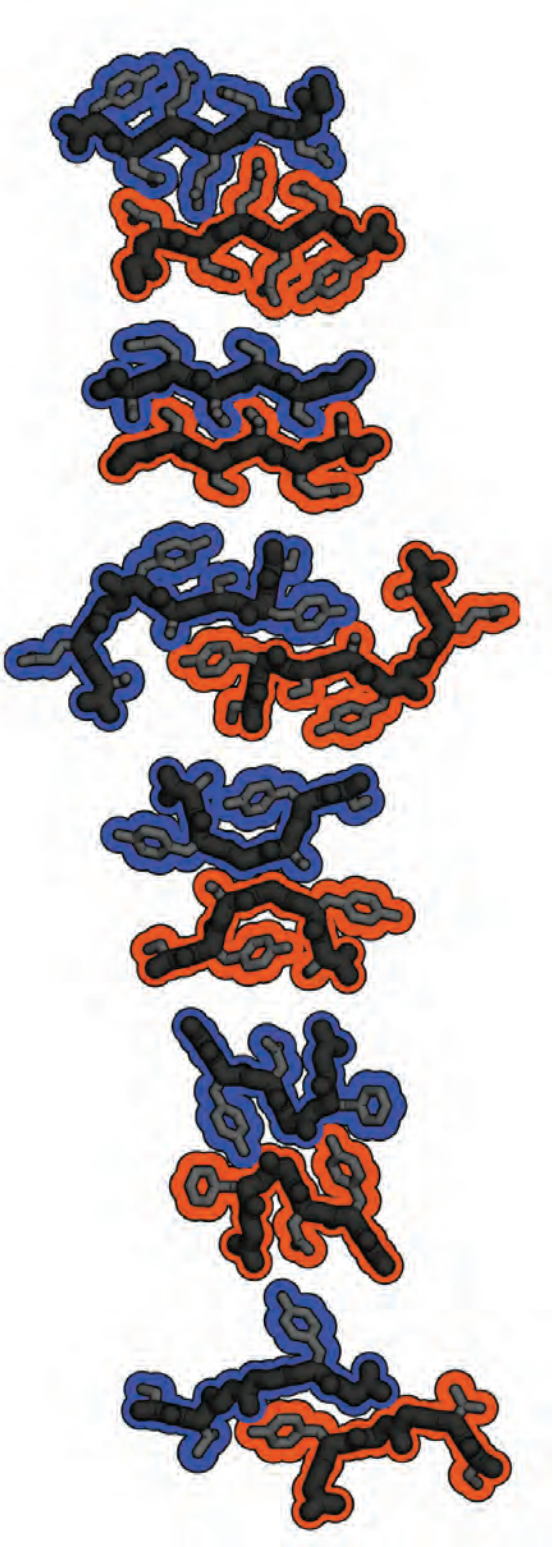

Fig. 1. Structures of low-complexity, aromatic-rich kinked segments (LARKS) shown as cartoons of the mating β sheets viewed parallel to the fibril axes. All structures are composed of two mating β sheets, one red and one blue. Credit: Michael Hughes

"Kinked" cont'd. from previous page

residues, which predominate in the structures providing stability both within segments and across segments. Hydrogen bonds also played a role stabilizing the sheets.

Pathogenic amyloid fibrils are also made from stacked β sheets, but the authors are quick to point out that LARKS stack differently. The steric zippers found in amyloid fibrils are extremely stable, while LARKS are more labile; the authors use the analogy that the amyloid's steric zippers are to molecular glue as LARKs in LCDs are to Velcro. In other words, the LARKs have lower binding energy than steric zippers, which was supported by a series of computations and experiments. First, the researchers calculated how much energy, on average, would it take to separate the LARKS interfaces, which was on the order of thermal energy. In amyloids, the energy is several times thermal energy. These calculations were backed up by experiments that showed LCD hydrogels transition to liquid phase under gentle heating.

As a next step, the researchers explored the human proteome looking for additional LCD candidates that could form the kinked β sheets. They used an approach called computational three-dimensional profiling, which threads protein sequences through a template structure, in this case the LARK's, and tests compatibility of the sequence with that structure. They found hundreds of proteins with such sequences potentially capable of forming kinked β sheets. As may be expected, many of these proteins are known to be associated with membraneless organelles.

These findings provide support for the assertion that kinked β sheets are a general motif that facilitates the formation and dissolution of membraneless organelles. Additional research will be needed to understand the cellular triggers that drive this activity. — Erika Gebel Berg

See: Michael P. Hughes, Michael R. Sawaya, David R. Boyer, Lukasz Goldschmidt, Jose A. Rodriguez, Duilio Cascio, Lisa Chong, Tamir Gonen, and David S. Eisenberg*, "Atomic structures of low-complexity protein segments reveal kinked β sheets that assemble networks," Science **359**, 698 (2018).
DOI: 10.1126/science.aan6398
Author affiliation: University of California, Los Angeles
Correspondence: * david@mbi.ucla.edu

The authors thank U.S. National Science Foundation MCB-1616265, National Institutes of Health (NIH) AG-054022, the U.S. Department of Energy (DOE), and the Howard Hughes Medical Institute for support. NE-CAT is funded by the National Institute of General Medical Sciences from the NIH (P41 GM103403). This research used resources of the Advanced Photon Source, a U.S. DOE Office of Science User Facility operated for the DOE Office of Science by Argonne National Laboratory under contract no. DE-AC02-06CH11357.

"Opioids" con't'd. from page 93

to other opioid receptors. Using this model, the researchers synthesized a new compound that was highly selective for the kappa receptor.

Now, opioid researchers around the world can use the structure of the active form of the receptor, which is available online in a public database, to simulate the binding of hundreds of millions of compounds to the kappa receptor. Scientists will then select the most promising molecules from these large-scale screenings to study their effects in cells and animal models. The results may one day yield drug candidates suitable for human trials, with the ultimate goal of identifying compounds that deliver pain relief without the deadly side effects associated with modern opioids. — Chris Palmer

See: Tao Che[1], Susruta Majumdar[2], Saheem A. Zaidi[3], Pauline Ondachi[4], John D. McCorvy[1], Sheng Wang[1], Philip D. Mosier[5], Rajendra Uprety[2], Eyal Vardy[1], Brian E. Krumm[1], Gye Won Han[3], Ming-Yue Lee[3,6,7], Els Pardon[8,1], Jan Steyaert[8,9], Xi-Ping Huang[1], Ryan T. Strachan[1], Alexandra R. Tribo[1], Gavril W. Pasternak[2], F. Ivy Carroll[4], Raymond C. Stevens[3], Vadim Cherezov[3], Vsevolod Katritch[3], Daniel Wacker[1]*, and Bryan L. Roth[1,10]**, "Structure of the Nanobody-Stabilized Active State of the Kappa Opioid Receptor," Cell **172**, 55 (January 11, 2018).
DOI: 10.1016/j.cell.2017.12.011
Author affiliations: [1]University of North Carolina at Chapel Hill School of Medicine, [2]Memorial Sloan Kettering Cancer Center, [3]University of Southern California, Los Angeles, [4]Research Triangle Institute, [5]Virginia Commonwealth University, [6]Arizona State University, [7]Nanjing Audit University, [8]Vrije Universiteit Brussel, [9]VIB-VUB Center for Structural Biology, [10]University of North Carolina at Chapel Hill
Correspondence: * dwacker@email.unc.edu,
** bryan_roth@med.unc.edu

This work was supported by National Institutes of Health (NIH) grants RO1MH61887 and U19MH82441, the National Institute of Mental Health NIMH Psychoactive Drug Screening Program Contract, and the Michael Hooker Distinguished Chair of Pharmacology (to B.L.R.), as well as grants from the National Institute on Drug Abuse to B.L.R., R.C.S., V.C., and V.K. (DA035764), to V.K. (DA038858), to G.W.P. (DA0624), and to S.M.(DA034106). This research was also funded by the Mayday Foundation and the Peter F. McManus Trust (to G.W.P.), (DA034106) (S.M.), and an NIH/National Cancer Institute Cancer Center support grant (P30 CA008748) (to Memorial Sloan Kettering Cancer Center). We thank J. Smith and R. Fischetti and the staff of GM/CA-XSD, which has been funded with Federal funds from the National Cancer Institute (ACB-12002) and the National Institute of General Medical Sciences (AGM-12006). The Eiger 16M detector on 23-ID-B was funded by an NIH–Office of Research Infrastructure Programs, High-End Instrumentation Grant (1S10OD012289-01A1). This research used resources of the Advanced Photon Source, a U.S. Department of Energy (DOE) Office of Science User Facility, operated for the DOE Office of Science by Argonne National Laboratory (contract no. DE-AC02-06CH11357).

New Research on Fluorine Could Transform Drug Development

The enzyme cysteine dioxygenase (CDO) plays a critical role in regulating the level of thiols (compounds that contain a sulfur atom bonded to a hydrogen atom) in the body. It also contains a cofactor consisting of a cysteine-to-tyrosine thioether bond (Cys-Tyr) that boosts the enzyme's catalytic efficiency. However, questions have persisted about the addition of this cofactor, which occurs after the enzyme is translated. Using x-ray diffraction data collected at the APS and the Stanford Synchrotron Radiation Lightsource, researchers investigated the structure of CDO. Unexpectedly, they found that, during formation of the cofactor, the enzyme could use oxygen to break down carbon-fluorine (C–F) bonds, which are considered to be the strongest bonds in organic chemistry. This novel finding not only increases scientists' understanding about fluorine chemistry, but could also have important implications for drug development, given the important role that fluorine plays in pharmaceutical chemistry.

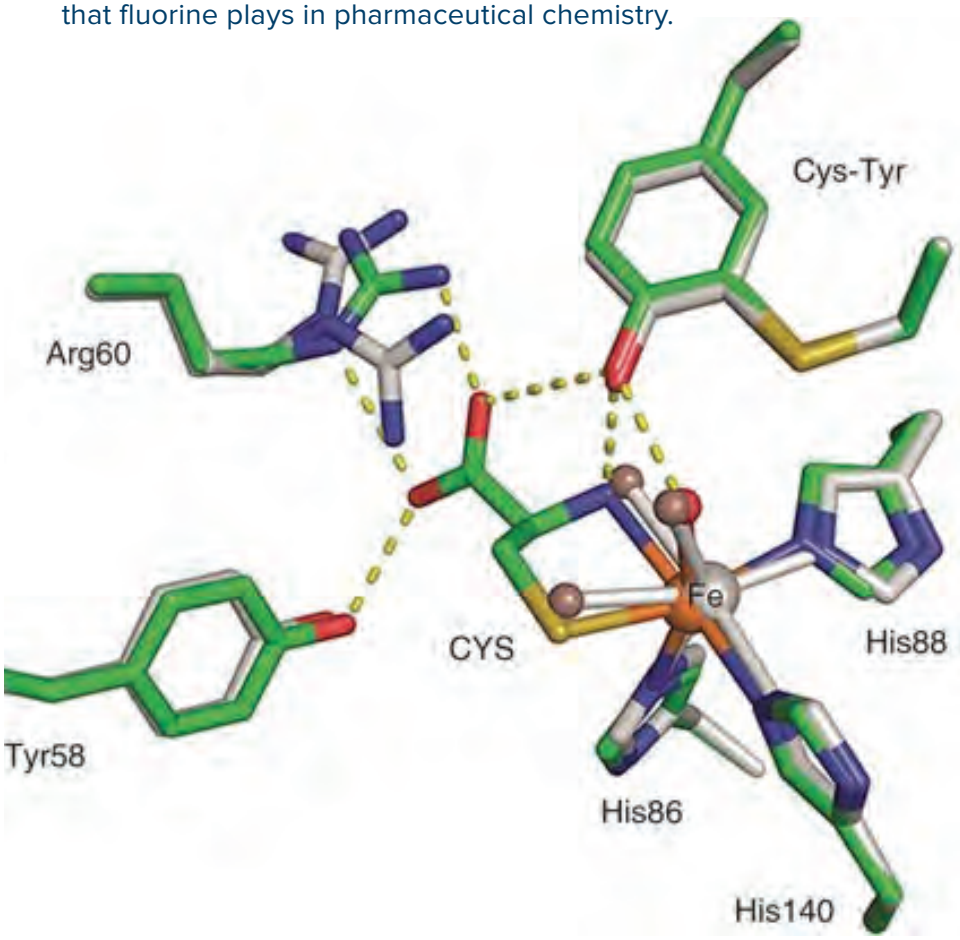

CDO is an important enzyme involved in metabolism of sulfur, and helps to regulate the body's levels of thiol. CDO catalyzes the conversion of the thiol-containing amino acid cysteine into cysteine sulfinic acid (CSA), by adding molecular oxygen to the sulfur of the amino acid. And abnormal or deficient CDO activity has been reported in patients with various diseases, including rheumatoid arthritis, breast cancer, Parkinson's disease, Alzheimer's disease.

Soon after it is translated, CDO also undergoes a modification that adds a unique cofactor to the enzyme's structure. This cofactor consists of a Cys-Tyr thioether bond that enhances CDO's catalytic efficiency. However, the mechanism by which CDO produces this cofactor has remained poorly understood.

With this in mind, researchers at The University of Texas at San Antonio (UTSA) conducted a study to further investigate the formation and function of this Cys-Tyr crosslink. Using a genetic technique, they replaced the tyrosine of the cofactor in human CDO with unnatural tyrosine compounds. To determine the crystal structures of CDO (Fig. 1), the researchers also used crystallographic data collected at SBC-CAT beamline 19-BM-D at the APS, and at Stanford Synchrotron Radiation Lightsource beamline BL9-2. In this way, they solved the structures of human CDO and the new forms of the enzyme created by incorporating the unnatural tyrosine compounds.

During formation of the cofactor in some of the new enzyme variants, the researchers found that CDO could catalyze oxidative breakage of C–F or carbon-chloride (C–Cl) bonds. This resulted in a marked change in conformation of both the cysteine and tyrosine components of the enzyme's cofactor during its assembly.

The breakage of the C-F bond was an unexpected finding because the C–F bond is one of the strongest covalent bonds in organic chemistry. Indeed, although recent studies have demonstrated breakage of an aromatic C–F bond by nitrogen-ligated nonheme iron model complexes, this UTSA study is the first to show that a protein can break the C-F bond.

The fluorine atom can play a significant role in medicinal chemistry. In particular, its selective incorporation into certain therapeutic agents can improve several of their properties, such as biological activity, and chemical or metabolic stability. For example, introducing fluorine to a compound at a site of metabolic attack has been used as a strategy to increase the metabolic stability of certain compounds. This is because the C-F bond is more resistant to attack than the carbon-hydrogen bond is. Because of its strength, the C-F bond has traditionally been considered to be resistant to breakage.

However, according to the researchers, this new discovery about fluorine and how other molecules bond with it widens the range of fluorine chemistry, and could transform drug design and development. — Nicola Parry

< Fig. 1. Crystal structure of the active sites of the ligand-free (gray) and substrate (CYS)-bound complex (green) crystal structures of human CDO. From J. Li et al., Nat. Chem. Biol. **14**, 843 (September 2018). © 2018 Springer Nature Publishing AG

See: Jiasong Li[1], Wendell P. Griffith[1], Ian Davis[1], Inchul Shin[1], Jiangyun Wang[2], Fahui Li[2], Yifan Wang[1], Daniel J. Wherritt[1], and Aimin Liu[1]*, "Cleavage of a carbon–fluorine bond by an engineered cysteine dioxygenase," Nat. Chem. Biol. **14**, 843 (September 2018). DOI: 10.1038/s41589-018-0085-5
Author affiliations: [1]The University of Texas at San Antonio, [2]Chinese Academy of Sciences
Correspondence: * Feradical@utsa.edu

The work is supported in part by the National Institutes of Health grants GM107529, GM108988, and MH107985, the U.S. National Science Foundation grant CHE-1623856, and the Lutcher Brown Distinguished Chair Endowment fund (to A.L.). J.W. acknowledges the support of the National Science Foundation of China grants 91527302, 31370016, and U1532150. The beamline staff scientists are acknowledged for the assistance of the remote data collections. The SSRL is supported by the U.S. Department of Energy (DOE) Office of Science-Basic Energy Sciences under Contract No. DE-AC02-76SF00515 and by the National Institutes of Health (P41GM103393). This research used resources of the Advanced Photon Source, a U.S. DOE Office of Science User Facility operated for the DOE Office of Science by Argonne National Laboratory under Contract No. DE-AC02-06CH11357.

Solving the Transmittal Riddle of the Influenza Type A Virus

The flu virus comes in three well-known types: A, B, and C. Type A accounts for all the virus pandemics in recorded history. The 20th century has witnessed three major Type A pandemics, resulting in many millions of deaths worldwide: the Spanish flu of 1918 (denoted as 1918 H1N1), the Asian flu of 1957 (1957 H2N2), and the Hong Kong flu of 1968 (1968 H3N2). The recent swine flu pandemic, in 2009 (2009 H1N1), caused about half million human deaths globally. Infections caused by Types A and B remain a major source of human morbidity and mortality. They also pose a potential threat as man-made bio-weapons. Work by researchers utilizing the APS offers a new insight into the transmission of influenza Type A in humans.

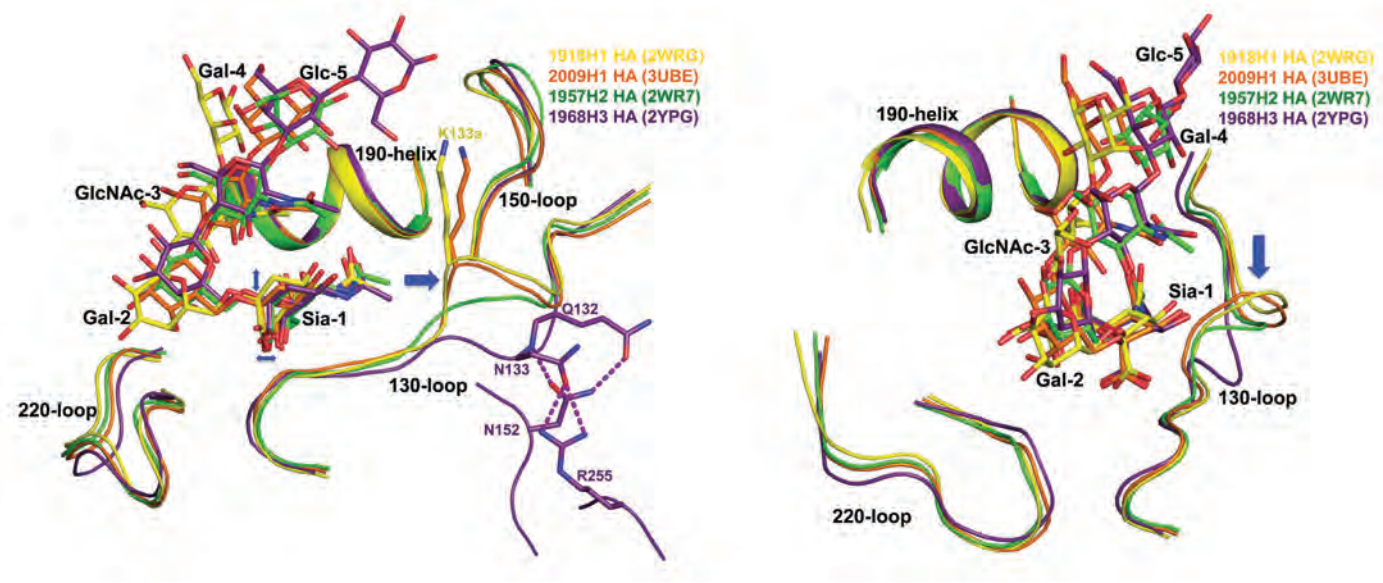

Fig. 1. Crystallographic ribbon structures for 1918H1, 1957H2, 1968H3, and 2009H1 hemagglutinin at the receptor binding site. Two different views displayed.

Influenza pandemics occur when a new strain from other animal species overwhelms inter-species barriers and infects the human population by means of efficient airborne transmission of the virus. Critical to this process is that the protein hemagglutinin undergoes a few key mutations to switch its binding from avian to human receptors. Of the 18 different hemagglutinin subtypes for the Type A virus, only three of them (H1, H2, and H3) have been commonly found in humans. These three are responsible for all the above pandemics and, together with influenza Type B viruses, for seasonal flu outbreaks. These subtypes use two sets of hallmark mutations to cause the switch from avian to human receptors: Q226L and G228S for H2 and H3 and E190D and G225D for H1.

In recent years, other hemagglutinin subtypes (H5, H6, H7, and H9) have resulted in some human deaths. These pose the threat of causing pandemics should a few mutations occur. Hence, a better understanding is urgently needed of the mutations that cause these viruses to become transmittable to humans through air.

The researchers in this study, from the Baylor College of Medicine and Northwestern University, compared the crystallographic structures of the human receptor analogue LSTc bound with hemagglutinin from the last four pandemic viruses: 1918H1, 1957H2, 1968H3, and 2009H1. As shown in Fig. 1, the receptor binding site con-

sists of four major structures: 190-helix, 220-loop, 150-loop, and 130-loop. The Sia-1 moiety of LSTc for 1918H1 sits higher and more toward the 130-loop than those in 1957H2 and 1968H3 (highlighted by two slim blue arrows). The large blue arrow in the center highlights the different lengths for the 130-loop of the four hemagglutinin structures. The authors addressed the question of whether the different lengths are responsible for the mutational routes mentioned above.

This study involved the preparation of the 1918H1 hemagglutinin and its mutants, determination of the apparent dissociation constants, and structural characterization by x-ray diffraction at the LS-CAT 21-ID-F and 21-ID-G x-ray beamlines at the APS.

The results indicated that single-residue deletion of the residue K133a converted 1918H1 into H2/H3-like hemagglutinin where the mutations Q226L and G228S imposed a preferential binding for human receptor. By sharp contrast, without the K113a deletion, no preferential binding for human or avian receptors occurred. Taken together, their receptor-binding and structural data suggest that the 130-loop defines the different sitting positions within the receptor-binding site of 1918H1 and H2/H3 hemagglutinin. Further analysis led to the finding that the 130-loop also dictates the modes of binding receptors in other subtypes of hemagglutinin (H4 to H7 and H9).

The authors conclude that the length of the 130-loop and, more importantly, the sitting position of the Sia-1 moiety can help determine whether a given hemagglutinin would likely behave as the H1 or H2/H3 subtypes. More broadly, this study has contributed to progress in gaining a deeper understanding of the molecular mechanism behind the switch in receptor preference from avian to human, and that understanding could help in the timely detection of newly emerging influenza strains that pose a pandemic threat. — Joseph E. Harmon

See: Fengyun Ni[1], Elena Kondrashkina[2], Qinghua Wang[1]*, "Determinant of receptor-preference switch in influenza hemagglutinin," Virology **513**, 98 (2018). DOI: 10.1016/j.virol.2017.10.010
Author affiliations: [1]Baylor College of Medicine, [2]Northwestern University
Correspondence: * qinghuaw@bcm.edu

Q.W. thanks support from the National Institutes of Health (R01-AI067839, R01-GM116280) and the Welch Foundation (Q-1826). Use of the Life Sciences Collaborative Access Team Sector 21 was supported by the Michigan Economic Development Corporation and the Michigan Technology Tri-Corridor (Grant 085P1000817). This research used resources of the Advanced Photon Source, a U.S. Department of Energy (DOE) Office of Science User Facility operated for the DOE Office of Science by Argonne National Laboratory under Contract No. DE-AC02-06CH11357.

A Brief History of Influenza Epidemics

1918 Pandemic (H1N1 virus)

The 1918 influenza pandemic, the most severe in recent history, was caused by an H1N1 virus with genes of avian origin. Although there is no consensus as to where it originated, it spread worldwide during 1918-1919. In the U.S., it was first identified in military personnel in spring 1918. About 500 million people, or one-third of the world's population, became infected with this virus. The number of deaths was estimated to be at least 50 million worldwide, some 675,000 occurring in the U.S. Mortality was high in people younger than 5, 20-40, and 65 years and up. The high mortality in healthy people, including those in the 20-40-year age group, was a unique feature of this pandemic. The properties that made it so devastating are not well understood. With no vaccine to protect against infection and no antibiotics to treat secondary bacterial infections associated with influenza, control efforts worldwide were limited to nisolation, quarantine, good personal hygiene, use of disinfectants, and limitations of public gatherings, which were applied unevenly.

1957-1958 Pandemic (H2N2 virus)

In February 1957, a new influenza A (H2N2) virus emerged in East Asia, triggering a pandemic ("Asian Flu"). It was reported in Singapore in February 1957, Hong Kong in April 1957, and in coastal cities in the U.S. in summer 1957. The estimated number of deaths was 1.1 million worldwide and 116,000 in the U.S.

1968 Pandemic (H3N2 virus)

The 1968 pandemic was caused by an influenza A (H3N2) virus comprising two genes from an avian influenza A virus, including a new H3 hemagglutinin, but also contained the N2 neuraminidase from the 1957 H2N2 virus. It was first noted in the U.S. in September 1968. The estimated number of deaths was 1 million worldwide and about 100,000 in the U.S. Most deaths were in people 65 years and older. This virus continues to circulate worldwide as a seasonal influenza A virus.

2009 H1N1 Pandemic (H1N1pdm09 virus)

In the spring 2009, a novel influenza A (H1N1) virus was detected first in the U.S. and spread quickly around the world. This virus contained a unique combination of influenza genes not previously identified in animals or people, and was designated as influenza A (H1N1)pdm09 virus. Few young people had any existing immunity to the virus, but nearly 1/3 of people over the age of 60 had antibodies against this virus, likely from an earlier exposure to an older H1N1 virus. The virus was very different from H1N1 viruses that were circulating at that time; vaccination with seasonal flu vaccines offered little cross-protection against it. While a vaccine was produced, it was not available in large quantities until late November 2009, after the peak of illness during the second wave had come and gone in the U.S. From April 12, 2009, to April 10, 2010, CDC estimated that there were ~61 million cases, ~274,000 hospitalizations, and ~12,500 deaths in the U.S. due to the virus, and that between 151,700 and 575,400 people worldwide died from the virus during the first year. Globally, CDC estimated that 80% of virus-associated deaths were in people younger than 65, which differs from typical seasonal influenza epidemics during which about 70% to 90% of deaths are estimated to occur in people 65 and older.
Source: Centers for Disease Control and Prevention, https://bit.ly/2ltBXNr

Unraveling the Mechanics of a Promising Anticancer Drug

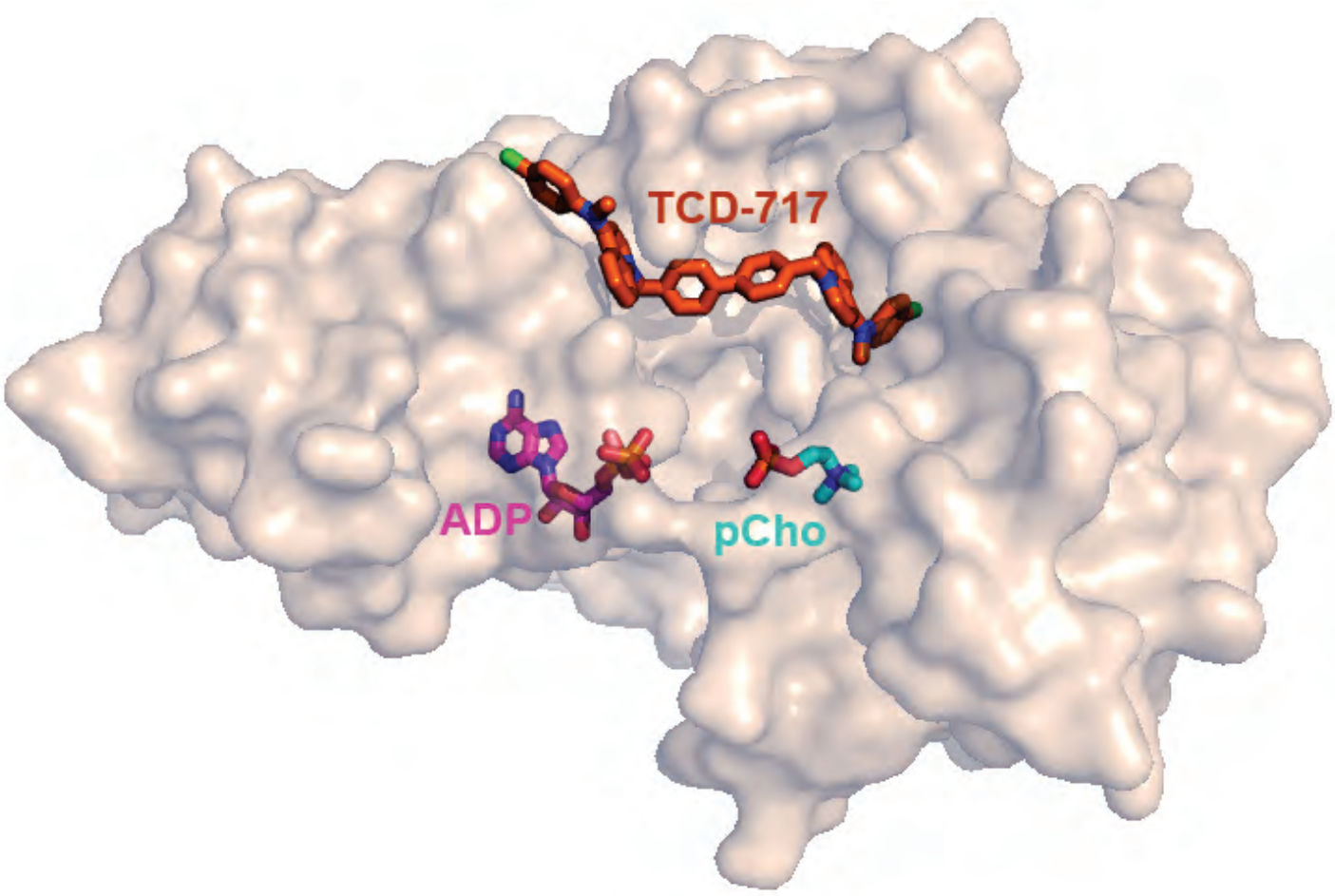

Fig. 1. ADP (magenta) and pCho (cyan), the products of the reaction catalyzed by ChoKα, are seen buried in the enzyme's deep binding pocket. When TCD-717 (orange) binds, rather than competing for a binding site in this pocket, it wraps around the entry point to the active site.

Choline kinase α (ChoKα) is an enzyme with an important role in the biosynthesis of phosphatidylcholine, a key structural component of cell membranes. This enzyme is implicated in tumor formation because its expression is increased in a variety of common cancers. Additional data have also highlighted ChoKα as an attractive target for development of cancer therapeutics, and one inhibitor of the enzyme, TCD-717, has completed phase 1 clinical trials. A big puzzle in the field is the fact that some ChoKα inhibitors cause cell arrest, whereas others cause cell death (apoptosis). To investigate this discrepancy, researchers employed high-brightness x-rays to collect diffraction data at the APS and found that TCD-717 binds to ChoKα at a different site from that where most other inhibitors bind. The researchers note that this could also be disruptive to protein–protein interactions that may be key to inducing apoptosis, and thus may have implications for scientists involved in developing ChoKα inhibitors.

The enzyme human ChoKα is responsible for the production of phosphocholine (pCho) in cells. It plays a key role in the biosynthesis of phosphatidylcholine, which is a major phospholipid component of cell membranes.

Lipid metabolism has been shown to be abnormal during cancer development, and ChoKα has been shown to be tumorigenic and upregulated in many types of cancer. The results of numerous studies have also suggested several links between ChoKα and cancer. For example, increased intracellular levels of the enzyme are associated with malignant phenotype and poor prognosis, and increased ChoKα activity levels correlate with higher tumor grade. Increased availability of pCho in the cell is also associated with a more aggressive cancer phenotype. Together, these findings indicate that ChoKα is a prime target for chemotherapeutic drug design for inhibiting tumor growth. Indeed, effective ChoKα inhibitors have been developed and have entered clinical trials. One such small-molecule inhibitor, TCD-717, has recently completed phase-1 trials.

The enzymatic activity of ChoKα can be ablated by using either ChoKα inhibitors or short interfering RNAs (siRNAs) of the genes encoding the enzyme. However, studies have also shown that, despite being very potent *in vitro*, some ChoKα inhibitors do not cause cancer cells to undergo apoptosis, but only halt tumor growth. However, genetic ablation of ChoKα does result in apoptosis and thus tumor reduction.

With this in mind, a group of scientists from the University of Illinois at Chicago, the University of Pennsylvania, and the Jesse Brown VA Medical Center conducted a study to further investigate why these two approaches lead to different cellular effects. They focused on the interaction between ChoKα and TCD-717, because the antitumor activity of this inhibitor does induce apoptosis. However, previous studies have not examined how TCD-717 interacts with the ChoKα enzyme.

The researchers wanted to determine what makes TCD-717 different from all other ChoKα inhibitors that have been examined. Utilizing the diffraction data collected at the LS-CAT 21-ID-F and 21-ID-G beamlines at the APS, the group solved the crystal structure of ChoKα in complex with the inhibitor TCD-717.

Their study showed that TCD-717 binds to ChoKα at a site that differs from where the other inhibitors bind. Although many other ChoKα inhibitors bind to the enzyme deep in the choline pocket in its structure, TCD-717 binds in a unique location, wrapping around the active site of the enzyme, near its surface (Fig. 1). This effectively clamps the enzyme shut so it cannot perform the reaction. It also has the added benefit of changing the surface properties of the enzyme, which potentially disrupts a critical protein-protein interaction made by ChoKα in the cell. According to the researchers, this protein–protein interaction may be necessary to cause the cells to undergo apoptosis. Hence, to assure cell-killing potency, further development of ChoKα inhibitors should take this into consideration. — Nicola Parry

See: Stefanie L. Kall[1], Edward J. Delikatny[2], and Arnon Lavie[1,3]*, "Identification of a Unique Inhibitor-Binding Site on Choline Kinase α," Biochem. **57**, 1316 (2018).
DOI: 10.1021/acs.biochem.7b01257
Author affiliations: [1]University of Illinois at Chicago, [2]University of Pennsylvania, [3]Jesse Brown VA Medical Center
Correspondence: * Lavie@uic.edu
Use of the Life Sciences Collaborative Access Team facility was supported by the Michigan Economic Development Corp. and the Michigan Technology Tri-Corridor (Grant 085P1000817). This research used resources of the Advanced Photon Source, a U.S. Department of Energy (DOE) O ce of Science User Facility operated for the DOE O ce of Science by Argonne National Laboratory under Contract DE-AC02-06CH11357.

APS users by institutional geographic distribution (FY 2018)

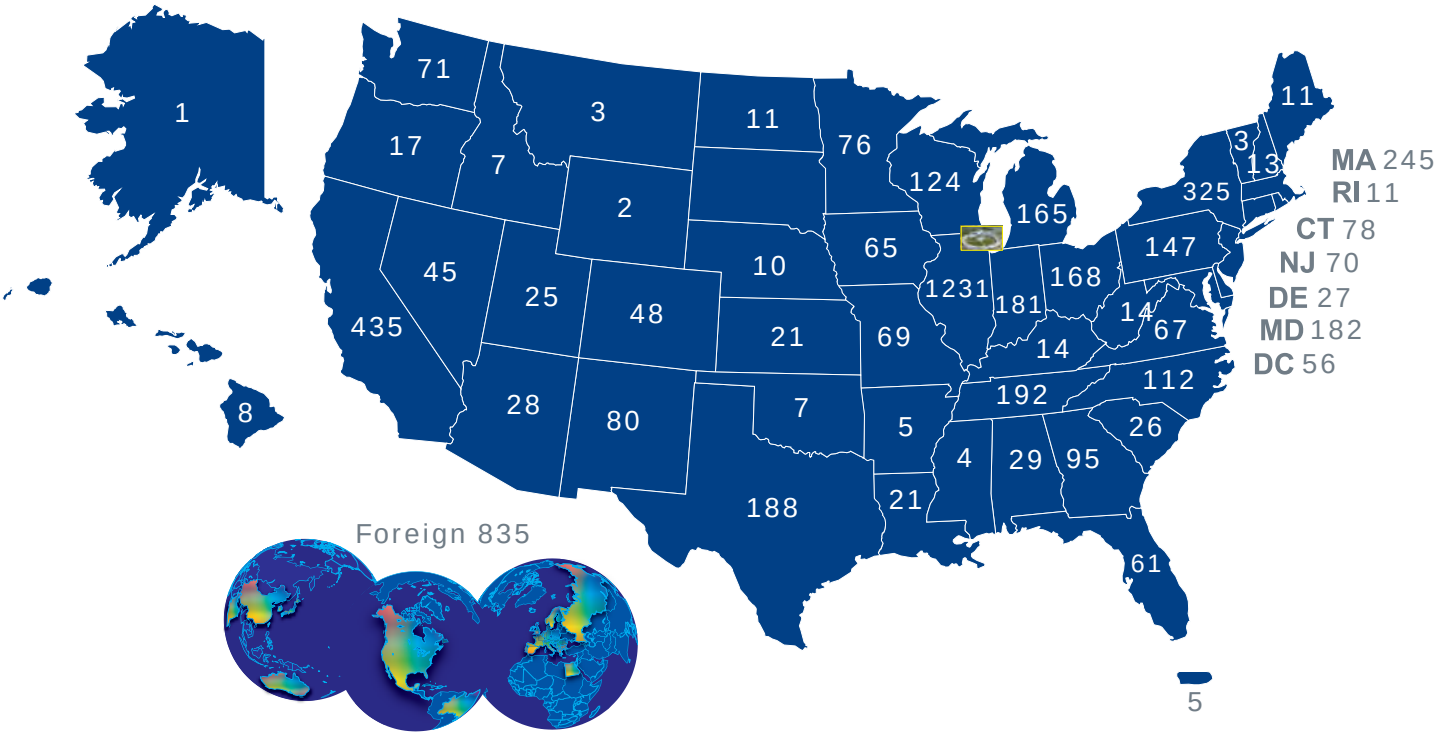

APS USER INSTITUTIONS x INSTITUTION TYPE (FY 2018)

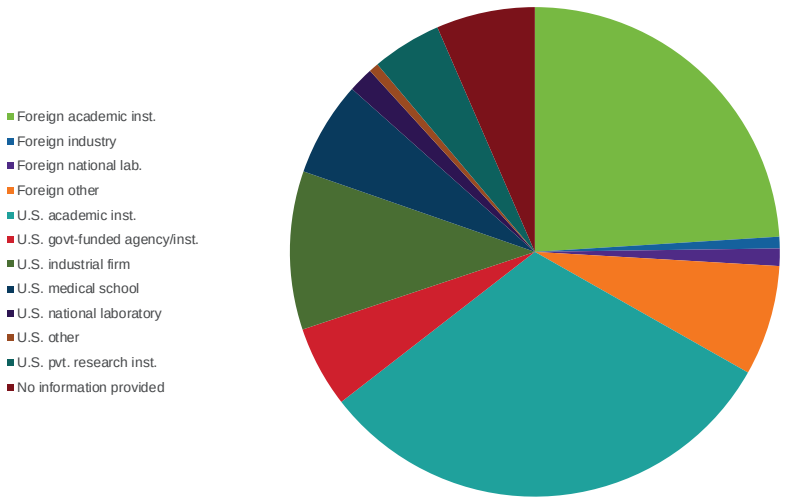

Environmental, Geological & Planetary Science

An Acidic Environment Increases the Solubility of Aerosol Iron

"Red tide" is the term commonly applied to a harmful algal bloom. Red tides make the news for their striking visual effect and their ability to disturb ecosystems through the sudden die-off of fish. What may be less well known is that the phytoplankton stimulated by easy access to iron can sequester a great deal of carbon dioxide. But phytoplankton are only able to access iron when in solution, and the solubility of iron depends on many factors. Research carried out at the APS examined the composition and oxidation states of aerosol iron and revealed that while many variables affect its solubility, including its source and the path it has traveled, an increase in acidity increases the solubility of aerosol iron. A better understanding of the role of aerosol iron has implications for insights about sequestration of carbon dioxide by marine algae and other biogeochemical impacts.

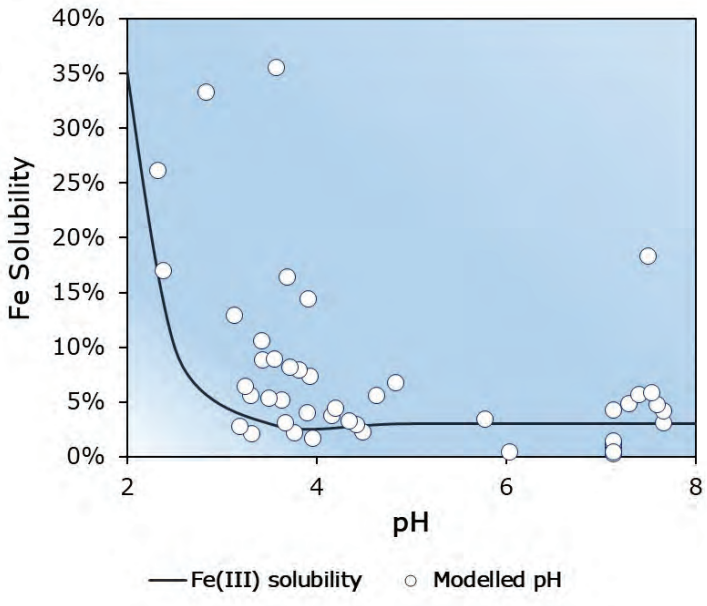

Fig. 1. The modelled pH of the samples show that only when the pH is below approximately 4, or under acidic conditions, does the pH affect the fractional solubility of the iron. This behavior of the aerosol iron is consistent with the speciation of Fe^{+3}.

Aerosol iron is sampled using air filters, which trap particulates. Since aerosols are airborne particles, a sample can include particulates from multiple sources depending on air currents. This transportation allows many events to physically and chemically affect the aerosol iron to increase its solubility, including rock weathering, cloud processing, and photoreduction. An international team of researchers from academia and government research institutions examined samples from locations distributed across the Earth and thus influenced by a variety of atmospheric and anthropogenic events. They focused on the speciation and oxidation state of aerosol iron to explore the commonalities across these influences, which affect aerosol iron solubility.

The aerosol samples were collected at five globally-diverse locales and gave details of Earth's atmosphere over these locations during differing spans of time. Total soluble iron was determined using the ferrozine technique, which turns different shades of magenta to indicate the speciation of iron. Additionally, these samples were examined using micro x-ray fluorescence and x-ray absorption near edge structure (XANES) spectroscopy at the XSD 2-ID-D beamline at the APS. The XANES spectroscopy was utilized to examine both individual particles and bulk aerosol properties. The team applied the XANES spectra to determine the oxidation state and mineral composition of the iron.

The team found that their samples exhibited a wide range of values for the total solubility of iron, but no clear pattern emerged until they looked at fractional solubility. On examining samples from the Mediterranean Sea, they found that the samples from European sources had the highest values, followed by those samples from marine sources. Samples from Bermuda, which were influenced by anthropogenic activities in North America, had higher fractional solubility than those most influenced by North African mineral dust.

Although previously published results have found Fe^{2+} to be more soluble than Fe^{3+}, in this work the team found higher amounts of Fe^{3+} than Fe^{2+}. This relationship was true for both the individual particle analysis as well

"Acidic" cont'd. on next page

"Acidic" cont'd. from previous page

as the bulk sample results. The team postulated this higher value of Fe^{3+} may be explained by the source of the aerosols being highly-weathered materials from land surfaces, which often contain higher quantities of iron oxides. The range of fractional iron solubilities measured by the team for different oxidation states gave no evidence for a relationship between iron's oxidation state and its fractional solubility.

However, when the team concentrated on pH, they found that the solubility of aerosol iron increased up to 35% as the pH dropped below 4. The team found no similar relationship as a function of specific compounds that participate in acidic reactions, such as inorganic acids or sulfuric acid. They conclude that only when a sufficient number of acidic species act on an aerosol iron particle will it become soluble.

The team looked at other factors, such as transport time, alteration of clay mineral phases, and source region, but found no clear relationship between these and solubility. They concluded that while other factors do play a role in the solubility of aerosol iron, and simply may not have been sufficiently present in their samples to show a relationship, their data emphasizes the importance of pH to increase aerosol iron solubility.

— Mary Alexandra Agner

See: Ellery D. Ingall[1]*, Yan Feng[2], Amelia F. Longo[1,] Barry Lai[2], Rachel U. Shelley[3], William M. Landing[3], Peter L. Morton[4], Athanasios Nenes[1,5,6], Nikolaos Mihalopoulos[6,7], Kalliopi Violaki[7], Yuan Gao[8], Shivraj Sahai[9,10], and Erin Castorina[1], "Enhanced Iron Solubility at Low pH in Global Aerosols," Atmosphere-Basel **9**, 201 (2018). DOI: 10.3390/atmos9050201

Author affiliations: [1]Georgia Institute of Technology, [2]Argonne National Laboratory, [3]Florida State University, [4]National High Magnetic Field Laboratory, [5]Foundation for Research and Technology–Hellas, [6]Institute for Environmental Research and Sustainable Development, [7]University of Crete, [8]Rutgers University at Newark, [9]Amity University, [10]Adigrat University
Correspondence: * ellery.ingall@eas.gatech.edu

This material is based upon work supported by the U.S. National Science Foundation (NSF) under Grants OCE 1357375 (EDI), OCE 1658181 (EDI), OCE-0929919 (WML), OCE-1034764 (WML), OCE-1658311 (PLM), OPP-0944589 (YG), and PLR-1341494 (YG). A portion of this work was performed at the National High Magnetic Field Laboratory, which is supported by the U.S. NSF Cooperative Agreement DMR-1157490 and the State of Florida. N.M. and K.V. acknowledge support from European Union (European Social Fund) and Greek national funds through the Operational Program "Education and Lifelong Learning" of the National Strategic Reference Framework Research Funding Program. This research used resources of the Advanced Photon Source, an Office of Science User Facility operated for the U.S. Department of Energy (DOE) Office of Science by Argonne National Laboratory under contract no. DE-AC02-06CH11357, and the Canadian Light Source and its funding partners.

What is a Red Tide?

Harmful algal blooms, or HABs, occur when colonies of algae — simple plants that live in the sea and freshwater — grow out of control while producing toxic or harmful effects on people, fish, shellfish, marine mammals, and birds. The human illnesses caused by HABs, though rare, can be debilitating or even fatal.

While many people call these blooms "red tides," scientists prefer "harmful algal bloom." One of the best known HABs in the nation occurs nearly every summer along Florida's Gulf Coast. This bloom, like many HABs, is caused by microscopic algae that produce toxins that kill fish and make shellfish dangerous to eat, and may also make the surrounding air difficult to breathe. As the name suggests, the bloom of algae often turns the water red.

HABs have been reported in every U.S. coastal state, and their occurrence may be on the rise. HABs are a national concern because they affect not only the health of people and marine ecosystems, but also the health of local and regional economies.

But not all algal blooms are harmful. Most blooms are beneficial because they are food for animals in the ocean. In fact, they are the major source of energy that fuels the ocean food web. A small percentage of algae produce the harmful toxins. HABs also include blooms of non-toxic species that have harmful effects on marine ecosystems. For example, when masses of algae die and decompose, the decaying process can deplete oxygen in the water, causing the water to become so low in oxygen that animals either leave the area or die.

Scientists at the National Ocean Service have been monitoring and studying this phenomenon for a number of years to determine how to detect and forecast the location of the blooms. The goal is to give communities advance warnings so they can adequately plan for and deal with the adverse environmental and health effects associated with these red-tide events. *Source: National Ocean Service, NOAA, https://oceanservice.noaa.gov/facts/redtide.html*

Red tide pic: melvil, wikimedia, https://commons.wikimedia.org/wiki/File:Red_tide_2017.jpg

A New Look into the Evolution of the Volcanic System of Nyamuragira

Nyamuragira, which is located in the Virunga region in the western branch of the East African Rift, and is one of the most active volcanoes in Africa, has provided a better understanding of the controls on redox behavior of heterovalent elements in silicate melts, in which atoms have their oxidation state changed. In samples of magmatic glass, the valence states of iron (Fe) and vanadium (V) provide an indirect measurement of the redox state of magma, acting as proxies for the melt's oxygen fugacity (fO_2). Sulfur (S) speciation is also strongly tied to changing magmatic redox; understanding the behavior of S is important for discerning primary controls on volcanic degassing and explosivity, and thus the causes and nature of volcanoes. New data resulting from this study, carried out at the APS, imply that storage history, rather than differences in fO_2, may have a larger influence on SO_2 emissions and eruption styles. However, further work is required to clarify these differences.

Researchers from Northeastern Illinois University and The University of Chicago utilized the GSECARS x-ray microprobe beamline 13-ID-E at the APS to perform microscale S, Fe, and V K-edge microscale x-ray absorption near edge structure (μ-XANES) measurements on samples from the Nyamuragira volcano. The μ-XANES analyses were executed on previous investigations of basanite and alkali basalt melt inclusion (MI) samples of lava from 1938 and 1948 eruptions and samples of tephra from 1986 and 2006 eruptions. The beam of the monochromator was focused to a secondary source aperture (SSA) by two horizontally deflecting mirrors with various coatings. Silicon stripes for S and V provided harmonic rejection, and rhodium stripes for Fe provided better reflectivity. The samples rotated on a highly stable air binding turntable of the monochromator. While V and Fe analyses were conducted in open air, S was conducted in a helium environment in order to minimize absorption of the x-ray fluorescence signal, the mode in which μ-XANES spectra were collected.

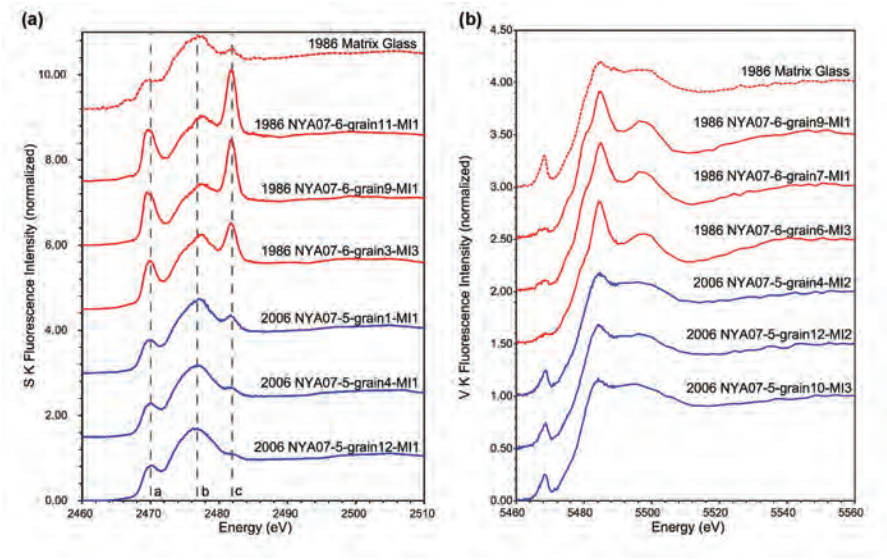

Fig. 1. Sulfur (a) and vanadium (b) K-edge XANES spectra from a suite of representative 1986 (in red) and 2006 (in blue) Nyamuragira MI. Individual spectra are offset vertically for clarity. In comparison to data collected from 1938, 1948, and 2006 MI, S XANES spectra for 1986 MI are characterized by a more intense spectral feature at ~ 2469.8 eV (peak *a*), similar to what is observed in crystalline Fe-S minerals, and a more intense and variable peak at ~ 2481.5 eV (peak *c*) that is characteristic of sulfate (S^{6+}) species. The 1986 MI V K-edge spectra are consistently more ordered and reduced than spectra from 1938, 1948, and 2006 MI. Also shown are S and V K-edge spectra for 1986 interstitial matrix glass (dashed red spectra), which are similar to spectra measured in 2006 MI in that they have low sulfate and a less structured V spectra with a higher average valence.

For MI samples taken from the 1938, 1948, and 2006 Nyamuragira eruptions, redox values showed a mean of FMQ-1 with a small variance of 0.6 log units. This demonstrates that any crystallization and water loss that may have happened following entrapment had not made any measurable changes, suggesting that some melt inclusions undergo significant H_2O loss with no impact to fO_2.

"Volcanic" cont'd. on next page

"Volcanic" cont'd. from previous page

The 1986 MI µ-XANES results were drastically different, however. V had smaller pre-edge peaks and lower energies, showing it is more ordered than other glasses. Fe data was more reduced with an FMQ -1.5 (±0.5). Sulfur, on the other hand, had a much higher intensity, indicating mixed population of sulfide and sulfate, and a difference in bonding of Fe-S (Fig. 1).

While confidence in coupled S, V, and Fe redox proxies increases with the agreement of 1938, 1948, and 2006 MI, 1986 must be further evaluated to understand its uniqueness and the variations in elemental speciation. Identified as a potential model to explain the differences, crystallization of nanoscale daughter minerals post-entrapment allows for the hypothesis that cooling and/or diffusion post-entrapment of H is most likely to lead to the spectroscopic features of V and S, and provides important information to interpret the ratios of Fe. Magnetite and sulfide nanolites' presence within the 1986 MI and not 2006 suggests that there are differences in the ascent and cooling. Although the specific mechanisms driving nanolite growth in 1986 are unclear, new data of this study gives clarity to the evolution of Nyramuragira's system.

The researchers note that their study shows that V and S µ-XANES spectroscopy could be extremely useful for identifying nanolite crystallization in olivine-hosted MI where other imaging techniques prove inadequate, due to XANES sensitivity to short-range order and ability to detect precipitates at the nanoscale.

— Gwenevier Johnson

See: Elisabet Head[1]*, Antonio Lanzirotti[2], Matthew Newville[2], and Stephen Sutton[2], "Vanadium, sulfur, and iron valences in melt inclusions as a window into magmatic processes: A case study at Nyamuragira volcano, Africa," Geochim. Cosmochim. Acta **226**, 149 (2018). DOI: 10.1016/j.gca.2018.01.033
Author affiliations: [1]Northeastern Illinois University, [2]The University of Chicago
Correspondence: * e-head@neiu.edu

GSECARS is supported by the National Science Foundation, Earth Sciences (EAR-1128799 and EAR-1634415) and the U.S. Department of Energy (DOE) Office of Science, Geosciences (DE-FG02-94ER14466). SEM analyses were supported by funds from the Northeastern Illinois University Earth Science Department and a Sigma Xi Grants-In-Aid research award to James Beer at Northeastern Illinois University, whom we acknowledge for his assistance during analysis. This research used resources of the Advanced Photon Source, an Office of Science User Facility operated for the U.S. DOE Office of Science by Argonne National Laboratory under contract no. DE-AC02-06CH11357, and the Canadian Light Source and its funding partners.

The Nyamuragira Volcano

Nyamuragira volcano crater on 31 January, 2014.

Nyamuragira, also known as Nyamulagira, is an active composite volcano near the city of Goma in the Virunga Mountains of the Democratic Republic of the Congo, situated about 25 km north of Lake Kivu. The name is derived from the Kifuru and Kishi verb *Kuragira ngavu*, meaning to herd cows. It has been described as Africa's most active volcano and has erupted over 40 times since 1885. As well as eruptions from the summit, there have been numerous eruptions from the flanks of the volcano, creating new, smaller volcanoes that have lasted only for a short time. It is 13 km north-northwest of Nyiragongo, the volcano that caused extensive damage to the city of Goma in 2002. Nyamuragira has a volume of 500 cubic km, and covers an area of 1500 km^2. It has a low shield profile, and contrasts with the adjacent steep-sided Nyiragongo volcano. Nyamuragira volcano is responsible for a large portion of the sulfur dioxide released into the atmosphere by volcanoes.

At dawn on 2 January, 2010, Nyamuragira began spewing out lava flows that could be seen on satellite. It erupted again on November 5, 2011, producing a 400-m-high column of lava, said to have been its largest eruption in 100 years.

In 2014, for the first time in 75 years, a new lava lake appeared at the volcano, one of the few volcanoes on Earth that has sustained lava lakes for several decades. The formation of the new lava lake occurred between June and August 2014. It has a depth of 500 m and is growing, and can produce lava flows in the future. The eruption did not affect the communities in the area but left ash and air pollution. Sulfate aerosols formed by volcanic sulfur dioxide from the eruptions were observed as far away as the central Amazon rain forest in South America. The lava lake has recently hardened and the activity has appeared to have stopped.

Source: https://en.wikipedia.org/wiki/Nyamuragira
Photo: MONUSCO Photos
commons.wikimedia.org/wiki/File:Nyamuragira_volcano_crater_on_31_January_2014_(12433170694).jpg

Ice Inclusions Indicate Deep Liquid Water

While it's easy to see how Earth's surface water plays a part in global cycles, water moving through the mantle contributes to these same cycles as mantle materials flow in such processes as volcanism and mantle plumes. The movement of water in the mantle enables the movement of heat-generating elements and isotopes such as thorium and uranium and the radioactive isotope 40K. To understand the effect of water in the mantle, we need to know how much water exists at different depths. However, it is difficult to directly sample the distribution of water throughout the mantle. Scientists use diamonds — especially the minerals encapsulated in them during their growth — to learn about the conditions in the mantle's depths where they formed. Recent research at the APS by a team examining diamonds from geologically-diverse sites confirms not only the presence of a water-based fluid but a water-based fluid within the lower mantle, supporting existing theories and laboratory results about the composition of the mantle across the transition zone.

The mantle makes up the majority of the Earth's interior by volume and comprises three layers: upper mantle, transition zone, and lower mantle. The transition zone is defined by changes in seismic wave velocities at depths of 410 km and 660 km. These velocity changes are associated with variations in crystal structure, with the peridotite rock of the mantle changing into different crystalline forms as increasing pressure rearranges its structure. Because the lower mantle materials do not bond with water, current theories postulate the lower mantle marks the depth at which water is released back into the mantle to be incorporated into upward-moving rock. These new results establish the presence of an aqueous fluid in diamonds which were formed below a depth of 660 km, thus indicating liquid water in the lower mantle. In addition to such deep pockets of aqueous fluid, the team also detected fluid across a range of depths within the upper mantle and transition zone.

The team from the University of Nevada, Las Vegas, The University of Chicago, the California Institute of Technology, the China University of Geosciences, the University of Hawaii at Manoa, and the Royal Ontario Museum (Canada) studied diamonds from China, Sierra Leone, and countries in southern Africa. They collected several types of x-ray data from the diamonds, including diffraction data using the GSECARS 13-ID-D and HP-CAT 16-ID-B x-ray beamlines at the APS; and x-ray microfluorescence maps using the GSECARS 13-ID-E beamline at the APS (Fig. 1). They also obtained infrared spectra at the U.S. DOE's Advanced Light Source (ALS) at Lawrence Berkeley National Laboratory, and with the Caltech Division of Geology and Planetary Sciences spectrometer.

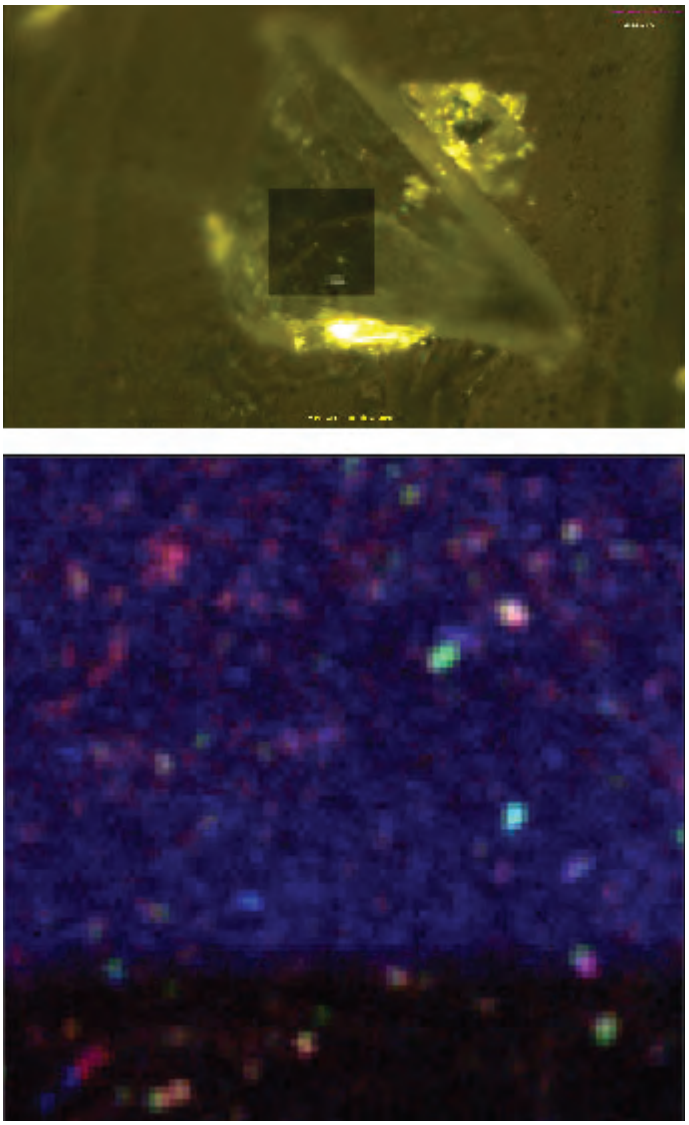

Fig. 1. Visible light and x-ray fluorescence images of samples. Top: Visible light microscope image of the holotype ice-VII-bearing diamond sample M57666 mounted at the diffractometer at GSECARS beamline 13-ID-D. Bottom: X-ray fluorescence map of a region in ice-VII-bearing diamonds specimen SM458. From O. Tschauner et al., Science **359**, 1136 (2018), Supp. Info.

They detected the presence of ice-VII inclusions in

"Ice" cont'd. on page 110

A New Understanding of Shock-Compressed Fused Silica

Silicon dioxide (SiO_2) is the most abundant oxide in the Earth's crust and serves as an archetype for silicate crystals and melts of the deep Earth. Due to its ubiquity in the Earth's crust, studies of the dynamic response of SiO_2 are critical for understanding meteorite impact events and other types of crustal explosions. While there have been numerous models of the dynamic response of SiO_2 , the *in situ* crystal structure under dynamic compression is largely unexplored. New capabilities at the DCS allow for real-time studies of the crystal structure of SiO_2 under dynamic loading. This research explains heretofore controversial features of the shock-compression behavior of fused silica and are consistent with recent molecular dynamics simulations.

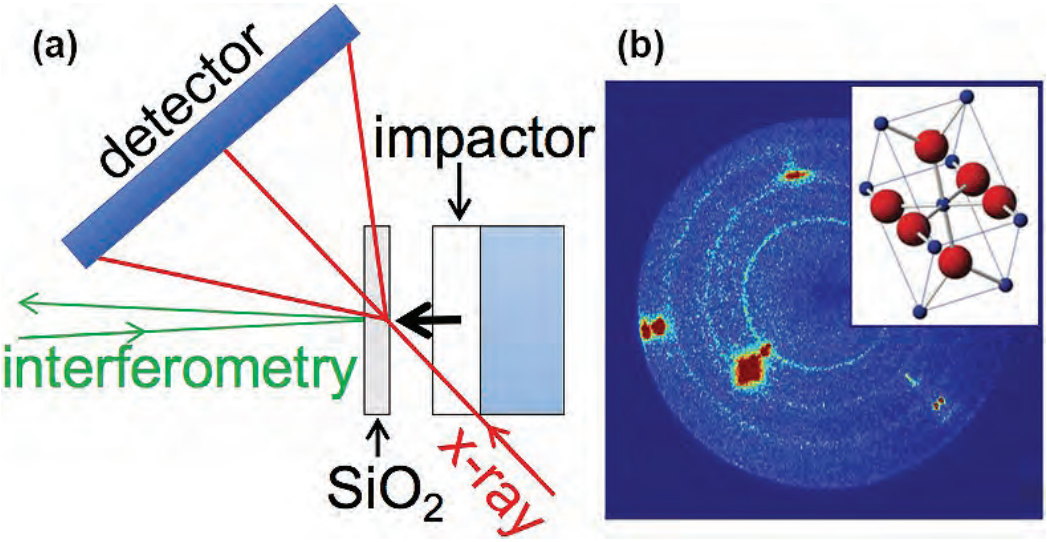

Fig. 1. a) The experimental configuration for *in situ* x-ray diffraction measurements under shock compression. b) Two-dimensional diffraction image taken at 41.8 GPa overlaid with crystal structure of high-pressure stishovite phase. The bright spots (red) are single-crystal diffraction from the LiF impactor.

The response of SiO_2 to shock loading can be broken up into three categories: (1) an elastic regime up to 8-9 GPa, (2) a highly compressible region, often described as the "mixed-phase region," 10-35 GPa, and (3) a dense/low-compressibility phase above 35 GPa. The crystal structure(s) of the mixed- and high-pressure regions have been a point of debate for over 50 years. It has often been assumed that the high-pressure crystal structure corresponds to crystalline stishovite (a dense, 6-coordinated structure observed in static compression experiments) and that the mixed-phase region is a mixture of low- and high-pressure phases, however this hypothesis lacks direct proof. Crystallization of stishovite requires a local 4- to 6-fold coordination change and it has been argued that this process is too sluggish to occur on shock wave timescales. Plate impact experiments utilizing the DCS 35-ID-B,C,D,E x-ray beamline at the APS have shed new light on these previous understandings.

In these experiments, a projectile was launched at high velocity and impacted the SiO_2, generating a shock wave in the sample, after which ultrafast x-ray diffraction was employed to determine the crystal structure during the transient (~100-nsec) high-pressure state. Using both a single-stage propellant gun and a two-stage light-gas gun, the researchers from Princeton University and Wash-

"Silica" cont'd. on page 110

"Ice" cont'd. from page 108

multiple diamond samples. Ice-VII, a type of water ice formed at high pressures, is stable at pressures above 2.4 GPa. Based on this study, ice-VII was recognized by the International Mineralogical Association as a mineral and can be used as an indicator of the pressures and temperatures under which it was included by its host diamond.

The team focused on the inclusions within the diamond samples. In addition to pockets of ice-VII, they detected nearby inclusions of silicates, carbonates, halides, and others. The diamond host crystal holds the ice-VII inclusions at pressures close to that of diamond formation even as the mantle material moves toward Earth's surface. By applying the equation of state for ice-VII, the team estimated a minimum pressure at which the diamond surrounding the ice-VII had formed. From this pressure, the team determined a minimum depth of formation for each diamond sample, allowing them to infer the depth of the aqueous fluid which crystallized into the ice-VII inclusions.

The diamond samples yielded depths ranging from 10 GPa (upper mantle) across the transition zone into 25 GPa (lower mantle). The team found that samples from locations close to each other exhibited this range of pressures. Additionally, samples located distant from each other also yielded formation pressures of similar values. Based on the total range of pressures, as well as the range of pressures at a single site, the team concluded that multiple regions of aqueous fluid exist in the mantle, some below the transition zone in the lower mantle.

— Mary Alexandra Agner

See: O. Tschauner[1]*, S. Huang[1], E. Greenberg[2], V.B. Prakapenka[2], C. Ma[3], G.R. Rossman[3], A.H. Shen[4], D. Zhang[2,5], M. Newville[2], A. Lanzirotti[2], and K. Tait[6], "Ice-VII inclusions in diamonds: Evidence for aqueous fluid in Earth's deep mantle," Science **359**, 1136 (2018). DOI: 10.1126/science.aao3030

Author affiliations: [1]University of Nevada, Las Vegas, [2]The University of Chicago, [3]California Institute of Technology, [4]China University of Geosciences, [5]University of Hawaii at Manoa, [6]Royal Ontario Museum
Correspondence: * olivert@physics.unlv.edu

This work supported by U.S. Department of Energy (DOE) awards DESC0005278, DE-FG02-94ER14466, and DE-NA0001974; by U.S. National Science Foundation (NSF) grants EAR-1634415, EAR-1128799, EAR-1322082, EAR-0318518, and DMR-0080065. GeoSoilEnviroCARS is supported by the U.S. NSF-Earth Sciences (EAR-1634415) and DOE- GeoSciences (DE-FG02-94ER14466). This research used resources of the Advanced Photon Source, a U.S. DOE Office of Science User Facility operated for the DOE Office of Science by Argonne National Laboratory under Contract No. DE-AC02-06CH11357. HP-CAT operations are supported by the DOE-National Nuclear Security Administration Office of Experimental Sciences. The Advanced Light Source is supported through contract DE-AC02-05CH11231.

"Silica" cont'd. from page 109

ington State University created planar shock waves in silica glass samples. A 10-mm-diameter disk of lithium fluoride (LiF) was mounted in a polycarbonate projectile and accelerated at a velocity of 1.8-5.6 km/s, generating uniform, well defined stress states ranging from 12 GPa to 63 GPa. After impact, a series of four x-ray diffraction images separated by 153.4 nsecs were recorded as the shock wave traversed the sample and during the subsequent release (Fig. 1). Each diffraction pattern was collected using a single bunch of photons (~100 psec) from the APS storage ring.

The x-ray diffraction patterns correspond to frames captured during a uniform stress state. Below 34 GPa there was no evidence of crystalline peaks, suggesting fused silica can be understood to be amorphous when shock compressed to these conditions. Above 36 GPa, transformation to a crystalline phase was evidenced by the emergence of sharp peaks in the x-ray diffraction data. Fits to the data in the high-pressure region patterns corresponded to stishovite with grain sizes ranging from 5 to 30 nm. Furthermore, the results suggest the "mixed-phase region" between 10 to 35 GPa corresponds to a region of glass densification rather than being a true mixture of low- and high-pressure phases, as had been previously assumed.

These results resolve the long controversy about the nature of fused silica under dynamic loading. Upon shock compression above the elastic limit up to 34 GPa, stishovite adopts a dense amorphous structure, comparable to its behavior under static compression and at shock pressures above 34 GPa, fused silica transforms to polycrystalline stishovite. — Gwenevier Johnson

See: Sally June Tracy[1]*, Stefan J. Turneaure[2], and Thomas S. Duffy[1], "*In situ* X-Ray Diffraction of Shock-Compressed Fused Silica," Phys. Rev. Lett. **120**, 135702 (2018).
DOI: 10.1103/PhysRevLett.120.135702

Author affiliations: [1]Princeton University, [2]Washigton State University
Correspondence: * sjtracy@princeton.edu

We thank Paulo Rigg and the staff of the Dynamic Compression Sector for assistance with impact experiments. This research was supported by the Defense Threat Reduction Agency Grant No. HDTRA1-15-1-0048. Washington State University provided experimental support through the U.S. Department of Energy (DOE) National Nuclear Security Agency (NNSA) Award No. DE-NA0002007. This work is based upon experiments performed at the Dynamic Compression Sector, which is operated by Washington State University under U.S. DOE/NNSA Award No. DE-NA0002442. This research used the resources of the Advanced Photon Source, a U.S. DOE Office of Science User Facility operated for the DOE Office of Science by Argonne National Laboratory under Contract No. DE-AC02-06CH11357.

Nanoscience

Weaving Gold and DNA into Metamaterials

Invisibility cloaks, super-speedy chemical reactions, and lenses that change their focus in response to their environment are just a few of the surprising technological tricks that could be performed by metamaterials. Metamaterials are designed materials carefully structured to manipulate electromagnetic radiation. They are often made of several different components — say, two different metals, or DNA plus gold — and the most exciting metamaterials are structured at the nano level so that they can manipulate visible light. Metamaterials are a rapidly advancing area of research, but building specific metamaterials rapidly and at scale is still an unsolved problem. Researchers utilized high-brightness x-rays at the APS to show that building metamaterials using templates that employ a combination of DNA and lithography to align the components is a viable method of creating bespoke materials at usable scales.

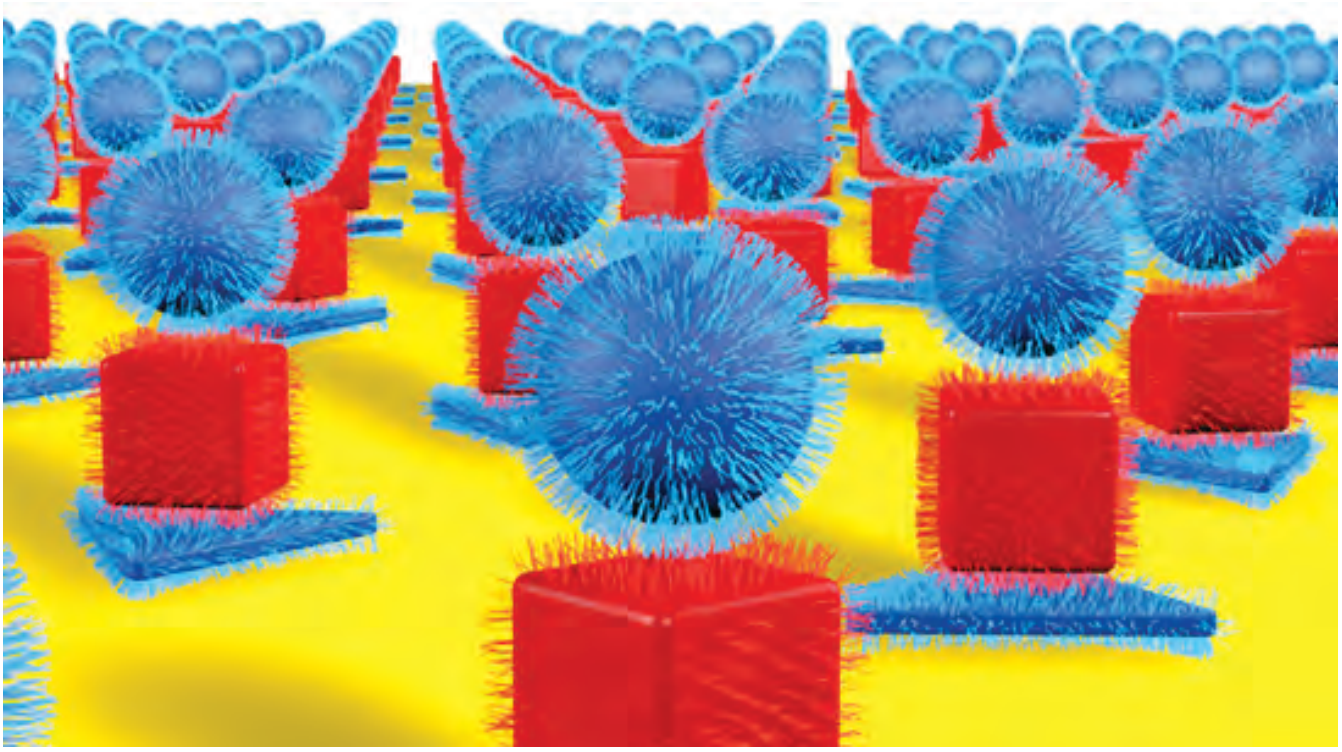

Fig. 1. Each unit cell of the nanoparticle superlattice consists of a gold surface, circular disk, cube, and sphere, with experimentally matched dimensions. Adapted from Q.-Y. Lin et al., Science **359**, 669 (2018).

DNA is best known as the instruction manual for life. It is written with four chemical "letters": G, A, T, and C, and usually hangs together in double strands that look like spiral ladders. Each rung of the ladder is made of two letters that fit together. A is always paired with T, and G always goes with C. Researchers at Northwestern University used DNA's desire to double as a tool to create elaborate metamaterial structures.

Their technique applied electron lithography, often used to write tiny circuitry on microchips, to arrange the DNA. First, a beam of electrons drew a pattern of pores through a 300-nm-thick slab of polymer down to the gold beneath it. Then the team attached strands of DNA to the gold at the bottom of each pore. A single strand of DNA stuck out of each pore, waiting for its "match." Gold nanoparticles with single strands of DNA attached to them were the matches; whenever a single strand of DNA sticking out of a pore met its complementary single strand on a gold nanoparticle, the two stuck together. In this way, particles of specific shapes could be assigned specific spots in the pattern. Multiple layers could be made by attaching a second strand of DNA to the other side of each particle. By layering particles and stringing them together with additional strands of DNA, it would be possible to build nanoparticle superlattices: many-layered structures with nanoparticles of specific shapes in precise locations (Fig. 1).

Previous attempts to do the same thing without DNA required multiple lithographic steps, metal evaporation, and perfect realignment for each new layer. Errors quickly built up, and the process was too time-consuming. By instead utilizing DNA to do the alignment, metamaterials can be built rapidly, automatically, and with precise alignment between layers, something critical to the performance of the finished material.

To see exactly what they had built, the research team and a colleague from Argonne performed grazing-incidence small-angle x-ray scattering (GISAXS) at the XSD 12-ID-B beamline at APS. The brightness and high flux of the x-ray photons from the APS make it an ideal place to perform this kind of analysis. GISAXS combines the small-angle scattering ability to image objects from one to thousands of angstroms in size on both the surface and the interior of a material with grazing incidence diffraction sensitivity to structures on the surface. Combining the two in GISAXS gives detailed information about nanostructured materials such as the gold and DNA metamaterials the team constructed.

The team found that the DNA and lithography templates did indeed build what they had designed them to build. After a bit of experimentation, they also found that if there were defects in the material, they could gently warm and agitate it, and the mismatched DNA strands would detach, while the properly assembled DNA strands held together. This allowed the team to fix defects in the materials without trashing the whole construct and starting over. The technique dramatically expands the size of the playground computational materials scientists have to work with, and will open new possibilities for new metamaterials of the future. — Kim Krieger

See: Qing-Yuan Lin[1], Jarad A. Mason[1], Zhongyang Li[1], Wenjie Zhou[1], Matthew N. O'Brien[1], Keith A. Brown[1], Matthew R. Jones[1], Serkan Butun[1], Byeongdu Lee[2], Vinayak P. Dravid[1]***, Koray Aydin[1]**, and Chad A. Mirkin[1]*, "Building superlattices from individual nanoparticles via template-confined DNA-mediated assembly," Science **359**, 669 (2018). DOI: 10.1126/science.aaq0591
Author affiliations: [1]Northwestern University, [2]Argonne National Laboratory
Correspondence: * chadnano@northwestern.edu, ** aydin@northwestern.edu, ** v-dravid@ northwestern.edu

This material is based on work supported by the Center for Bio-Inspired Energy Science, an Energy Frontier Research Center funded by the U.S. Department of Energy (DOE) Office of Science-Basic Energy Sciences, under award DE-SC0000989; and the Air Force Office of Scientific Research under awards FA9550-12-1-0280, FA9550-14-1-0274, and FA9550-17-1-0348. Use of the Center for Nanoscale Materials, an Office of Science user facility at Argonne National Laboratory, and GISAXS experiments at the Advanced Photon Source at Argonne National Laboratory were supported by the U.S. Department of Energy (DOE) Office of Science-Basic Energy Sciences, under contract DE-AC02-06CH11357. This work made use of the Electron Probe Instrumentation Center facility of the Northwestern University Atomic and Nanoscale Characterization Experimental Center at Northwestern University, which has received support from the Soft and Hybrid Nanotechnology Experimental (SHyNE) Resource (NSF NNCI-1542205); the Materials Research Science and Engineering Center program (NSF DMR-1121262) at the Materials Research Center; the International Institute for Nanotechnology (IIN); the Keck Foundation; and the State of Illinois, through the IIN. Q.-Y.L., Z.L., and M.R.J. gratefully acknowledge support from the Ryan Fellowship at Northwestern University, and M.N.O. gratefully acknowledges the National Science Foundation for a Graduate Research Fellowship.

Living on the Edge for Pt Nanoparticles during Methane Oxidation

Metal nanoparticles are often utilized as catalysts for applications in energy conversion and environmental technologies. These materials have several characteristics that make them well suited for this role, including a large surface-to-volume ratio for reaction species to settle on, and an abundance of "under-coordinated" atoms with the capacity to bind these species. These under-coordinated sites can improve the efficiency of catalytic reactions by breaking chemical bonds in the reactants or splitting them into smaller species. Identifying exactly where catalytic reactions take place on metal nanoparticle catalysts, areas known as the "active sites," can shed light on the reaction mechanism and help researchers develop ways to improve reaction efficiency. Studies have shown that when reactant species interact with metal nanoparticle catalysts, they can change the nanoparticles' shapes or sizes. However, the structural changes that take place at active sites aren't well studied. To better understand this phenomenon, researchers carried out studies at the APS. Their experiments revealed severe distortions of the crystal lattice in platinum (Pt) nanocrystals as they adsorbed oxygen at their edges, a strain that disappeared and allowed the lattice to return to its original state after the reaction was complete. These findings were in good agreement with simulations. The authors suggest that these results could provide insights that might eventually help researchers design better nanoscale catalysts.

The researchers from Sogang University (Korea), Argonne, the Deutsches Elektronen-Synchrotron (DESY), and Seoul National University of Science and Technology (Korea) examined the Pt catalysts as they catalyzed the methane oxidation reaction. To do this, they employed the Bragg coherent x-ray diffraction technique at the XSD 34-ID-C beamline at the APS. Before the start of the reaction, the researchers saw the 6-fold symmetry characteristic of a nanocrystal with a truncated octahedral shape. After allowing 20% oxygen gas to flow into the reaction chamber, the researchers imaged the Pt nanocrystals again. Their results showed deformation through the entirety of the nanocrystals' volume. This distortion increased even more once methane gas was introduced and continued throughout the methane oxidation reaction, receding only once the reaction was complete.

Employing reactive molecular dynamics simulation, a computer modeling technique, the team found that the most likely places for dissociated oxygen atoms to bind were the nanocrystals' edges and corners. In this simulation, methane then bound to these oxygen atoms for the methane oxidation reaction to take place.

When the researchers compared experimental results to this model, it was clear that the lattice distortion was due to strong contraction that originates at the crystal edges and propagates to the interior of the crystal. Once the reaction was complete and the oxidated methane left the Pt nanocatalysts, this contraction was released.

The team further compared these findings to those generated with finite element analysis, a different type of computer modeling technique. Remarkably, their results meshed with the experimental findings in terms of the magnitude of the lattice displacement and further confirmed the molecular dynamics simulation, providing even more evidence that the under-coordinated corners and edges of the Pt nanocrystal act as preferential adsorption sites for oxygen.

Together, the researchers say, these results show that the Pt nanocrystal edges and corners act as active sites for the methane oxidation reaction. The under-coordi-

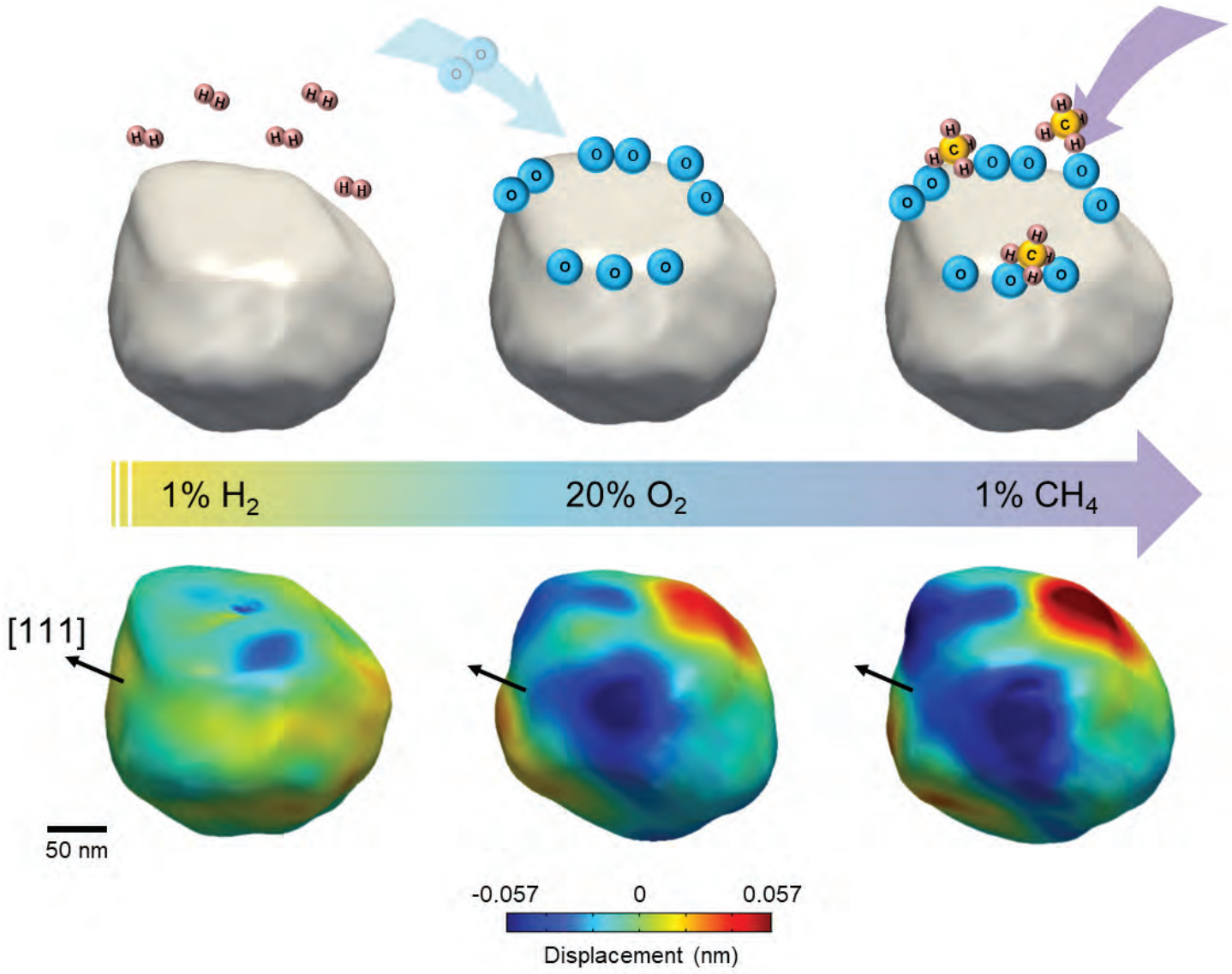

Fig. 1. Upper image: The schematic process of oxygen adsorption and methane oxidation at the edges of Pt nanoparticles. Lower image: The strain observed during the process above. The lattice displacement and strain are observed at active site edges of the nanoparticles. In the end of the catalytic methane oxidation process, the lattice displacement and strain are recovered to the initial stage.

nated atoms on these sites bind oxygen, allowing an oxidation reaction to take place once methane is introduced. This oxygen binding, and the subsequent binding of methane to the oxygen, causes the edges to contract significantly, distorting the Pt crystal lattice throughout its volume. Gaining a better grasp on how this reaction takes place, the researchers suggest, could lead to engineered nanocatalysts that allow this process to take place even more efficiently, saving time and money.

— Christen Brownlee

See: Dongjin Kim[1], Myungwoo Chung[1], Jerome Carnis[1], Sungwon Kim[1], Kyuseok Yun[1], Jinback Kang[1], Wonsuk Cha[2], Mathew J. Cherukara[2], Evan Maxey[2], Ross Harder[2], Kiran Sasikumar[2], Subramanian K.R.S. Sankaranarayanan[2], Alexey Zozulya[3], Michael Sprung[3], Dohhyung Riu[4], and Hyunjung Kim[1]*, "Active site localization of methane oxidation on Pt nanocrystals," Nat. Commun. **9**, 3422 (2018). DOI: 10.1038/s41467-018-05464-2
Author affiliations: [1]Sogang University, [2]Argonne National Laboratory, [3]Deutsches Elektronen-Synchrotron (DESY), [4]Seoul National University of Science and Technology
Correspondence: * hkim@sogang.ac.kr

This research was supported by the National Research Foundation of Korea (NRF-2014R1A2A1A10052454, 2015R1A5A1009962, 2016R1A6B2A02005468, and 2017K1A3A7A09016379). This research used resources of the National Energy Research Scientific Computing Center, a U.S. Department of Energy (DOE) Office of Science User Facility supported by the Office of Science of the U.S. DOE under contract no. DE-AC02-05CH11231. M.J.C. acknowledges funding from Argonne LDRD 2018-019-N0: A.I.C.D.I.: Atomistically Informed Coherent Diffraction Imaging. Use of the Advanced Photon Source and computational resources at the Center for Nanoscale Materials were supported by the U.S. DOE Office of Science-Basic Energy Sciences, under contract no. DE-AC02-06CH11357.

Giant Molecules as a Unique Platform for Unconventional Nanostructures

The engineering of materials into ordered structures is always a critical step to transfer and amplify microscopic molecular functionalities to macroscopic material properties. Tremendous efforts have been made toward understanding the relationship between molecules and the corresponding supramolecular structures as the base for further study of structure-property relationship. Giant molecules are a family of macromolecules with well-defined composition, geometry, and topology built up from molecular nanoparticles with precise chemical structures. They typically include folded globular proteins, polyhedral oligomeric silsesquioxane (POSS), fullerene (C60), and polyoxometalates (POMs). A multitude of studies have demonstrated that they are a unique and efficient platform upon which to construct various ordered patterns in a desired feature size. Researchers utilizing the APS have shown that altering the composition and sequence of giant molecules answers some fundamental questions about how giant molecules can be used for the assembly of controllable, well-defined, self-assembled nanostructures.

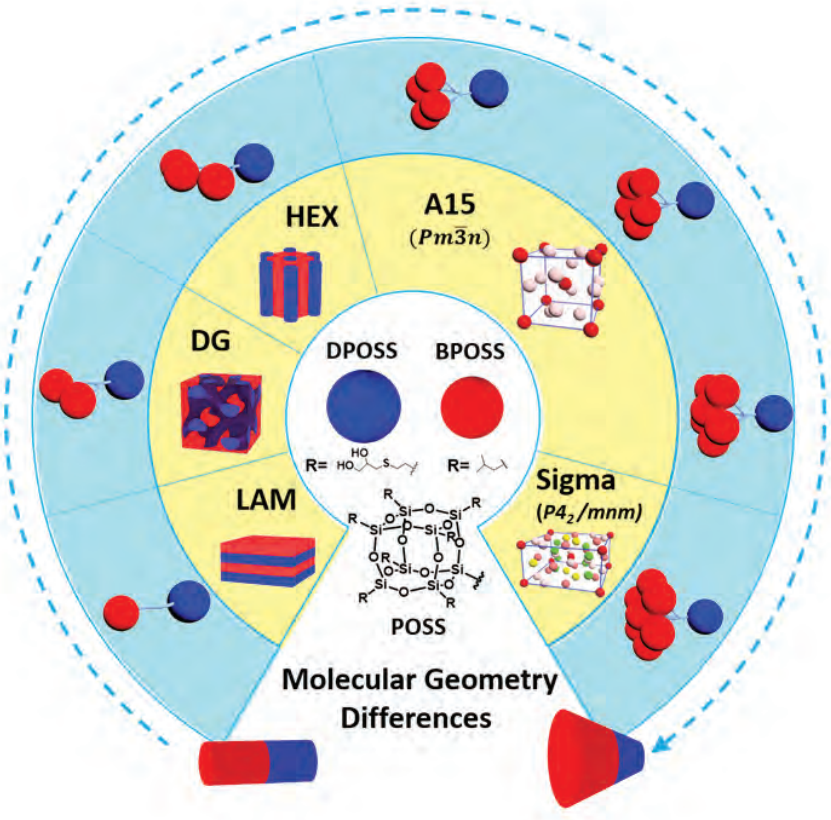

Fig. 1. Summary of self-assembly behaviors of a set of DPOSS-BPOSSn giant shape amphiphiles. Structural evolution is directed by variations of molecular geometric shape. From X. Feng et al. ACS Central Sci. **3**, 860 (2017). Copyright © 2018 American Chemical Society

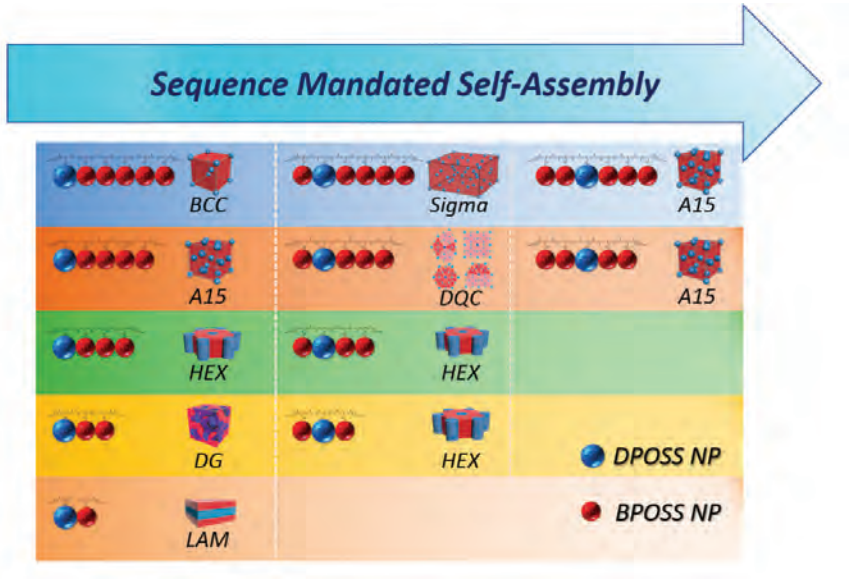

Fig. 2. Schematic illustration of the influence of composition and sequence on the self-assembled supramolecular structures in POSS based precisely defined chain-like giant molecule system.

As shown in Fig. 1, a set of giant molecules were constructed by linking one hydrophilic polyhedral oligomeric silsesquioxane nanoparticle (DPOSS, 14 hydroxyl groups functionalized POSS) with different numbers (*n*) of hydrophobic POSS(s) (BPOSS, 7 isobutyl groups functionalized POSS). The self-assembly study shows that a supramolecular structure formation sequence ranging from lamella (LAM), double gyroid (DG), hexagonal closed packed cylinders (HEX), to Frank-Kasper (F-K) A15, and further to F-K Sigma phase could be observed by turning the number of hydrophobic BPOSS (structure cartoons, Fig. 1). The phase formation sequence here is dominated by a change of the geometry of whole molecules. Increasing the number of BPOSS, the shape of the whole molecules changes from a linear shape (which forms LAM), to fan-like shape (which forms HEX), and further to cone-like shape (which forms the F-K A15 and F-K Sigma phase). The samples were well-characterized by small-angle x-ray scattering (SAXS) and transmission electron microscopy by a team of researchers from the University of Akron, Northern Illinois University, Sichuan University (China), Argonne, RIKEN CLST-JEOL Collaboration Center (Japan), JEOL RESONANCE Inc., South China University of Technology (China), and Peking University (China). The SAXS work was performed at the XSD 12-ID-B,C beamline at the APS.

Besides the composition factor, sequence controlled giant molecules were also designed and studied. A series of sequence controlled chain-like giant molecules based on one hydrophilic DPOSS and multiple hydrophobic BPOSS nanoparticles were synthesized. As shown in Fig. 2, besides the compositional variation (shown in the vertical direction of the table), the sequence of the giant molecule chain also plays an important role in the supramolecular phase formation process (shown in the horizontal direction of the table), resulting in versatile supramolecular structures.

This set of samples provides a model system for understanding the structural evolution pathways and relationships among different phases. They also offer the opportunities to design and synthesize functional molecules with certain microscopic assembly structures, and further introduce macroscopic properties to the materials with potential applications in catalysts and nano-medicine. — Tao Li

See: Xueyan Feng[1], Ruimeng Zhang[1], Yiwen Li[2], You-lee Hong[4,5], Dong Guo[1], Kening Lang[1], Kuan-Yi Wu[1], Mingjun Huang[1], Jialin Mao[1], Chrys Wesdemiotis[1], Yusuke Nishiyama[4,5], Wei Zhang[1], Wei Zhang[6], Toshikazu Miyoshi[1], Tao Li[3], and Stephen ZD Cheng[1]*, "Hierarchical Self-Organization of ABn Dendron-like Molecules into a Supramolecular Lattice Sequence," ACS Central Sci. **3**, 860 (2017). DOI: 10.1021/acscentsci.7b00188

and

Wei Zhang[1], Xinlin Lu[1], Jialin Mao[1], Chih-Hao Hsu[1], Gaoyan Mu[1], Mingjun Huang[1], Qingyun Guo[1], Hao Liu[1], Chrys Wesdemiotis[1], Tao Li[3], Wen-Bin Zhang[7], Yiwen Li[2], and Stephen ZD Cheng[1]*, "Sequence-Mandated, Distinct Assembly of Giant Molecules," Angew. Chem. Int. Ed. **56**, 15014 (2017). DOI: 10.1002/anie.201709354

Author affiliations: [1]University of Akron, [2]Sichuan University, [3]Northern Illinois University/Argonne National Laboratory, [4]RIKEN CLST-JEOL Collaboration Center, [5]JEOL RESONANCE, Inc., [6]South China University of Technology, [7]Peking University

Correspondence: * scheng@uakron.edu

This work was supported by National Science Foundation DMR-1408872 (to S.Z.D.C) and National Science Foundation of China (51603133 to Y.L., 21674003, 91427304 to W.-B.Z.), Grant-in Aid for JSPS Research Fellow 16F16047 (to Y.H.). This research used resources of the Advanced Photon Source, a U.S. Department of Energy (DOE) Office of Science User Facility operated for the U.S. DOE Office of Science by Argonne National Laboratory under Contract No. DE-AC02-06CH11357.

X-ray Availability and Reliability

In fiscal year 2018*, the APS x-ray source continued to function as a highly reliable delivery system for synchrotron x-ray beams for research. Several factors support the overall growth in both the APS user community and the number of experiments carried out by that community. But there is a direct correlation between the number of x-ray hours available to users; the success of the APS experiment program; and the physicists, engineers, and technicians responsible for achieving and maintaining optimum x-ray source performance. Below are definitions of important measures for the delivery of x-ray beam to users (latest data shown graphically).

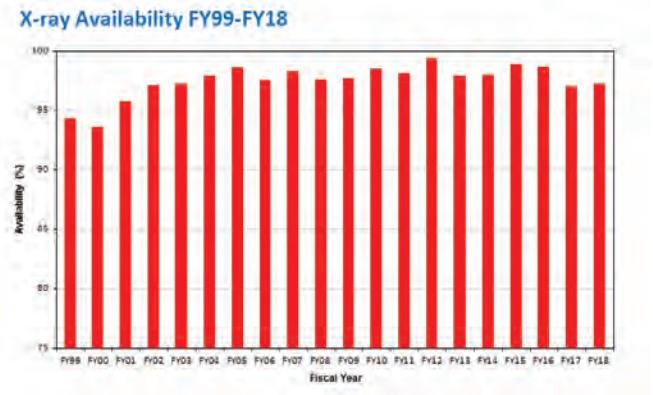

X-ray Availability: The number of hours that beam is available to users divided by the number of hours of scheduled beam delivery prior to the beginning of a run. The specific definition of available beam is that the APS main control room has granted permission to users to open shutters, and there is more than 50-mA stored

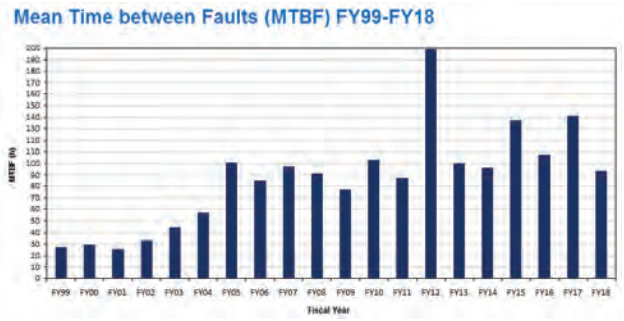

beam in the storage ring.

Storage Ring Reliability: A measure of the mean time between beam losses (faults), or MTBF, calculated by taking the delivered beam and dividing by the total number of faults. The APS targets, and routinely exceeds, 70 h MTBF. A fault is defined as complete unavailability of beam either via beam loss or removal of shutter permit not related to weather. A fault also occurs when beam has decayed to the point where stability and orbit can no longer be considered reliable (50 mA).

* While the highlights in, and title of, this report cover calendar year 2018, data on accelerator performance and user statistics are measured on the basis of fiscal years.

Typical APS Machine Parameters

Linac

Output energy	425 MeV
Maximum energy	500 MeV
Output beam charge	0.3–3 nC
Normalized emittance	5–20 mm-mrad
Frequency	2.856 GHz
Modulator pulse rep rate	30 Hz
Gun rep rate	2–12 Hz
(1–6 pulses, 33.3 ms apart every 0.5 s)	
Beam pulse length	8–15 ns
Bunch length	1–10 ps FWHM

Particle Accumulator Ring

Nominal energy	425 MeV
Maximum energy	450 MeV
Circumference	30.66 m
Cycle time	500 ms or 1000 ms
Fundamental radio frequency (RF1)	9.77 MHz
12th harmonic RF frequency (RF12)	117.3 MHz
RMS bunch length	0.34 ns
(after compression)	

Injector Synchrotron (Booster)

Nominal extraction energy	7.0 GeV
Injection energy	425 MeV
Circumference	368.0 m
Lattice structure	10 FODO cells/ quadrant
Ramping rep rate	2 Hz or 1 Hz
Natural emittance	87 nm-rad (actual)
	132 nm-rad (nominal)
Radio frequency	351.930 MHz

Storage Ring System

Nominal energy	7.0 GeV
Circumference	1104 m
Number of sectors	40
Length available for insertion device	5.0 m
Nominal circulating current, multibunch	100 mA
Natural emittance	2.5 nm-rad
RMS momentum spread	0.096%
Effective emittance	3.1 nm-rad
Vertical emittance	0.040 nm-rad
Coupling (operating)	1.5%
Revolution frequency	271.555 kHz
Radio frequency	351.935 MHz
Operating number of bunches	24 to 324
RMS bunch lengths	33 ps to 25 ps
RMS bunch length of 16 mA in hybrid mode	50 ps

Novel Accelerator & X-ray Techniques & Instrumentation

A Monocrystalline Device for Room-Temperature Serial Diffraction

The techniques of macromolecular x-ray crystallography (MX) have revolutionized biology, making possible the study of life down to the level of individual atoms in proteins. But frustrating technical limitations remain, such as the need to cryogenically freeze protein crystals in order to limit damage from the x-ray beam, making it difficult for MX researchers to observe working proteins at room temperature. Serial crystallography techniques that combine data from large batches of crystals at room temperature offer an alternative strategy, but need a large number of protein crystals. Specialized devices to grow crystals and contain them for *in situ* study have been implemented, but many such devices can introduce background x-ray scattering, thus reducing data quality. A research team has developed "crystal-on-crystal" chip devices made of a monocrystalline quartz substrate that can be used for large-scale, *in situ* serial diffraction studies on protein crystals of all sizes at both synchrotron and x-ray free-electron laser facilities. They demonstrated the applications of the devices with Laue diffraction experiments at the APS on two different types of protein crystals.

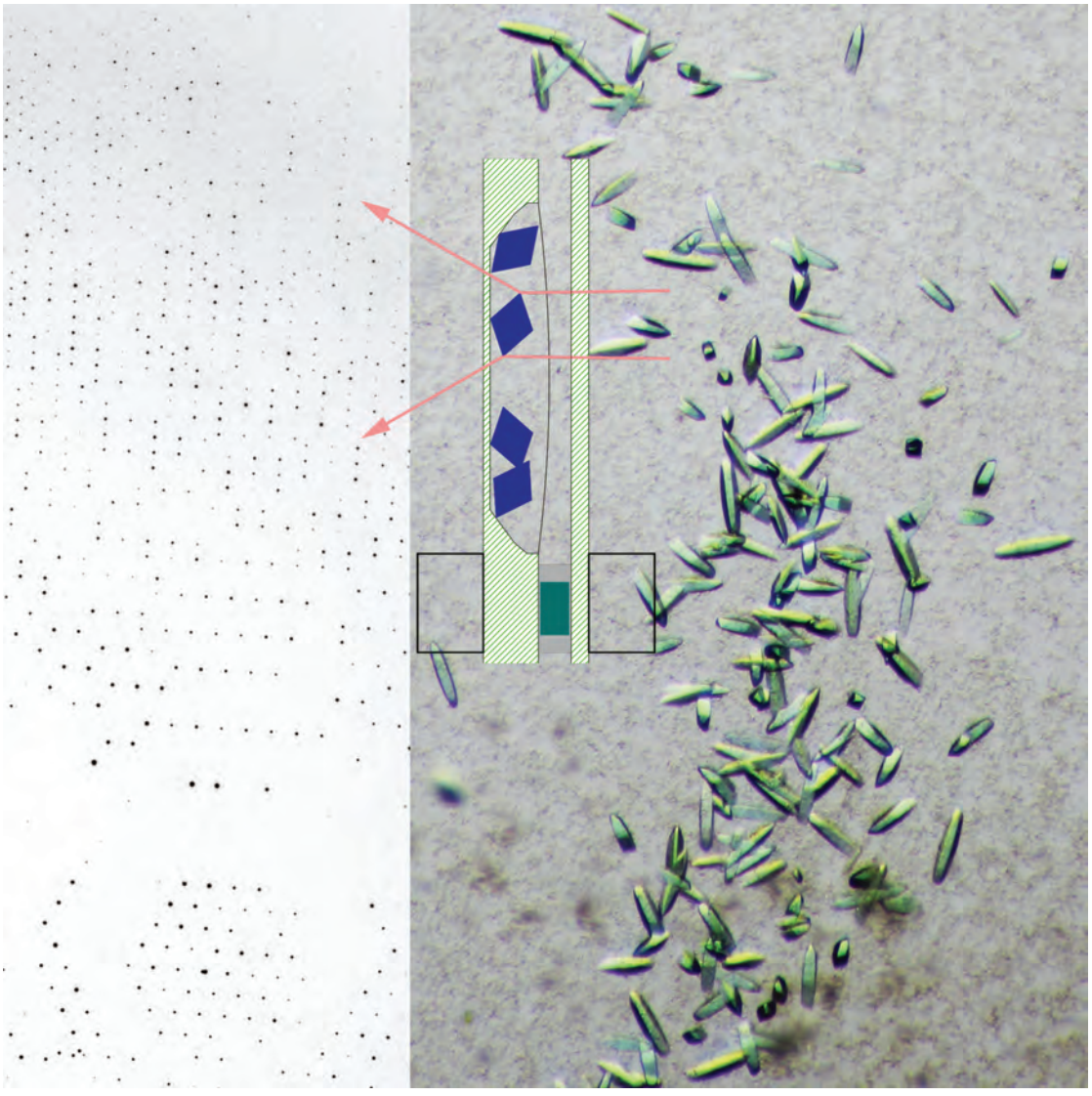

Because most protein crystals tend to be fragile at room temperature, it is important to protect them from damaging changes in sample environment such as pressure, temperature, and humidity. Vibrations or other physical touches can also damage them and thus compromise diffraction data. The crystal-on-crystal device developed by this team will enable the conduct of large-scale and high-throughput diffraction experiments from hundreds and thousands of crystals without the use of injection, screening, or other procedures so that the native crystal states can be preserved as closely as possible.

The experimenters in this study from The University of Illinois at Chicago and Renz Research, Inc., chose monocrystalline quartz as a substrate material for its lack of permeability and thus resistance to vapor loss over a long time, its wide transparency over broad wavelengths, and its minimal x-ray scattering as opposed to other commonly used glass or plastic materials, despite prior concerns that single-crystal materials might create severe interference from their Bragg reflections. The team has tested Z-cut wafers and successfully avoided Bragg reflections altogether from the quartz material (Fig. 1).

Laue diffraction studies were conducted on samples of UVR8, a plant photoreceptor protein, and PhrB, a DNA repair protein, each grown in different devices. Protein crystallization was tested using both the hanging drop vapor diffusion and microbatch methods. Both monochromatic diffraction and polychromatic Laue diffraction studies were performed with the devices mounted on a goniometer at the BioCARS 14-ID-B beamline at the APS. The researchers were able to obtain nearly complete datasets from hundreds of crystals, with a greater number of usable frames compared to previous serial Laue diffraction studies. With further improvements in data processing techniques, they expect to obtain thousands of frames per dataset.

Serial crystallography obtains a dataset not from an individual crystal but rather many thousands, with each crystal often contributing only one frame. The nature of injector-based methods inevitably rules out repeated exposures of an individual crystal. Repeated exposures from the same crystal are also difficult because they can quickly induce x-ray damage at room temperature. However, the experiment team notes that their crystal-on-crystal chip can facilitate second and subsequent x-ray exposures from the same crystal but with different volumes with the use of crystal recognition and shot planning software, improving dynamic imaging capabilities.

The researchers observe that both injection-based and fixed-target sampling systems often display a low "hit rate," defined as the number of images containing any diffraction signal out of the total attempted hits. Considering an alternative parameter they call "yield," which is the percentage of total crystals that produce diffraction data, the team notes that the current experiments produced a yield of nearly 100%, indicating that almost all of the prepared crystals were imaged, although not all gave usable data.

This work spotlights a number of significant advantages of monocrystalline devices for room temperature x-ray diffraction studies. Compared to non-crystalline plastic or glass materials, the "crystal-on-crystal" quartz devices offer greatly improved signal-to-noise ratio, optical transparency, stable crystallization, excellent data yield, and compatibility with different crystallographic techniques. The concept is also readily suited for both synchrotron-based and XFEL work, making both static and dynamic room temperature serial crystallography of biological structures and processes a scientific tool as versatile and valuable as cryo-crystallography.

— Mark Wolverton

< Fig. 1. An *in situ* diffraction platform for serial crystallography at room temperature. A micrograph of bacteriophytochrome crystals grown on the device is shown on the right. These crystals and the entire device can be mounted on an APS beamline directly for diffraction experiments. As shown in the inset, an x-ray beam through the monocrystalline device substrate will not cause any interfering Bragg diffraction or diffuse scattering. A diffraction image on the left shows very clean data from protein diffraction only.

See: Zhong Ren[1,2]*, Medine Ayhan[1], Sepalika Bandara[1], Kalinga Bowatte[1], Indika Kumarapperuma[1], Semini Gunawardana[1], Heewhan Shin[1], Cong Wang[1], Xiaoli Zeng[1‡], and Xiaojing Yang[1]**, "Crystal-on-crystal chips for *in situ* serial diffraction at room temperature," Lab Chip **18**, 2246 (2018). DOI: 10.1039/c8lc00489g
Author affiliations: [1]University of Illinois at Chicago, [2]Renz Research, Inc. ‡Present address: Chinese Academy of Sciences
Correspondence: *zren@uic.edu, **xiaojing@uic.edu

This work is supported in part by grants from the University of Illinois at Chicago and National Institutes of Health (R01EY024363) to XY. Use of BioCARS was supported by the National Institute of General Medical Sciences of the National Institutes of Health under grant number R24GM111072. The content is solely the responsibility of the authors and does not necessarily represent the official views of the National Institutes of Health. This research used resources of the Advanced Photon Source, an Office of Science User Facility operated for the U.S. DOE Office of Science by Argonne National Laboratory under contract no. DE-AC02-06CH11357, and the Canadian Light Source and its funding partners.

Extending Non-resonant Valence-to-Core Emission Spectroscopy to Niobium Chemistry

Non-resonant valence-to-core (V2C) x-ray emission spectroscopy (XES) promises to be a powerful complement to other structure characterization methods, in that the emerging technique as applied to 3*d* transition metals has been found to clearly distinguish ligand atoms that are similar in atomic mass, which other structure determination tools often cannot do. This motivated a team of researchers to begin investigating the use of nonresonant V2C XES with 4*d* metals, whose V2C *Kβ* emission spectroscopy has not been extensively investigated. All data were measured using a recently developed optimized/high-resolution spectrometer at the APS. The spectrometer was specifically designed to operate efficiently in the energy range required for nonresonant V2C XES of the 4*d* transition metals. The amplitudes and positions of the $K\beta_{2,4}$ and $K\beta''$ V2C XES peaks were identified using software that was developed to process and analyze the data generated by the recently developed spectrometer. Density functional theory was combined with calculations of the Bethe-Salpeter equation of motion to interpret the results.

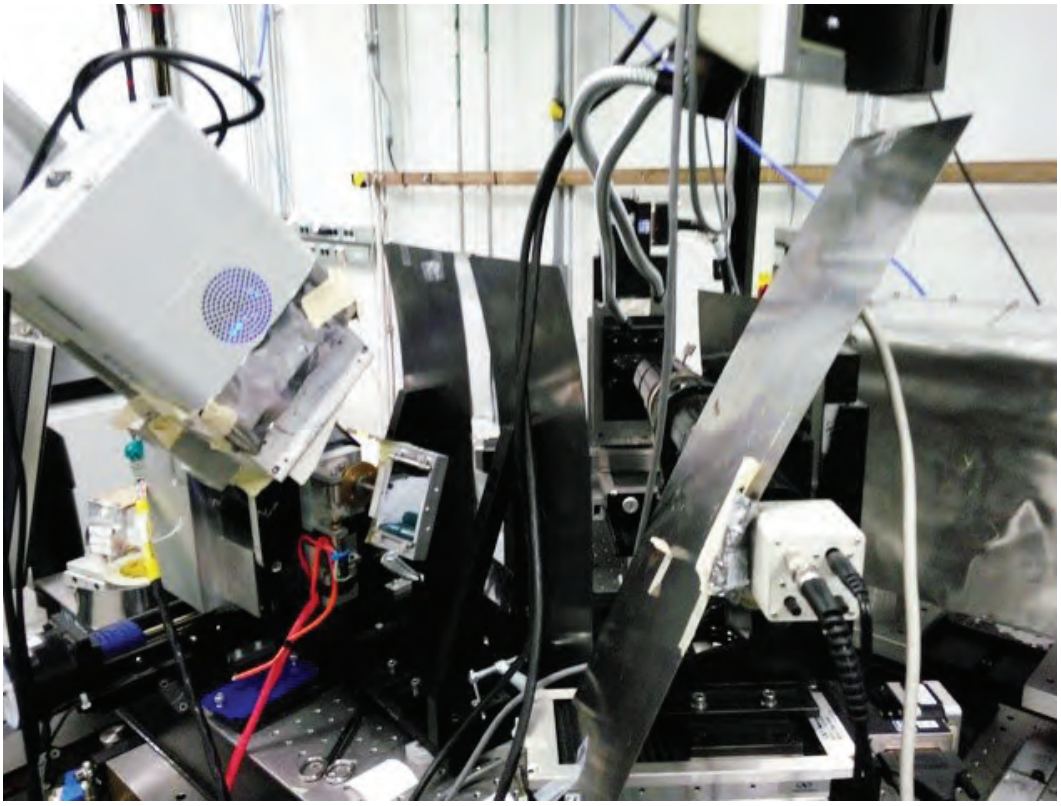

Fig. 1. The recently developed spectrometer at the MR-CAT 10-ID-B beamline, which uses a bent Laue analyzer crystal and an area detector for excellent energy resolution at high x-ray energies.

V2C XES measurements involving the metal atoms of a material can complement the more established structural determination techniques by providing a specific sensitivity to the ligands bound to the metal atoms. In an x-ray emission measurement, the incident x-ray beam is used to excite a 1s electron of the metal atom, creating a photoelectron and leaving behind a core hole. When the core hole is refilled by some other electron, a secondary photon is emitted by the atom. The energy of that secondary photon identifies the state of that other electron before it refilled the core hole. The *Kβ″* peak in V2C XES is of particular interest as it arises from the transition of the ligand 2s electron filling the metal 1s core hole. In the case of the 3*d* transition metal series (Ti to Zn), the position of the *Kβ″* peak shifts many electron volts to lower energy as the ligand changes from carbon to nitrogen, oxygen, or fluorine.

Utilizing the spectrometer at the MR-CAT 10-ID-B x-ray beamline at the APS (Fig. 1), the research team from the National Institute of Standards and Technology, Argonne, Stony Brook University, Brookhaven National Laboratory, and the University of Sheffield (UK) explored the ligand dependence of nonresonant V2C XES for the niobium compounds NbC, NbN, N_2O_5, and NbF_5, showing that the *Kβ″* peaks of this 4*d* metal demonstrate the well-defined dependence on ligand species that was found for 3*d* metals and molybdenum, the only other 4*d* metal studied using the non-resonant V2C XES technique.

The nonresonant V2C XES $K\beta_{2,4}$ spectra for the Nb^{4+} compound NbC and the Nb^{5+} compounds Nb_2O_5 and NbF_5 were measured with photons having an incident energy of 19100 eV, which is 114 eV above the Nb *K*-edge energy of 18986 eV (Fig. 2). As with the 3*d* metals, the position of the *Kβ″* peak was found to be ligand dependent, with shifts by many electron volts among the ligands C, O, and F, which were well within the detection limit of the researcher's spectrometer.

The study showed that the position and intensity of the *Kβ″* peak can be used to positively identify ligand species, even in situations where x-ray diffraction, x-ray absorption fine structure (XAFS), neutron diffraction, or other structural measurements cannot resolve that information. The nonresonant V2C XES measurement does not contain as much information about the chemical state of the material as measurements made in the resonant regime, with the incident photon energy being close to the core hole excitation energy. It is, however, a relatively simple and quick measurement that can be added to an XAFS or diffraction measurement campaign at a synchrotron.

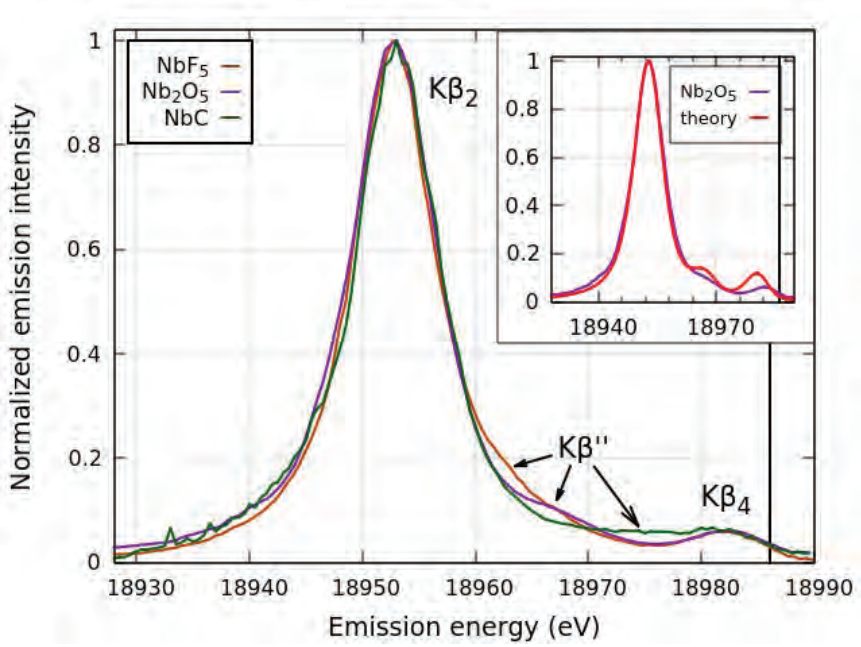

Fig. 2. V2C XES measurements on three Nb compounds. Note that the *Kβ″* peak shifts by over 10 eV from C to F. Inset: comparison of measured V2C XES data with theory for Nb_2O_5, showing good agreement with all three *Kβ* peaks.

— Vic Comello

See: Bruce Ravel[1]*, A. Jeremy Kropf[2], Dali Yang[2], Mengen Wang[3], Mehmet Topsakal[4], Deyu Lu[4], Martin C. Stennett[5], and Neil C. Hyatt[5], "Nonresonant valence-to-core x-ray emission spectroscopy of niobium," Phys. Rev. B **97**, 125139 (2018). DOI: 10.1103/PhysRevB.97.125139
Author affiliations: [1]National Institute of Standards and Technology, [2]Argonne National Laboratory, [3]Stony Brook University, [4]Brookhaven National Laboratory, [5]The University of Sheffield
Correspondence: *bravel@bnl.gov

M.T. was supported by Laboratory Directed Research and Development Grant No. 16-039 at Brookhaven National Laboratory. N.C.H. received financial support from the Engineering and Physical Sciences Research Council under Grant No. EP/M026566/1. Materials Research Collaborative Access Team operations are supported by the U.S. Department of Energy (DOE) and Materials Research Collaborative Access Team member institutions. The research used resources of the Center for Functional Nanomaterials, which is a DOE Office of Science Facility at Brookhaven National Laboratory under Contract No. DE-SC0012704. This research used resources of the Advanced Photon Source, a DOE Office of Science User Facility operated for the DOE Office of Science by Argonne National Laboratory under Contract No. DE-AC02-06CH11357.

Trapping Short-lived Intermediates to Peek at their Structure

How do chemists characterize pesky, reactive intermediates? Pinning down these complexes long enough to study them can be a challenge. In particular, complexes with late transition metal M-L multiply bonds are highly reactive and notoriously difficult to characterize. But what if there was a way to trap these fleeting intermediates long enough to get a good look? Photocrystallography is a rapidly developing crystallographic technique that allows scientists to observe the three-dimendional structure of short-lived molecules by photogenerating and trapping them in a crystalline matrix. This innovative technique uses synchrotron experiments to irradiate a single crystal and collect x-ray diffraction patterns of reaction species. Recently, researchers working at the APS used photocrystallography to achieve the first-ever direct characterization of a reactive di-ruthenium nitride intermediate. These results position photocrystallography as a feasible and powerful tool for assessing the structures of highly reactive M-L multiply bonded intermediates.

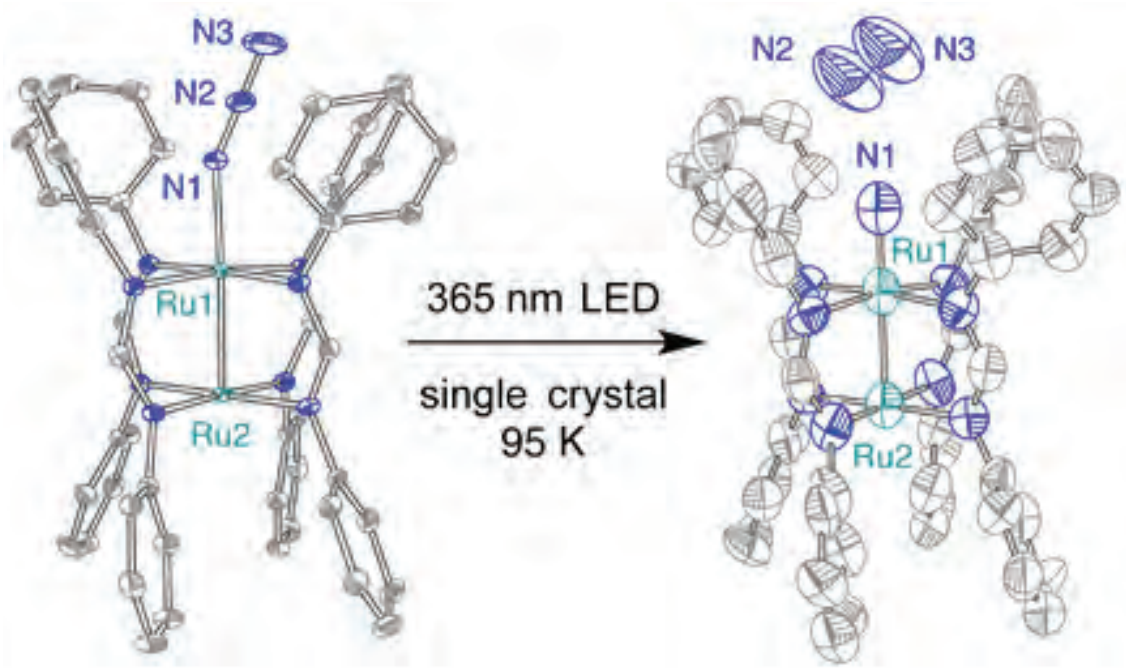

Metal-oxo and metal-nitrido complexes have proven to be powerful workhorses in the field of catalysis. Metal-nitrido coordination complexes contain at least one terminal nitrogen atom that is multiply bonded to a transition metal. These reactive species are critical intermediates in a variety of important catalytic reactions, such as nitrogen fixation and C-H amination.

The reactivity of complexes with metal-to-ligand (M-L) multiple bonds is determined in part by the valency of the metal. Complexes with mid-to-late transition metals tend to be less stable than their early transition metal, M-L multiply bonded complex counterparts due to an increased number of d electrons across the M-L bonds. Although the reactivity of these mid-to-late transition metal complexes lends beautifully to their use as catalysts, their instability makes them very difficult to isolate and characterize. Previous attempts to study these intermediates relied on synthetically stabilizing the reactive ligand or metal fragments of interest, which allowed for isolation but resulted in an undesired decrease in reactivity--not a great result when the intended application is catalysis.

In order to circumvent the need for synthetic modifications, the researchers applied a novel crystallographic technique called photocrystallography that they believed would allow them to directly determine the structure of a highly reactive M-L multiply bonded complex. The technique of photocrystallography involves irradiating a crystalline sample to photogenerate reactive species that are confined in crytalline matrices and can be studied at low temperature. Researchers can then rapidly collect x-ray diffraction data on the photogenerated sample using a synchrotron source.

To benchmark this photocrystallographic technique with reactive ruthenium intermediates, researchers selected Ru_2 nitride **2** (Fig. 1), which can be generated by photolysis of Ru_2 azide **1** at low temperatures. Since the precursor **1** is stable, researchers postulated that they could use photocrystallography to generate **2** *in situ* using photolysis without disturbing the crystal lattice, and conduct x-ray diffraction to determine its structure. Researchers conducted the experiment at ChemMatCARS beamline 15-ID-B,C,D at the APS, where they mounted a crystal of the intermediate precursor **1**, irradiated it with a LED source, and monitored the real-time reaction progress with x-ray diffraction. During irradiation, the Ru_2 azide **1** complex undergoes a bond-angle linearization, resulting in a phase transition, but continued irradiation eventually leads to the formation of **2**. The researchers confirmed the successful photo-generation of **2** by comparing the EPR signals to a standard, which appeared nearly identical.

With these promising results, photocrystallography has emerged as a feasible and powerful tool for assessing the structures of highly reactive M-L multiply bonded intermediates. By confining these reactive intermediates within a lattice structure under low temperature conditions, researchers were able to avoid synthetically modifying the compound, and instead were able to directly determine the compound's three-dimensional structure using photocrystallography. — Alicia Surrao

< Fig. 1. Upon single-crystal photolysis, the Ru_2 azide (left) extrudes N_2 extrusion to generate a reactive Ru_2 nitride (right). These structures were determined by photocrystallography.

See: Anuvab Das[1], Joseph H. Reibenspies[1], Yu-Sheng Chen[2], and David C. Powers[1]*, "Direct Characterization of a Reactive Lattice-Confined Ru2 Nitride by Photocrystallography," J. Am. Chem. Soc. **139**, 2912 (2017). DOI: 10.1021/jacs.6b13357
Author affiliations: [1]Texas A&M University, [2]The University of Chicago
Correspondence: * david.powers@chem.tamu.edu

The authors thank Texas A&M University and the Welch Foundation (A-1907) for financial support. Chem-MatCARS Sector 15 is principally supported by the U.S. National Science Foundation under grant number NSF/CHE-1346572. This research used resources of the Advanced Photon Source, a U.S. Department of Energy (DOE) Office of Science User Facility operated for the DOE Office of Science by Argonne National Laboratory under Contract No. DE-AC02-06CH11357.

This highlight was inadvertantly omitted from *APS Science 2017*.

Lisa Keefe (IMCA-CAT Director) was elected President of the American Crystallographic Association, Inc.

APS guest student **Daikang Yan** (Northwestern University) received the 2018 IEEE CSC Graduate Study Fellowship Award in Applied Superconductivity.

Yang Ren (physicist with the XSD Structural Science Group) joined eight colleagues and co-authors as co-winners of the American Iron and Steel Institute "2018 Institute Medal" for their paper, "Deformation Mode and Strain Path Dependence of Martensite Phase Transformation in a Medium Manganese TRIP Steel."

David Keavney (physicist with the XSD Magnetic Materials Group) has been awarded an AAAS Science and Technology Policy Fellowship at the U.S. Department of State, Bureau of Energy Resources for 2018-2019.

Brian Toby (left, APS Chief Computational Scientist and XSD Computational X-ray Science [CSX] Group Leader) and **Robert Von Dreele** (right, senior physicist in the CSX Group) were selected as the recipients of the American Crystallographic Association 2019 Trueblood Award in recognition of their "seminal contribution to the crystallographic community, in the creation and support of widely-used open-source software (GSAS-II, GSAS, and EXPGUI), in development of new instrumentation, new diffraction techniques, and in training." **Von Dreele** was also named a Fellow of the American Crystallographic Association

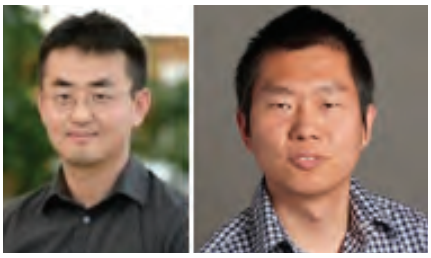

Qingteng Zhang (left, XSD Time Resolved Research Group postdoc) and **Cang Zhao** (XSD Imaging Group postdoc) received an award for Outstanding Postdoctoral Performance in the Area of Applied Science from Argonne National Laboratory.

Zhang Jiang (physicist with the XSD Time Resolved Research Group) was among the 84 U.S. scientists chosen to receive a DOE 2018 Early Career Research Program award, for developing coherence surface scattering imaging, which will support research to better control the synthesis and fabrication of advanced materials, which is a challenge due to their complexity and heterogeneity.

APS Organization Chart

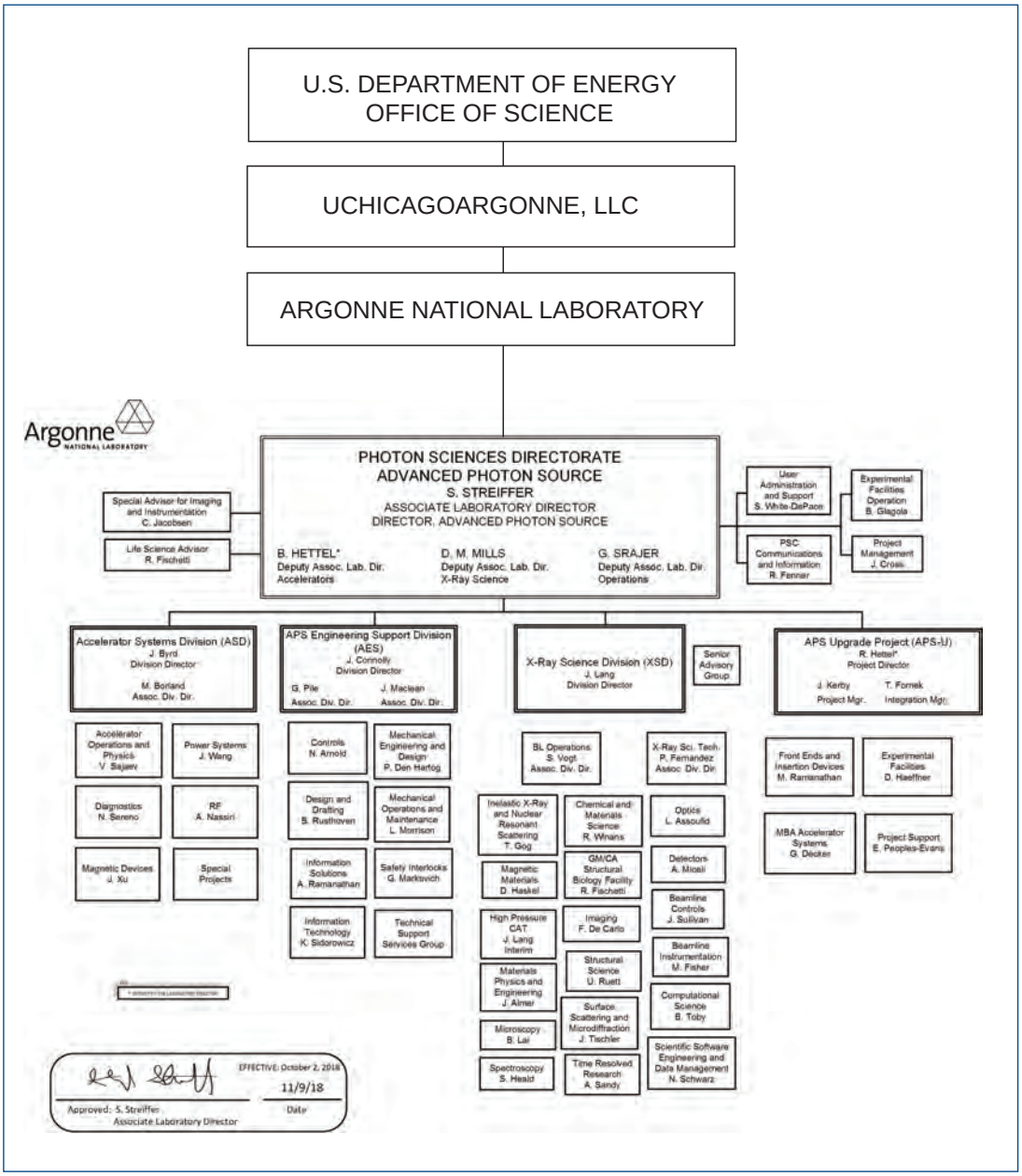

APS Funding (FY 2006 - FY 2018)

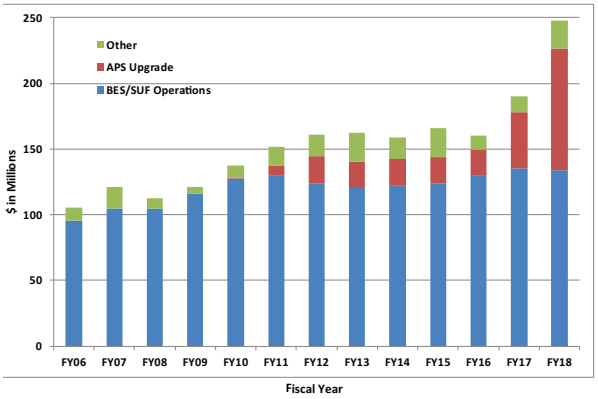

APS Staffing (FY 2007- FY 2018)

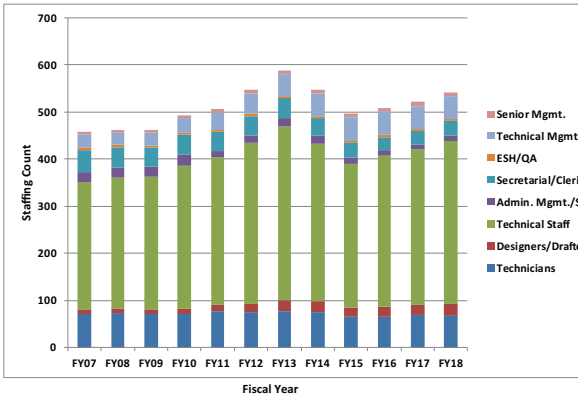

APS Source Parameters

Undulator A (31 insertion devices [IDs] in 25 sectors)

Period: 3.30 cm
Length: 2.1 m in sectors 16, 21, 23, 24, 28, 34; 2.3 m in Sector 6; 2.4 m in sectors 1, 2, 5, 7, 8, 9, 10, 11, 15, 17, 18, 19, 20, 22, 26, 28, 31, 32, 33
Minimum gap: 10.5 mm
B_{max}/K_{max}: 0.892 T/2.75 (effective; at minimum gap)
Tuning range: 3.0–13.0 keV (1st harmonic)
3.0–45.0 keV (1st–5th harmonic)
On-axis brilliance at 7 keV (ph/s/mrad^2/mm^2/0.1%bw):
4.1 x 10^{19} (2.4 m), 4.0 x 10^{19} (2.3 m), 3.3 x 10^{19} (2.1 m)
Source size and divergence at 8 keV:
Σ_x: 276 μm Σ_y: 11 μm
$\Sigma_{x'}$: 12.7 μrad (2.4 m), 12.8 μrad (2.3 m), 12.9 μrad (2.1 m)
$\Sigma_{y'}$: 6.7 μrad (2.4 m), 6.8 μrad (2.3 m), 7.1 μrad (2.1 m)

2.30-cm Undulator (2 IDs in sectors 11, 14)

Period: 2.30 cm Length: 2.4 m
Minimum gap: 10.5 mm
B_{max}/K_{max}: 0.558 T/1.20 (effective; at minimum gap)
Tuning range: 11.8–20.0 keV (1st harmonic)
11.8–70.0 keV (1st-5th harmonic, non-contiguous)
On-axis brilliance at 12 keV (ph/s/mrad^2/mm^2/0.1%bw): 6.9 x 10^{19}
Source size and divergence at 12 keV:
Σ_x: 276 μm Σ_y: 11 μm
$\Sigma_{x'}$: 12.3 μrad $\Sigma_{y'}$: 5.9 μrad

2.70-cm Undulator (5 IDs in sectors 3, 12, 14, 35)

Period: 2.70 cm
Length: 2.1 m in Sector 12; 2.4 m in sectors 3, 14, and 35
Minimum gap: 10.5 mm
B_{max}/K_{max}: 0.698 T/1.76 (effective; at minimum gap)
Tuning range: 6.7–16.0 keV (1st harmonic)
6.7–60.0 keV (1st-5th harmonic, non-contiguous)
On-axis brilliance at 8.5 keV (ph/s/mrad^2/mm^2/0.1%bw):
5.7 x 10^{19} (2.4 m), 4.7 x 10^{19} (2.1 m)
Source size and divergence at 8 keV:
Σ_x: 276 μm Σ_y: 11 μm
$\Sigma_{x'}$: 12.7 μrad (2.4 m), 12.9 μrad (2.1 m)
$\Sigma_{y'}$: 6.7 μrad (2.4 m), 7.1 μrad (2.1 m)

3.00-cm Undulator (8 IDs in sectors 12, 13, 16, 21, 23, 27, 34)

Period: 3.00 cm
Length: 2.1 m in sectors 12, 13, 16, 21, 23, 34; 2.4 m in Sector 27
Minimum gap: 10.5 mm
B_{max}/K_{max}: 0.787 T/2.20 (effective; at minimum gap)
Tuning range: 4.6–14.5 keV (1st harmonic)
4.6–50.0 keV (1st-5th harmonic)
On-axis brilliance at 8 keV (ph/s/mrad^2/mm^2/0.1%bw):
4.8 x 10^{19} (2.4 m), 3.9 x 10^{19} (2.1 m)
Source size and divergence at 8 keV:
Σ_x: 276 μm Σ_y: 11 μm
$\Sigma_{x'}$: 12.7 μrad (2.4 m), 12.9 μrad (2.1 m)
$\Sigma_{y'}$: 6.7 μrad (2.4 m), 7.1 μrad (2.1 m)

3.50-cm SmCo Undulator (Sector 4)

Period: 3.50 cm Length: 2.4 m
Minimum gap: 9.75 mm
B_{max}/K_{max}: 0.918 T/3.00 (effective; at minimum gap)
Tuning range: 2.4–12.5 keV (1st harmonic)
2.4–42.0 keV (1st-5th harmonic)
On-axis brilliance at 7 keV (ph/s/mrad^2/mm^2/0.1%bw): 3.7 x 10^{19}
Source size and divergence at 8 keV:
Σ_x: 276 μm Σ_y: 11 μm
$\Sigma_{x'}$: 12.7 μrad $\Sigma_{y'}$: 6.7 μrad

3.60-cm Undulator (Sector 13)

Period: 3.60 cm
Length: 2.1 m
Minimum gap: 11.0 mm
B_{max}/K_{max}: 0.936 T/3.15 (effective; at minimum gap)
Tuning range: 2.2–11.8 keV (1st harmonic)
2.2–40.0 keV (1st-5th harmonic)
On-axis brilliance at 6.5 keV (ph/s/mrad^2/mm^2/0.1%bw): 2.8 x 10^{19}
Source size and divergence at 8 keV:
Σ_x: 276 μm Σ_y: 11 μm
$\Sigma_{x'}$: 12.9 μrad $\Sigma_{y'}$: 7.1 μrad

1.72-cm Undulator (3 IDs in sectors 30, 35)

Period: 1.72 cm
Length: 4.8 m (2 x 2.4 m) in Sector 30; 2.4 m in Sector 35
Minimum gap: 10.6 mm
B_{max}/K_{max}: 0.330 T/0.53 (effective; at minimum gap)
Tuning range: 23.7–26.3 keV (1st harmonic)
On-axis brilliance at 23.7 keV (ph/s/mrad^2/mm^2/0.1%bw):
1.0 x 10^{20} (4.8 m), 4.4 x 10^{19} (2.4 m)
Source size and divergence at 23.7 keV:
Σ_x: 276 μm Σ_y: 11 μm
$\Sigma_{x'}$: 11.6 μrad (4.8 m) 11.9 μrad (2.4 m)
$\Sigma_{y'}$: 4.3 μrad (4.8 m), 4.9 μrad (2.4 m)

1.80-cm Undulator (Sector 32)

Period: 1.80 cm
Length: 2.4 m
Minimum gap: 11.0 mm
B_{max}/K_{max}: 0.244 T/0.41 (effective; at minimum gap)
Tuning range: 23.8 - 25.3 keV (1st harmonic)
71.4 - 75.9 keV (3rd harmonic)
On-axis brilliance at 23.8 keV (ph/s/mrad^2/mm^2/0.1%bw): 2.8 x 10^{19}
Source size and divergence at 23.8 keV:
Σ_x: 276 um Σ_y: 11 um
$\Sigma_{x'}$: 11.9 urad $\Sigma_{y'}$: 4.9 urad

IEX 12.5-cm Quasi-Periodic Polarizing Undulator (Sector 29)

Period: 12.5 cm
Length: 4.8 m
Circular polarization mode:
Max. currents: horizontal coils 34.4 A, vertical coils 20.7 A
K_{max}: 2.73 (effective; at max. currents)
B_{max}: 0.27 T (peak; at max. currents)
Tuning range: 0.44–3.5 keV (1st harmonic)
On-axis brilliance at 1.8 keV (ph/s/mrad^2/mm^2/0.1%bw): 1.4 x 10^{19}
Linear horizontal polarization mode:
Max. current: vertical coils 47.6 A
K_{max}: 5.39 (effective; at max. current
B_{max}: 0.54 T (peak; at max. current)
Tuning range: 0.24–3.5 keV (1st harmonic)
0.24–11.0 keV (1st–5th harmonic)
On-axis brilliance at 2.1 keV (ph/s/mrad^2/mm^2/0.1%bw): 1.1 x 10^{19}
Linear vertical polarization mode:
Max. current: horizontal coils 50.3 A
K_{max}: 3.86 (effective; at max. current)
B_{max}: 0.37 T (peak; at max. current)
Tuning range: 0.44–3.5 keV (1st harmonic)
0.44–11.0 keV (1st–5th harmonic)
On-axis brilliance at 2.1 keV (ph/s/mrad^2/mm^2/0.1%bw): 1.1 x 10^{19}
Fast polarization switching not required
Source size and divergence at 2 keV:
Σ_x: 276 μm Σ_y: 13 μm
$\Sigma_{x'}$: 13.9 μrad $\Sigma_{y'}$: 8.8 μrad

12.8-cm Circularly Polarizing Undulator (Sector 4)

Period: 12.8 cm
Length: 2.1 m
Circular polarization mode:
Max. currents: horizontal coils 1.34 kA, vertical coils 0.40 kA
K_{max}: 2.85 (effective; at max. currents)
B_{max}: 0.30 T (peak; at max. currents)
Tuning range: 0.4–3.0 keV (1st harmonic)
On-axis brilliance at 1.8 keV (ph/s/mrad^2/mm^2/0.1%bw): 3.1 x 10^{18}
Linear horizontal polarization mode:
Max. current: vertical coils 0.40 kA
K_{max}: 2.85 (effective; at max. current)
B_{max}: 0.30 T (peak; at max. current)
Tuning range: 0.72–3.0 keV (1st harmonic)
0.72–10.0 keV (1st–5th harmonic)
On-axis brilliance at 2.1 keV (ph/s/mrad^2/mm^2/0.1%bw): 2.3 x 10^{18}
Linear vertical polarization mode:
Max. current: horizontal coils 1.60 kA
K_{max}: 3.23 (effective; at max. current)
B_{max}: 0.34 T (peak; at max. current)
Tuning range: 0.58–3.0 keV (1st harmonic)
0.58–10.0 keV (1st–5th harmonic)
On-axis brilliance at 2.1 keV (ph/s/mrad^2/mm^2/0.1%bw): 2.3 x 10^{18}
Switching frequency (limited by storage ring operation): 0–0.5 Hz
Switching rise time: 50 ms
Source size and divergence at 2 keV:
Σ_x: 276 μm Σ_y: 12 μm
$\Sigma_{x'}$: 16.7 μrad $\Sigma_{y'}$: 12.7 μrad

1.80-cm Superconducting Undulator (2 IDs in sectors 1, 6)

Period: 1.80 cm
Length: 1.1 m
Gap: 9.5 mm (fixed)
Max. current: 450 A
B_{max}/K_{max}: 0.962 T/1.61 (effective; at maximum current)
Tuning range: 11.2–24.7 keV (1st harmonic)
11.2–150.0 keV (1st-13th harmonic, non-contiguous)
On-axis brilliance at 13 keV (ph/s/mrad^2/mm^2/0.1%bw): 3.2 x 10^{19}
Source size and divergence at 13 keV:
Σ_x: 276 μm Σ_y: 11 μm
$\Sigma_{x'}$: 13.2 μrad $\Sigma_{y'}$: 7.5 μrad

3.15-cm Helical Superconducting Undulator (Sector 7)

Period: 3.15 cm
Length: 1.2 m
Coil winding diameter: 31.0 mm
Max. current: 450 A
B_{max}/K_{max}: 0.413 T/1.213 (B_x=B_y effective; at maximum current)
Tuning range: 6.0-13.0 keV (1st harmonic)
On-axis brilliance at 6.0 keV (ph/s/mrad^2/mm^2/0.1%bw): 2.2 x 10^{19}
Source size and divergence at 6 keV:
Σ_x: 276 μm Σ_y: 11 μm
$\Sigma_{x'}$: 14.7 μrad $\Sigma_{y'}$: 10.0 μrad

APS Bending Magnet

Critical energy: 19.51 keV
Energy range: 1–100 keV
On-axis brilliance at 16 keV (ph/s/mrad^2/mm^2/0.1%bw): 5.4 x 10^{15}
On-axis angular flux density at 16 keV (ph/s/mrad^2/0.1%bw): 9.6 x 10^{13}
Horizontal angular flux density at 6 keV (ph/s/mradh/0.1%bw): 1.6 x 10^{13}
Source size and divergence at the critical energy:
Σ_x: 92 μm Σ_y: 31 μm
$\Sigma_{x'}$: 6 μrad $\Sigma_{y'}$: 47 μrad

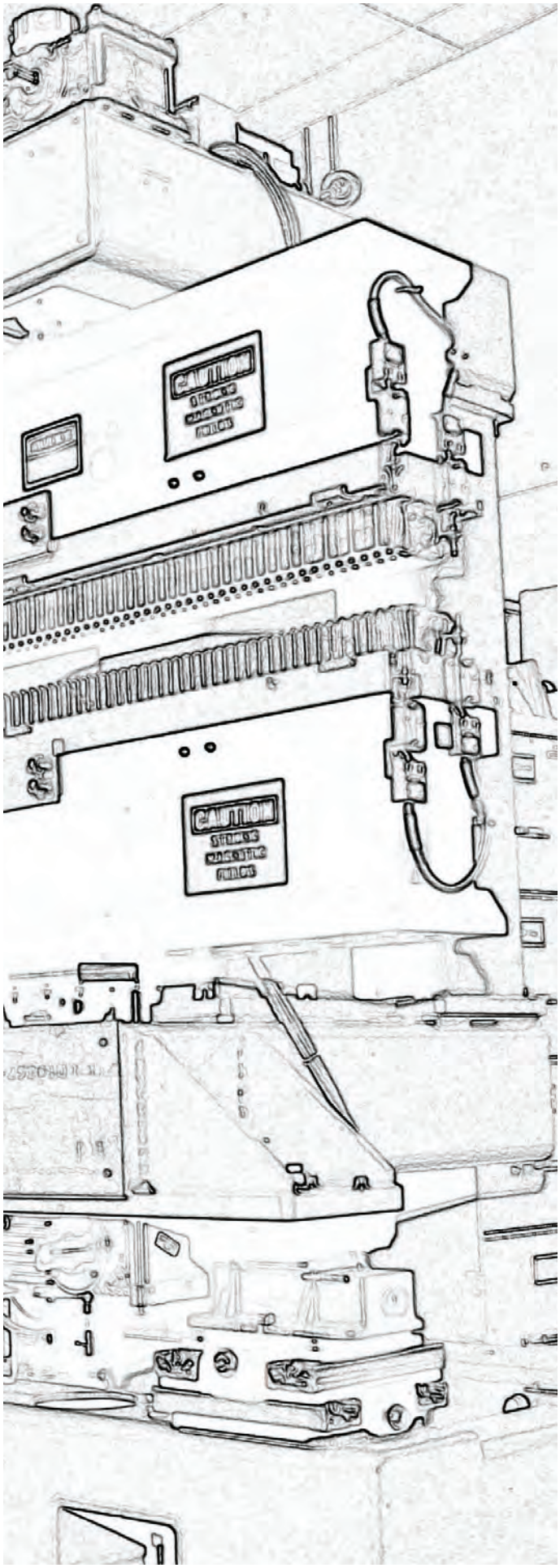

Acknowledgments

APS Science 2018 Editorial Board:

Mark A. Beno (ANL-PSC), John Byrd (ANL-ASD), John P. Connolly (ANL-AES), Robert Fischetti (ANL-XSD), Robert O. Hettel (ANL-PSC), Jonathan C. Lang (ANL-XSD), Dennis M. Mills, (ANL-PSC), George Srajer (ANL-PSC), Stephen K. Streiffer (ANL-PSC), Stefan Vogt (ANL-XSD)

Unless otherwise noted, the research highlights in this report were written by:

Mary Alexandra Agner (marymary@suberic.net)
Christen Brownlee (christenbrownlee@gmail.com)
Erika Gebel Berg (erikagebel@gmail.com)
David Bradley (david@sciencebase.com)
Vic Comello ANL-CPA - retired (vcomello@anl.gov)
Dana Desonie (desonie@cox.net)
Sandy Field (sfield@fieldscientific.com)
Amanda Grennell (amanda.jnb@gmail.com)
Gwenevier Johnson (gjpandcwriting@gmail.com)
Joseph E. Harmon ANL-BIS - (harmon@anl.gov)
Emma Nichols (emma@nascentmc.com)
Philip Koth (philkoth@comcast.net)
Kim Krieger (mskrieger@gmail.com)
David Lindley (dxlindley@gmail.com)
Chris Palmer (crpalmer2009@gmail.com)
Nicola Parry (nicola@parrymedicalwriting.com)
Neil Savage (neil@stefan.com)
Michael Schirber (mschirber@gmail.com)
Alicia Surrao (alicia@untoldcontent.com)
Mark Wolverton (exetermw@earthlink.net)

Photography: Wes P. Agresta, Mark L. Lopez (both ANL-CPA)
Aerial photograph of the APS: John Hill (Tigerhill Studio, http://www.tigerhillstudio.com)
Publications, contracts, rights and permissions, circulation: Jessie L. Skwarek (ANL-PSC)
Printing oversight: Gary R. Weidner (ANL-CPA)
Editorial, project coordination, design, photography: Richard B. Fenner (ANL-PSC)

Our thanks to the corresponding authors and others who assisted in the preparation of the research highlights, to the users and APS personnel who wrote articles for the report, and our apologies to anyone inadvertently left off this list. To all: your contributions are appreciated.

The Advanced Photon Source is a U.S. Department of Energy (DOE) Office of Science User Facility
operated for the DOE Office of Science by Argonne National Laboratory under Contract No. DE-AC02-06CH11357.

About Argonne National Laboratory

Argonne is a U.S. Department of Energy laboratory managed by UChicago Argonne, LLC under contract DE-AC02-06CH11357. The Laboratory's main facility is outside Chicago, at 9700 South Cass Avenue, Argonne, Illinois 60439. For information about Argonne and its pioneering science and technology programs, see www.anl.gov.

DOCUMENT AVAILABILITY

Online Access: U.S. Department of Energy (DOE) reports produced after 1991 and a growing number of pre-1991 documents are available free via DOE's SciTech Connect (http://www.osti.gov/scitech/)

Reports not in digital format may be purchased by the public from the National Technical Information Service (NTIS):

U.S. Department of Commerce
National Technical Information Service
5301 Shawnee Rd
Alexandra, VA 22312
www.ntis.gov
Phone: (800) 553-NTIS (6847) or (703) 605-6000
Fax: (703) 605-6900
Email: orders@ntis.gov

Reports not in digital format are available to DOE and DOE contractors from the Office of Scientific and Technical Information (OSTI):

U.S. Department of Energy
Office of Scientific and Technical Information
P.O. Box 62
Oak Ridge, TN 37831-0062
www.osti.gov
Phone: (865) 576-8401
Fax: (865) 576-5728
Email: reports@osti.gov

U.S. DEPARTMENT OF
ENERGY

Office of Science

Advanced Photon Source
Argonne National Laboratory
9700 S. Cass Ave.
Argonne, IL 60439 USA
www.anl.gov • www.aps.anl.gov